

UNIVERSITÉ DE TOURS

ÉCOLE DOCTORALE Santé, Sciences Biologiques, Chimie du Vivant

EA 7502 - Synthèse et Isolement de Molécules BioActives

THÈSE

présentée par:

Abdulrahim Altoam ALZAIN

soutenue le: **27 Novembre 2020**

pour obtenir le grade de:

Docteur de l'université de Tours

Discipline/ Spécialité: Chimie thérapeutique

Conception, synthèse, évaluation biologique et analyse 3D-QSAR de nouvelles imidazo[1,2-*a*:4,5-*c'*]dipyridines bioinspirées à activités antiproliférative, anti-migration et anti-invasion dans le cancer du sein triple négatif

THÈSE co-dirigée par:

Mme ENGUEHARD-GUEIFFIER Cécile

Mr ELHUSSEIN Magdi A. M.

Professeur, Université de Tours

Professeur, Université de la Khartoum, Soudan

THÈSE co-encadrée par:

Mr DELAYE Pierre-Olivier

MCU, Université de Tours

RAPPORTEURS:

Mr CARATO Pascal

Mr BOISBRUN Michel

Professeur, Université de Poitiers

MCU-HDR, Université de Lorraine

JURY:

Mme BERQUE-BESTEL Isabelle

Mr ELHADI Mohammed

Mr DELAYE Pierre-Olivier

Mr ROGER Sébastien

Mr CARATO Pascal

Mr BOISBRUN Michel

Mme ENGUEHARD-GUEIFFIER Cécile

Mr ELHUSSEIN Magdi A. M.

Professeur, Université de Bordeaux

Professeur, Université de la Gezira, Soudan

MCU, Université de Tours (co-encadrant)

MCU-HDR, Université de Tours

Professeur, Université de Poitiers

MCU-HDR, Université de Lorraine

Professeur, Université de Tours

Professeur, Université de la Khartoum, Soudan

Dedication

Dedicated to my beloved family for their endless love, support and encouragement especially my parents, my wife Reem and my son Gesan.
Thank you.

Acknowledgment

As my Ph.D. path comes to an end, I look back to three years ago when I moved to Tour naïve and inexperienced, but ascertained to do my Ph.D. in Medicinal Chemistry. What I did not recognize was that the next three years would be one of the most enriching and life-changing experience of my life both professionally and personally.

First and foremost, I would like to express my deepest appreciation to my academic advisors Prof. Cécile Enguehard-Gueiffier and Prof. Magdi A. M. Elhussein for their guidance, and encouragements during my research at Tour University. Prof. Cécile, thank you for accepting me in your lab and giving me a research project on which I have always wanted to work. I admire your hard work, and high standards for conducting research. I am also grateful to Dr. Sébastien Roger, thank you for generously opening your biology lab.

My appreciation goes to two distinguished lab mentors Pierre-Olivier Delaye in Chemistry lab and Lucie Brisson in biology lab for their support during my most uncertain times, I am deeply grateful, and I hope to emulate their mentorship style in my future career. I would also like to express my sincere appreciation for Dr. Stephan Chevalier and Dr. Pierre Besson for all their help and advice. I would also like to thank Mélanie Pénichon in helping synthesis of some compounds. My thanks extend to Stéphanie Chadet for her helping and guidance for the flow cytometry experiments. I also thank Prof. Hassan Allouchi for the X-Ray crystallography contained in this thesis.

Amanda have been fantastic labmate and we spent many time in lab talking about chemistry and musing over what to expect from graduate school.

Lastly, my gratitude towards my friends within and outside of professional sphere especially Gindeel, Mubarak, Mohamed A. Alrahman, Yousfi, Mohammed Hassan, Anas, Ahmed, Omer and Abbas.

Résumé

Le fardeau actuel du cancer du sein dans le monde, combiné aux difficultés liées au développement de nouveaux médicaments pour le traitement du cancer du sein triple négatif (TNBC) métastatique, constituent les principales motivations pour la découverte de nouveaux agents anticancéreux. Le développement des métastases est une cascade complexe qui implique une première et nécessaire étape d'invasion, avec l'acquisition de la capacité par les cellules malignes de se dégrader et de migrer à travers des matrices extracellulaires vers des tissus éloignés. Ainsi, l'inhibition de la prolifération, de la migration et de l'invasion des cellules TNBC constitue une approche très intéressante. Ces dernières années, nos laboratoires ont décrit une synthèse efficace pour la préparation d'imidazo[1,2-*a*:4,5-*c'*]dipyridines, analogues de la structure β -carboline présente dans de nombreux alcaloïdes naturels. Les β -carboline telles que l'harmine et ses dérivés présentent plusieurs activités pharmacologiques, en particulier des effets anticancéreux. Il est communément rapporté que les alcaloïdes de noyau β -carboline, tant naturels que synthétiques, induisent leurs activités anticancéreuses par de multiples mécanismes.

Dans le cadre de cette thèse, un travail approfondi a été réalisé pour développer de nouveaux agents anticancéreux de structure imidazo[1,2-*a*:4,5-*c'*]dipyridine. Un aperçu des β -carboline décrites dans la littérature est donné dans le chapitre 2, ainsi qu'une analyse des relations structure-activité (SAR) anticancéreuse de ce squelette. Cette thèse décrit dans le chapitre 3 nos efforts pour introduire une variabilité structurale sur quatre positions du noyau imidazo[1,2-*a*:4,5-*c'*]dipyridine. Ensuite, les produits cibles ont été testés pour leur capacité à inhiber la prolifération, la migration et l'invasion des cellules TNBC (chapitre 4). Les composés anti-prolifératifs les plus puissants [$IC_{50} \leq 6 \mu M$] contre les quatre lignées cellulaires TNBC étudiées ont été testés quant à leur capacité d'induire l'apoptose. De plus, deux composés ont réduit l'expression nucléaire de KI67, démontrant une activité inhibitrice de la prolifération cellulaire. Enfin, de nombreux analogues ont présenté de puissantes activités anti-migratoires sur MDA-MB-435s à $1 \mu M$. En outre, un composé a inhibé l'invasion des cellules murines 4T1 à $1 \mu M$.

μM. Dans le chapitre 5, nous discutons de l'étude *in silico* des relations structure-activité quantitatives tridimensionnelles (3D-QSAR) de nos composés.

En résumé, de nouveaux inhibiteurs puissants de la prolifération, de la migration et de l'invasion des cellules du cancer du sein ont été mis au point au cours de cette recherche doctorale.

Mots-clés: Cancer du sein triple négatif (TNBC); imidazo[1,2-*a*:4,5-*c'*]dipyridine, activité antiproliférative; apoptose; activité anti-migratoire; activité anti-invasion.

Summary

The current worldwide breast cancer burden combined with the difficulties associated with the development of novel drugs for the treatment of metastatic triple-negative breast cancer (TNBC) form the major motivations for the discovery of new anti-cancer agents. Metastasis development is a complex cascade that involves a first and necessary step of invasion, with the acquisition of the ability by malignant cells to degrade and migrate through extracellular matrices to distant tissues. Thus, inhibition of proliferation, migration, and invasion of TNBC cells constitutes highly interesting approaches. In recent years, our laboratories have described an efficient one-pot sequence for the preparation of imidazo[1,2-*a*:4,5-*c'*]dipyridines, analogues of the β -carboline scaffold present in many naturally occurring alkaloids. β -Carbolines such as harmine and its derivatives display several pharmacological activities, particularly anticancer effects. It is commonly reported that both natural and synthetic β -carboline alkaloids elicit their anticancer activities through multiple mechanisms.

In this thesis, an extensive work was done to develop new anticancer agents based on the imidazo[1,2-*a*:4,5-*c'*]dipyridine scaffold. An overview of β -carbolines described in the literature was given in Chapter 2, together with an analysis of the anticancer structure-activity relationships (SAR) of this skeleton. This thesis describes in Chapter 3 our efforts to introduce modifications at four positions of imidazo[1,2-*a*:4,5-*c'*]dipyridine core. Then, the target products were tested for their ability to inhibit the proliferation, migration, and invasion of TNBC cells (Chapter 4). The most potent anti-proliferative compounds [$IC_{50} \leq 6 \mu M$] against all four TNBC cell lines studied, were tested for their apoptotic induction capacity. Also, two compounds reduced nuclear Ki-67 staining indicating a decrease in cell proliferation. Many analogues exhibited potent anti-migratory activities against MDA-MB-435s at $1 \mu M$. Besides, one compound inhibited murine 4T1 cell invasion at $1 \mu M$. In chapter 5, we discuss the *in silico* three dimensional-quantitative structure-activity relationships (3D-QSAR) study of these compounds.

In summary, novel potent inhibitors of breast cancer cell proliferation, migration, and invasion were developed during this doctoral research, which may lead to novel anti-cancer agents.

Keywords: Triple-negative breast cancer (TNBC); imidazo[1,2-*a*:4,5-*c'*]dipyridine, antiproliferative activity; apoptosis; anti-migrative activity; anti-Invasion activity.

Table of Contents

Résumé	1
Summary	3
Table of Contents	5
List of Tables	8
List of Figures	9
List of Schemes.....	12
List of Abbreviations	14
Introduction	17
Chapter 1: Breast Cancer	23
I. Introduction	25
II. Epidemiology.....	25
III. Hallmarks of Cancer Cell	26
III-1. Sustaining Proliferative Signaling.....	27
III-2. Evading Growth Suppressors	28
III-3. Enabling Replicative Immortality	28
III-4. Inducing Angiogenesis	28
III-5. Activating Invasion and Metastasis	29
III-6. Resisting Cell Death	30
IV. Classification of Breast Cancer.....	32
IV-1. Luminal Breast Cancer	32
IV-2. Human Epidermal Growth Factor Receptor Breast Cancer.....	33
IV-3. Basal-Like/Triple-Negative Breast Cancers.....	33
V. Molecular Targets and Therapy in Breast Cancer.....	34
V-1. Targeting ER in Breast Cancer.....	34
V-2. Targeting HER2 in Breast Cancer	35
V-3. Novel Targeted Treatments in ER Positive Breast Cancer.....	36
V-4. BRCA-Associated Tumors and PARP Inhibitors.....	37
VI. Conclusion.....	38
Chapter 2: <i>Peganum harmala</i> L. and β -carboline	41
I. Introduction	43
II. Botanical Description of <i>Peganum Harmala</i>	43
III. Alkaloidic Composition.....	44

IV. Medicinal Uses.....	45
V. β -carboline Scaffold	47
V-1. General Presentation of β -carboline Derivatives	47
V-2. Synthesis of β -carboline Skeleton	48
V-3. Biological Activities	52
V-4. β -carbolines as Anticancer Agents	59
VI. Conclusion.....	83
Chapter 3: Design and Synthesis of New Imidazo[1,2- <i>a</i> :4,5- <i>b'</i>]dipyridines.....	85
I. Genesis of the Project	87
II. Background on the Synthetic Pathway	91
III. Design of the New Series of Compounds.....	93
IV. Personal Work.....	94
IV-1. Synthesis of the 3-Iodo-2-cyanoimidazo[1,2- <i>a</i>]pyridines as Common Starting Materials.....	94
IV-2. Sonogashira Cross-Coupling Reaction at Position 3	97
IV-3. Heterocyclization	101
IV-4. Suzuki-Miyaura and Copper-Catalyzed Cross-Coupling Reactions on the 7 Position.....	110
IV-5. Synthesis of Imidazo[1,2- <i>a</i> :4,5- <i>c'</i>]dipyridine Salt Analogues	115
V. Conclusion.....	119
Chapter 4: Biological Evaluation of Imidazo[1,2- <i>a</i> :4,5- <i>b'</i>]dipyridines	123
I. Introduction	125
II. <i>In Vitro</i> Cancer Growth Inhibition Activities	126
III. Studies of the Imidazo[1,2- <i>a</i> :4,5- <i>c'</i>]dipyridines Cellular Mechanism	130
III-1. Apoptosis Induction Activity of Imidazo[1,2- <i>a</i> :4,5- <i>c'</i>]dipyridines	131
III-2. Cellular Molecular Effects of Imidazo[1,2- <i>a</i> :4,5- <i>c'</i>]dipyridines	134
III-3. Ki-67 Staining Assay	135
IV. Anti-Migratory Activities.....	136
V. Selection and Further Tests Toward <i>In Vivo</i> Murine Evaluation	140
V-1. <i>In Vitro</i> Growth Inhibition Activity against Murine 4T1-luc Cells	141
V-2. <i>In Vitro</i> Migration and Invasion Inhibition Activities against Murine 4T1-luc Cells	142
VI. Selectivity Study against MCF-10A Cells	144
VII. Conclusion.....	146
Chapter 5: 3D-QSAR Study of Imidazo[1,2- <i>a</i> :4,5- <i>b'</i>]dipyridines	149
I. Introduction	151
II. 3D-QSAR Study	152
II-1. Data Set.....	152

II-2. Structure Optimization and Alignment.....	152
II-3. CoMFA and CoMISA Studies	154
II-4. Partial Least Squares (PLS) Analysis	154
II-5. Results.....	155
III. Conclusion.....	160
Conclusion and Perspectives	161
I. Conclusions	163
II. Perspectives	164
Experimental Part	165
I. Introduction	167
II. Chemistry	167
II-1. Reagents and Solvents	167
II-2. Physical and Spectroscopic Characterization	167
II-3. Chromatography.....	168
II-4. Synthesis and Characterization.....	168
III. Biology.....	205
III-1. Cell Culture Techniques	205
III-2. Evaluation of the Effects of Test Compounds on Cancer Cell Viability.....	207
III-3. Study of <i>In Vitro</i> Cell Migration and Invasiveness	212
III-4. Statistics	214
Bibliography	215

List of Tables

Table 1: Molecular classification of BC and correlation with biomarker staining.....	32
Table 2: Efficacy of PARP inhibitors currently under clinical evaluation for TNBC	38
Table 3: Chemical constituents of harmala seeds and their main biological activities.....	46
Table 4: Cancer cells viability effects of preliminary imidazo[1,2- <i>a</i> :4,5- <i>c'</i>]dipyridines.....	90
Table 5: Yields for the synthesis of 5a-h using terminal alkynes through Sonogashira reaction	99
Table 6: Attempts for coupling 4a-b with ethynyltrimethylsilane	101
Table 7: Yields for the synthesis of 7-hydrogenated 6a-h using Grignard reagents	103
Table 8: Yields for the synthesis of 7-brominated 6i-o using Grignard reagents.....	104
Table 9: Attempts for cyclizing 5e and 5g with Grignard reagents	105
Table 10: Yields for the synthesis of 6q-v using methoxide reagent	107
Table 11: Attempts for cyclizing 5c using sodium alkoxide nucleophiles	108
Table 12: Attempts for Sonogashira cross-coupling.....	113
Table 13: Isolated yields for imidazo[1,2- <i>a</i> :4,5- <i>c'</i>]dipyridine target salts 8-29	116
Table 14: Attempts for salt formations using benzyl bromide/ benzyl chloride.....	118
Table 15: Characteristics of the human breast cancer cell lines used in the study	126
Table 16: <i>In vitro</i> growth inhibition activities of imidazo[1,2- <i>a</i> :4,5- <i>c'</i>]dipyridines	128
Table 17: Cell proliferation activity of 13 , 18 , and 27-28 using Ki-67 assay.....	135
Table 18: Wound closure values for imidazo[1,2- <i>a</i> :4,5- <i>c'</i>]dipyridines.....	138
Table 19: <i>In vitro</i> growth inhibition activities of selected imidazo[1,2- <i>a</i> :4,5- <i>c'</i>]dipyridines.....	142
Table 20: 15h migration and invasion assay on 4T1-luc cells after treatment with 20 at 1 μ M	143
Table 21: <i>In vitro</i> 5 d cytotoxicity assay results for selected imidazo[1,2- <i>a</i> :4,5- <i>c'</i>]dipyridines .	145
Table 22: In vitro growth inhibition activities of analogues against MDA-MB-435s-luc.....	153
Table 23: The experimental <i>pIC</i> ₅₀ and predicted <i>pIC</i> ₅₀ of the training and test set molecules .	155
Table 24: PLS Statistical results of CoMFA and CoMSIA Models.....	157
Table 25: CoMFA and CoMSIA predictive <i>pIC</i> ₅₀ values of the test set	157
Table 26: List of primary antibodies used in western blotting.....	211
Table 27: List of secondary antibodies used in western blotting.....	211

List of Figures

Figure 1: Estimated number of female BC incidence cases worldwide	25
Figure 2: Estimated age-standardized incidence rates of BC in 2018 per 100,000 women	26
Figure 3: Hallmarks of cancer cells	27
Figure 4: Metastatic cascade steps in breast tumors	29
Figure 5: Intrinsic (mitochondrial) pathway of apoptosis	31
Figure 6: Molecular structures of palbociclib, ribociclib, and abemaciclib	37
Figure 7: (A) Harmala plant bearing flowers and fruit; (B) flower; (C) fruit; (D) seeds	44
Figure 8: Some chemical constituents of harmala seeds	45
Figure 9: Structures and nomenclature of carbolines (pyridoindoles)	47
Figure 10: Pinoline	48
Figure 11: Manzamine A and 8-hydroxymanzamine A with antimalarial activity	53
Figure 12: Some 1-amino- β -carboline derivatives I-VIII with antimalarial activity.....	53
Figure 13: 1-amino-6-halo- β -carboline derivatives IX-X with antimalarial activity	54
Figure 14: General structure of indolylglyoxylamides.....	54
Figure 15: Some β -carboline-1,3,5-triazine hybrids XI-XIV with antileishmanial activity.....	55
Figure 16: the semisynthetic 1,2,3,4-tetrahydromanzamine A with antifungal activity	55
Figure 17: β -carboline chalcones skeleton and their bromide salts with antibacterial activity ..	56
Figure 18: 1-methoxycanthinone with anti-HIV activity	56
Figure 19: 9-butylharmine with anti-HIV activity	56
Figure 20: 1-Formyl- β -carboline-3-carboxylic acid methyl ester with anti-HIV activity	57
Figure 21: 1-(thiophen-2-yl)- β -carboline derivative XV with anti-HIV activity	57
Figure 22: 3-piperazinoyl- β -carboline derivatives XVI-XX with anti-HIV activity.....	57
Figure 23: Tadalafil.....	58
Figure 24: FG-7142 and compounds XXI-XXII	59
Figure 25: 1-amino- β -carbolines derivatives XXIII-XXV and manzamine	60
Figure 26: 1-carboxamide β -carbolines XXVI-XXVIII and 1-amino β -carbolines XXIX-XXXIII	60
Figure 27: β -carboline with indolyl moiety at C-1 XXXIV with anticancer activity.....	61

Figure 28: 3-substituted- β -carbolines XXXV-XXXIX with anticancer activity.....	61
Figure 29: Compounds XL-XLII with potent anticancer activity	62
Figure 30: Compound XLIII and the Mannich bases XLIV-L with anticancer activity	63
Figure 31: (<i>N</i> -acetyl)pyrazole-linked β -carboline hybrids LI-LVI with anticancer activity	64
Figure 32: Compound LVII with potent anticancer activity.....	64
Figure 33: β -carboline-3-dithiocarbamate LVIII with anticancer activity	65
Figure 34: β -carbolines with bulky alkoxy substituent moiety at C-7 LIX-LXIII	66
Figure 35: 9-aralkylated substituted β -carboline LXIV with anticancer activity	67
Figure 36: 9-aralkylated substituted β -carboline derivatives LXV-LXVI with anticancer activity	67
Figure 37: 2-benzyl-1-styryl- β -carbolinium bromides LXVII-LXIX	68
Figure 38: <i>N</i> 2-benzylated quaternary β -carboline amino acid ester conjugates LXX-LXXI	69
Figure 39: 2-alkylated quaternary β -carboline LXXII with potent anticancer activity	69
Figure 40: 2,7,9-substituted β -carbolines LXXIII-LXXIV with potent anticancer activity	70
Figure 41: SAHA and β -carboline-based hydroxamic acid derivative LXXV	71
Figure 42: C3-substituted β -carboline-based hydroxamic acid LXXVI with anticancer activity...	72
Figure 43: C-1 and C-3 substituted β -carboline-based hydroxamic acid derivative LXXVII	73
Figure 44: 3-chalcone- β -carboline hybrid LXXVIII with anticancer activity	74
Figure 45: 1-chalcone- β -carbolinium bromide LXXIX with anticancer activity	74
Figure 46: β -carbolines/salicylic acid hybrid LXXX , salicylic acid and aspirin.....	75
Figure 47: Acylhydrazone-linked β -carboline hybrid LXXXI with potent anticancer effect	76
Figure 48: β -carboline-podophyllotoxin hybrids LXXXII-LXXXIII with anticancer effect.....	77
Figure 49: β -carbolines dimer LXXXIV with potent anticancer activity	78
Figure 50: Asymmetric β -carbolines dimer LXXXV with potent anticancer activity	78
Figure 51: Semi-synthetic β -carboline dimer B-9-3 with potent anticancer activity	79
Figure 52: Dimeric β -carboline LXXXVI with potent anticancer activity	79
Figure 53: Ruthenium (II) β -carboline complexes LXXXVII- XCI with potent anticancer activity	81
Figure 54: Pt (II) or Cu (II) β -carboline complex XCII with potent anticancer activity.....	81
Figure 55: Ni (II) β -carboline complex XCIII with potent anticancer activity	82
Figure 56: Highlighted biological activities of β -carbolines and anticancer SAR.....	84

Figure 57: β -carboline, harmine and imidazo[1,2- <i>a</i> :4,5- <i>c'</i>]dipyridine structures	88
Figure 58: Electrostatic potential map for the imidazo[1,2- <i>a</i> :4,5- <i>c'</i>]dipyridine using Gaussian..	88
Figure 59: X-ray crystal structure of imidazo[1,2- <i>a</i> :4,5- <i>c'</i>]dipyridine salt.....	89
Figure 60: Overview of the planned modifications on imidazo[1,2- <i>a</i> :4,5- <i>c'</i>]dipyridine motif.....	93
Figure 61. Electrostatic potential maps for 7b and 7e	117
Figure 62: The screening cascade adopted in the biological evaluation of compounds	125
Figure 63: MTT cell viability assay	127
Figure 64: Selective analogues 13 , 18 , and 27-28 with potent growth inhibition activity	131
Figure 65: Principles of the FITC Annexin V Apoptosis Assay	132
Figure 66: Annexin V and P.I. double staining flow cytometry of MDA-MB-231 cells treated with 13 , 18 , and 27-28 at 3 and 30 μ M for 48 hours	133
Figure 67: Western blot analysis of markers associated with apoptosis in MDA-MB-231 cells treated with compounds 13 , 18 , and 27-28 at 30 μ M for 48h	134
Figure 68: Ki-67 staining by the green colour of GFP for detection of cell proliferation of MDA- MB-231 cells treated with compounds 13 , 18 , and 27-28 at 30 μ M for 48h.....	136
Figure 69: Inserts used in cell migration assay.	137
Figure 70: Wound healing activity of 28 (1 μ M) and DMSO (0.1%) against MDA-MB-435s-luc cells at selected periods	140
Figure 71: Analogues 13 , 18 , 20 and 28 which will be used for the <i>in vivo</i> biological activities	141
Figure 72: Matrigel invasion chamber used in cell invasiveness assays	143
Figure 73: Invasion inhibitory activity of compound 20 against 4T1-luc cells.	144
Figure 74: SAR analysis of imidazo[1,2- <i>a</i> :4,5- <i>c'</i>]dipyridines.....	146
Figure 75: Effects of imidazo[1,2- <i>a</i> :4,5- <i>c'</i>]dipyridines on human breast cancer	147
Figure 76: The workflow adapted in the 3D-QSAR study	151
Figure 77: Database alignment method.	154
Figure 78: Predicted pIC_{50} vs. experimental pIC_{50} values for the 13 training set molecules obtained by PLS analysis using CoMFA and CoMSIA models	156
Figure 79: Contour maps of (A) CoMFA and (B) CoMSIA in combination with compound 18 ...	158
Figure 80: SAR summarized based on the 3D-QSAR analysis.....	160

List of Schemes

Scheme 1: Synthetic Route developed by our laboratory for the synthesis of imidazo[1,2- <i>a</i> :4,5- <i>c'</i>]dipyridines that mimic the structure of β -carbolines	20
Scheme 2: Synthesis of the β -carboline skeleton by Pictet-Spengler reaction.....	49
Scheme 3: Synthesis of β -carboline skeleton starting from <i>tert</i> -butylimines of <i>N</i> -substituted indole carboxaldehydes.....	49
Scheme 4: Synthesis of β -carboline skeleton starting from indolecarboxamides	50
Scheme 5: Synthesis of β -carboline skeleton starting from substituted indole	50
Scheme 6: Ruthenium-catalyzed method for the synthesis of the β -carboline skeleton.....	51
Scheme 7: Two-step protocol for the synthesis of β -carbolines developed by Ray group.....	51
Scheme 8: Synthesis of imidazo[1,2- <i>a</i> :4,5- <i>c'</i>]dipyridines.....	87
Scheme 9: Synthetic protocol towards target tricyclic compounds.....	92
Scheme 10: Retrosynthesis of target compounds.....	94
Scheme 11: Gram Scale reactions toward synthesis of 4a and its 7-brominated derivative 4b . ..	95
Scheme 12: Mechanisms for the synthesis of intermediates 1a-4a	96
Scheme 13: Mechanism of Sonogashira cross-coupling	98
Scheme 14: Synthetic protocol towards key intermediate 5i	99
Scheme 15: A plausible mechanism of decarboxylative Sonogashira reaction	100
Scheme 16: Proposed reaction mechanism for the imidazo[1,2- <i>a</i> :4,5- <i>c'</i>]dipyridine formation through Grignard reactions.....	102
Scheme 17: Synthetic protocol towards target compound 6p and attempts for synthesizing 1-methypiperazine and 1-piperidine analogues.....	105
Scheme 18: Proposed reaction mechanism for the formation of 6p	106
Scheme 19: Possible reaction mechanism for synthesis of 1-OMe analogues	108
Scheme 20: Effects of Pt(II) Parkins catalyst on carbonitrile reported by Li group.....	109
Scheme 21: Synthetic protocol towards target compounds 7a-d	110
Scheme 22: General mechanism for SM cross-coupling reaction.....	111
Scheme 23: Synthetic protocol towards target compound 7e	112

Scheme 24: Synthetic protocol towards target analogue 7h	114
Scheme 25: Proposed reaction mechanism for the formation of 7h	114
Scheme 26: Synthetic protocol towards 7-methoxy based analogue.....	115
Scheme 27: Mechanism of salt formation.....	115
Scheme 28: Synthetic pathways utilized to obtain target analogues	121

List of Abbreviations

¹³ C NMR	Carbon Nuclear Magnetic Resonance
¹ H NMR	Proton Nuclear Magnetic Resonance
Å	Ångstrom
α	Alpha
β	Beta
γ	Gamma
B	
Bak	Bcl-2 homologous antagonist/killer
Bax	Bcl-2-associated X protein
Bcl-XL	B-cell lymphoma-extra large
Bid	BH3 interacting domain death agonist
Bn	Benzyl
C	
°C	Degrees Celsius
<i>ca.</i>	Circa (around)
Calc.	Calculated
CoMFA	Comparative molecular field analysis
CoMISA	Comparative similarity indices analysis
CPME	Cyclopentyl methyl ether
c-Pr	Cyclopropyl
D	
Dapi	4',6-diamidino-2-phenylindole
dba	Dibenzylideneacetone
DME	1,2-dimethoxyethane
DMF	dimethylformamide
DMEM	Dulbecco's Modified Eagle Medium
DMSO	Dimethyl sulfoxide
E	
EDTA	Ethylenediaminetetraacetic Acid
eq.	Equivalent
ERK1/2	Extracellularly-Regulated Kinase-1 and -2
<i>et al.</i>	Et Alii (and others)
Et	Ethyl
F	
FITC	Fluorescein isothiocyanate

G

g	Gram(s)
G ₀ /G ₁	Quiescence/growth phase1 (cell cycle analysis)
GFP	Green fluorescent protein
G ₂ /M	Growth phase 2/mitosis

H

h	Hour
HRMS (ESI)	High resolution mass spectroscopy (Electrospray ionization)

K

Kcal	Kilo calorie
------	--------------

L

L	Liter(s)
---	----------

M

Me	Methyl
m.p	Melting point
mg	Milligram
mL	Milliliter
mol	Mole(s)
mM	Millimolar
mmol	Millimole
μm	Micrometer
μM	Micromolar (micromoles per liter)
μl	Microliter
mTOR	Mammalian target of rapamycin
MW	Microwave

N

NADH	Nicotinamide adenine dinucleotide (NAD) + hydrogen (H)
nm	Nanometer

O

OMe	Methoxy
OTf	Trifluoromethansulfonate

P

Ph	Phenyl
PPh ₃	Triphenyl phosphine
Pyr	Pyridinyl

R

R	Generalized group
RPMI	Roswell Park Memorial Institute
RT	Room temperature

T

<i>t</i> -Bu	<i>Tertiary</i> -Butyl
TEA	Triethylamine
THF	Tetrahydrofuran
Tris	Tris(hydroxymethyl)aminomethane

Introduction

This thesis research is a joint Ph.D. program in cotutelle between Prof. Cécile Enguehard-Gueiffier of the University of Tours in France and Prof. Magdi A. M. Elhussein of the University of Gezira in Sudan. This project is at the chemistry/biology interface in the field of cancerology. I synthesized and evaluated in *in vitro* biological tests all the compounds presented herein.

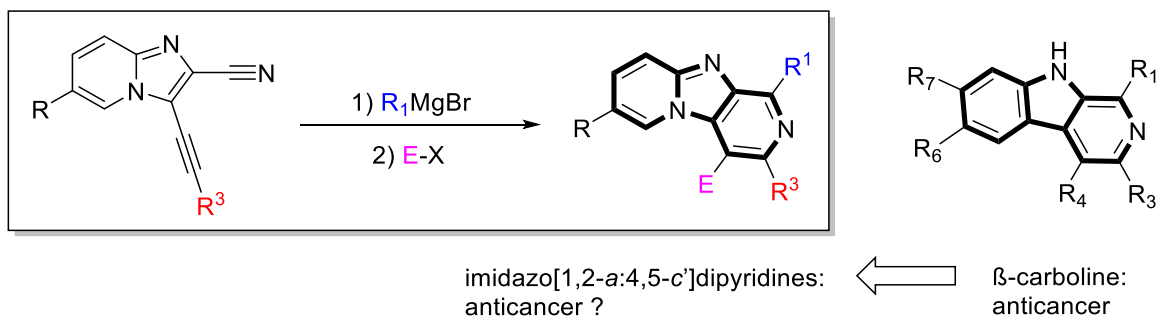
The synthesis of compounds was conducted in EA 7502 “Synthèse et Isolement de Molécules BioActives” (SIMBA) research group, at the Faculty of Pharmacy of Tours. Research in this laboratory focuses on the design of molecules for anticancer purposes inspired by natural molecules and new anti-infective therapies (antiviral, antibacterial, and antifungal). The chemical series historically studied at the faculty of pharmacy are nitrogen bridgehead bicycles, e.g., imidazo[1,2-*a*]pyridines and imidazo[1,2-*b*]pyridazines. The research team includes 13 institutional members and 8 Ph.D. or post-doctoral students.

The biological evaluation of compounds was conducted in UMR INSERM 1069 “Nutrition, Croissance et Cancer” (N2C) and EA 4245 “Transplantation, immunologie et inflammation” (T2I) at the Faculty of Medicine of Tours. UMR 1069 is a multidisciplinary single team unit (expertise in areas of biology, physiology, oncology, nutrition, at preclinical and clinical stages) composed of 33 institutional members and 7 Ph.D. or post-doctoral students. T2I unit is interested in understanding the interactions between cells of stressed tissue (cardiac cells, normal or cancerous epithelial cells) and immune cells for immuno-inflammatory response modulation in hypoxia/ischemia. T2I is composed of 18 institutional members and 6 Ph.D. or post-doctoral students.

The compounds investigated in this project were inspired by the structure of the β -carboline alkaloids (**Scheme 1**). The β -carbolines, which possess a common tricyclic pyrido[3,4-*b*]indole ring, represent a large group of synthetic or naturally occurring alkaloids, extracted and characterized from various plants and marine creatures. These alkaloids are notably abundant in *Peganum harmala*, a plant used as a traditional medicine in the Middle East, America, and Central Asia.¹ Indeed, these compounds demonstrated many important biochemical effects and pharmacological properties, such as anticancer, antithrombotic, antiparasitic, antimicrobial, and antiviral activities.² Interestingly, β -carbolines were extensively studied in the literature and were identified as highly potent anticancer compounds.³ In particular, natural β -carboline harmine

present in *Peganum harmala*, has potent anticancer effect and exert its activity through different mechanisms such as the inhibition of DYRK1A, a protein kinase linked to tumorigenesis, and DNA intercalating properties.⁴⁻⁷

In the ongoing effort of our lab to develop new methods for synthesizing imidazo[1,2-*a*]pyridine-based heterocycles, we have recently described efficient methods for the preparation of imidazo[1,2-*a*:4,5-*c'*]dipyridines as shown in **Scheme 1**.^{8,9} This core mimics the β -carbolines which inspired us to explore its anticancer activity.



Scheme 1: Synthetic Route developed by our laboratory for the synthesis of imidazo[1,2-*a*:4,5-*c'*]dipyridines that mimic the structure of β -carbolines

A preliminary biological evaluation of few imidazo[1,2-*a*:4,5-*c'*]dipyridines from our chemical library confirmed the promising anticancer activity of this new series of compounds. Encouraged by these preliminary results, this thesis research project aims to conduct further medicinal chemistry exploratory studies with respect to hit-to-lead optimization. This entailed design, synthesis, biological assessment, as well as structure-activity relationship analyses, in efforts to explore the opportunities and liabilities associated with the imidazo[1,2-*a*:4,5-*c'*]dipyridine class of compounds as potential anticancer agents. The project was funded by the French association “Ligue contre le Cancer”.

The thesis is divided into 5 chapters. After this introduction, chapter 1 provides a brief overview of breast cancer (BC) and its treatment. Chapter 2 reviews the literature concerning *Peganum harmala* L. and its β -carboline alkaloids that inspired this thesis project. Chapter 3 addresses the design and synthesis of the original bioinspired imidazo[1,2-*a*:4,5-*c'*]dipyridines.

Chapter 4 describes the biological activities of the synthesized imidazo[1,2-*a*:4,5-*c'*]dipyridines. Chapter 5 puts forward the *in silico* studies which support the experimental findings. The conclusion section highlights the major findings of the thesis, and propose issues inviting future research. Finally, the experimental part concentrates on the experimental details used in the project.

Chapter 1:

Breast Cancer

I. Introduction

In this chapter, a brief overview of breast cancer (BC) and its treatment is provided. BC is highlighted with respect to epidemiology and hallmarks of cancer, classification of breast cancer, as well as advances made in molecular targets and therapy in breast cancer.

II. Epidemiology

Breast cancer is the most common cancer among women, with an estimated 2.1 million newly diagnosed women each year worldwide (**Figure 1**). In 2018, nearly 627,000 women died of breast cancer, making it the second-leading cause of deaths among women after cardiovascular disorders worldwide, representing 23% and 7% of deaths in the USA and India, respectively.^{10,11}

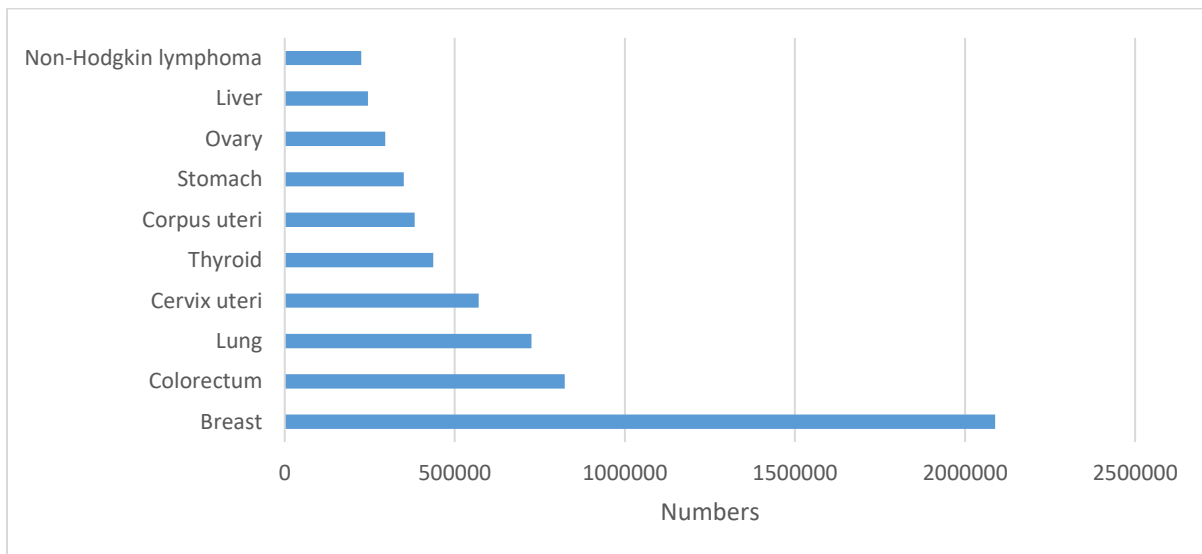


Figure 1: Estimated number of female BC incidence cases worldwide (Source: gco.iarc.fr/today/home)

Worldwide, the incidence rates are increasing, though, there is a great difference between developed and developing countries (**Figure 2**). The highest incidence rates remain in the more developed regions; in Western Europe, the incidence of breast cancer has reached more than 90 new cases per 100,000 women per year, compared with 20/100,000 in North Africa. This variation in incidence rates shows differences in the distribution of breast cancer risk factors and differences among the population's ability access to screening.

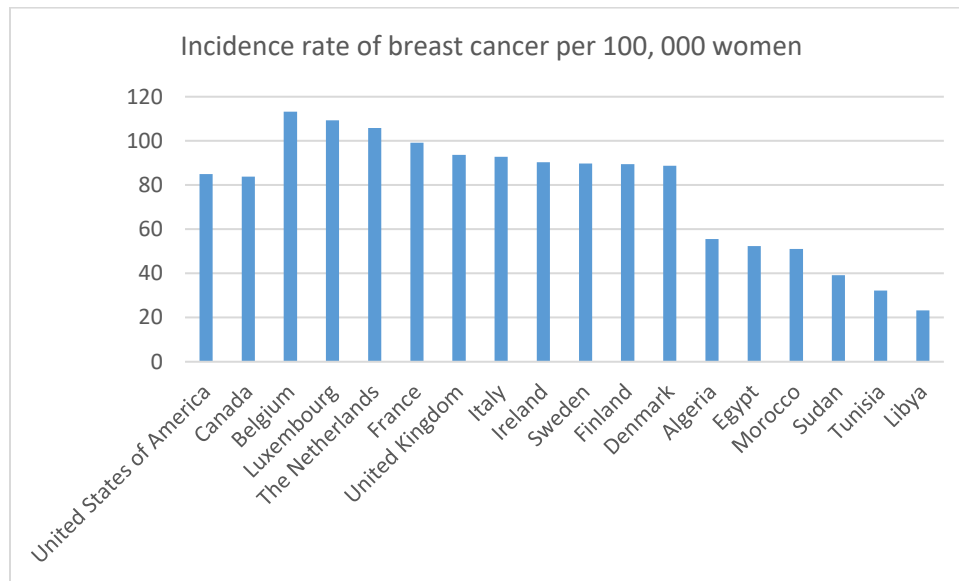


Figure 2: Estimated age-standardized incidence rates of BC in 2018 per 100,000 women (Source: gco.iarc.fr/today/home)

III. Hallmarks of Cancer Cell

The complexity of a cancer cell is derived collectively from essential alterations in cell physiology that cause malignant cell growth: sustaining proliferative signaling, evading growth suppressors, resisting cell death, inducing angiogenesis, enabling replicative immortality, and activating invasion and metastasis as shown in **Figure 3**.¹²

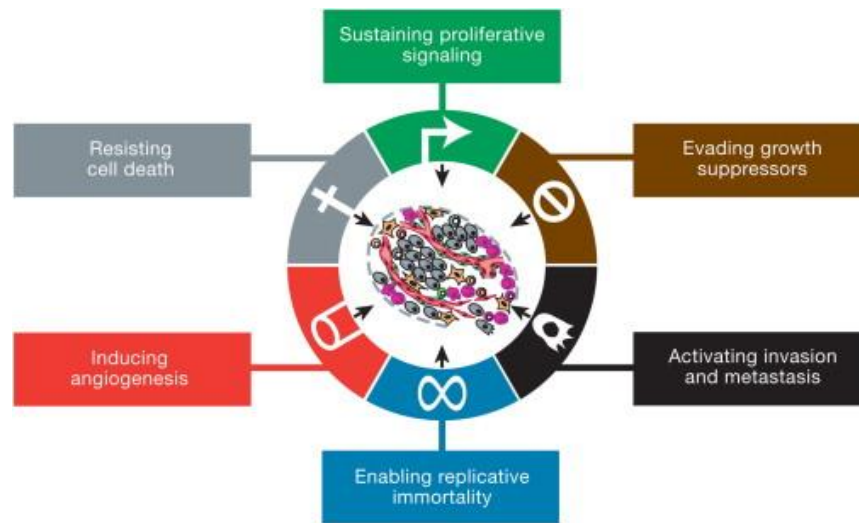


Figure 3: Hallmarks of cancer cells¹²

III-1. Sustaining Proliferative Signaling

Improved and sustainable cell proliferation is a core cancer-driving trait and one of the most important hallmarks of cancer that can be identified using several histologic, biochemical, and flow cytometry analysis.¹³ Under normal conditions, there is control over the production and release of growth factors that regulate cell growth and division. Normal cell regulation is related either to their dependency on other cells for growth factors or by an overproduction of a specific growth receptor required to respond to the corresponding growth factor. Through bypassing the normal regulatory mechanisms, cancer cells have self-sufficiency of growth property. The estrogen receptor (ER) signaling, vascular endothelial growth factor (VEGF) receptor family signaling, and human epidermal growth factor receptor-2 (HER2) signaling are the most commonly known proliferation-inducing pathways in breast cancer.¹⁴ The proliferative activity of breast cancer cells is often quantified through Ki-67, a nuclear protein that is expressed exclusively during the active cell cycle phases. Ki-67 is present in all proliferating cells and absent in nonproliferating cells.¹⁵

III-2. Evading Growth Suppressors

Cancer cells can evade a variety of growth suppression mechanisms in the extracellular matrix or on the surface of nearby cells. Cell growth and proliferation are limited by dozens of cancer suppressors, of which, RB (retinoblastoma)-associated and p53 proteins are considered prototype cancer suppressor proteins which function as fundamental regulatory points. Then, loss of function mutations are commonly observed for these proteins in cancer.¹⁶

III-3. Enabling Replicative Immortality

Telomeres are the caps and repetitive nucleotide sequences that are located at the ends of the linear chromosomes of most eukaryotic organisms. Telomeres have important functions in protecting the chromosomal structure. The telomerase, a DNA polymerase enzyme that is involved in maintaining telomere length, can add nucleotide repeats—TTAGGG oriented 5'-to-3' at the end of the chromosomes. However, telomerase is not capable to completely copy DNA at the very ends of chromosomes; therefore, approximately 50 nucleotides are lost during each cell cycle, which results in gradual telomere length shortening.¹⁷⁻¹⁹ Their progressive shortening during successive cell divisions induces chromosomal instability. Cancer cells usually overcome this issue by upregulating telomerase.

III-4. Inducing Angiogenesis

Cancer acquires abnormal and sustained angiogenesis, with the growth of new vessels from existing vasculature, that transports oxygen and nutrients to cancer cells and evacuates the waste and carbon dioxide.²⁰ A balance of angiogenic and angiostatic growth factors controls physiological angiogenesis. Disturbing this balance towards a pro-angiogenic environment is termed the 'angiogenic switch' and occurs in situations such as tissue hypoxia, inflammation, or tumor. 'Angiogenic switch' activates growth factors that stimulate endothelial cells (EC) to proliferate. The vascular endothelial growth factor (VEGF) family comprises major angiogenic

growth factors. VEGF-A is a potent activator of angiogenesis that stimulates EC proliferation and survival and results in the growth of new vessels into the tumor.²¹

III-5. Activating Invasion and Metastasis

Cancer metastasis is the leading cause of cancer patients mortality.²² Metastasis involves a series of distinct biological processes known as the metastatic cascade as shown in **Figure 4**.²³ Tumor cells invade the microenvironment of the primary tumor, intravasate and circulate into the blood or lymphatic circulation, reach distant organs, extravasate from the circulation into the metastatic site, colonize this organ, proliferate and establish the secondary tumor(s).²⁴ It has been proposed that during the epithelial-to-mesenchymal transition (EMT) process, the epithelial cells acquire mesenchymal features including motility and invasive properties.^{25,26} Since most of the metastases present a low degree of EMT, it has been suggested that EMT tumor cells undergo a mesenchymal-to-epithelial transition (MET) at the metastatic site.²⁴

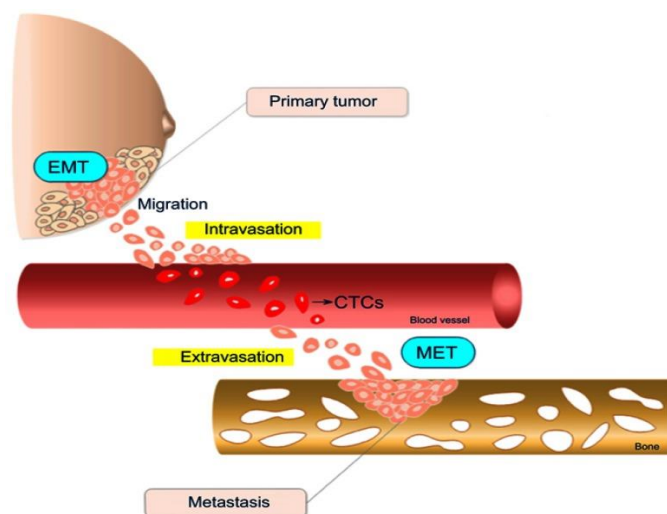


Figure 4: Metastatic cascade steps in breast tumors. Cells in the primary tumor undergo epithelial-mesenchymal transition (EMT), gaining migratory and invasive properties. After leaving the primary tumor, cells intravasate into circulatory or lymphatic vessels until extravasation to a distant metastatic secondary site (e.g., bone). Once established at the secondary site, cells suffer an inverse EMT process called mesenchymal-epithelial transition (MET). CTC, circulating tumor cells

Within the primary tumor, the hypoxic microenvironment stimulates the proliferation and migration of endothelial cells to afford the tumor with new vascular networks, which will permit growth and further dissemination to secondary sites. In the tumor tissue, there is an imbalance between oxygen demand and oxygen supply, and as the distance between cells and the existing vasculature increases, oxygen diffusion is reduced, thus, contributing to the development of a hypoxic environment.²⁷ This hypoxia induces many intracellular signaling pathways including the hypoxia-inducible factor (HIF) pathway which mediates the upregulation of angiogenic and hematopoietic growth factor genes. The angiogenic switch requires the overexpression of pro-angiogenic growth factors, including the VEGF. During hypoxia, HIF-1 binds the regulatory region of the VEGF gene, inducing its transcription and initiating its expression. VEGF is proteolytically released from the tumor matrix by matrix metalloproteases (MMPs), predominantly by the MMP-9 secreted into the tumor microenvironment by both tumor cells and tumor-infiltrating leukocytes. High levels of VEGF also increase local vascular permeability, which in turn would help tumor cells to both enter and exit the bloodstream.²³ Thus, a new approach called vessel normalization has become an interesting strategy to reduce metastatic dissemination and increase the response to treatments. The main target for vascular normalization is VEGF and its receptors, VEGFR-1, VEGFR-2, or its co-receptors.²⁸ Additionally, MMPs and other factors might be considered in the search for new targets for treatments against metastasis.²³

III-6. Resisting Cell Death

Apoptosis or programmed cell death is a process in which a cell actively terminates itself by the destruction of vital cellular components or DNA through various molecular signaling pathways. Apoptosis results in cell shrinkage, membrane blebbing, and fragmentation leading to the formation of apoptotic bodies which are then cleared by phagocytes of the immune system.²⁹ Apoptosis is important for embryogenesis, tissue homeostasis, and immunity. Any defects in apoptosis can lead to a myriad of diseases: insufficient apoptosis can lead to cancer and autoimmunity disorders whereas excessive cell death can cause neurodegenerative disorders.³⁰

Caspases, a family of intracellular cysteine proteases, play a foremost and an important role in apoptosis; they cleave cellular proteins that are involved in DNA repair, cytoskeletal organization, nuclear integrity, and cell survival. Two major apoptotic pathways for activating caspases have been identified in mammalian cells: the extrinsic pathway or death receptor-dependent pathway and the intrinsic (mitochondrial) pathway.

The B-cell lymphoma-2 (Bcl-2) family of proteins regulates the intrinsic (mitochondrial) pathway of apoptosis through a network of protein-protein interactions between pro- and anti-apoptotic members as shown in **Figure 5**.³¹ Over 25 Bcl-2 family members have been identified. These can be divided into two classes based on their functions: anti-apoptotic proteins which inhibit apoptosis such as Bcl-2 and Bcl-xL and pro-apoptotic proteins which promote apoptosis such as Bax and Bak. Overexpression of the anti-apoptotic Bcl-2 family members such as Bcl-2 and Bcl-xL have been reported in 70% of breast cancers, and efforts have been focused on developing therapeutics against this protein's family for the cancer treatments.³² Selective and potent small molecule inhibitors have been successfully developed against Bcl-2³³, Bcl-xL³⁴, and Bcl-2/Bcl-xL³⁵.

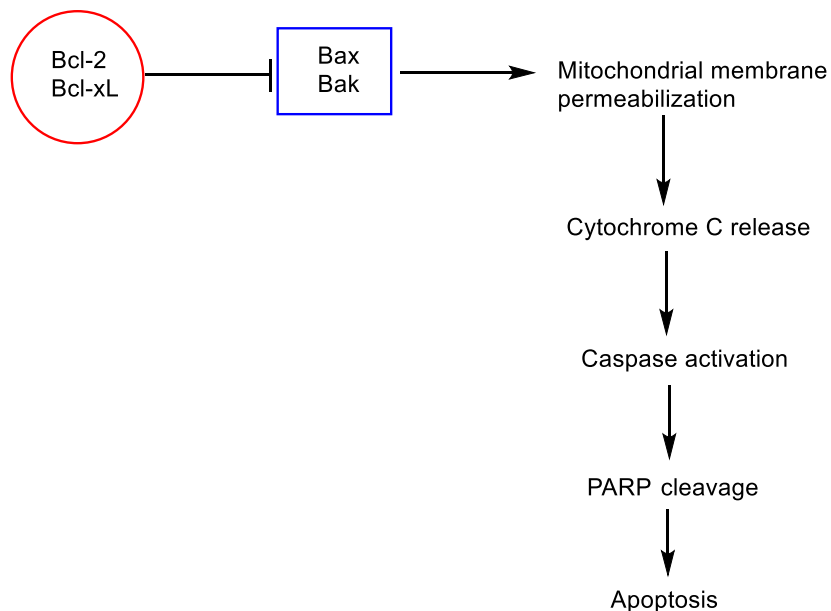


Figure 5: Intrinsic (mitochondrial) pathway of apoptosis

IV. Classification of Breast Cancer

The introduction of next-generation sequencing (NGS) appears to have opened new research areas for cracking breast cancer molecular complexity, refining molecular classification, and identifying novel therapeutic targets. These molecular techniques may enhance diagnosis, prediction of outcomes and behavior, and assist the selection of therapies for individual patients.³⁶ Broadly, based on the gene expression profiling, Perou and coll.²⁵ and Sorlie and coll.²⁶ classified breast cancers into four intrinsic subtypes, namely, Luminal ER-positive (Luminal A and Luminal B), HER2 enriched, and basal-like (**Table 1**).

Table 1: Molecular classification of BC and correlation with biomarker staining

Biological Subtypes	Phenotype			
	ER		PR	HER2
Luminal A	Positive	and/or	Positive	Negative
Luminal B1	Positive	and/or	Positive or negative	Negative
Luminal B2	Positive	and/or	Positive or negative	Positive
HER2	Negative		Negative	Positive
Triple-negative or basal-like	Negative		Negative	Negative

Abbreviations: ER, estrogen receptor; PR, progesterone receptor; HER2, type 2 receptor of human epidermal growth factor.

IV-1. Luminal Breast Cancer

Luminal breast cancers are ER-positive tumors and can be subclassified into 2 subgroups based on the expression of proliferation-related genes. Luminal A tumors are associated with a highly favorable prognosis and high expression of ER-related genes, and lack the cell proliferation protein Ki-67.³⁷ In contrast, Luminal B tumors are associated with a more intermediate prognosis when compared with the Luminal A molecular subtype and high expression of the Ki-67 protein.

The Luminal A group is probably to benefit from hormonal therapy alone, whereas Luminal B tumors with their increased proliferation may be candidates for chemotherapy.^{15,37,38}

IV-2. Human Epidermal Growth Factor Receptor Breast Cancer

The human epidermal growth factor receptor (HER) network is a family of four proteins with an extracellular ligand-binding domain and cytoplasmic tyrosine kinase domain that result in a potent cell signaling.³⁹ Human epidermal growth factor receptor (HER) family includes the epidermal growth factor receptor (EGFR), HER2, HER3, and HER4. HER3 has been considered as an inactive receptor. Despite of its weak kinase activity, HER3 serves as a vital co-receptor of HER2 and its expression is essential for HER2-mediated breast cancer cell growth, proliferation, and differentiation. Thus, HER3 has to form dimers with HER2 in order to fully transduce PI-3K/Akt signaling.^{40–42} Breast cancer that overexpresses HER2 forms accounting for 15–20% of cases, with decreased overall survival and increased risk of metastasis to liver, lung, bone, and CNS.^{43,44}

IV-3. Basal-Like/Triple-Negative Breast Cancers

Triple-negative breast cancer (TNBC) is defined by the absence of the estrogen receptor, progesterone receptor, and HER2 overexpression, accounting for 15% to 20% of all invasive breast cancers.⁴⁵ TNBC is more aggressive than other BC, with a trend to early relapse and metastatic spread to the lung, liver and central nervous system, and has a higher three-year recurrence rate and five-year mortality rate after treatment.⁴⁶

One of the first molecular insights into TNBCs was the observation that they are likely to arise in BRCA1 mutation carriers. BRCA1 plays an essential role in DNA double-strand break repair that maintains DNA stability. A major breakthrough in targeted treatment of BRCA1-mutant cancers was heralded by the finding that BRCA1-mutant cells are exquisitely sensitive to poly(ADP-ribose)polymerase (PARP) inhibitors. PARP activity plays a critical role in mediating

some of the chromatin changes required for efficient DNA repair.⁴⁷ Other investigations identifying molecular markers of TNBC, such as VEGF, EGFR, Src, and mTOR.⁴⁸

Two basal groups (A and B) have been identified by gene expression profiling of breast cancer cell lines. Basal A cell lines, such as MDA-MB-468, display epithelial characteristics and are associated with *BRCA1* gene signatures, while basal B cell lines such as MDA-MB-231 and MDA-MB-435 are more invasive and display mesenchymal and stem-like characteristics.^{48,49}

Due to the absence of targetable hormone receptors ER, PR and HER2 expression, TNBC is characterized by lack of broad choice therapeutic agents, hence, it is considered as a very interesting and challenging topic for breast cancer research.⁵⁰

V. Molecular Targets and Therapy in Breast Cancer

The treatment response of each tumor to any treatment regimen can be highly variable. Recent advances in therapeutics development are getting more targeted toward specific tumor-associated molecular defects. Such targeted therapies are more precise in their mechanism for tumor inhibition or destruction than traditional cytotoxic chemotherapy.⁵¹ Breast cancer proved clinical efficacy to targeted therapy. Characterization of biomarker targets, estrogen receptor (ER), progesterone receptor (PR), and HER2 is important for the appropriate treatment of breast cancer.

V-1. Targeting ER in Breast Cancer

The majority of breast cancers is estrogen receptor (ER)-positive representing 80% of breast cancer cases. Hormonal therapy for ER-positive breast cancer is the paradigm for the development of targeted therapies in breast cancer care. In advanced breast cancer, response rates and time to tumor progression were entirely relying on quantitative levels of ER and/or PR expression; the higher ER expression, the higher were tumor response rates and time to tumor progression.⁵²

Recently, specific acquired mutations in the ER have been discovered during anti-estrogen treatment. These mutations affect the receptor hormone-binding site and may play an essential role in acquired endocrine therapy resistance. However, they have only been found to date in a small percentage of tumors; for most ER-positive breast cancers, ER signaling remains operational despite overt clinical progression, and subsequent lines of endocrine treatment can still be clinically effective.⁵³ Thus, several breast cancer hormonal therapies including tamoxifen, aromatase inhibitors, and fulvestrant have become common for use in advanced diseases.⁵⁴ Antiestrogens (e.g., tamoxifen) are frequently used to treat premenopausal patients with breast cancer. Fulvestrant, an ER antagonist that degrades ER, was found to be more effective than tamoxifen. Aromatase inhibitors (e.g. letrozole, anastrozole, and exemestane), which inhibit the synthesis of estrogens, are now in use to treat postmenopausal women.⁵⁵ Moreover, GnRH analogues (e.g. Triptorelin) are administered in combination with estrogen antagonists (e.g., tamoxifen) or aromatase inhibitors in early-stage hormone-sensitive breast cancer in women at high risk for recurrence, confirmed as not menopausal following chemotherapy.⁵⁶

The success of endocrine therapy for advanced breast cancer permitted clinical trials of adjuvant therapy for early-stage disease, showing how breast cancer targeted therapy has served as the model for the development of targeted agents in cancer therapy.⁵²

V-2. Targeting HER2 in Breast Cancer

Estrogen receptor-targeted therapy was primarily observed in women receiving endocrine treatment, and retrospective studies that showed a correlation between ER and endocrine treatment outcomes. By contrast, anti-HER2 therapy development was prompted by the recognition of gene amplification and overexpression of the HER2 oncogene as a poor prognostic factor in breast cancer.⁵⁷ HER2 overexpression arises in approximately 20%—30% of invasive breast cancer.⁵⁸

Preclinical studies proved that anti-HER2 antibodies would only have potency in tumors that overexpressed HER2. Subsequently, the trastuzumab antibody was shown to have substantial clinical activity in advanced breast cancer when combined with standard

chemotherapy.⁵⁹ A few years later, trastuzumab became a standard adjuvant option for an early stage, HER2 overexpressing breast cancer.⁶⁰ However, the development of resistance is a major obstacle: only 30% of patients will respond to a first line of trastuzumab and of these responders, 70% will relapse after a year of treatment.

The success of the initial antiHER2 treatment, trastuzumab, led to the development of multiple anti-HER2 therapies.⁶¹ Lapatinib, a dual inhibitor of EGFR and HER2 tyrosine kinases, has activity in trastuzumab-refractory breast cancer. Pertuzumab in combination with chemotherapy and trastuzumab, is a standard first-line treatment for HER2 positive advanced breast cancer based on improvement in response rates, time to progression, and overall survival.⁶² Finally neratinib, an irreversible pan-HER inhibitor, is given following adjuvant treatment with trastuzumab.

V-3. Novel Targeted Treatments in ER Positive Breast Cancer

Activation of the PI3K/AKT/mTOR pathway is implicated in the tumorigenesis of ER+ breast cancer and resistance to endocrine therapy.⁶³ Genomic sequencing has discovered mutations in this pathway in a large percentage of Luminal (ER-positive) breast cancers. For these reasons, a variety of clinical trials have analyzed the addition of mTOR inhibitors and PI3-kinase inhibitors for the treatment of advanced breast cancer. Everolimus, an mTOR inhibitor, has been approved by the FDA for the treatment of advanced renal cell carcinoma, pancreatic neuroendocrine tumors, and advanced breast cancer.⁶⁴

Currently, drug discovery is focusing on the cyclin-dependent kinases 4 and 6, critical mediators of the cell cycle control in many cancer cells.⁶⁵ Heterocyclic drugs such as palbociclib, ribociclib, and abemaciclib (**Figure 6**), inhibitors of CDK-4 and 6, are currently available for the treatment of locally advanced or metastatic breast cancer (ER+ and HER-).

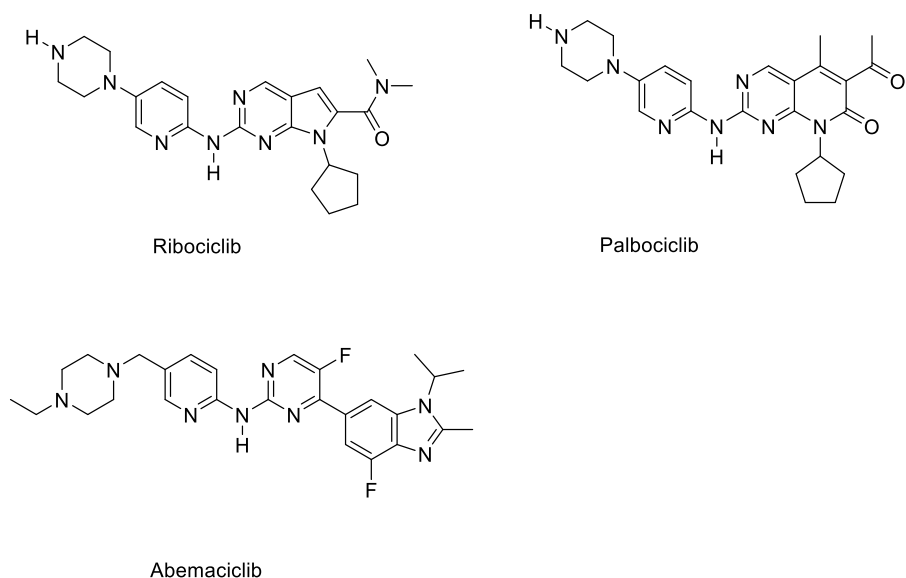


Figure 6: Molecular structures of palbociclib, ribociclib, and abemaciclib

V-4. BRCA-Associated Tumors and PARP Inhibitors

Hereditary BRCA1 and BRCA2 mutations result in high risks of developing breast and ovarian cancer.⁶⁶ Poly (ADP-ribose) polymerases (PARP) inhibitors have displayed activity against BRCA-associated cancers in early clinical studies. PARP1, the first described enzyme of the PARP family, plays an essential role in the repair of DNA single-strand breaks via base excision repair. Studies display that PARP1 inhibitors have the most potent anticancer effects in BRCA-associated cancers, as double-strand break repair via homologous recombination is not available in BRCA-defective cells.⁶⁷ **Table 2** showed three inhibitors targeting PARP enzymes including veliparib, olaparib, and talazoparib. The latter two are FDA-approved PARP inhibitors in 2018 in gBRCA-mutated breast cancer (HER-2 negative) but are still under clinical evaluation.⁶⁸

Table 2: Efficacy of PARP inhibitors currently under clinical evaluation for TNBC

Name	Potency and clinical implication	NCT number	Clinical trial identifier
Veliparib	An orally active PARP1/2 inhibitor also known as ABT888 and 912444-00-9	NCT02595905	Phase II study to compare the efficacy of veliparib plus cisplatin to that of cisplatin alone in mTNBC and BRCA mutated breast cancer.
		NCT02032277	Phase III study of veliparib plus carboplatin or carboplatin alone in TNBC
Olaparib		NCT02032823	The phase III, randomized OlympiA trial is evaluating adjuvant use of olaparib in patients with high-risk HER2-negative breast cancer with gBRCA mutations.
Talazoparib	An orally active PARP inhibitor.	NCT02401347	Phase II trial investigating talazoparib monotherapy in advance, triple negative, or HER2 negative BRCA1/2 wild-type breast cancer.

VI. Conclusion

This chapter reviews selected topics in breast cancer studied in this thesis work. Many interesting points are worth to mention.

- Improved and sustainable cell proliferation is a core cancer-driving trait and one of the most important hallmarks of cancer that can be identified using many histologic, biochemical, and flow cytometry analyses. The proliferative activity of breast cancer cells is often quantified through Ki-67 protein.
- Apoptosis has long been recognized as one of the major mechanisms of programmed cell death in response to cancer therapies. Moreover, apoptosis is regulated by a large set of genes. Among them, the bcl-2 family proteins play a key role. Some of them promote apoptosis (Bax, Bak) whereas others are anti-apoptotic (Bcl-2, Bcl-xL).

- Tumor metastasis is a complex multi-step process that is regulated by multiple signaling pathways. The process of tumor metastasis is also called the invasion-metastasis cascade.
- Triple-negative breast cancer (TNBC) is defined by lack of expression of human epidermal growth factor receptor 2 (HER-2), estrogen receptor (ER), and progesterone receptor (PR), which accounts for approximately 15–20% of invasive breast cancers as it can rapidly metastasize to distant organs, which finally resulted in a very poor prognosis and high recurrence.
- Two basal groups (A and B) have been identified by gene expression profiling of breast cancer cell lines. Basal A cell lines, such as MDA-MB-468, have epithelial characteristics and are associated with BRCA1 gene signatures, while basal B cell lines such as MDA-MB-231 and MDA-MB-435 are more invasive and display mesenchymal and stem-like characteristics.
- Poly(ADP-ribose) polymerases (PARP) inhibitors (olaparib and talazoparib) are currently available for the treatment of locally advanced or metastatic BRCA-associated and HER2 negative cancers.
- CDK4/6i (palbociclib, ribociclib, and abemaciclib) are small heterocyclic molecules that are currently available for the treatment of locally advanced or metastatic breast cancer (ER+ and HER-).

The following chapter reviews the *Peganum harmala* and β -carboline studies which inspired us to investigate the anticancer activity of imidazo[1,2-*a*:4,5-*c'*]dipyridines in this thesis project.

Chapter 2:

***Peganum harmala* L. and β -carbolines**

I. Introduction

In this chapter, I will review in more depth the scientific work that has provided the base of this thesis work. This chapter reviews the literature concerning *Peganum harmala* L. and its β -carboline alkaloids that inspired this thesis project on the imidazo[1,2-*a*:4,5-*c'*]dipyridines series.

The general characteristics of *Peganum harmala* L. will be successively described in terms of botanical description, alkaloidic composition, and medicinal uses. Interestingly, *P. harmala* is traditionally used as analgesic, anthelmintic, antispasmodic, antiepileptic, antidepressant, and anticancer.

Then, the β -carbolines will be presented: their natural derivatives, synthesis, and biological activities, as well as, an in-depth review of the literature concerning their anticancer activity.

II. Botanical Description of *Peganum Harmala*

Harmala (*Peganum harmala* L.) is a member of the family *Nitrariaceae*.⁶⁹ It has various common names, including harmala, harmal, Syrian rue, and African rue. Its habitat is represented by the arid regions mostly from North Africa to East Asia, but also in North America and Australia.⁷⁰

Harmala is a much-branched perennial, herbaceous, glabrous plant that grows up to 60 cm tall with short creeping roots (**Figure 7**). It possesses narrow leaves arranged alternately on fleshy, bright green stiff stems. The flowers are small, white or yellowish-white, and 5-petaled. The fruit capsule is 6 mm to 10 mm across with 3 chambers.⁷¹

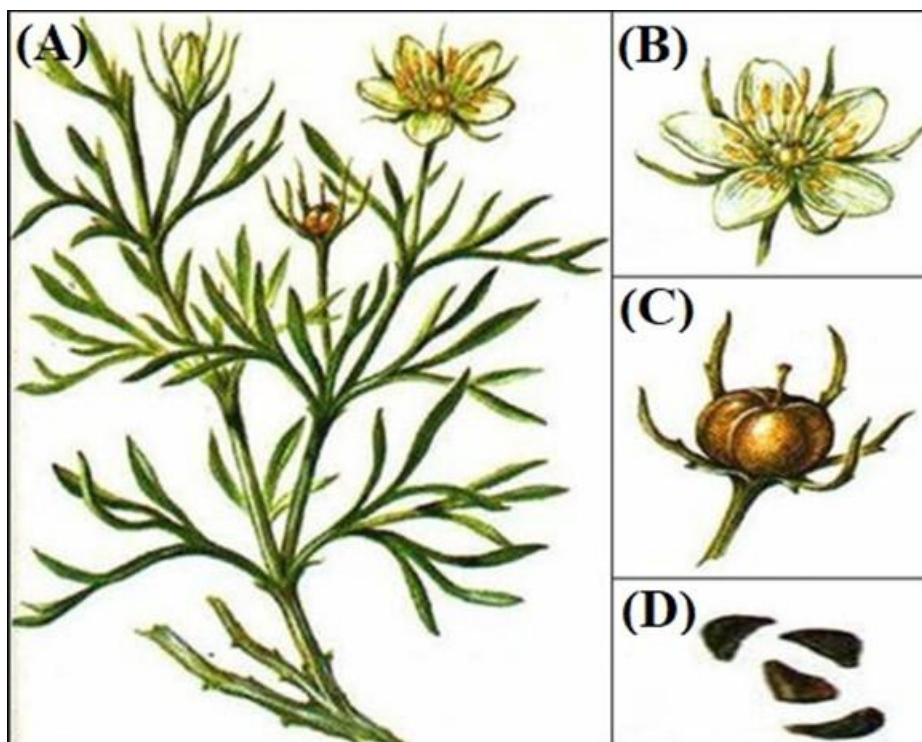


Figure 7: (A) Harmala plant bearing flowers and fruit; (B) flower; (C) fruit; (D) seeds (Source: healthyhomegardening.com/Plant.php?pid=638)

III. Alkaloidic Composition

The active constituents of harmala are found especially in the seeds and roots. The alkaloids in *P. harmala* seeds are of two known types: the quinazoline alkaloids, exemplified by peganine (vasicine), deoxypeganine and vasicinone, or the β -carboline class, such as harman, harmine, isoharmine, harmaline, harmalidine and harmalol (**Figure 8**).³ Harmaline and harmine are the most important alkaloids that are generally responsible for the pharmacological effects of *P. harmala*, even if other alkaloids present in this plant also have some roles. Lipids, proteins, and mineral elements are also found in the seeds.⁷²

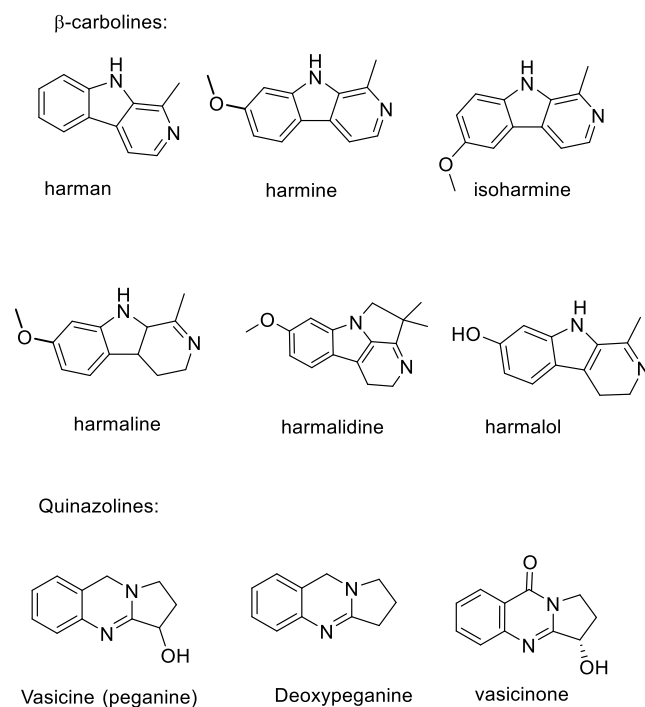


Figure 8: Some chemical constituents of harmala seeds

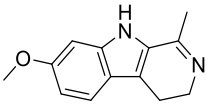
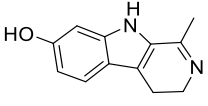
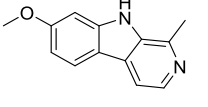
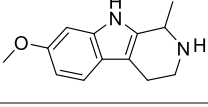
IV. Medicinal Uses

Peganum harmala is being used as an effective herbal medicine possessing hallucinogenic, hypothermic, anthelmintic, abortifacient, galactagogue and emmenagogue properties. Most parts of the herb are used in the traditional systems of medicine: seeds, fruits, root, and bark. The extracts of the seeds have been traditionally used for hundreds of years to treat the digestive tract cancers and malaria in Northwest China.³

In Morocco, *P. harmala* seeds are also regarded as traditional therapeutic for cancers. Moreover, the seeds are used as anthelmintic, antispasmodic, emetic, and for treatment of asthma, malaria, diarrhea, diabetes, jaundice, lumbago, and hypertension.^{68–70} **Table 3** presents the chemical constituents of *P. harmala* seeds and their biological activities.

Anticancer activity of *P. harmala* extract and its alkaloids on cancer cells has been reported in various studies. It showed an antiproliferative effect on leukemic cell lines, metastasis inhibitory effect and apoptosis induction on melanoma cells.^{71–73} Lately, the alkaloids extracts of *P. harmala* showed anticancer effect towards nearly all cancer cell lines tested (lung (A549), astroglioma (U373), oligodendroglioma (Hs683), breast (MCF7), melanoma (B16F10 and SKMEL-28) cancer cells).⁷⁶ Besides, it has been reported that harmine induces autophagy in human gastric cancer cells (MGC-803 and SGC-7901 cells).¹

Table 3: Chemical constituents of harmala seeds and their main biological activities

Compound	Molecular Structure	Activities	References
Harmaline		Antimalarial, Antibacterial, and antiprotozoal	77
		Anticancer	78
		Vasodilator	79
		Human monoamine oxidase Inhibitor	80
		Central nervous system (CNS) stimulator	81
Harmalol		Antibacterial and antiprotozoal	78
Harmine		Antimalarial	77
		Antibacterial, antiprotozoal	78
		Anticancer, Vasodilator	79
		Human monoamine oxidase Inhibitor	80
		Central nervous system (CNS) stimulator	81
Tetrahydroharmine		CNS stimulator	81

V. β -carboline Scaffold

This section gives general features of β -carboline nucleus, and presents the synthetic pathway allowing their production. In addition, this section discusses the biological activity of β -carbolines with regard to their antiprotozoal, antibacterial, antifungal, anti-HIV, Phosphodiesterase-5 (PDE5) inhibition, and neuropharmacological activities.

V-1. General Presentation of β -carboline Derivatives

The carbolines represent a group of isomeric pyridoindoles compounds which differ from one another with respect to the nitrogen atom position within the pyridine ring (**Figure 9**). The nitrogen of β -carbolines (β Cs) is at N-2 compared to α - and γ -carbolines, which have the nitrogen atom in other positions.⁸² Molecular diversity of β -carbolines is due to distinct substituents both at the pyridine and benzene ring as well as different degrees of saturation in the pyridine ring. According to the saturation of their pyridine ring, β -carbolines can be categorized into different classes. Fully unsaturated members are named as β -carbolines (β Cs), whereas, partially unsaturated and completely saturated ones are known as dihydro- β -carboline (DH β Cs) and tetrahydro- β -carbolines (TH β Cs), respectively.³

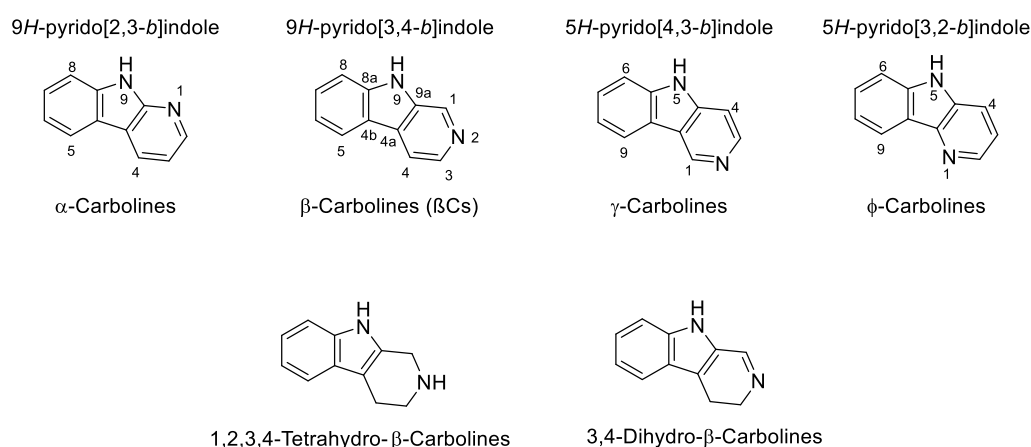


Figure 9: Structures and nomenclature of carbolines (pyridoindoles)

β -carbolines are widely distributed in numerous natural sources like plants, marine life, human tissues, and body fluids.³ First β -carboline alkaloid harmaline was isolated in 1841, from *Peganum harmala* (Nitrariaceae). β -carboline alkaloids were also isolated from the South American vine *Banisteriopsis caapi* (Malpighiaceae), an important plant ingredient in the hallucinogenic beverage Ayahuasca and some religious spirits used in South America.⁸³ During the last three decades more β -carboline alkaloids were found in foods, fruits, fruit-derived products, alcoholic and non-alcoholic beverages.³ Consumption of these beverages having β -carboline alkaloids contributed significantly for their endogenous presence in mammalian tissues along with endogenous bio-synthesis.⁸⁴ The first endogenous β -carboline alkaloid isolated from the extraction of pineal gland tissue was pinoline (**Figure 10**) in 1961, followed by isolation of other β -carboline derivatives from various body fluids and tissues of mammals.⁸⁵

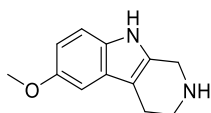


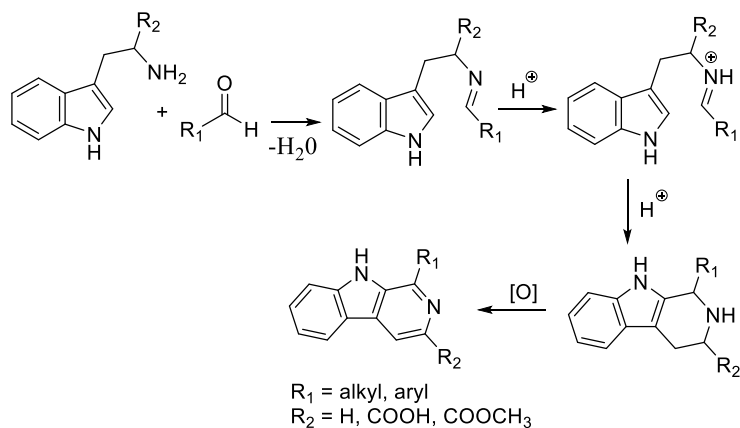
Figure 10: Pinoline

V-2. Synthesis of β -carboline Skeleton

The β -carboline skeleton is found in numerous pharmacologically interesting compounds and hence these alkaloids have been in the focus of extensive synthetic efforts for a long time. The most popular synthetic routes utilize Pictet-Spengler cyclization. Herein, I describe rapidly the synthesis of the β -carboline skeleton using several metal-catalyzed protocols starting from substituted indoles as well as substituted anilines.

V-2.1. Synthesis protocol from substituted indoles

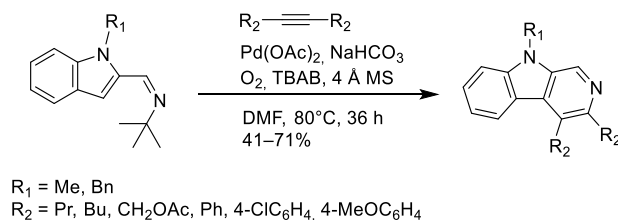
The synthesis of the β -carboline skeleton from indoles takes place through the Pictet-Spengler reaction (**Scheme 2**). The mechanism of this reaction proceeds via formation of an iminium cation intermediate (Schiff base) and cyclization to give TH β Cs.⁸⁶



Scheme 2: Synthesis of the β -carboline skeleton by Pictet-Spengler reaction

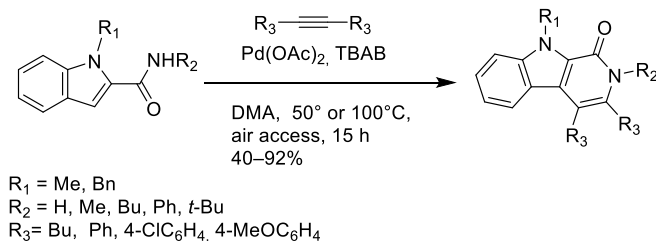
Besides the traditional Pictet—Spengler reaction, several methods have been discovered for the construction of the β -carboline skeleton.

Ding *et al.* published the palladium-catalyzed direct dehydrogenative annulation reaction of internal alkynes and *tert*-butylimines of *N*-substituted indole carboxaldehydes, which produced the corresponding β -carboline derivatives (**Scheme 3**). In this protocol, elemental oxygen was used for the activation of C—H bond.⁸⁷



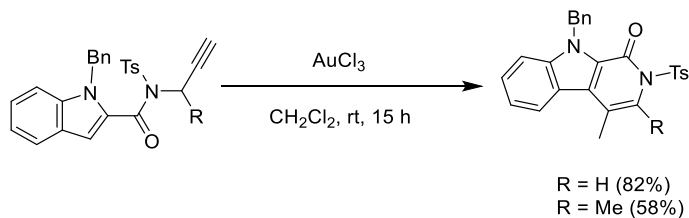
Scheme 3: Synthesis of β -carboline skeleton starting from *tert*-butylimines of *N*-substituted indole carboxaldehydes. TBAB = *tetra-n*-butylammonium bromide

In the next study by the same group, β -carbolinones have been synthesized under similar reaction conditions starting from indolecarboxamides and acetylenes (**Scheme 4**).⁸⁸ It is worth mentioning that these reactions were also tested with unsymmetrical alkynes and the appropriate products were frequently obtained in good regioselectivity.



Scheme 4: Synthesis of β -carboline skeleton starting from indolecarboxamides. *N,N*-dimethylacetamide (DMA), tetra-*n*-butylammonium acetate (TBAA)

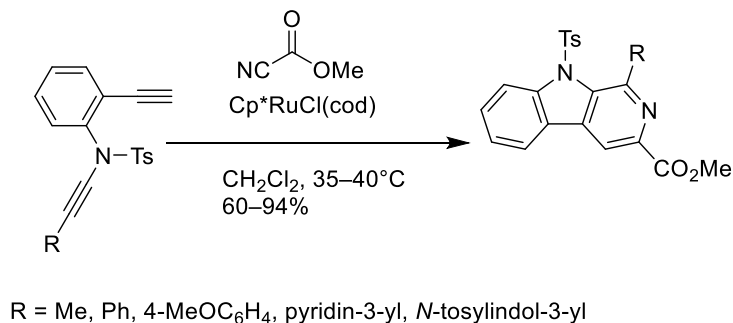
N-Tosyl- β -carbolinones were synthesized under mild conditions from indole substituted in position 2 with *N*-propargylamides via AuCl_3 -catalyzed 6-exo-*dig* cyclization.⁸⁹ The resulting 3-substituted-4-methylcarbolinones were transformed into several important derivatives by treatment with POCl_3 or PCl_3 (**Scheme 5**).



Scheme 5: Synthesis of β -carboline skeleton starting from substituted indole

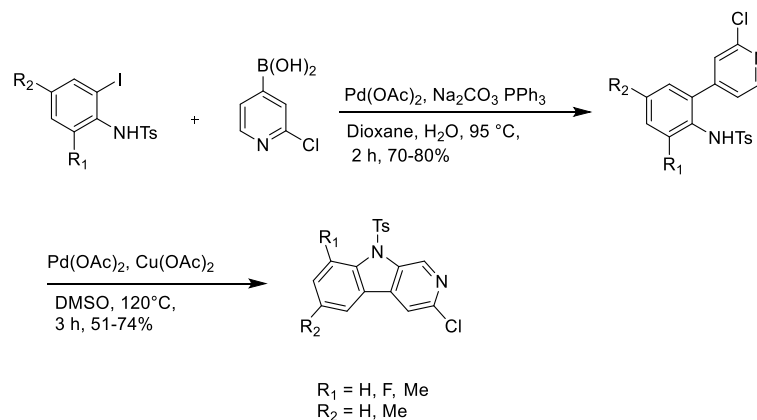
V-2.2. Synthesis protocol from substituted anilines

Witulski *et al.* published the ruthenium-catalyzed method for the synthesis of the β -carboline skeleton.⁹⁰ The required yne-ynamides were prepared in five steps starting from readily available 2-iodoaniline. The $\text{Cp}^*\text{RuCl}(\text{cod})$ -catalyzed [2 + 2 + 2] cycloaddition of yne-ynamides with methyl cyanoformate yielded the corresponding β -carbolines (**Scheme 6**).



Scheme 6: Ruthenium-catalyzed method for the synthesis of the β -carboline skeleton

Ray and co-workers developed a two-step protocol for the synthesis of β -carbolines.⁹¹ Precursors were prepared by using Suzuki coupling on *N*-tosylated 2-iodoanilines with (2-chloropyridin-4-yl)boronic acid. Subsequent ring closure *via* Pd-mediated C–H/N–H activation yielded the target molecules in moderate yields. The easily obtained chloro- β -carbolines can be engaged in different cross-coupling reactions (**Scheme 7**).



Scheme 7: Two-step protocol for the synthesis of β -carbolines developed by Ray group

V-3. Biological Activities

During the last two decades, β -carboline-based natural products have been the interest of many investigations. Several β -carboline-based molecules of natural or synthetic origin are ascribed with different pharmacological properties. In this section, I review their antiprotozoal, antibacterial, antifungal, antiviral, anticancer, antithrombotic, anti-inflammatory activities and their phosphodiesterase-5 inhibition. In the following section, the anticancer activities of β -carbolines will be reviewed extensively.

V-3.1. Antiprotozoal activity

Several natural β -carboline alkaloids and their synthetic derivatives have been reported to exhibit antiprotozoal activity such as antimalaria, antileishmania, antitrypanosomes and antitoxoplasma properties.

➤ Antimalarial activity

The natural β -carboline alkaloids, harmine and harmaline isolated from *Peganum harmala* showed *in vitro* antimalarial activity against *Plasmodium falciparum*.⁷⁷

Manzamines are natural alkaloids bearing β -carboline moiety attached to a pentacyclic diamine ring, present in various species of marine sponges found in the Indian and Pacific oceans.⁹² Many of these isolated alkaloids showed potent antimalarial activity against drug-sensitive and -resistant strains. Among these alkaloids, manzamine A and 8-hydroxymanzamine A (**Figure 11**) exhibited a potent *in vitro* activity against both chloroquine-sensitive D6 and resistant W2 strains of *P. falciparum* (IC₅₀= 20.8 (D6) and 25.8 (W2) vs. 19.5 (D6) and 22.0 (W2) μ M, respectively).⁹³

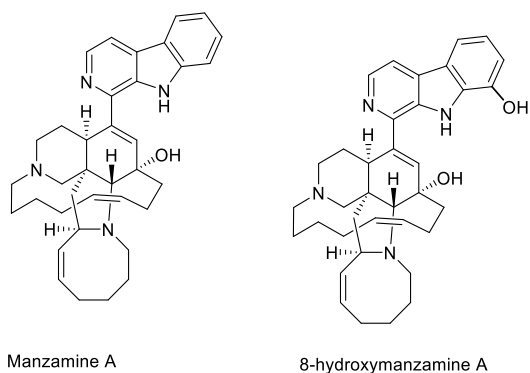


Figure 11: Manzamine A and 8-hydroxymanzamine A with antimalarial activity

Boursereau *et al.* in 2004, reported the antimalarial activity of some 1-amino- β -carboline derivatives. Eight derivatives (I-VIII) (**Figure 12**) displayed potent antimalarial activity against *P. falciparum* with IC_{50} values of 0.4-3.4 μM .⁹⁴

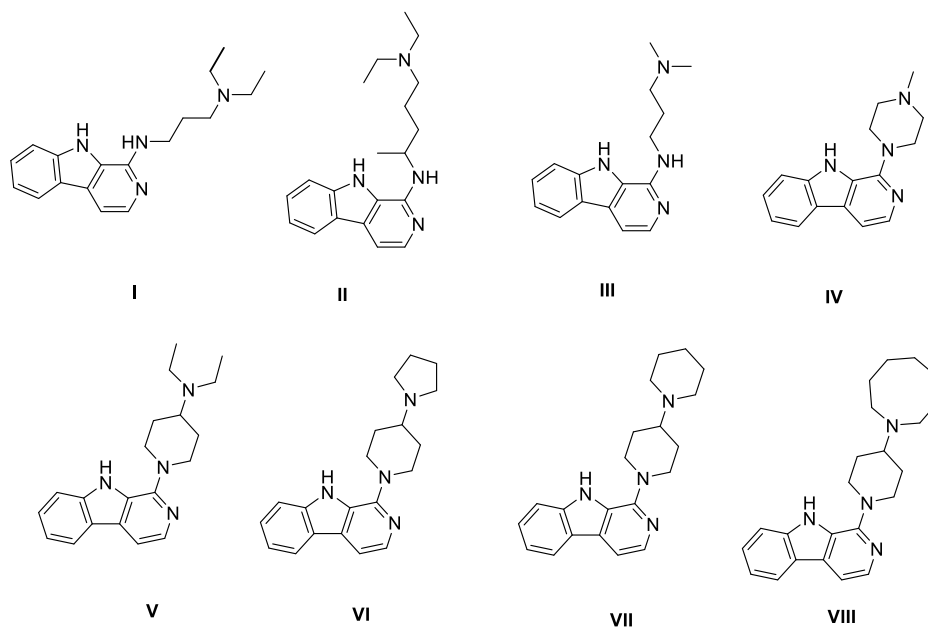


Figure 12: Some 1-amino- β -carboline derivatives I-VIII with antimalarial activity

In another study, the same group reported the antimalarial activity of a series of 1-amino- β -carboline derivatives with 6-halo group. Among these derivatives, 1-amino-6-halogeno-- β -

carboline analogues **IX-X** (**Figure 13**) exhibited greater antimalarial bioactivity with IC_{50} values of 0.15 to 1.08 μM against two *P. falciparum* strains (3D7 and K1).⁹⁵

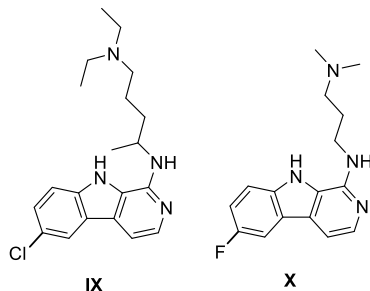


Figure 13: 1-amino-6-halo- β -carboline derivatives **IX-X** with antimalarial activity

➤ Antileishmanial activity

In addition to antimalarial studies, β Cs have recently also gained attention as potential antileishmanial and trypanocidal compounds. Chauhan *et al.* reported good antileishmanial activities of novel derivatives of indolylglyoxylamides (**Figure 14**) against *Leishmania donovani* with IC_{50} values ranged from 3.79 to 5.17 μM .⁹⁶

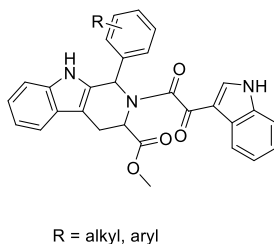
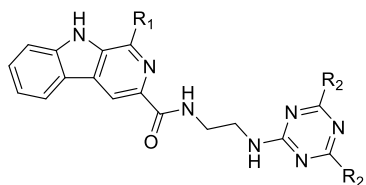


Figure 14: General structure of indolylglyoxylamides

Several studies investigated the activity of 1,3,5-triazine derivatives as antileishmanial agents. Recently, Baréa *et al.* reported the synthesis and biological evaluation of a series of hybrids β -carboline-1,3,5-triazine against *Leishmania*. Among these, the hybrids **XI-XIV** (**Figure 15**) exhibited potent activity against *Leishmania amazonensis* with IC_{50} values of 7.6, 5.1, 7.5, and 6.2 μM , respectively.⁹⁷



XI $R_1 = 2\text{-Cl-Ph}$, $R_2 = \text{Cl}$

XII $R_1 = 3\text{-NO}_2\text{-Ph}$, $R_2 = \text{Cl}$

XIII $R_1 = \text{Ph}$, $R_2 = \text{N(CH}_3)_2$

XIV $R_1 = 4\text{-OCH}_3\text{-Ph}$, $R_2 = \text{N(CH}_3)_2$

Figure 15: Some β -carboline-1,3,5-triazine hybrids **XI-XIV** with antileishmanial activity

V-3.2. Antibacterial and antifungal activities

Semi-synthetic manzamine derivative, 1,2,3,4-tetrahydromanzamine A (**Figure 16**) showed potent antifungal activity against *Candida neoformans* ($\text{IC}_{50} = 0.9 \mu\text{g/ml}$).⁹⁸

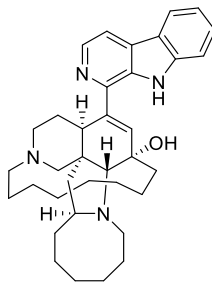


Figure 16: the semisynthetic 1,2,3,4-tetrahydromanzamine A with antifungal activity

Venkataramana Reddy *et al.* reported the moderate antibacterial activity of sixteen β -carboline chalcones and their bromide salts with general structures illustrated in **Figure 17** against two Gram-positive bacterial strains *Staphylococcus aureus*, *Bacillus subtilis* and three Gram-negative bacterial strains *Escherichia coli*, *Pseudomonas aeruginosa* and *Enterococcus cloacae*.⁹⁹

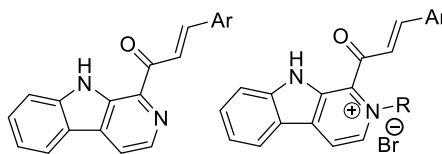
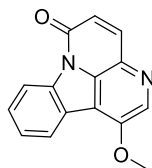


Figure 17: β -carboline chalcones skeleton and their bromide salts with antibacterial activity

V-3.3. Anti-HIV activity

The alkaloid, 1-methoxycanthinone (**Figure 18**) belonging to canthin-6-one alkaloids was isolated from *Leitneria floridana* and evaluated for anti-HIV bioactivity. It showed potent anti-HIV activity in H9 cell line ($EC_{50} = 0.26 \mu\text{g/mL}$).¹⁰⁰



1-methoxycanthinone

Figure 18: 1-methoxycanthinone with anti-HIV activity

Natural alkaloid harmine displayed moderate anti-HIV activity and among its synthetic derivatives, 9-butylharmine (**Figure 19**) showed slightly enhanced anti-HIV activity compared to zidovudine ($EC_{50} = 0.037$ and $0.045 \mu\text{M}$, respectively).¹⁰¹

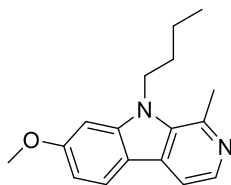


Figure 19: 9-butylharmine with anti-HIV activity

In another study, Brahmbhatt *et al.* reported that 1-formyl- β -carboline-3-carboxylic acid methyl ester (**Figure 20**) exhibited inhibition of HIV at IC_{50} of $2.9 \mu\text{M}$.¹⁰²

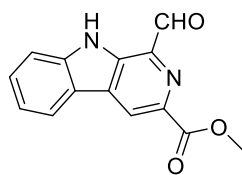


Figure 20: 1-Formyl-β-carboline-3-carboxylic acid methyl ester with anti-HIV activity

Ashok *et al.* reported the synthesis of a new series of 1-(thiophen-2-yl)-β-carboline derivatives and evaluated their inhibitory potency against HIV-1 replication. Among them, **XV** (**Figure 21**) exhibited significant anti-HIV activity with EC_{50} value of 0.53 μ M.¹⁰³

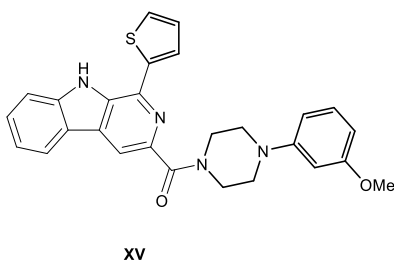
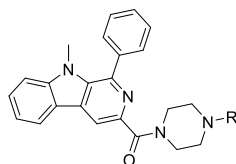


Figure 21: 1-(thiophen-2-yl)-β-carboline derivative **XV** with anti-HIV activity

Furthermore, they reported the synthesis and biological activity of a new series of 1-phenyl-3-piperazinoyl-β-carboline derivatives against HIV-1 and HIV-2 strains. Among these derivatives, compounds **XVI-XX** (**Figure 22**) showed selective inhibition against HIV-2 strain (ROD), a subtype isolated from a Cape Verdian with EC_{50} values of 2.6 to 29.4 μ M.¹⁰⁴



XVI R = C₆H₅
XVII R = 4-CH₃C₆H₄
XVIII R = 2-OCH₃C₆H₄
XIX R = 4-FC₆H₄
XX R = 2-FC₆H₄

Figure 22: 3-piperazinoyl-β-carboline derivatives **XVI-XX** with anti-HIV activity

V-3.4. Phosphodiesterase-5 (PDE5) inhibition activity

Phosphodiesterases are enzymes that catalyze the conversion of cyclic guanosine monophosphate (cGMP) to guanosine monophosphate (GMP). PDE5 has traditionally been a target for treating erectile dysfunction (ED) and pulmonary arterial hypertension. Tadalafil (**Figure 23**) is a PDE5 inhibitor approved by US-FDA for the treatment of ED and approved for the treatment of pulmonary arterial hypertension.

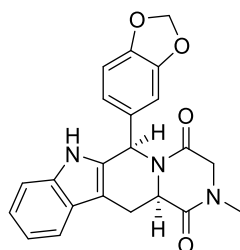


Figure 23: Tadalafil

With the discovery of tadalafil, large numbers of tetrahydro-β-carboline derivatives were evaluated for PDE5 inhibitory activity. Most of these THβ-carboline derivatives exhibited significant inhibition of PDE5.^{105,106}

V-3.5. Neuropharmacological activity

The neuropharmacological effects of some β-carbolines may partially be due to their interaction with various receptor systems in the mammalian CNS, such as serotonergic receptors and benzodiazepine receptors.³ For instance, a study showed that the β-carboline **FG-7142** activates a recognized anxiety-related neural networks and interacts with noradrenergic, serotonergic, dopaminergic, and cholinergic modulatory systems within that network. Moreover, **FG-7142** has been found to induce anxiety-related behavioral and physiological responses in numerous mammalian and non-mammalian species, including humans.¹⁰⁷ In another study, β-carboline esters **XXI-XXII** exhibited high affinity for the brain benzodiazepine recognition site as inverse agonists (**Figure 24**).¹⁰⁸

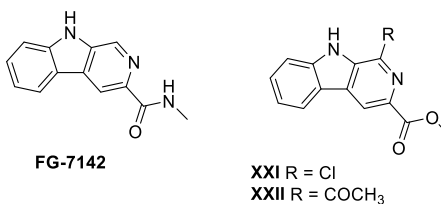


Figure 24: FG-7142 and compounds **XXI-XXII**

V-4. β -carbolines as Anticancer Agents

Some β -carbolines, initially isolated from *Peganum harmala* which are commonly used as a traditional remedy herb in China and Morocco in digestive tract cancers, were proven to possess considerable anticancer effects. Extensive efforts have been made to design and synthesize β -carboline derivatives with better anticancer activities and pharmacokinetics properties such as solubility. This section offers a careful discussion on SAR and includes recent reports in the area. This section has been structured according to the type and position of the main pharmacophoric substituent on the β -carboline core.

V-4.1. β -carbolines substituted at C-1 and/or C-3

Boursereau and Coldham reported the anticancer activity of manzamine A and simple β -carbolines with 1-amino moieties. Among these, compounds **XXIII-XXV** (**Figure 25**) were selected to be tested against a panel of 60 cancer cell lines and showed submicromolar activities. The β -carboline **XXIII** displayed the best activity with a 50% growth inhibition (GI₅₀) value of 0.38 μ M against non-small cell lung cancer (HOP-92). Besides, the natural product **manzamine A** showed potent activity against all cell lines, especially HOP-92 (0.25 μ M).⁹⁴

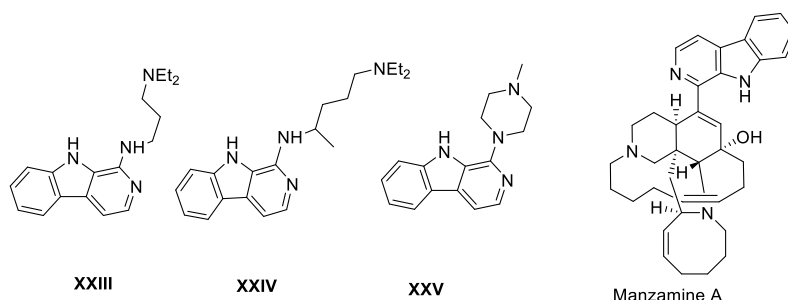


Figure 25: 1-amino-β-carbolines derivatives **XXIII-XXV** and manzamine

In another study, some β-carboline-1-carboxamides and 1-amino-β-carbolines (**Figure 26**) were prepared by Ma *et al.* and tested for their anticancer activity against breast (MCF-7), gastric (BGC823), prostate (22RV1), liver (HepG2), renal (OS-RC-2, 786-O and 769-P), colon (HT-29), nasopharynx epidermoid (KB) carcinoma and melanoma (A375) in comparison to cisplatin as reference drug. The *in vitro* biological evaluation of compounds revealed that 1-amino derivatives displayed superior potency than their 1-carboxamide congeners. Among 1-carboxamide derivatives, **XXVI** displayed moderate activity ($IC_{50} = 55.6 \mu M$) against colon (HT-29) cancer cells and **XXVII-XXVIII** showed moderate activities against prostate (22RV1) cancer cells with IC_{50} values of 33.6 and 46.2 μM , respectively. Of all the 1-amino-β-carboline compounds, *N*-9-aralkylated β-carbolines **XXIX-XXXIII** showed the highest inhibitory activity against the tested human cancer cell lines with IC_{50} values below 20 μM .¹⁰⁹

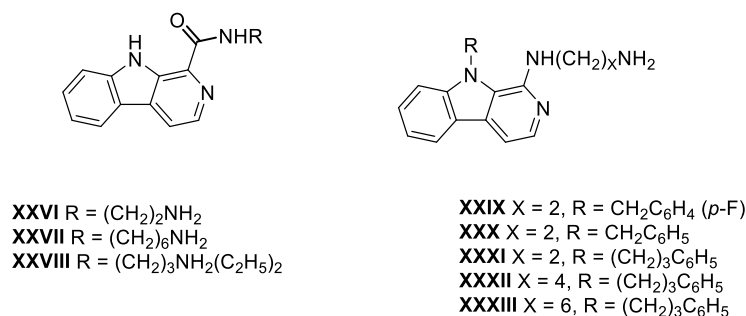


Figure 26: 1-carboxamide β-carbolines **XXVI-XXVIII** and 1-amino β-carbolines **XXIX-XXXIII**

Liew *et al.* have synthesized a series of 1-indolyl substituted β -carboline derivatives. Most of the compounds showed weak anticancer effects against a panel of 60 human cancer cell lines except for compound **XXXIV** (**Figure 27**) which exhibited interesting anti-leukemic activity towards the HL-60 (TB) cell line with median lethal dose (LC₅₀) value of 4.2 μ M.¹¹⁰

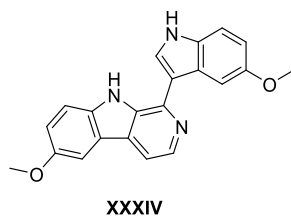
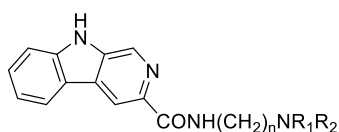


Figure 27: β -carboline with indolyl moiety at C-1 **XXXIV** with anticancer activity

Xiao *et al.* studied the anticancer properties of 3-substituted- β -carbolines (**Figure 28**) against human leukemia cancer (HL-60), human gastric cancer (BGC), nasopharynx epidermoid carcinoma (KB), and cervical Hela cell lines. In these reported novel β -carboline derivatives, all compounds **XXXV-XXXIX** showed relative inhibitory interaction to several human cancer cell lines. In particular, compound **XXXVII** exhibited high activities against human leukemia and human gastric cancer cell lines with IC₅₀ values of 1.9 μ M and 8.6 μ M, respectively.¹¹¹



XXXV n=2 R₁ = H, R₂ = H
XXXVI n=2 R₁ = C₂H₅, R₂ = C₂H₅
XXXVII n=4 R₁ = H, R₂ = H
XXXVIII n=4 R₁ = CH₃, R₂ = CH₃
XXXIX n=6 R₁ = H, R₂ = H

Figure 28: 3-substituted- β -carbolines **XXXV-XXXIX** with anticancer activity

Formagio *et al.* reported biological evaluation of a library of 1-substituted-phenyl- β -carbolines bearing the 1,3,4-oxadiazol-5-yl and 1,2,4-triazol-3-yl at C-3 (**Figure 29**) against eight cancer cell lines including, breast (MCF-7), melanoma (UACC-62), lung (NCI-460), colon (HT29), prostate (PCO-3), leukemia (K-562), ovarian (OVCAR), and renal (786-0) cancer cell lines. In this

β -carboline library, compounds **XL-XLI**, bearing the 3-(2-methylthio-1,3,4-oxadiazol-5-yl) moiety, exhibited high potent anticancer activity against ovarian cell line with GI_{50} values of 10 nM. Besides, compound **XLII** bearing 1-(*N,N*-dimethylaminophenyl) and 3-(5-thioxo-1,2,4-triazol-3-yl) groups was the most active compound on lung cell line (GI_{50} = 0.06 μ M).¹¹²

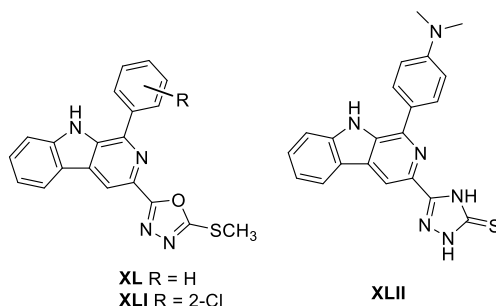
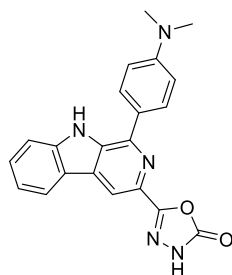
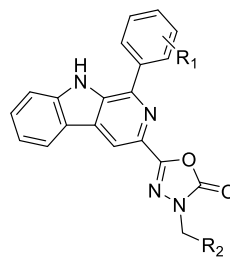


Figure 29: Compounds **XL-XLII** with potent anticancer activity

The same group investigated further the pharmacomodulation of the 1,3,4-oxadiazolyl moiety. Accordingly, a family of substituted phenyl at C-1 of 3-(2-oxo-1,3,4-oxadiazol-5-yl)- β -carbolines and their corresponding Mannich bases were synthesized and screened for their *in vitro* anticancer activity against a panel of seven cell lines [breast (MCF7), colon (HT29), ovarian resistant (NCI/ADR-RES), prostate (PC-3), lung (NCI-H460), melanoma (UACC-62), and ovarian (OVCAR-03) cancers]. Compound **XLIII** (**Figure 30**) having the *N,N*-dimethylaminophenyl group at C-1, showed the highest activity with GI_{50} in the range of 0.67–3.20 μ M. Moreover, some Mannich bases showed high selectivity and potent activity especially towards resistant ovarian (NCI-ADR/RES) cell lines (**XLIV-XLVII** and **XLIX**), and ovarian (OVCAR-03) cell lines (**XLV-L**). In addition, UV and fluorescence spectroscopy studies suggested that compound **XLIII** interacts with calf thymus DNA (ctDNA), a natural DNA isolated from the thymus of male and female calves that is used in studies of DNA binding anticancer agents and DNA interacting molecules.¹¹³



XLIII



XLIV $R_1 = H$, $R_2 = -NHC_3H_7$

XLV $R_1 = p-N(CH_3)_2$, $R_2 = -NHC_3H_7$

XLVI $R_1 = H$, $R_2 = -NHC_4H_9$

XLVII $R_1 = o-Cl$, $R_2 = -NHC_4H_9$

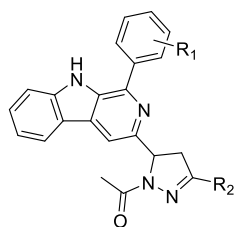
XLVIII $R_1 = H$, $R_2 = -N \begin{array}{c} \diagup \diagdown \\ \text{O} \end{array}$

XLIX $R_1 = p-N(CH_3)_2$, $R_2 = -N \begin{array}{c} \diagup \diagdown \\ \text{O} \end{array}$

L $R_1 = o-Cl$, $R_2 = -N \begin{array}{c} \diagup \diagdown \\ \text{O} \end{array}$

Figure 30: Compound **XLIII** and the Mannich bases **XLIV-L** with anticancer activity

To develop new anticancer agents, Kamal and co-workers designed pyrazole-linked β -carboline analogues. Different series of the target compounds were synthesized. They examined the anticancer activity of the hybrids on a panel of human cancer cell lines including human breast (MCF-7), lung carcinoma (A549), prostate cancer (DU-145), cervix (HeLa), renal adenocarcinoma (ACHN) and normal human embryonic kidney (HEK-293) cell lines. Among them, compounds **LI-LVI** (**Figure 31**) exhibited a potent anticancer effect against all cell lines tested with IC_{50} values of 1.9-8.7 μ M. Based on Annexin V-FITC, Hoechst staining, and DNA fragmentation analysis, the hybrids demonstrated apoptosis induction. Additionally, based on DNA fragmentation assay, these hybrids were able to cross the cell membrane barrier and cause DNA damage under normal cellular conditions. Finally, compound **LIV** inhibited DNA topoisomerase I activity and preserved DNA in the supercoiled form.¹¹⁴



- LI** $R_1 = 4\text{-CF}_3$, $R_2 = 2\text{-pyrrolyl}$
LII $R_1 = 4\text{-CF}_3$, $R_2 = 2\text{-furanyl}$
LIII $R_1 = 3,4,5\text{-(OCH}_3)_3$, $R_2 = 2\text{-thiophenyl}$
LIV $R_1 = 3,4,5\text{-(OCH}_3)_3$, $R_2 = 2\text{-furanyl}$
LV $R_1 = 3,4\text{-diF}$, $R_2 = 2\text{-thiophenyl}$
LVI $R_1 = 3,4\text{-diF}$, $R_2 = 2\text{-furanyl}$

Figure 31: (*N*-acetyl)pyrazole-linked β -carboline hybrids **LI-LVI** with anticancer activity

Barbosa *et al.* reported the synthesis and biological evaluation of a novel series of 1-(substituted-phenyl)- β -carbolines bearing a substituted-carbohydrazide moiety at C-3 (**Figure 32**) against a panel of cancer cells consisting of the breast (MCF-7), melanoma (UACC-62), lung (NCI-460), colon (HT29), prostate (PCO-3), leukemia (K-562), ovarian (OVCAR), and renal (786-0) cancer cell lines. Compound **LVII** exhibited the most significant activity toward all tested cell lines, with a remarkable activity against renal (786-0) cell lines ($IC_{50} = 0.04 \mu\text{M}$). Further, compound **LVII** was investigated in an *in vivo* Ehrlich solid carcinoma experimental model in mice paw and demonstrated systemic effectiveness as an inhibitor of cancer growth.¹¹⁵

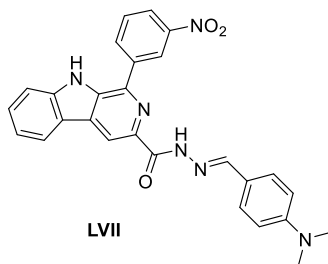


Figure 32: Compound **LVII** with potent anticancer activity

Dithiocarbamates are a common class of organic compounds that have a diverse range of biological activities including antibacterial, antifungal, and anticancer activity.^{116,117} Kamal *et al.* reported the synthesis and anticancer activity of 1-(substituted-phenyl)- β -carbolines having

dithiocarbamates moiety at C-3 against breast (MCF-7), lung (A549), cervical (HeLa), and prostate (DU-145) cancer cell lines. Among them, the derivative **LVIII** (**Figure 33**) displayed profound anticancer activity with IC_{50} values of 1.34 μ M on prostate cancer cells. Furthermore, the induction of apoptosis was confirmed by Annexin V-FITC and Hoechst staining assays. Besides, these derivatives also inhibit DNA topoisomerase II enzymatic activity. The present study emphasizes the importance of linking a dithiocarbamate moiety to the β -carboline nucleus for displaying remarkable activity.¹¹⁸

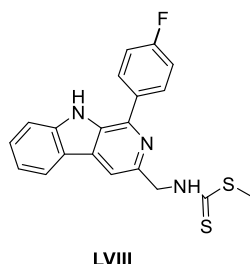


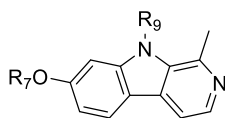
Figure 33: β -carboline-3-dithiocarbamate **LVIII** with anticancer activity

V-4.2. β -carbolines substituted at C-7 and/or N-9

In an early study, Ishida *et al.* concluded that installing an oxygenated substituent at C-7 enhanced anticancer activity compared to unsubstituted C-7 analogues and the length of the C-7-alkoxy chain affected both activity and cell line specificity. In particular, harmine bearing 7-methoxy moiety displayed potent activity against nasopharynx (KB), non-small cell lung (A549), renal (Caki-1), ovarian (1A9) and embryonic lung fibroblast (HEL) cancer cells (EC_{50} = 1.6-2.4 μ g/mL).⁷

Cao *et al.* tried to elucidate the anticancer SARs of harmine derivatives in finer detail by investigating new analogues of harmine bearing variable alkoxy moieties in 7-position and various alkyl or aralkyl groups in 9-position against breast (MCF-7), cervical (Hela), renal (769-P, 786-O and OS-RC-2), liver (Bel-7402 and HepG2), gastric (BGC-823), melanoma (A375), nasopharynx (KB), non-small cell lung (A549), colon (HT-29), malignant bladder (Blu-87), glioma (U251), and bladder squamous (SCaBER) cancer cells by MTT assay. The harmine analogues bearing relatively large and bulky alkoxy substituent in 7-position **LIX-LXIII** (**Figure 34**) showed

weak or no anticancer activities against several human cancer cell lines, and this might be due to poor water solubility of these compounds.¹¹⁹



LIX $R_9 = C_2H_5$, $R_7 = n-C_{10}H_{21}$

LX $R_9 = C_2H_5$, $R_7 = CH_2C_6H_5$

LXI $R_9 = n-C_4H_9$, $R_7 = n-C_8H_{17}$

LXII $R_9 = n-C_4H_9$, $R_7 = CH_2C_6F_5$

LXIII $R_9 = (CH_2)_3C_6H_5$, $R_7 = CH_2CH(CH_3)_2$

Figure 34: β -carboline with bulky alkoxy substituent moiety at C-7 **LIX-LXIII**

Synthesis and evaluation of a series of water-soluble 9-substituted β -carboline bearing a flexible amino side chain in the 3 position were reported by Chen and co-workers, against a panel of cancer cell lines consisting of breast (MCF-7), renal (769-P, 786-O and OS-RC-2), nasopharynx (KB), prostate (22RV1), gastric (BGC-823), liver (HepG2), and colon (HT-29) carcinoma and melanoma (A375). Of all 9-substituted β -carboline, the 9-aralkylated-substituted compounds exhibited more potent anticancer activities than the 9-alkylated analogues. In particular, compound **LXIV** (**Figure 35**) was found to be the most active towards eight human cancer cell lines with IC_{50} values lower than 10 μM . In particular, **LXIV** exhibited profound activity against HT-29 cell line ($IC_{50} = 2.6 \mu M$). The SAR revealed that the 9-aralkylated substituents of the β -carboline core played an important role in the anticancer potency modulation. Based on the significant spectral changes (red-shift and hypochromism), helix melting temperature (ΔT_m) value, and fluorescence quenching effects, these compounds displayed significant DNA-binding affinity.¹²⁰

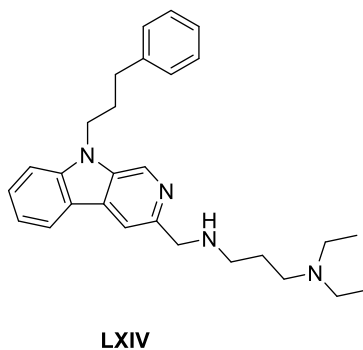


Figure 35: 9-alkylated substituted β -carboline **LXIV** with anticancer activity

In the next study by the same group, a new series of water-soluble β -carbolines bearing the same flexible amino side chain in position 3, were synthesized to find out better anticancer agents with improved pharmacological profile against a panel of cancer cell lines including MCF-7, KB, BGC-823, HepG2, A375, HT-29, 22RV1, 769-P, 786-0 and OS-RC-2. As expected, the 9-alkylated substituted β -carbolines represented the most interesting anticancer agents. Of which, compounds **LXV-LXVI** (**Figure 36**) were found to exhibit the most potency against ten human cancer cell lines ($IC_{50} < 10 \mu M$). In particular, both compounds displayed excellent activity against HepG2 cancer cells with IC_{50} values of 1.7 and 2.1 μM , respectively. The results confirmed that the 9-alkylated substituents of β -carboline had a crucial role in the modulation of the anticancer potency. Moreover, the interaction with the DNA of these derivatives was also examined, these compounds showed significant DNA binding affinity.¹²¹

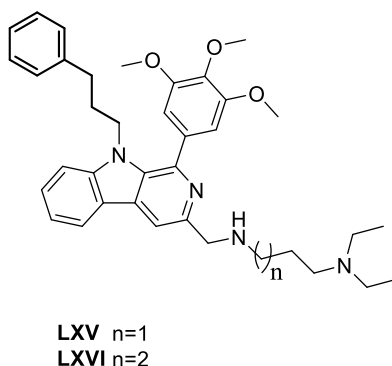


Figure 36: 9-alkylated substituted β -carboline derivatives **LXV-LXVI** with anticancer activity

V-4.3. Influence of 2-substitution of β -carbolines

A family of 2-benzyl-1-styryl- β -carbolines (**Figure 37**) was prepared and evaluated as anticancer agents against cervical (HeLa), nasopharynx (KB), colon (HT-29), liver (Bel-7402 and HepG2), gastric (BGC-823), melanoma (A375), non-small cell lung (A549), and renal carcinoma (786-0 and 769-P). Among the synthesized compounds, 2-benzylated β -carbolinium bromides **LXVII-LXIX** showed the highest inhibitory activity against the tested human cancer cell lines with IC_{50} values below 10 μ M.¹²²

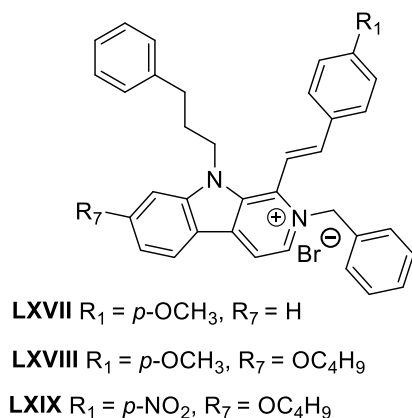
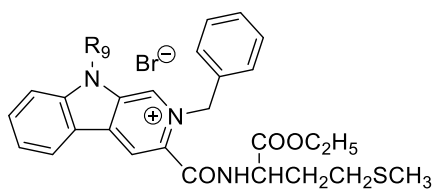


Figure 37: 2-benzyl-1-styryl- β -carbolinium bromides **LXVII-LXIX**

A series of β -carboline amino acid ester conjugates and their 2-benzylated analogues were prepared and screened for anticancer activity against renal (769-P and 786-0), gastric (BGC-823), nasopharynx (KB), carcinoma and melanoma (A375). The 2-benzylated quaternary β -carboline amino acid ester conjugates showed interesting anticancer activities. In particular, compounds **LXX-LXXI** (**Figure 38**) were found to be the most potent derivatives with IC_{50} values lower than 20 μ M against all human cancer cell lines studied compared to more than 100 μ M for non-substituted analogues on the 2 position. These results concluded that the 2-benzyl substituent on the β -carboline core played a very important role in the modulation of the anticancer potencies.¹²³



LXX $R_9 = n\text{-C}_4\text{H}_9$
LXXI $R_9 = (\text{CH}_2)_3\text{C}_6\text{H}_5$

Figure 38: N2-benzylated quaternary β -carboline amino acid ester conjugates **LXX-LXXI**

In another study, Zhang *et al.* reported the *in vitro* activity of 2-alkylated quaternary β -carbolines which were pharmacomodulated on positions 1, 2, 7 and 9 of the β -carboline skeleton with various alkyl and aralkyl substituents against ten human cancer cell lines: breast (MCF-7), liver (HepG2), gastric (BGC-823), prostate (22RV1), colon (HT-29), renal (769-P), Lewis lung (LLC), esophageal (Eca-109), ovarian (SK-OV-3) carcinomas, and malignant melanoma (A375). Some of these compounds exhibited potent anticancer effects in animal models. Mice bearing Sarcoma 180 was more susceptible to this series of compounds than mice bearing Lewis lung cancer. Compound **LXXII** (**Figure 39**) having a benzyl group at position 2 displayed the most potent antitumor effect with the cancer inhibition rate of 63.5 and 60.6% against mice bearing Sarcoma 180 and Lewis lung cancer, respectively. The Structure-Activity Relationships (SARs) investigations revealed that the benzyl substituent in position 2 of the β -carboline skeleton, was the optimal group for significant anticancer effects.¹²⁴

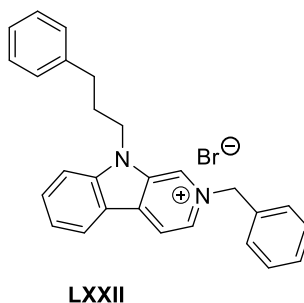
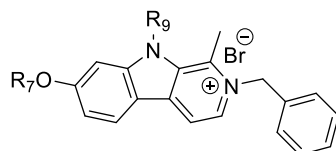


Figure 39: 2-alkylated quaternary β -carboline **LXXII** with potent anticancer activity

In another study, Cao group synthesized and evaluated a new series of harmine derivatives possessing 2-benzyl moiety and different alkyl moieties in positions 7 and 9. Among derivatives, compounds **LXXIII-LXXIV (Figure 40)** were the most active anticancer agents with the cancer inhibition rate of 53.1 and 52.6% in mice bearing Sarcoma 180 model, respectively.¹¹⁹



LXXIII $R_9 = C_2H_5$, $R_7 = (CH_2)_3C_6H_5$

LXXIV $R_9 = CH_2CH(CH_3)_2$, $R_7 = CH_2C_6H_5$

Figure 40: 2,7,9-substituted β -carbolines **LXXIII-LXXIV** with potent anticancer activity

V-4.4. β -carbolines hybrids

Hybrid drugs combine two distinct biologically active compounds that act at different targets, into one new chemical entity to synergize the effects of each compound. Hybrid drugs are usually defined as a structure in which a linker, often a simple hydrocarbon chain, connects the two drug molecules that are not much altered with regard to their initial chemical structure. Hybridization of drugs is a powerful tool to develop better treatments for several human diseases, particularly for cancer.¹²⁵ Herein, I review the anticancer activity of a variety of β -carboline hybrids including hydroxamate-linked β -carboline hybrids, chalcone-linked β -carboline hybrids, salicylic acid-linked β -carboline hybrids, and podophyllotoxin-linked β -carboline hybrids.

➤ Hydroxamate-linked β -carboline hybrids

The key regulatory enzymes involved in post-translational modifications are histone acetyltransferases (HATs) and histone deacetylases (HDACs) which are responsible for reversible processes of acetylation and deacetylation of histones. Post-translational histones modifications often result in the remodeling of chromatin that is partially responsible for the epigenetic regulation of gene expression.^{126,127} Many HDACs are overexpressed in various cancer types, showing their importance in cancer growth. HDACs play a key role in carcinogenesis, including

the transcription and gene regulation involved in cell proliferation, apoptosis, and cell-cycle regulation.^{128,129} HDAC inhibitors (HDACis) have been found to induce apoptosis, differentiation, and cell cycle arrest, and to inhibit cell migration, cell invasion, and angiogenesis in many cancer cell lines. Additionally, these compounds inhibit cancer growth in animal models and in patients.^{130,131} Moreover, many anticancer agents exhibit synergistic inhibitory effects with HDACis including those targeting DNA or topoisomerase, in the induction of apoptosis and suppression of proliferation in cancer cells.^{132–134} Generally, HDACis are structurally grouped into four classes: hydroxamic acids (e.g., SAHA or Vorinostat), benzamides (e.g., entinostat), cyclic tetrapeptides (e.g. trapoxin B) and short-chain fatty acids (e.g., valproic acid).¹³⁵ Hydroxamic acid-based compounds represent the most extensively studied class of HDACis that has entered clinical studies and therapeutic arsenal as anticancer drugs (e.g., Vorinostat ZOLINZA®, Panobinostat FARYDAK®, belinostat BELEODAK®).^{136–138}

Ling *et al.* have prepared a novel series of hybrids from β -carboline and hydroxamic acid linked with urea and evaluated their anticancer activity as well as their mechanisms against colon cancer cell lines (HCT116, SW620, SW480, and LOVO) in comparison to harmine and SAHA as reference drugs. Among these hybrids, compound **LXXV** (**Figure 41**) showed superior anticancer potency as well as induced more significant cancer cell apoptosis than SAHA by cleavage of both poly(ADP-ribose)polymerase (PARP) and caspase 3 in a dose-dependent effect. Moreover, the potent anticancer activity of compound **LXXV** was related to HDAC inhibition, p53 signaling pathway activation, and DNA damage. Finally, compound **LXXV** displayed low acute toxicity in mice and showed superior growth inhibition of implanted human colorectal cancer (CRC) in mice than SAHA.¹³⁹

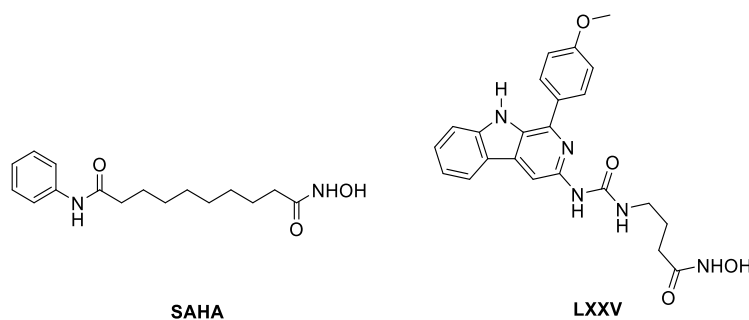


Figure 41: SAHA and β -carboline-based hydroxamic acid derivative **LXXV**

In the next study by the same research group, a novel series of C3-substituted β -carboline-based hydroxamic acids with amide linker were synthesized and evaluated for their HDAC inhibition and anticancer activities against lung cancer cells (H1299), colon cancer cells (HCT116), and human hepatocellular carcinoma cells (HepG2 and SMMC-7721). Both SAHA and harmine were used as positive controls. Most of these derivatives exhibited significant HDAC inhibition and good anticancer activity, with IC_{50} values in the low micromolar range. Among them, compound **LXXVI** (**Figure 42**) displayed superior HDAC inhibition than SAHA. Additionally, **LXXVI** enhanced histone H3 and α -tubulin acetylation, induced DNA damage as confirmed by hypochromism, and improved phosphorylation of histone H2AX. It also suppressed Stat3, Akt, and ERK signaling, important cell-growth-promoting pathways that are activated in most cancers. Finally, compound **LXXVI** exhibited reasonable solubility and permeability in Caco-2 cells.¹⁴⁰

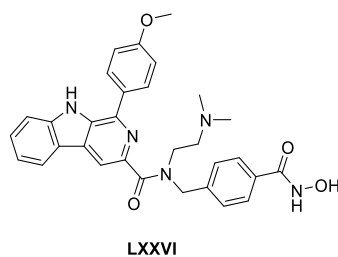


Figure 42: C3-substituted β -carboline-based hydroxamic acid **LXXVI** with anticancer activity

Recently, they also synthesized and evaluated a family of novel β -carboline-based hydroxamic acid derivatives in which β -carboline core is connected to a benzylic linker with an amino group instead of urea and amide linkers and evaluated their anticancer activity against human breast adenocarcinoma cells (MCF-7), hepatocellular carcinoma cells (HepG2, SMMC-7721, and Huh7), and human colon cancer cells (HCT116) in comparison to β -carboline analog harmine and SAHA as reference compounds. Many of these compounds displayed excellent HDAC1/3/6 inhibitory effects as well as significant anticancer activities against the five human cancer cell lines. In particular, compound **LXXVII** (**Figure 43**) displayed the highest anticancer potency against cancer cell lines with low IC_{50} values of 0.53-1.56 μ M, compared to harmine and SAHA with IC_{50} values of 46.70-55.30 μ M and 4.48-6.26 μ M, respectively. Further, **LXXVII** dose-dependently suppressed acetylation of histone H3 and α -tubulin as evidence of its HDAC

inhibitory effects. Furthermore, it significantly arrested HepG2 cells at the G2/M phase in a concentration-dependent manner. Finally, compound **LXXVII** displayed strong antimetastasis activity by simultaneously decreasing MMP2 and MMP9 protein levels, and MAPK signaling pathway inhibition.¹⁴¹

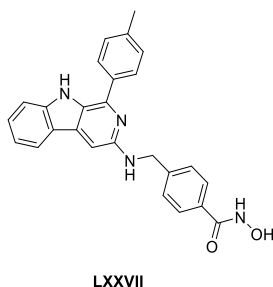


Figure 43: C-1 and C-3 substituted β -carboline-based hydroxamic acid derivative **LXXVII**

➤ Chalcone-linked β -carboline hybrids

Chalcones are attractive for broad-range biological activities such as hepatoprotective, anticancer, antimalarial, antimicrobial, and anti-HIV activities.^{142,143} Among these, anticancer and antiangiogenic activities account for the research interest of these compounds.¹⁴⁴ Based on the attractive anticancer properties of β -carboline and chalcone units, diverse chalcones linked to C-1 and C-3 of β -carboline were evaluated for their anticancer effect.

In a study by Shankaraiah *et al.*, a series of chalcones were introduced at C-3 of β -carbolines and examined for their *in vitro* anticancer potential and DNA-binding affinity against cervical carcinoma (HeLa), mouse melanoma (B-16), colon cancer (HT-29), lung adenocarcinoma (A-549) and prostate cancer (PC-3) cell lines. Among them, compound **LXXVIII** (**Figure 44**) displayed potent activities against A-549 and PC-3 with IC_{50} values of 5.3 and 6.4 μ M, respectively. Moreover, the SARs derived from anticancer and DNA-binding affinity studies revealed that the nitro, amino, trimethoxy and hydroxyl substitutions on the chalcone part of the ring could play a crucial role in improving activities.¹⁴⁵

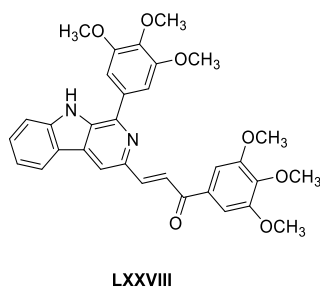


Figure 44: 3-chalcone-β-carboline hybrid **LXXVIII** with anticancer activity

Recently, a series of chalcones at C-1 of β-carboline with their bromide salts were designed, prepared and screened for anticancer properties against six cancer cell lines including, breast carcinoma (MDA-MB-231), pancreatic cancer (BxPC-3), human prostate cancer (PC-3), cervical cancer (HeLa), human embryonic kidney 293 (HEK293T) and castration-resistant prostate cancer (C4-2) cells using MTT assay. Among them, 2-alkylated-β-carboline chalcone **LXXIX** (**Figure 45**) showed anticancer activity with IC_{50} values of 16.1 μ M against C4-2 cancer cells. Besides, **LXXIX** markedly induced apoptosis in MDA-MB-231 cells in dual acridine orange/ethidium bromide (AO/EB) fluorescent staining.⁹⁹

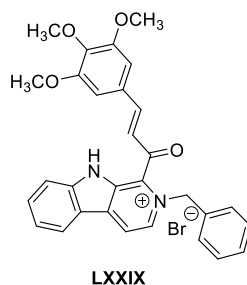


Figure 45: 1-chalcone-β-carbolinium bromide **LXXIX** with anticancer activity

➤ **Salicylic acid-linked β -carboline hybrids**

Aspirin, also known as acetylsalicylic acid, is daily used as antipyretic analgesics but also exhibit high potency in the treatment of cancer.^{146–152} Epidemiological studies and randomized clinical trials revealed that aspirin decreases the incidence of cancers, including colorectal, gastrointestinal, and lung cancer.^{153–155} Aspirin was more effective against colorectal cancers (CRC) than against cancers of other tissues such as breast, prostate, liver, lung, and skin.^{156–159} Recently, several studies suggested that aspirin and its metabolite salicylic acid and their derivatives could induce apoptosis in several CRC cell lines.^{156,160–163}

Qi-Bing *et al.* combined β -carboline and salicylic acid moieties to synthesize a series of novel β -carbolines/salicylic acid hybrids as anticancer agents. Most of the hybrids showed potent anticancer activity against all the five tested cancer cell lines including human colon cancer (HCT116), hepatocellular carcinoma (SMMC-7721 and Hep G2), human lung cancer (H460), and human bladder carcinoma (EJ) cell lines. Particularly, compound **LXXX** (**Figure 46**) was selective to liver cancer SMMC-7721 with IC_{50} values of 7.0 μ M. Moreover, compound **LXXX** showed apoptosis induction in an Annexin V-FITC/propidium iodide flow cytometry assay and triggered the mitochondrial/caspase apoptosis. It was concluded that combining β -carboline and salicylic acid moieties into one molecule is an effective method to obtain promising therapeutics candidate for the intervention in human cancers.¹⁶⁴

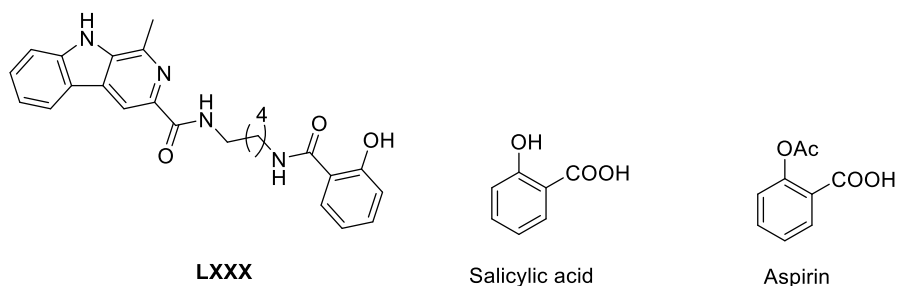


Figure 46: β -carbolines/salicylic acid hybrid **LXXX**, salicylic acid and aspirin

➤ **Acylhydrazone-linked β -carboline hybrids**

Acylhydrazone scaffold (-CONHNH=) has received considerable interest for decades due to the broad applications of their pharmacological properties, including antibacterial and anticancer activities.^{165–173}

Li *et al.* conjugated acylhydrazone and β -carboline cores, and subjected the resultant hybrids to anticancer evaluation against a panel of cancer cell lines: breast (MCF-7 and MDA-MB-231), lymphoma (Raji), lung (H460), paclitaxel-resistant human lung (A549/T), vinblastine resistant human colon (HCT-8/V), paclitaxel-resistant human ovarian (A2780/T), and adriamycin resistant human breast (MCF-7/ADR) cancer cell lines. Compound **LXXXI** (**Figure 47**) exhibited the highest activity among the tested compounds with IC₅₀ values of 1–2 μ M against a panel of cancer cell lines and retained remarkable activity in multidrug-resistant cancer cells. Besides, **LXXXI** induced late apoptosis on both MCF-7 and MCF-7/ADR cancer cells. Moreover, it displayed anticancer effect *in vivo* (average growth-inhibition = 17.2%) with low toxic and side effects and without significant body weight loss.¹⁷⁴

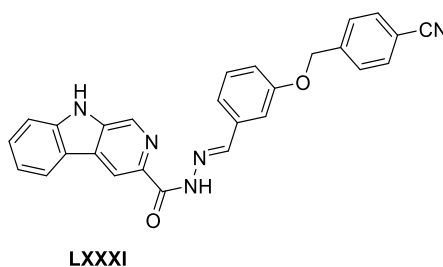
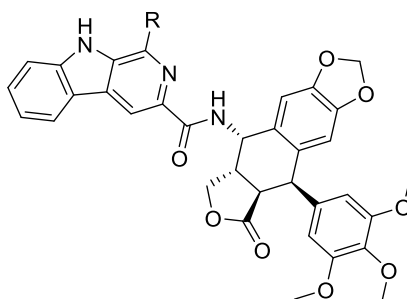


Figure 47: Acylhydrazone-linked β -carboline hybrid **LXXXI** with potent anticancer effect

➤ **Podophyllotoxin-linked β -carboline hybrids**

Podophyllotoxin is a natural compound and can be semi-synthesized commercially. Podophyllotoxin has potent anticancer activity against many several types of cancers such as cervical carcinoma, colon cancer, breast cancer, prostate cancer, small cell lung cancer, osteosarcoma, nasopharyngeal carcinoma, and testicular carcinoma.^{175–180} Semi-synthetic podophyllotoxin derivatives etoposide (CELLTOP®) and teniposide are used as chemotherapeutic agents acting as inhibitors of DNA-topoisomerase II.¹⁸¹

Sathish *et al.* reported podophyllotoxin based hybrids and quoted two significant leads (**LXXXII-LXXXIII**) (**Figure 48**) for anticancer activity with IC_{50} values of 1.07 and 1.14 μM , respectively against prostate cancer (DU-145) cell line. Based on biological and docking studies, these hybrids inhibited DNA interaction with topoisomerase II.¹⁸²



LXXXII R = 2,5-(OCH₃)₂C₆H₃

LXXXIII R = 3,4-diFC₆H₃

Figure 48: β -carboline-podophyllotoxin hybrids **LXXXII-LXXXIII** with anticancer effect

➤ β -carbolines dimers

Since a β -carboline dimer was unexpectedly synthesized in 1962, researchers began to focus on them.¹⁸³ Natural β -Carboline dimers were first isolated from the tree bark of *Picrasma quassioides* Bennet in 1984.¹⁸⁴ In general, the motif could be directly linked by carbon chains, heteroatoms, heterocycles, amides, esters, and amino-groups on their connected sites that mainly consist of positions 1, 2, 3, and 9. Herein, we provide a rapid overview of their anticancer effect.

Shi *et al.* have accomplished the synthesis of β -carbolines dimers which were screened for anticancer activity. Compound **LXXXIV** (**Figure 49**) showed good anticancer activities with IC_{50} values of 3.8-8.5 μM against gastric carcinoma (BGC-823), malignant melanoma (A375), ovarian adenocarcinoma (SK-OV-3), and epidermoid carcinoma of the nasopharynx (KB) cell lines.¹⁸⁵

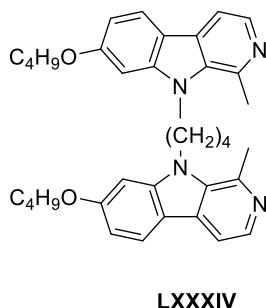


Figure 49: β -carboline dimer **LXXXIV** with potent anticancer activity

From the same group, a recent report mentioned the synthesis of asymmetric dimeric β -carboline and their biological evaluation against nine cell lines. Among tested compounds, compound **LXXXV** (**Figure 50**) displayed the most potent tumor inhibition rate of 54.6% and 48.1% in a Sarcoma 180 or Lewis lung cancer-bearing mice model respectively. Further, **LXXXV** had migration inhibitory effects in wound healing assay and displayed angiogenesis inhibition in the chicken chorioallantoic membrane (CAM) assay.¹⁸⁶

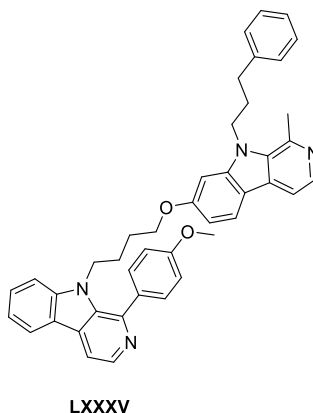
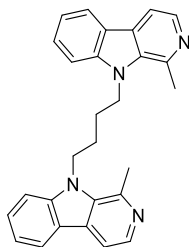


Figure 50: Asymmetric β -carboline dimer **LXXXV** with potent anticancer activity

Daoud *et al.* evaluated the anticancer activity of a semi-synthetic compound **B-9-3** (**Figure 51**) that is formed of two harmane molecules bound by a butyl group. The compound exhibited remarkable anticancer activity against human lung (NCI-H460), human breast (T47D), and human colorectal (HCT-116) cancer cell lines with IC_{50} values of 3.6-9.6 μ M. Additionally, the

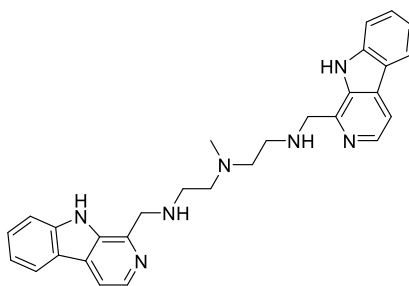
compound induced dose-dependent apoptosis, or necroptosis, and inhibited cancer cell migration. The compound had anti-angiogenesis activity evidenced by inhibition of tube formation in a human umbilical vascular endothelial cell line (HUVEC).¹⁸⁷



B-9-3

Figure 51: Semi-synthetic β -carboline dimer **B-9-3** with potent anticancer activity

A dimeric β -carboline **LXXXVI** (**Figure 52**) was synthesized by Chatwichien and co-workers with diethylenetriamine as linker. The *in vitro* cancer inhibition of the dimer compound was studied against several non-small cell lung carcinoma (NSCLC) cell lines. The compound exhibited superior potency than the corresponding monomer. Further, the compound induced apoptosis through caspase-dependent pathway mediated by PUMA (p53 upregulated modulator of apoptosis) in a dose-dependent manner.¹⁸⁸



LXXXVI

Figure 52: Dimeric β -carboline **LXXXVI** with potent anticancer activity

V-4.5. β -carboline metal complexes

➤ Ruthenium (II) β -carboline complexes

The discovery of cisplatin as a metal-based anticancer agent opened a new era in cancer chemotherapy.¹⁸⁹ However, its severe side effects and cross drug resistance stimulated the development of non-platinum metal-based anticancer agents.^{190–192} Ruthenium compounds turned out to be the most promising alternatives because of their rich synthetic chemistry, variable oxidation states and potential use as therapeutic anticancer agents with low systemic toxicity.^{193–195} Several ruthenium compounds display promising anticancer activity, and some of them exhibit an anticancer potency similar to or better than that of cisplatin.^{196–200}

Tan group studied the anticancer activity of different ruthenium (II) β -carboline complexes **LXXXVII-XCI** in many reports as depicted in **Figure 53**. **LXXXVII** displayed superior cell growth inhibition activities (IC_{50} values below 6 μ M) than those of cisplatin (IC_{50} values above 16.7 μ M) against breast (MCF-7), cervix (HeLa), and liver (HepG2) cancer cell lines by inducing apoptosis and triggering G0/G1 phase arrest.²⁰¹ In a second study, **LXXXVIII** exhibited a broad spectrum of inhibition on human cancer cells, with IC_{50} values ranging from 15 to 46 μ M, which were comparable with those of cisplatin by inducing apoptosis.²⁰² In a third study, **LXXXIX** had a cancer inhibition rate greater than 45% against MCF-7 and HepG2 in mice model.²⁰³ Finally, **XC-XCI** exhibited potent anticancer activities against a panel of human cancer cell lines with IC_{50} values lower (1.9–18.4 μ M) than those of cisplatin by inducing apoptosis and mediating cycle arrest in the G0/G1 phase.²⁰⁴

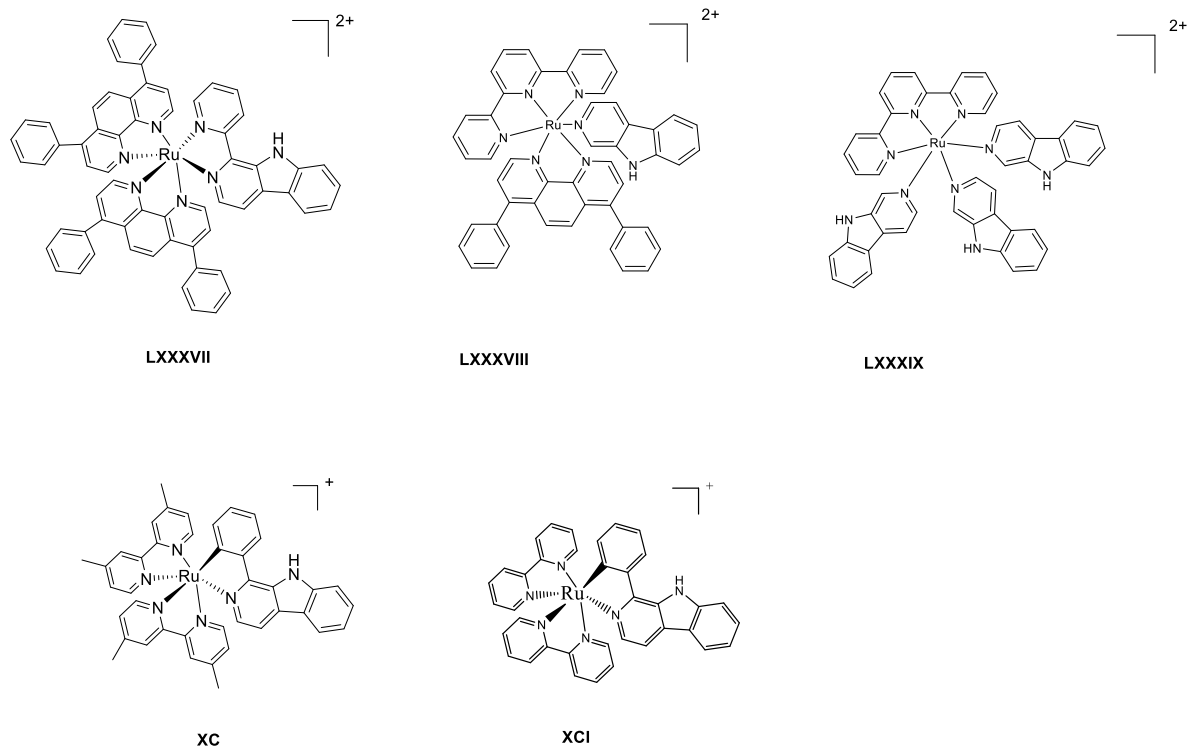


Figure 53: Ruthenium (II) β -carboline complexes LXXXVII- XCI with potent anticancer activity

➤ Other β -carboline metal complexes

Jin *et al.* synthesized a series of Pt (II), Cu (II), Co (II) and Ni (II) complexes with β -carboline. The Cu (II) and Pt (II) complexes **XCII** (**Figure 54**) displayed superior DNA binding and DNA cleavage ability than that of the other two. Furthermore, the two complexes were toxic against lung (A549) and cervix (HeLa) cancer cells but relatively safe to normal cells (Helf).²⁰⁵

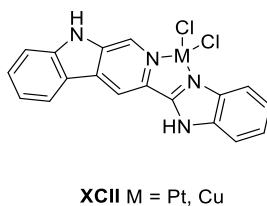


Figure 54: Pt (II) or Cu (II) β -carboline complex **XCII** with potent anticancer activity

Yang *et al.* reviewed a novel β -carboline derivative-based nickel (II) complex series, discovering compound **XCIII** (**Figure 55**). They evaluated their anticancer towards six cancer cell lines, with IC_{50} values in the micromolar range (3.8–15.1 μM), lower than cisplatin in MGC-803, Hep G2, T24, OS-RC-2, NCI-H460, and SK-OV-3 cancer cell lines. In particular, the IC_{50} value of **XCIII** for MGC-803 was 3.8 μM , which is 4.6 times lower than that of cisplatin (17.6 μM). The anticancer activity of compound **XCIII** was mainly attributed to its ability to induce cell cycle arrest at the S phase and intrinsic apoptosis.²⁰⁶

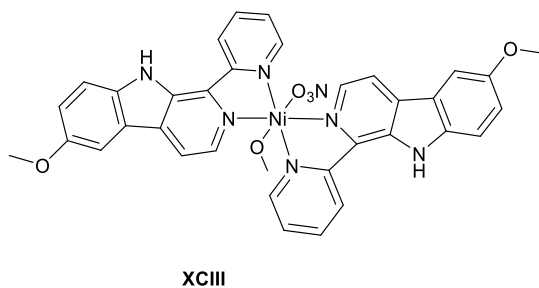


Figure 55: Ni (II) β -carboline complex **XCIII** with potent anticancer activity

VI. Conclusion

This chapter provides a comprehensive overview of *Peganum harmala* and its alkaloidic composition. In the first section, we reviewed the general characteristics of *Peganum harmala* in terms of botanical description, alkaloidic composition, and medicinal uses. Then, we highlighted the biological activities of β -carbolines and their potential development as a drug.

The amount of data described in the previous sections allows us to postulate a few conclusions on the SAR of β -carboline analogues as anticancer agents (**Figure 56**):

- The use of carboxamides and amino groups at C-1 improve the activity.
- Installing appropriate substituted phenyl moieties such as halo-phenyl at C-1 and appropriate groups such as heteroaryls and dithiocarbamates at C-3 enhance the efficacy.
- 7-Methoxy group enhances the activity.
- 9 and 2-alkyl substituents do increase the β -carbolines activity.

Several β -carboline hybrids displayed potent anticancer effects including β -carboline linked to hydroxamic acids, chalcones, salicylic acid, acylhydrazone and podophyllotoxin. Besides, many symmetric and asymmetric dimeric β -carbolines with different linkers showed superior potency than the corresponding monomer. Various ruthenium (II), platinum (II), copper (II), and nickel (II) β -carboline complexes exhibited potent growth inhibitory effect in cancer cells.

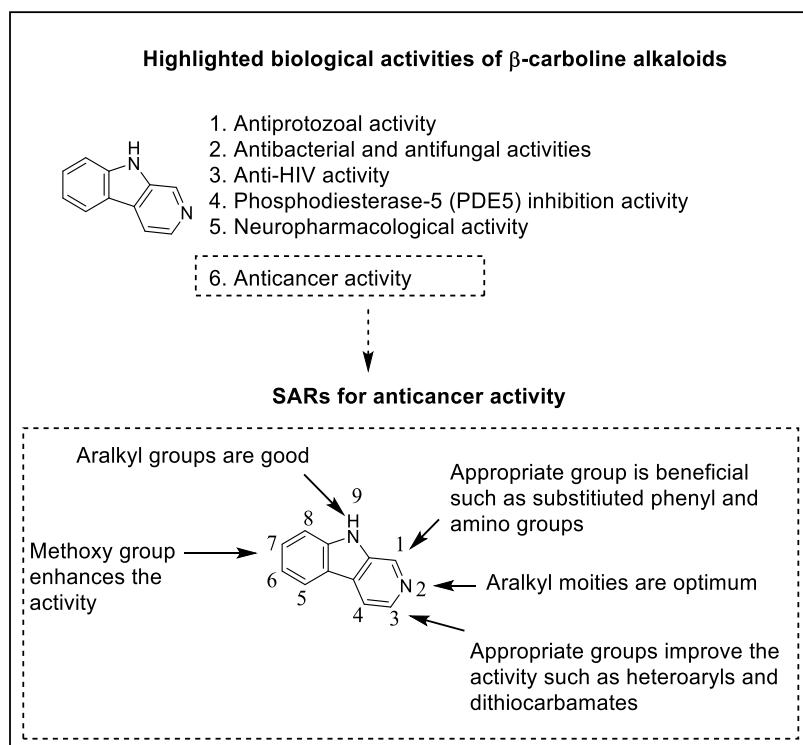


Figure 56: Highlighted biological activities of β -carbolines and anticancer SAR

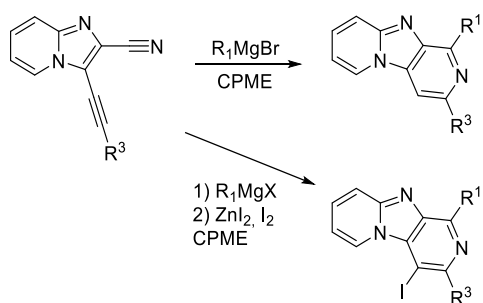
Chapter 3:

Design and Synthesis of New Imidazo[1,2- α :4,5- b']dipyridines

I. Genesis of the Project

As previously reviewed in chapter 2, a considerable amount of data supports the idea that β -carbolines are promising anticancer agents. Many studies revealed that β -carboline harmine exhibits significant anticancer activities *in vitro* and *in vivo*, through proliferation, migration and invasion inhibition and induction of apoptosis. Harmine inhibits the growth of many types of cancer, including lung, gastric, breast and hepatic cancer.²⁰⁷ Harmine induces autophagy and apoptosis through mTOR and ERK1/2 signaling pathways, increases the expression of pro-apoptotic factors, including caspases 3/8/9, Bax and Bid, and reduces the level of pro-inflammatory cytokines in melanoma and gastric cancer.^{3,207,208}

During the last decade, a tremendous effort by our research group has been devoted to the development of new synthetic methodologies for the preparation of imidazo[1,2-*a*]pyridine-based heterocycles. Notably, the preparation of imidazo[1,2-*a*:4,5-*c'*]dipyridines was described in our laboratory in a one-pot sequence from Grignard addition to nitrile at position 2 followed by cyclization on alkyne at position 3.⁹ These reaction conditions were then optimized to allow the straightforward synthesis of 1,3-disubstituted 4-iodoimidazo[1,2-*a*:4,5-*c'*]dipyridines (Scheme 8).⁸



Scheme 8: Synthesis of imidazo[1,2-*a*:4,5-*c'*]dipyridines

As can be seen in **Figure 57**, the newly developed imidazo[1,2-*a*:4,5-*c'*]dipyridines are structurally very close from the β -carboline scaffold. The only difference is the presence of supplementary nitrogen in imidazo[1,2-*a*:4,5-*c'*]dipyridines.

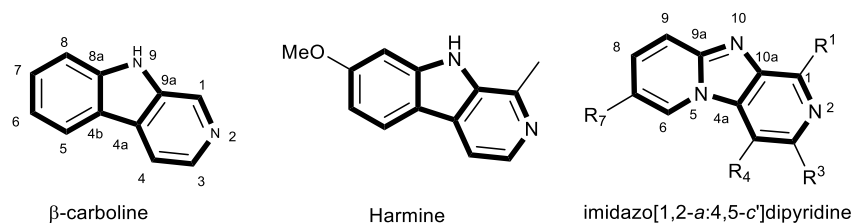


Figure 57: β -carboline, harmine and imidazo[1,2-*a*:4,5-*c'*]dipyridine structures

We were encouraged by the remarkable anticancer activity exhibited by the β -carbolines to pursue and investigate imidazo[1,2-*a*:4,5-*c'*]dipyridines as potential anticancer agents. We were curious to determine the potential effect of the second pyridine ring on the chemical reactivity, the solubility and the capacity to interact with the target(s) of this new series of compounds. For instance, β -carboline derivatives are generally difficult to develop as lead compounds for preclinical studies because of their poor solubility.^{209,210} Interestingly, we found that imidazo[1,2-*a*:4,5-*c'*]dipyridine salts have excellent solubility. In converse to β -carboline, we noticed in the preliminary study that position 2 of imidazo[1,2-*a*:4,5-*c'*]dipyridines could not be explored. Indeed, N-2 of pyridine ring was less nucleophilic than N-10 of imidazole ring in this series of compounds. This was supported by the electrostatic potential map (Gaussian09 using DFT method at B3LYP/6-31G(d) level of theory) which displayed higher electron density around N-9 compared to that of N-2 (**Figure 58**) and confirmed by X-ray crystallographic analysis of the first salt synthesized (**Figure 59**).

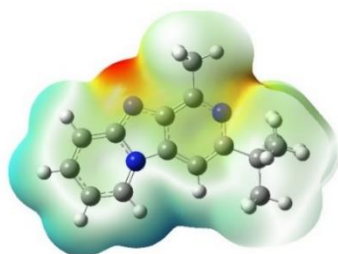


Figure 58: Electrostatic potential map for the imidazo[1,2-*a*:4,5-*c'*]dipyridine using Gaussian

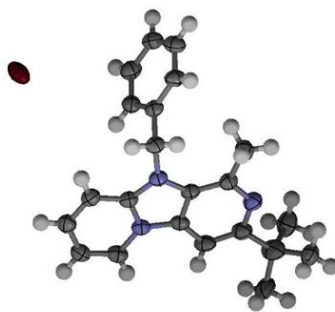
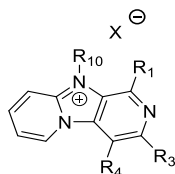


Figure 59. X-ray crystal structure of imidazo[1,2-*a*:4,5-*c'*]dipyridine salt

Our efforts to determine the anticancer potentialities of our series of compounds began with a preliminary study conducted in a collaboration with UMR INSERM 1069 N2C of the Faculty of Medicine of Tours. In this preliminary study, six compounds previously synthesized were converted to salt and evaluated *in vitro* for their cancer cell growth inhibition activity against two triple-negative breast cancer (TNBC) cell lines, namely, MDA-MB 435s-Luc (basal-B) and MDA-MB 468-Luc (basal-A) via 3-(4,5-dimethylthiazol-2-yl)-2,5-diphenyltetrazolium bromide (MTT) assay. Human cancer cells divide through a sequence of steps that are collectively called the cell cycle which lasts 24h or less. Thus, we treated the cancer cells with our compounds for 5 days to investigate their effect on cancer growth. Besides, we explored the cytotoxic activity of these compounds by evaluating cell survival after one-day treatment to exclude any compound with an acute toxic effect that could induce high toxicity *in vivo*.

To determine the growth inhibition activity of compounds **POD114**, **POD128**, **POD118**, **POD108**, **POD110** and **POD147** on MDA-MB 468-luc and MDA-MB 435s-luc cells, the cells were treated with tested compounds for 5 days and 50% inhibitory concentration (IC₅₀) was determined by MTT assay.

Table 4: Cancer cells viability effects of preliminary imidazo[1,2-*a*:4,5-*c'*]dipyridines

	R ₁	R ₃	R ₄	R ₁₀	X	5 days- cell viabilities (IC ₅₀ , μM ± SEM)		24h-cell viabilities (IC ₅₀ , μM ± SEM)
						MDA-MB 468-luc	MDA-MB 435s-luc	MDA-MB 435s-luc
POD114	Ph	n-Bu	I	H	Br	>100	>100	>100
POD128	Me	c-Pr	I	H	CF ₃ SO ₃ ⁻	>100	>100	>100
POD118	Me	c-Pr	H	Bn	Br	30.7±11.5	43.9±14.1	>100
POD108	Me	<i>t</i> -Bu	H	Bn	Br	18.4±6.1	16.4±3.1	74.4±28
POD110	Me	c-Pr	4Cl-C ₆ H ₄ S-	Bn	Br	2.4±0.1	0.6±0.2	6.2±2.4
POD147	Me	CO ₂ Et	H	Bn	Br	>100	>100	>100

Table 4 summarizes the IC₅₀ values and revealed that the 10-benzylated compound **POD108** presents interesting inhibitory activities on MDA-MB 468-luc and MDA-MB 435s-luc cells with IC₅₀ of 18.4 and 16.4 μM, respectively, compared to the completely inactive 10-hydrogenated compounds **POD114** and **POD128**. The substitution of N-10 with a benzyl group seems to be important for the growth inhibition activity as a first approximation. The same remark applies to the 10-benzylated **POD118** (R₃ = cyclopropyl, IC₅₀ of 30.7 and 43.9 μM respectively) compared to the 10-hydrogenated inactive analogue **POD128**. 10-Benzylated compound **POD110** (R₃ = 4-Cl-C₆H₄S-) displayed high cytotoxic effects against both cell lines after 5 days treatment; however, it was not pursued further because of 24h acute toxic effect to the cells. Moreover, these first results gave a trend for the C-3 position: *t*-butyl (**POD108**)> *c*-propyl (**POD118**)>> CO₂Et (**POD147**). Indeed, **POD147** was completely inactive.

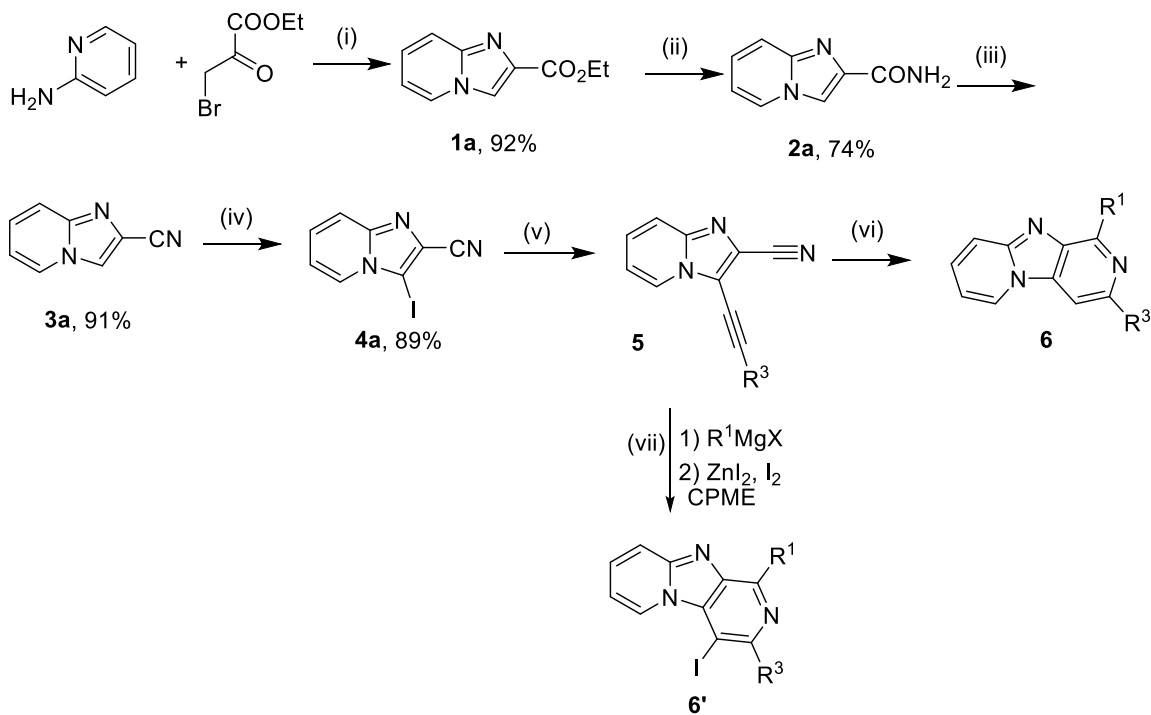
Encouraged by these preliminary results, this thesis research project aimed to conduct further medicinal chemistry exploratory studies. This entailed design, synthesis, biological assessment, as well as three dimensional-quantitative Structure-Activity Relationship (3D-QSAR) analyses, in efforts to explore the opportunities and liabilities associated with the imidazo[1,2-*a*:4,5-*c'*]dipyridine class of compounds as potential anticancer agents.

II. Background on the Synthetic Pathway

The synthesis of the imidazo[1,2-*a*:4,5-*c'*]dipyridines explored in this thesis work was previously described in two articles published by EA 7502 SIMBA.^{8,9} This synthetic pathway started with the cyclocondensation of the commercially available 2-aminopyridine with ethyl bromopyruvate to afford ethyl imidazo[1,2-*a*]pyridin-2-carboxylate **1a** in high yields (92%) (**Scheme 9**). Ester **1a** was transformed into imidazo[1,2-*a*]pyridin-2-carboxamide **2a** through aminolysis reaction using an aqueous solution of ammonia (30%) at room temperature overnight (74%). The dehydration of amide **2a** afforded the imidazo[1,2-*a*]pyridin-2-carbonitrile **3a** in 91% yield, by heating the amide in phosphorus oxychloride (POCl₃). The next step was an iodination reaction in the 3 position, which was accomplished by cooling nitrile **3a** in chloroform (CHCl₃) in the presence of iodine monochloride (ICl) to furnish the key intermediate 3-iodoimidazo[1,2-*a*]pyridin-2-carbonitrile **4a** (89%). Then, Sonogashira cross-coupling reactions were applied to **4a** with the appropriate alkynes in the presence of Pd₂(dba)₃ and copper iodide (CuI) as catalysts. Thereafter, the tricyclic imidazo[1,2-*a*:4,5-*c'*]dipyridines **6** were obtained by a Grignard reagent addition sequence to the nitrile group, followed by a *6-endo-dig* cyclization on the triple bond at room temperature for 30 minutes to two hours. The Grignard reagent-promoted *6-endo-dig* cyclization developed by our lab features mild reaction conditions and allows the functionalization at positions 1 and 3 of the tricyclic compounds **6** with alkyl or aryl groups.

Moreover, our lab expanded the scope of this reaction to the functionalization of the 4 position of the tricyclic compound, by adding ZnI₂ and I₂ to the reaction mixture, leading to the 4-iodinated **6'**. This iodine atom allows the functionalization of position 4 using various metal-

catalyzed reactions.⁸ The two steps of Sonogashira coupling reaction and heterocyclization present the advantage to be performed in very short reaction time and good yields.



Scheme 9: Synthetic protocol towards target tricyclic compounds. Reagents and conditions: (i) a) DME, RT, overnight b) EtOH, Reflux, overnight; (ii) THF, NH₄OH, RT, overnight; (iii) POCl₃ (20 eq), 115 °C, 1 h; (iv) ICl (2.5 eq), CHCl₃, RT, overnight; (v) Dioxane, TEA, appropriate alkyne (1.2 eq), Pd₂(dba)₃ 5%, CuI 10%, RT, 5 min. (vi) CPME, appropriate Grignard reagent (R₁MgBr) (2 eq), RT, 30 min-1 h. (vii) CPME, appropriate Grignard reagent (R₁MgBr) (2 eq), ZnI₂ (1 eq), I₂ (3 eq), RT, 30 min – 1 h

III. Design of the New Series of Compounds

The objective of this work is the synthesis of new and potent imidazo[1,2-*a*:4,5-*c'*]dipyridines as anticancer agents. From the preliminary screening, we chose **POD108** and **POD118** as hit compounds, because of their promising activity.

Taking into account the β -carbolines SAR described in the conclusion of chapter 2 and to ensure variety in terms of electronic, steric, and hydrophobicity effects on target analogues, four main strategies toward new imidazo[1,2-*a*:4,5-*c'*]dipyridine analogues are proposed (**Figure 60**):

1. Introducing secondary amines, phenyl, halo substituted phenyl, methyl, methoxy, and other alkyl and aryl moieties at position 1.
2. As we are limited with the commercial availability of the corresponding alkynes to install the desired heteroaryls in 3-position, we will in a first time investigate the effect of introducing pyridinyl, methyl, phenyl, and hydrogen moieties at this position.
3. Installing bromine and different alkyl, alkynyl and aryl moieties at position 7 as the position 6 of β -carbolines (position 7 in our series) was poorly studied.⁷ In addition, introducing 7-methoxy moiety by analogy with harmine (**R**₇= OMe).
4. Introducing benzyl and ethyl groups at position 10.

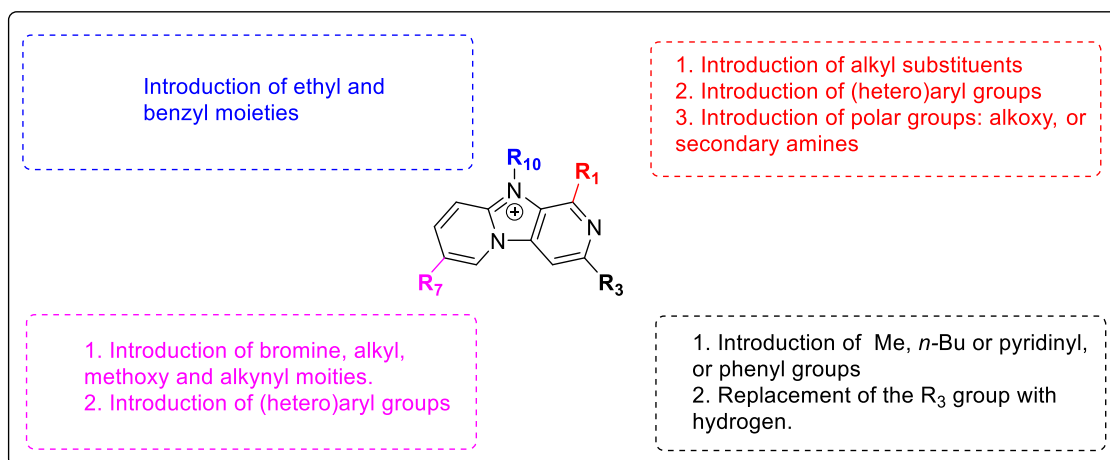
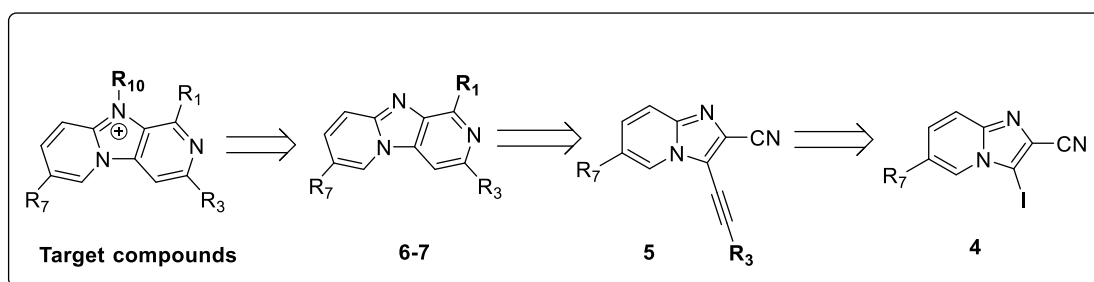


Figure 60: Overview of the planned modifications on imidazo[1,2-*a*:4,5-*c'*]dipyridine motif

The overall design strategy was then to combine the best structural features from **R₁**, **R₃**, **R₇** and **R₁₀** to produce analogues with improved anticancer activity.

IV. Personal Work

Herein, I describe the synthetic approaches that were utilized to access target compounds with the desired moieties at **R₁**, **R₃**, **R₇** and **R₁₀** as shown in **Scheme 10**.



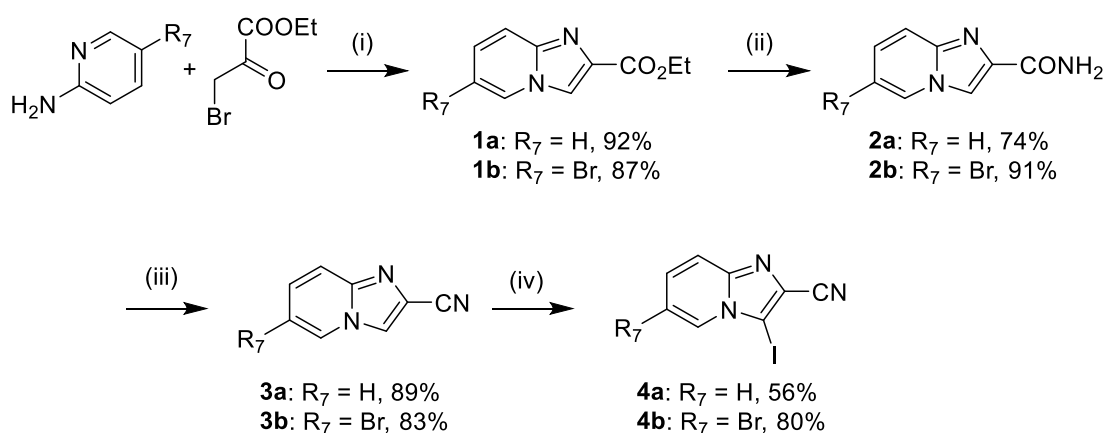
Scheme 10: Retrosynthesis of target compounds

IV-1. Synthesis of the 3-Iodo-2-cyanoimidazo[1,2-*a*]pyridines as Common Starting Materials

The synthetic route described in the previous publications has been scaled up to yield more than 3 g of **4a** (**Scheme 11**) which was subsequently used as a common starting material for the following reactions. These large-scale reactions were carried out using 5 g (53 mmol) of 2-aminopyridine; good yields were obtained for the three subsequent products **1a**, **2a**, and **3a** (92, 74, 89%, respectively). Nitrile **3a** in the presence of ICl in chloroform produced **4a** in a moderate yield (56%).

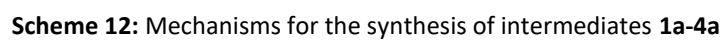
With the aim to explore the 6 position of the scaffold (the 7 position of the future tricyclic compound), I extended during my thesis this synthetic route to 2-amino-5-bromopyridine starting material (**Scheme 11**) leading to compound **4b** in gram scale reactions using similar

reaction conditions for the synthesis of **1b**, **2b** and **3b** (87, 91, 83%, respectively). In order to improve the yield of the iodination step, I used another protocol previously used in the laboratory, using *N*-iodosuccinimide (NIS) in refluxing acetonitrile for the synthesis of **4b** that appears to be more efficient, and gave excellent yield (80%) using 8.4 g (37.8 mmol) of compound **3b**.²¹¹



Scheme 11: Gram Scale reactions toward synthesis of **4a** and its 7-brominated derivative **4b**. *Reagents and conditions:* (i) a) DME, RT, 5h b) EtOH, Reflux (90 °C), overnight; (ii) THF, NH₄OH, RT, overnight; (iii) POCl₃ (20 eq), 115 °C, 1-3 h; (iv) **4a:** ICl (2.5 eq), CHCl₃, RT, overnight; **4b:** NIS (1.3 eq), CH₃CN, Reflux, overnight

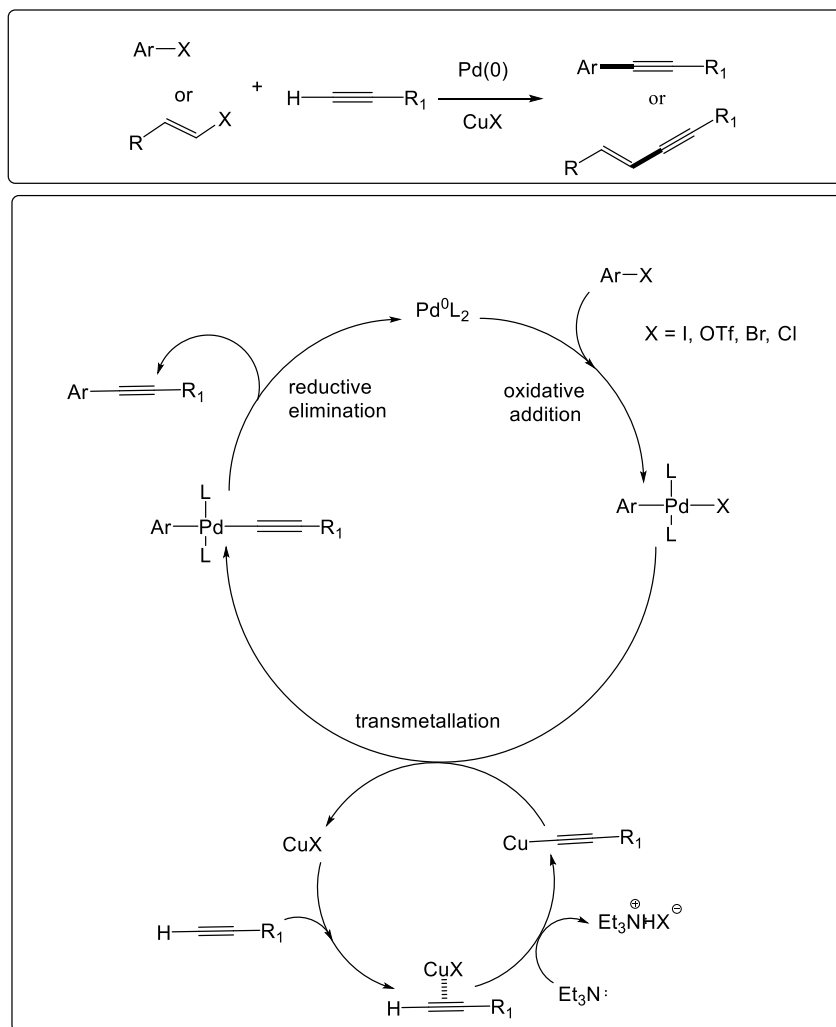
The reaction mechanisms for the synthesis of intermediates **1a-4a** are summarized in **Scheme 12**. Firstly, the nitrogen of pyridine serves as a nucleophile in making a new bond to C-3 of ethyl bromopyruvate. The extracyclic amino group attack the carbonyl carbon which then undergoes heterocyclization to afford ester **1a**. Then, NH₃ bonds to the electrophilic carbonyl carbon atom of ester **1a** to create a tetrahedral intermediate. This intermediate then undergoes elimination of ethanol to yield the amide **2a**. After, the dehydration of amide **2a** to produce nitrile **3a** occurs by the initial reaction of POCl₃ on the nucleophilic amide oxygen atom, followed by deprotonation and a subsequent E2-like elimination reaction. Lastly, the electrophile I⁺ attacks the C-3 of **3a** to form a cation. Then the proton was removed from the carbon that formed the bond with the electrophile to afford **4a**.



IV-2. Sonogashira Cross-Coupling Reaction at Position 3

Sonogashira cross-coupling reaction is a copper-palladium catalyzed coupling of terminal alkynes with aryl and vinyl halides or triflates to form sp^2 - sp C-C bond. The reaction requires a base to neutralize the hydrogen halide produced as the by-product of this coupling reaction. The reactivity order of the leaving group is as: $I \approx OTf > Br \gg Cl$.²¹²

Sonogashira cross-coupling reaction proceeds via a catalytic cycle as shown in **Scheme 13**. Organohalides ($Ar-I$) and $Pd(0)$ participate in ligand coupling processes. $Pd(0)$ is readily oxidized to $Pd(II)$, with simultaneous oxidative addition into the C-I bond, to give a *cis*-organopalladium complex, which rapidly equilibrates to the *trans*-system. The base triethylamine deprotonates the alkyne, to give an acetylide anion, which reacts with the copper iodide to give a copper acetylide. The *trans*-palladium complex undergoes transmetalation (metal-metal exchange) with the copper acetylide to give a new palladium complex, with the two principal ligands in a *trans*-arrangement. Equilibration to the *cis*-system permits reductive elimination, giving the attempted product, and releases $Pd(0)L_2$ which then catalyzes the next reaction. There are two hypothesis for the formation of $[Pd(0)L_2]$ complex: 1) it can be formed from $Pd(0)$ complexes like $Pd(PPh_3)_4$ or, 2) from $Pd(II)$ complexes like $PdCl_2(PPh_3)_2$.

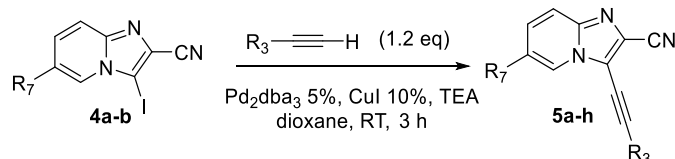


Scheme 13: Mechanism of Sonogashira cross-coupling

Table 5 depicts different alkynes that were coupled to **4a-b**. High yields values (74-94%) were obtained for the synthesis of **5b-c** and the 7-brominated analogues **5f-g** using ethynylcyclopropane and 3,3-dimethylbut-1-yne. The phenylethynyl **5d** and its 7-brominated analogue **5h** were obtained in moderate yields of 62 and 50% respectively, using phenylacetylene. Furthermore, the use of less reactive hept-1-yne and ethynylpyridine gave **5a** and **5e** with yield values of 21 and 27%, respectively.²¹³

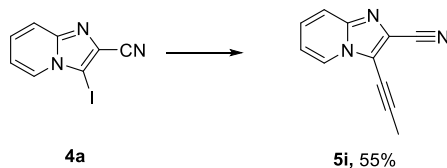
As expected, the Sonogashira coupling reactions occurred on the iodine at position 3 and did not occur at bromine in position 7. Moreover, no clear effect of the bromine atom at the 7 position on the reactivity of the scaffold was noticed.

Table 5: Yields for the synthesis of **5a-h** using terminal alkynes through Sonogashira reaction



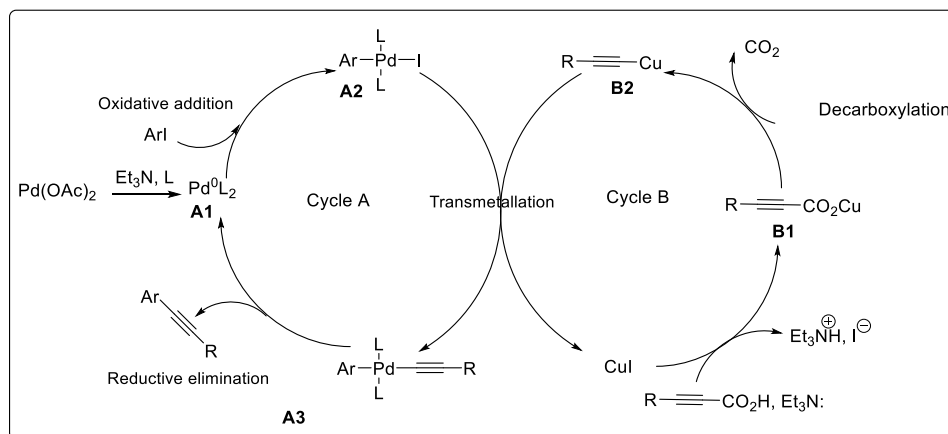
Compound	R ₃	R ₇	Yield
5a	<i>n</i> -Bu	H	21%
5b	<i>c</i> -Pr	H	83%
5c	<i>t</i> -Bu	H	74%
5d	Ph	H	62%
5e	Pyridin-2-yl	H	27%
5f	<i>c</i> -Pr	Br	74%
5g	<i>t</i> -Bu	Br	94%
5h	Ph	Br	50%

Next attention was directed to produce analogues with a smaller functional group such as methyl or hydrogen moieties at position 3. The iodinated intermediate **4a** was successfully coupled with the alkyne 2-butyneic acid through a decarboxylative Sonogashira reaction to yield **5i** (55%) according to the synthetic protocol described by Thibonnet's group (EA SIMBA 7502) (**Scheme 14**).²¹⁴



Scheme 14: Synthetic protocol towards key intermediate **5i**. Reagents and conditions: DMF, TEA, 2-butyneic acid (2 eq), Pd(OAc)₂ 10%, PPh₃ 10%, CuI 5%, MW (50 °C), 2h

The proposed mechanism of decarboxylative Sonogashira reaction (**Scheme 15**) is based on two catalytic cycles: Cycle A which includes the C–C bond coupling with palladium salts, and Cycle B that includes the decarboxylation of alkynyl carboxylic acid catalyzed by copper salts. In the presence of a base such as TEA and CuI, alkynyl carboxylic acid lead to the formation of copper carboxylate **B1** which is subjected to decarboxylation. The formed alkynyl copper **B2** is a common intermediate in Sonogashira coupling reaction. Palladium salts permit the formation of C–C bond via a common mechanism: first, an oxidative addition producing the intermediate **A2** followed by a transmetalation with alkynyl copper **B2** that yield to the complex **A3**. Lastly, a reductive elimination produces the expected arylalkyne target compound and regenerates palladium (0) **A1**.

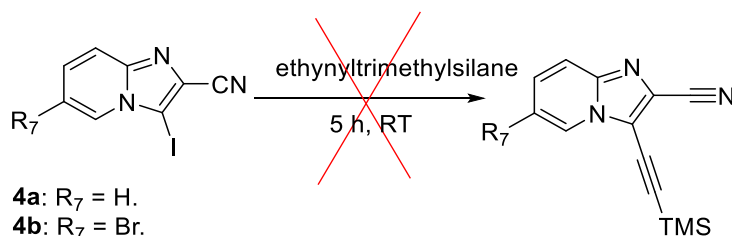


Scheme 15. A plausible mechanism of decarboxylative Sonogashira reaction

In order to synthesize tricyclic intermediates with hydrogen at C-3, we pursued several attempts of coupling reactions with the alkyne ethynyltrimethylsilane as shown in **Table 6**, with the aim to eliminate the trimethylsilane group in a second step. In the first attempt, we adopted a synthetic protocol described by Matulenko *et. al* (entry 1) to couple **4a** to the alkyne, in the presence of $\text{PdCl}_2(\text{PPh}_3)_2$ and TEA in acetonitrile.²¹⁵ This proved to be unsuccessful, forcing us to try another established route using $\text{PdCl}_2(\text{PPh}_3)_2$, CuI and *N,N*-diisopropylethylamine (DIPEA) in acetonitrile (entry 2).²¹⁶ This was unsuccessful too which led us to switch $\text{PdCl}_2(\text{PPh}_3)_2$ to

$\text{Pd}_2(\text{dba})_3$, acetonitrile to less polar solvent dioxane and DIPEA to nucleophilic TEA, also without success (entry 3).

Table 6: Attempts for coupling **4a-b** with ethynyltrimethylsilane



Entry	Starting Material	Catalyst/ligand	Solvent/Base	Result
1	4a	$\text{PdCl}_2(\text{PPh}_3)_2$ 5%	Acetonitrile (3 ml/mol)/ TEA (3 ml/mol)	NR
2	4a	CuI 10%, $\text{PdCl}_2(\text{PPh}_3)_2$ 5%	Acetonitrile (3 ml/mol)/ DIPEA (1 ml/mol)	NR
3	4b	CuI 10%, $\text{Pd}_2(\text{dba})_3$ 5%	Dioxane (1 ml/mol)/ TEA (1 ml/mol)	NR

NR= no reaction.

IV-3. Heterocyclization

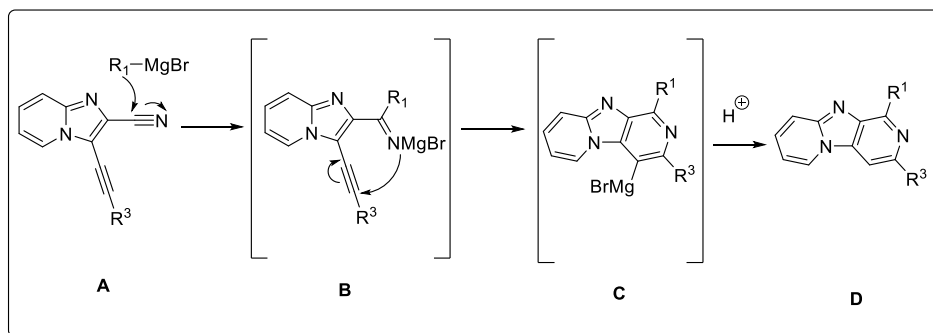
The heterocyclization leading to the imidazo[1,2-*a*:4,5-*c'*]dipyridine scaffold was performed using Grignard reagents as previously described in the publications. In order to extend the scope of the pharmacomodulation at position 1, new alternative protocols were explored to obtain methoxy and amino-substituted compounds.

IV-3.1. Grignard reagent

The tricyclic imidazo[1,2-*a*:4,5-*c'*]dipyridines were obtained by a sequence of addition of Grignard reagent to the nitrile, followed by domino 6-*endo-dig* cyclization reaction on the triple bond at room temperature for 30 minutes to one hour. The Grignard reagent is an organometallic reagent represented by the general formula RMgX , where R is an organic moiety usually alkyl, alkynyl, alkenyl, or aryl group and X a halide (F, Cl, Br, I). Grignard reagent has a partial negative charge on carbon atom, and it can react with a variety of electrophiles (electrophilic centers).

Grignard reagents have been the most widely used organometallic reagents in chemical synthesis since their discovery over a century ago due partly to their ease of preparations from organic halides and magnesium metal in ethereal solvents (diethyl ether and THF).

The 6-*endo-dig* cyclization reaction mechanism involved in the synthesis of imidazo[1,2-*a*:4,5-*c'*]dipyridines through Grignard reactions is proposed to proceed as shown in **Scheme 16**.⁸ The potential mechanism for the cyclization of 3-ethynylimidazo[1,2-*a*]pyridine-2-carbonitriles **A** starts with Grignard reagent addition. This mechanism probably involves an attack by the imine salt intermediates **B** on the triple bond, leading to organomagnesians of type **C**. On addition of aqueous acid, these intermediates are protonated to yield the corresponding imidazo[1,2-*a*:4,5-*c'*]dipyridines **D**.



Scheme 16: Proposed reaction mechanism for the imidazo[1,2-*a*:4,5-*c'*]dipyridine formation through Grignard reactions

As indicated in **Tables 7** and **8**, various Grignard reagents were utilized to access the corresponding tricyclic **6a-o** from the 7-hydrogeno **5b-d** or 7-bromo **5f-h** starting materials, respectively.

As shown in **Table 7**, compounds **6a** and **6b** ($R_3 = \text{Ph}$) were produced in low yield (42%) using phenyl and methylmagnesium bromide, while **6c** and **6d** ($R_3 = t\text{-Bu}$) were produced in high yield of 77 and 83%, respectively. Apparently, the reactivity of the starting material seems to be affected by the nature of the alkyne substitution at C-3. Moreover, **6f-h** ($R_3 = c\text{-Pr}$) were synthesized in moderate to high yield of 84, 60, 72% respectively. Only **6e** ($R_3 = t\text{-Bu}$) was obtained in 40% yield contrarily to **6c-d**.

Table 7: Yields for the synthesis of 7-hydrogenated **6a-h** using Grignard reagents

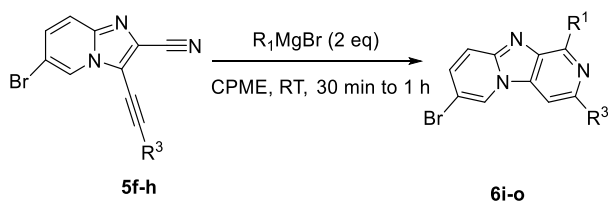
Reaction scheme: **5b-d** $\xrightarrow[\text{CPME, RT, 30 min to 1 h}]{R_1\text{MgBr (2 eq)}}$ **6a-h**

Compound	R_1	R_3	Yield
6a	Ph	Ph	42%
6b	Me	Ph	42%
6c	Ph	<i>t</i> -Bu	77%
6d	Me	<i>t</i> -Bu	83%
6e	Et	<i>t</i> -Bu	40%
6f	Ph	<i>c</i> -Pr	84%
6g	Me	<i>c</i> -Pr	60%
6h	Et	<i>c</i> -Pr	72%

Table 8 illustrates the synthesis of 7-brominated analogues **6i-o** using more diverse Grignard reagents. Apparently, introducing 7-bromo moiety does increase the reactivity of the scaffold toward phenylmagnesiumbromide leading to **6i** and **6j** in excellent yields (85 and 91%, respectively) compared to their non-brominated peers **6a** (42%) and **6c** (77%), respectively. Also, the same yields were observed for the formation of **6o** (74%) and its non-brominated peer **6h** (72%) using ethylmagnesiumbromide. Nevertheless, using more original Grignard reagents, their nature also deeply affects the yield of the reaction. In particular, 4-bisphenylmagnesiumbromide and 4-fluorophenylmagnesiumbromide afforded **6l** and **6n** in low yields (40 and 34%, respectively)

which may be due to the steric effect of the biphenyl group and the presence of fluorine deactivation group, respectively. Finally, thienylmagnesiumbromide reagent produced **6m** in moderate yield (63%).

Table 8: Yields for the synthesis of 7-brominated **6i-o** using Grignard reagents

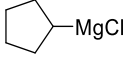
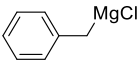
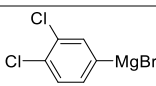


Compound	R ₁	R ₃	Yield
6i	Ph	Ph	85%
6j	Ph	<i>t</i> -Bu	91%
6k	Me	<i>t</i> -Bu	42%
6l	4-Bisphenyl	<i>t</i> -Bu	40%
6m	Thien-2-yl	<i>t</i> -Bu	63%
6n	4-Fluorophenyl	<i>t</i> -Bu	34%
6o	Et	<i>c</i> -Pr	74%

Many Grignard reactions failed to produce clean products as illustrated in **Table 9**. In each attempt, the desired product was never cleanly separated from other contaminants preventing us to provide an unambiguous structure of the target compounds from the NMR spectrum. The presence of the ethynylpyridine substituent at position 3 (entry 1) may prevent the heterocyclization of **5g** to produce the desired derivative. As expected, the use of organomagnesium chloride such as cyclopentylmagnesium chloride or benzylmagnesium chloride affected their reactivity toward **5e** (entries 2 and 3) compared to the bromide analogues. Also, the two chlorine atoms in the 3,4-dichlorophenylmagnesium bromide inhibited the nucleophilic addition by deactivating the Grignard reagent (entry 4). Further, reaction entries 2 and 4 were attempted twice without obtaining the desired products.

Table 9: Attempts for cyclizing **5e** and **5g** with Grignard reagents

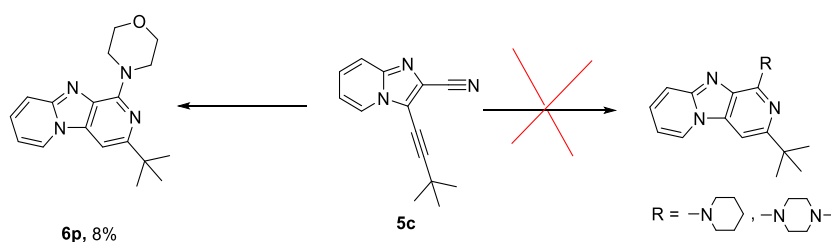
5e and 5g

Entry	Grignard reagent	R ₃	R ₇	Result
1	CH ₃ MgBr 3M	Pyridin-2-yl	H	CM
2	 12M	<i>t</i> -Bu	Br	CM
3	 1.4M	<i>t</i> -Bu	Br	CM
4	 0.5M	<i>t</i> -Bu	Br	CM

CM= complex mixtures.

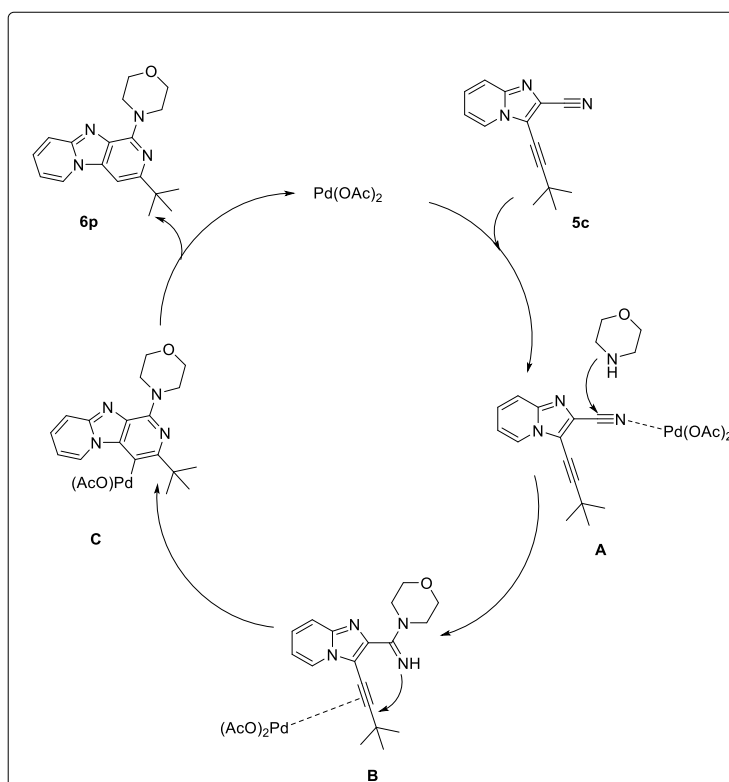
IV-3.2. Secondary amines reagent

Intending to generate secondary amines at C-1, we adopted a synthetic protocol described by Kumar group on 2-chloroquinoline-3-carbonitriles.²¹⁷ They used Pd(OAc)₂ (5%), PPh₃ (10%), morpholine (2 eq) and K₂CO₃ (2 eq) in acetonitrile at 80 °C overnight to afford the desired amine form carbonitriles. No reaction occurred using piperidine and 1-methylpiperazine, whereas morpholine gave the desired product **6p** in very low yield (8%) and in mixture with the starting material (**Scheme 17**).



Scheme 17: Synthetic protocol towards target compound **6p** and attempts for synthesizing 1-methylpiperazine and 1-piperidine analogues. *Reagents and conditions:* Secondary amines reagent (such as morpholine, 1-methylpiperazine, and piperidine; 2 eq), acetonitrile, PPh₃ 10%, Pd(OAc)₂ 5%, K₂CO₃ (2 eq), 80 °C, overnight

The proposed reaction mechanism was depicted in **Scheme 18**. In this reaction, $\text{Pd}(\text{OAc})_2$ plays two roles: firstly as a Lewis acid, which forms complex **A** with the nitrogen atom of the cyano group, facilitating the nucleophilic attack of the amine on the carbon atom of the cyano group; secondly, as a transition-metal catalyst, which forms complex **B** with the π -electrons of the alkyne. The intermediate **B** undergoes heterocyclization to yields the intermediate **C**, which upon protodemetalation, gives compound **6p**.



Scheme 18: Proposed reaction mechanism for the formation of **6p**

IV-3.3. Alkoxide reagent

In order to extend the scope of the pharmacomodulation at position 1, a new alternative protocol was developed using sodium methoxide as a nucleophile, in refluxing methanol overnight, to obtain the 1-methoxy substituted compounds.

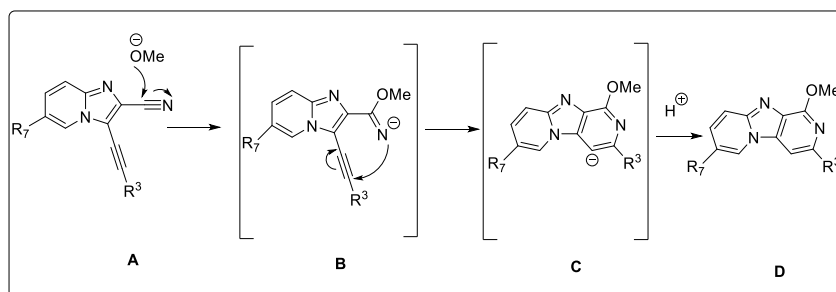
As illustrated in **Table 10**, tricyclic **6q-v** were obtained in low to moderate yields (traces to 57%), which were lower than those obtained using Grignard reagents. This may be attributed to the lower strength of alkoxides compared to carbanion nucleophiles. A low yield was obtained for **6q** (21%) with methyl at position 3. Presence of a bulky moiety at 3-position enhanced the yield as displayed by **6r**, **6s**, and **6t** (39-57%) with *c*-Pr, *t*-Bu and Ph at 3-position. In the reaction of MeONa with **5a** (R_3 = *n*-Bu), a trace amount of a new product was observed (entry 4), however, the poor yield precluded characterization. Moreover, slightly improved yield values were obtained for the synthesis of the 7-bromo derivatives **6u** and **6v** (43 and 47%), compared to their 7-unsubstituted analogues **6s** and **6t** (39 and 44%), respectively.

Table 10: Yields for the synthesis of **6q-v** using methoxide reagent

Reaction scheme: **5a-d, 5g-i** + MeONa 5% / MeOH, Δ overnight \rightarrow **6q-v**

Entry	SM	Product	R_3	R_7	Yield
1	5i	6q	Me	H	21%
2	5b	6r	<i>c</i> -Pr	H	57%
3	5c	6s	<i>t</i> -Bu	H	39%
4	5a	-	<i>n</i> -Bu	H	Trace
5	5d	6t	Ph	H	44%
6	5g	6u	<i>t</i> -Bu	Br	43%
7	5h	6v	Ph	Br	47%

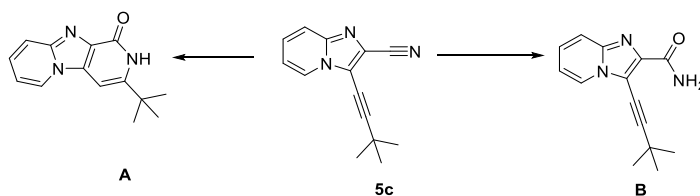
The formation of 1-methoxyimidazo[1,2-*a*:4,5-*c'*]dipyridines can be rationalized in terms of an initial nucleophilic addition of $\text{CH}_3\text{O}^-\text{Na}^+$ on the slightly positive carbon center of the carbonitrile **A** to give the intermediate **B** which cyclized to give **C**. This intermediate is protonated to yield the corresponding imidazo[1,2-*a*:4,5-*c'*]dipyridine derivative **D** (**Scheme 19**).²¹⁸



Scheme 19: Possible reaction mechanism for synthesis of 1-OMe analogues

Having successfully performed the nucleophilic addition and the subsequent cyclization as described above, we decided to explore a similar strategy for the synthesis of new alkoxy analogues such as 1-ethoxy and 1-isopropoxy moieties (**Table 11**). However, upon applying the above-mentioned conditions for cyclization of **5c** ($\text{R}_3 = t\text{-butyl}$) using nucleophiles EtONa and *i*-PrONa at refluxing ethanol at 80°C overnight, we noticed the formation of an O-dealkylated product that could be identified as pyridone **A** (entry 1). We tried to avoid the formation of **A** by using EtONa at 90°C under microwave irradiation for 1h (entry 2), also without success.

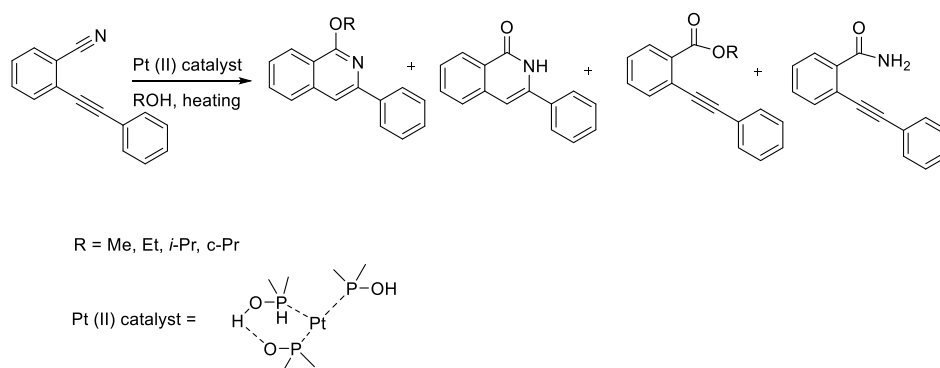
Table 11: Attempts for cyclizing **5c** using sodium alkoxide nucleophiles



Entry	Reagent	Solvent	Temp./ time	Result
1	EtONa (10 eq)	Ethanol (10 ml/mol)	80 °C, Overnight	A
2	EtONa (10 eq)	Ethanol (10 ml/mol)	90 °C MW, 1 h	A
3	<i>i</i> -PrONa (10 eq)	Isopropanol (10 ml/mol)	80 °C, Overnight	A
4	Pt (II) catalyst (0.1 eq)	Ethanol (10 ml/mol)	80 °C, Overnight	B
5	Pt (II) catalyst (0.1 eq)	Isopropanol (10 ml/mol)	80 °C, Overnight	B

The bad results obtained using EtONa and *i*-PrONa nucleophiles urged us to try out other strategies. We found an article published by Li group which discuss the use of [PtH{(PMe₂O)₂H}(PMe₂OH)], known as Parkins catalyst, to synthesize various alkoxy derivatives.²¹⁹ Using 10 % of Pt(II) catalyst in refluxing ethanol or isopropanol for 16h, the authors obtained the attempted 1-ethoxy or 1-isopropoxy derivatives, respectively. We decided to adopt this approach using Pt(II) catalyst to synthesize tricyclic derivatives with ethoxy or isopropoxy group at C-1 (entries 4-5) in our series. The reactions were followed by TLC, nitrile **5c** was hydrolyzed to amide **B** in both attempts.

In their publication, Li group also documented that the reaction of carbonitriles using MeOH, EtOH, *i*-PrOH, *c*-PrOH and Pt(II) catalyst produced a mixture of products including 1-alkoxy pyridine compounds, pyridone, esters and amides derivatives as shown in **Scheme 20**. Fortunately, we did not encounter this problem during the synthesis of various 1-methoxy derivatives using sodium methoxide nucleophile but only with sodium ethoxide and sodium isopropoxide. With these unpromising results and no precedent for such reactions, this approach was not pursued any further.



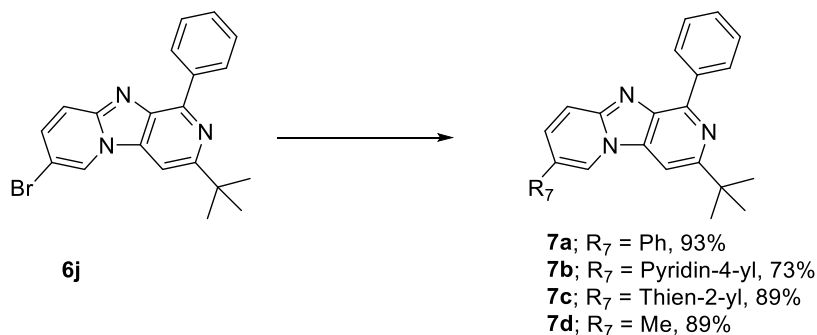
Scheme 20: Effects of Pt(II) Parkins catalyst on carbonitrile reported by Li group

IV-4. Suzuki-Miyaura and Copper-Catalyzed Cross-Coupling Reactions on the 7 Position

We chose **6j** and **6u** as starting materials to produce new analogues with a variety of moieties at C-7 using various palladium-catalyzed Suzuki-Miyaura and Sonogashira cross-coupling, and copper-catalyzed cross-coupling of amides.

IV-4.1. Suzuki-Miyaura cross-coupling

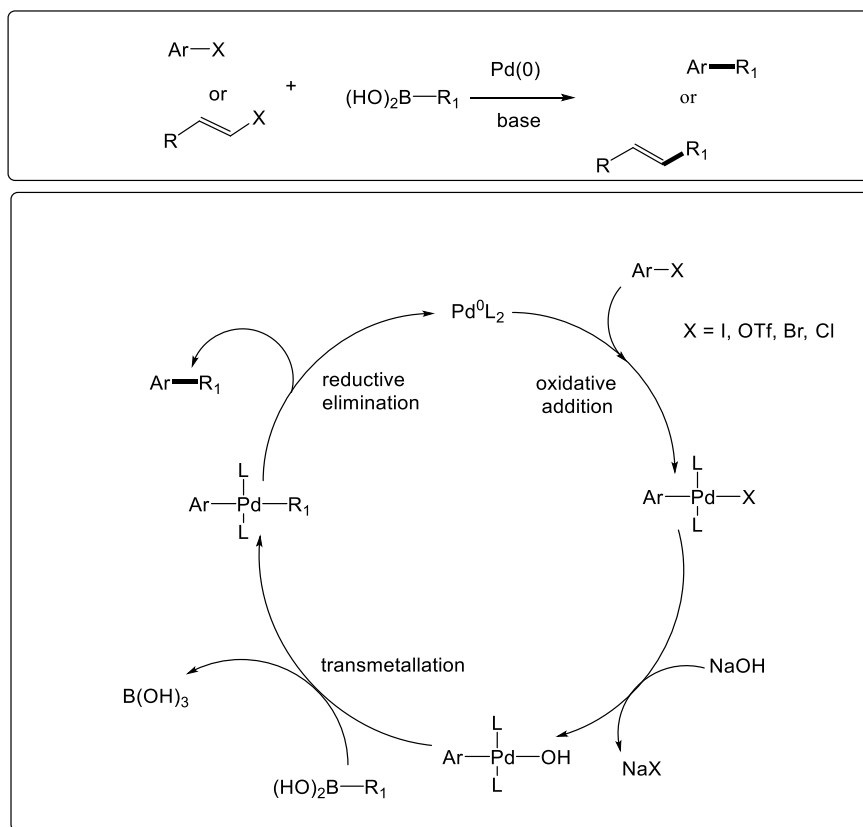
Using organoboron reagents in Suzuki-Miyaura cross-coupling conditions, we introduced at position 7 a small alkyl group (methyl), an aryl (phenyl) or an heteroaryl (thienyl or pyridyl) moieties. Starting from **6j** in the presence of boronic acids and using 5 mol% PdCl₂(PPh₃)₂ as catalyst, Na₂CO₃ as base and DMF/water as solvents, the expected compounds **7a–d** were obtained in high yields (73-93%) (**Scheme 21**).³²



Scheme 21: Synthetic protocol towards target compounds **7a–d**. *Reagents and conditions:* DME/H₂O, R₇B(OH)₂ (1.1 eq), Na₂CO₃ (2 eq), PdCl₂(PPh₃)₂ 10%, MW (100 °C), 2h

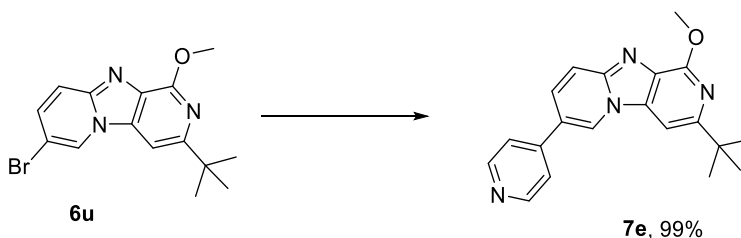
Suzuki-Miyaura (SM) reaction is one of the most efficient and well-known cross-coupling reactions, first published in 1979 by Norio Miyaura, Kinji Yamada, and Akira Suzuki.²²⁰ This palladium-catalyzed coupling is conducted in the presence of a base, to combine an organoboron and an organohalide molecules to form a biaryl through the formation of a new C–C bond. Although, couplings such as Negishi, Stille and Himaya can form C–C bonds, the SM reaction provides several advantages. The popularity of this cross-coupling is due to its exceptional

functional group tolerance, mild reaction conditions and high chemoselectivity. The SM reaction is both air and moisture tolerant, and is conducted at low temperatures and in a variety of solvents, including water.^{221,222} Boronic acids are the most commonly used SM organoboron reagents. The use of boronic acids also assists purification of the cross-coupling product, as the by-product, boric acid, can be easily removed by aqueous base extraction. The general mechanism of the SM reaction is shown in **Scheme 22**.²²³



Scheme 22: General mechanism for SM cross-coupling reaction

The same work was then performed using **6u** ($\text{R}_1 = \text{OMe}$). We successfully synthesized the desired analogue **7e** in the same previously described conditions in excellent yield (99%) (**Scheme 23**).

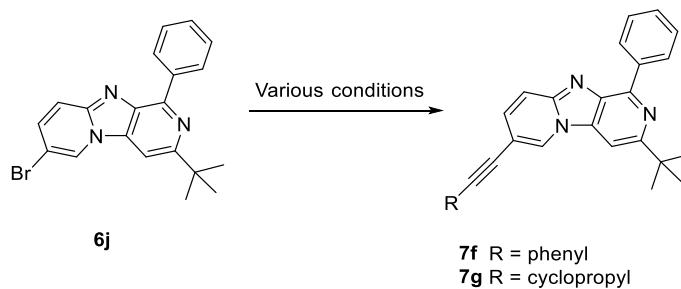


Scheme 23: Synthetic protocol towards target compound **7e**. *Reagents and conditions:* DME/H₂O, 4-pyridylB(OH)₂ (1.1 eq), Na₂CO₃ (2 eq), PdCl₂(PPh₃)₂ 10%, MW (100 °C), 2h

IV-4.2. Sonogashira cross-coupling

Synthesis of imidazo[1,2-*a*:4,5-*c'*]dipyridine analogues with alkynyl moiety at 7-position was planned. Many difficulties (**Table 12**) were encountered when we attempted the coupling of 7-brominated **6j** with alkynes (entries 1-4) as aryl bromides are less reactive than aryl iodides. The first attempt (entry 1) was based on Pd-catalyzed coupling reaction between phenylacetylene and **6j** in the presence of PdCl₂(PPh₃)₂ 6%, DIPEA (2 ml/mol), and CuI 10% in THF at room temperature for 4 h then 60 °C overnight, without success. In the second attempt (entry 2), we used less polar solvent dioxane, nucleophilic TEA, and Pd₂(dba)₃ catalyst at room temperature for 4 h then 80 °C overnight, but the result was not different. In the third attempt (entry 3), a successful synthesis of compound **7f** was finally achieved in 69% yield using PdCl₂(PPh₃)₂ as catalyst, TEA, CuI 10% in DMF at 80 °C for 5h.

We decided to explore the same strategy for the synthesis of 7-cyclopropylethynyl substituent from **6j** (entry 4). This route was successful to lead to analogue **7g** in a low yield (19%) due to the presence of a products mixture difficult to purify.

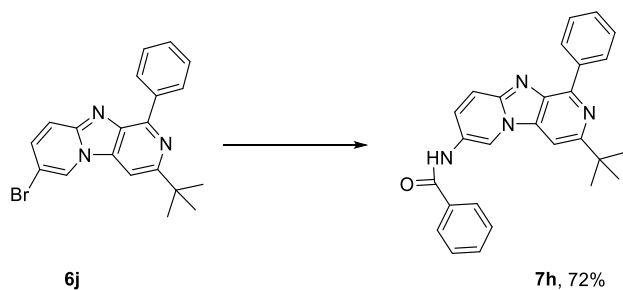
Table 12: Attempts for Sonogashira cross-coupling

Entry	Catalyst/ligand	Solvent, Base	Temperature/ time	Result	Yield
1	Phenylacetylene (1.5 eq), PdCl ₂ (PPh ₃) ₂ 6%, CuI 10%	THF (2 mL/mol), DIPEA (2 mL/mol)	RT for 4 h then 60 °C overnight	NR	-
2	Phenylacetylene (2.2 eq), Pd ₂ (dba) ₃ 5%, CuI 10%	Dioxane (1 mL/mol), TEA (1 mL/mol)	RT for 4 h then 80 °C overnight	NR	-
3	Phenylacetylene (2 eq), PdCl ₂ (PPh ₃) ₂ 10%, CuI 10%	DMF (0.25 mL), TEA (0.25 mL)	80 °C, 5h	7f	69%
4	Ethynylcyclopropane (2 eq), PdCl ₂ (PPh ₃) ₂ 10%, CuI 10%	DMF (0.25 mL), TEA (0.25 mL)	80 °C, 5h	7g	19%

NR = no reaction

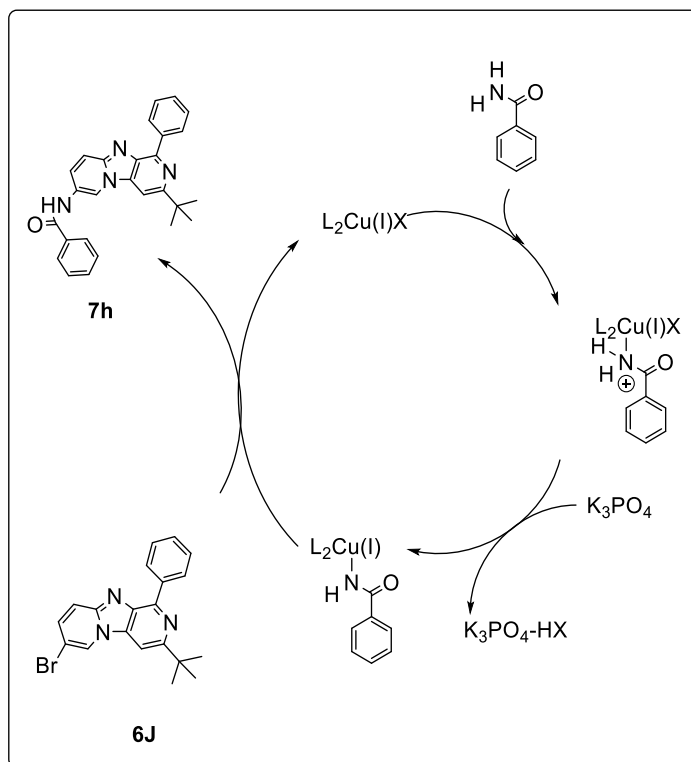
IV-4.3. Copper-catalyzed cross-coupling of amide

From the experience of the laboratory²²⁴, we wished to investigate the effect of introducing amide moiety at C-7. The copper-catalyzed *N*-arylation of benzamide with aryl bromide **6j** proceeded in the presence of CuI, *trans* *N,N'*-dimethylcyclohexane-1,2-diamine as a ligand and K₃PO₄ in toluene under microwaves irradiation at 100°C for 30 min and then at 130°C for 30 minutes leading to compound **7h** (72%) (**Scheme 24**).



Scheme 24: Synthetic protocol towards target analogue **7h**. *Reagents and conditions:* Toluene, benzamide (1.2 eq), *trans* *N,N'*-dimethylcyclohexane-1,2-diamine (0.1 eq), CuI 10%, K₃PO₄ (2eq), MW, 100°C for 30 min then 130 °C for 30 min

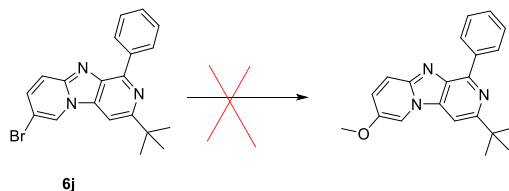
The proposed mechanism of Cu-catalyzed cross-coupling of amides with aryl halides is depicted in **Scheme 25**. Cu-catalyzed amidation reactions of aryl halides initiate by addition of the nucleophile to a L₂Cu(I)X complex to provide an L₂Cu(I)amidate, followed by product formation.²²⁵



Scheme 25: Proposed reaction mechanism for the formation of **7h**

IV-4.4. Copper-catalyzed methoxylation

We wished to investigate the effect of introducing 7-methoxy to the imidazo[1,2-*a*:4,5-*c'*]dipyridine core by analogy with harmine (**R**₇= OMe) using optimized protocol described by Sato group (**Scheme 26**).²²⁶ Unfortunately, the synthetic effort towards this compound was nonproductive, ending with the debrominated derivative.



Scheme 26: Synthetic protocol towards 7-methoxy based analogue. *Reagents and conditions:* DMF, MeONa (10 eq), CuI 10%, 150 °C, 24h

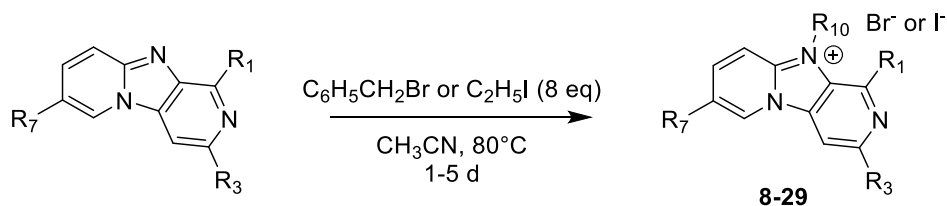
IV-5. Synthesis of Imidazo[1,2-*a*:4,5-*c'*]dipyridine Salt Analogues

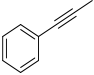
When we tried to test the newly synthesized imidazo[1,2-*a*:4,5-*c'*]dipyridines *in vitro*, we encountered problems of poor solubility. To solve this problem, all these compounds were converted into quaternary ammonium salts **8-29**, after nucleophilic substitution reaction with benzyl bromide or ethyl iodide in acetonitrile at 80°C for 1-5 days as depicted in **Table 13**. The mechanism is illustrated in **Scheme 27** in which the N-10 functions as the nucleophile and attacks the electrophilic C of the BnBr displacing the bromide and creating the new C-N bond. Salt formation not only aimed to improve the solubility but also to introduce substituent on the 10-position, which has already been shown to be beneficial for antiproliferative activity against cancer cell lines in the β -carboline series (See chapter 2, section VI.).



Scheme 27: Mechanism of salt formation

Table 13: Isolated yields for imidazo[1,2-*a*:4,5-*c'*]dipyridine target salts **8-29**



Compound	R ₁	R ₃	R ₇	R ₁₀	Yield
8	Et	<i>c</i> -Pr	H	Et	15%
9	Et	<i>c</i> -Pr	Br	Bn	20%
10	Ph	<i>c</i> -Pr	H	Et	44%
11	Ph	<i>c</i> -Pr	H	Bn	55%
12	OMe	<i>c</i> -Pr	H	Et	47%*
13	OMe	<i>c</i> -Pr	H	Bn	43%*
14	Me	<i>t</i> -Bu	Br	Bn	99%
15	Me	<i>t</i> -Bu	H	Et	63%
16	Et	<i>t</i> -Bu	H	Bn	40%
17	OH	<i>t</i> -Bu	H	Bn	80%
18	OMe	<i>t</i> -Bu	H	Bn	50%*
19	Ph	<i>t</i> -Bu	H	Bn	34%
20	Ph	<i>t</i> -Bu	Br	Bn	33%
21	Ph	<i>t</i> -Bu	Me	Bn	53%
22	Ph	<i>t</i> -Bu	Thien-2-yl	Bn	90%
23	Ph	<i>t</i> -Bu	1-benzylpyridinium-4-yl	H	97%
24	Ph	<i>t</i> -Bu	Ph	Bn	97%
25	Ph	<i>t</i> -Bu		Bn	56%
26	OMe	<i>t</i> -Bu	1-benzylpyridinium-4-yl	Bn	32%*
27	Me	Ph	H	Bn	30%
28	OMe	Ph	H	Bn	49%*
29	OMe	Ph	Br	Bn	85%*

* Salts were prepared using 1.5 eq of benzyl bromide or ethyl iodide.

In most of these nucleophilic substitution reactions, the salt transformations were very slow and took very long time (1-5d) to obtain the desired products in acceptable yields. This may be due to the weak nucleophilicity of N-10 of imidazo[1,2-*a*:4,5-*c'*]dipyridine core that affects these SN2 reactions. Moreover, no clear effect of the substituents at positions 1, 3 and 7 on the reactivity of the scaffold was noticed.

During the salt formation, compound **6s** ($R_1 = \text{OMe}$, $R_3 = t\text{-Bu}$, $R_7 = \text{H}$) underwent a demethylation of the methoxy group leading to the 1-hydroxy derivative **17**. To avoid this demethylation, the reaction time with benzyl bromide was limited to 24h and lower amount of the electrophile (1.5 eq instead of 8 eq) was used leading to compound 1-methoxy analogue **18**. This optimization was adopted for the synthesis of all 1-methoxy analogues.

Analogue **7b** ($R_1 = \text{Ph}$, $R_3 = t\text{-Bu}$, $R_7 = \text{pyridin-4-yl}$) was benzylated only on the pyridine moiety to afford compound **23** while **7e** ($R_1 = \text{OMe}$, $R_3 = t\text{-Bu}$, $R_7 = \text{pyridin-4-yl}$) was methylated on both 7 and 10 positions leading to **26**. This is supported by electrostatic potential maps around **7b** and **7e** (Figure 61) which displayed higher electron density around 7-pyridine's nitrogen than that of 10 position for analogue **7b**, and high electron densities around both 7-pyridine's nitrogen and 10 position for **7e**.

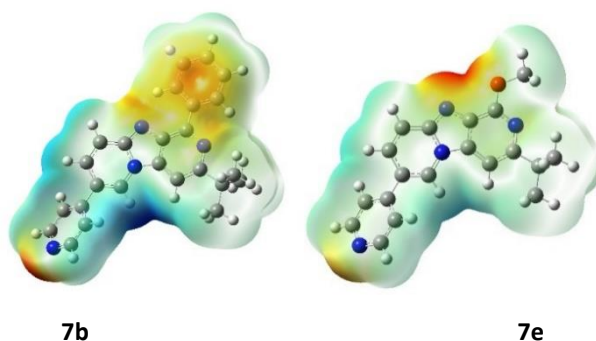


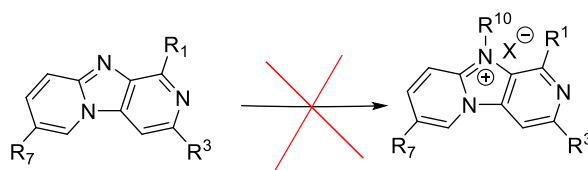
Figure 61. Electrostatic potential maps for **7b** and **7e**.

For the preparation of salts for the biological evaluation we solubilize these salts in DMSO to prepare 100 mM stock solution and further diluting them in the growth medium to obtain five different concentrations (0.01, 0.1, 1, 10, and 100 μM). Salt **25** was soluble in DMSO but not

soluble enough in the growth medium. Moreover, salt **29** was not soluble in either DMSO or methanol. Hence, both compounds were not subjected to biological evaluation.

Despite these salts were successfully synthesized, unfortunately some others were unsuccessful. Many attempts for nucleophilic substitution for salt formation were performed under various conditions to improve the yield: reagent amounts, switch to another more polar aprotic solvent, change of the ratio and reaction duration as illustrated in **Table 14**.

Table 14: Attempts for salt formations using benzyl bromide



Entry	SM	R ₁	R ₃	R ₇	Reagent	Solvent	Temp. /time	Result
1	6a	Ph	Ph	H	BnBr (8 eq)	CH ₃ CN (10 ml/mol)	80°C, 2 d	CM
2	6a	Ph	Ph	H	BnBr (8 eq)	DMF (2.5 ml/mol)	80 °C, 3 d	NR
3	6i	Ph	Ph	Br	BnBr (8 eq)	CH ₃ CN (2.5ml/mol)	80°C, 4 d	NR
4	6l	4-Bisphenyl	t-Bu	Br	BnBr (1.5 eq)	CH ₃ CN (10 ml/mol)	80°C, 2 d	NR
5	6m	Thien-2-yl	t-Bu	Br	BnBr (1.5 eq)	CH ₃ CN (10 ml/mol)	80°C, 2 d	CM
6	6q	OMe	Me	H	BnBr (1.5 eq)	CH ₃ CN (10 ml/mol)	80°C, 2 d	Pyridone
7	7g	Ph	t-Bu	cyclopropylethynyl	BnBr (8 eq)	CH ₃ CN (0.47 ml/mol)	80°C, 5 d	CM
8	7h	Ph	t-Bu	Benzamide	BnBr (8 eq)	CH ₃ CN (1.7 ml/mol)	80°C, 4 d	CM
9	6p	morpholine	t-Bu	H	BnBr (1.5 eq)	CH ₃ CN (10 ml/mol)	80°C, 2 d	Trace

CM= complex mixture, NR= no reaction

Salt formation reactions of **6a** and **6i** with phenyl moieties at C-1 and C-3 (entries 1-3) were the first salts that did not succeed. In the first attempt, **6a** and benzyl bromide in acetonitrile

(entry 1) produced a complex mixture that was difficult to purify. In the second attempt, we tried to use more polar aprotic solvent DMF (entry 2) without success. The third attempt was performed on 7-brominated analogue **6i** (entry 3) in acetonitrile (2.5 ml/mol), also unsuccessfully. These reaction failures may be due to the steric hindrance of phenyl moieties. Thus, **6l** (R_1 = 4-Bisphenyl) (entry 4) was found to be also unreactive to salt formation.

Benzylation of **6m**, **6e** and **7g-h** (entries 5 and 7-8) afforded a mixture of products that were difficult to purify and characterized. Also, **6q** (entry 6) was demethylated in C-1 to produce pyridone. Besides, benzylation of **6p** (entry 9) yielded a trace amount of a new product, however, the yield was poor and precluded characterization.

V. Conclusion

This chapter described the design and synthesis of imidazo[1,2-*a*:4,5-*c'*]dipyridine derivatives. The analogues were designed by employing rational medicinal chemistry principles, and thereafter successfully synthesized by protocols adapted from developed and published synthetic methods.

Different synthetic approaches were utilized to access target compounds with the desired moieties at R_1 , R_3 , R_7 and R_{10} on imidazo[1,2-*a*:4,5-*c'*]dipyridine scaffold summarized in **Scheme 28**.

Desired moieties were coupled at position 3 using terminal alkynes through Sonogashira cross-coupling reactions. Several attempts of coupling reactions with the alkyne ethynyltrimethylsilane to synthesize tricyclic intermediates with hydrogen at C-3 failed to produce the desired product.

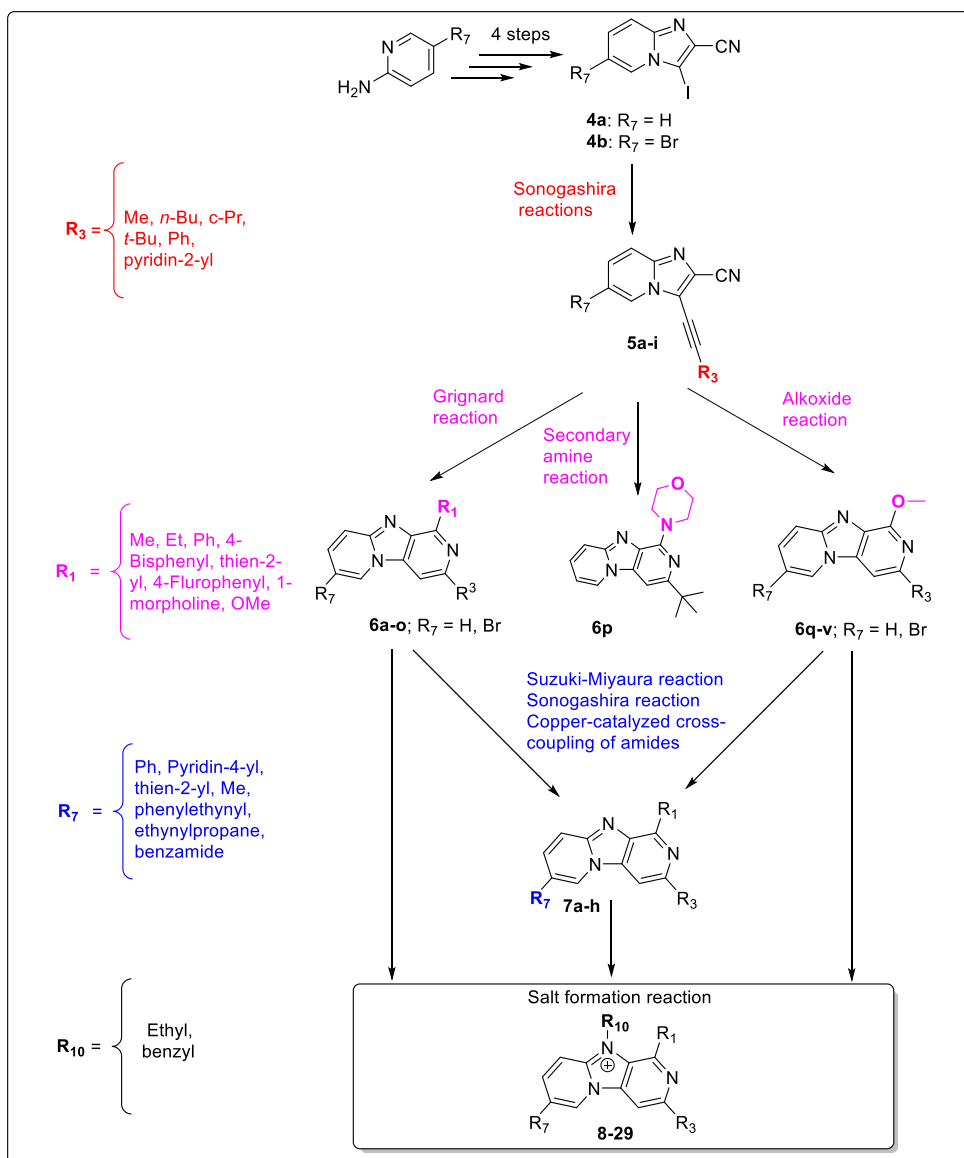
Desired substituents were installed at position 1 through *6-endo-dig* cyclization reactions using Grignard, secondary amine and alkoxide reagents, yielding the tricyclic imidazo[1,2-*a*:4,5-*c'*]dipyridines. The reactivity of the starting material toward Grignard reagents appears to be affected by the nature of the alkyne substitution at C-3. Also, the nature of Grignard reagent greatly affects the reactivity. The use of secondary amine reagent morpholine gave the desired

product in very low yield and in mixture with the starting material, whereas no reaction occurred using piperidine and 1-methylpiperazine. Using alkoxide reagents, desired tricyclics were obtained in lower yield than those obtained using Grignard reagents. Many attempts to synthesize tricyclic with 1-ethoxy and 1-isopropoxy moieties failed to afford the desired product, leading to pyridones and amides.

Desired groups were placed at position 7 through metal cross-coupling reactions using organoboron, and terminal alkynes reagents. Copper-catalyzed methoxylation at C-7 was nonproductive to yield the desired product.

Ethyl and benzyl moieties were attached at position 10 using ethyl iodide and benzyl bromide, respectively, affording target salts **8-29** to improve the solubility and enhance the anticancer activity. Eight compounds could not be salified.

Solutions of salts were prepared and then subjected to biological evaluation which are discussed in chapter 4.



Scheme 28: Synthetic pathways utilized to obtain target analogues

Chapter 4:

Biological Evaluation of Imidazo[1,2-*a*:4,5-*b'*]dipyridines

I. Introduction

Chapter 4 reviews the biological studies that were carried out to evaluate the synthesized analogues for growth inhibition, anti-migratory, and anti-invasion activities. Subsequently, these studies followed a well-defined screening cascade as shown in **Figure 62**, which also showed the criteria that informed the advancement of compounds to various assays.

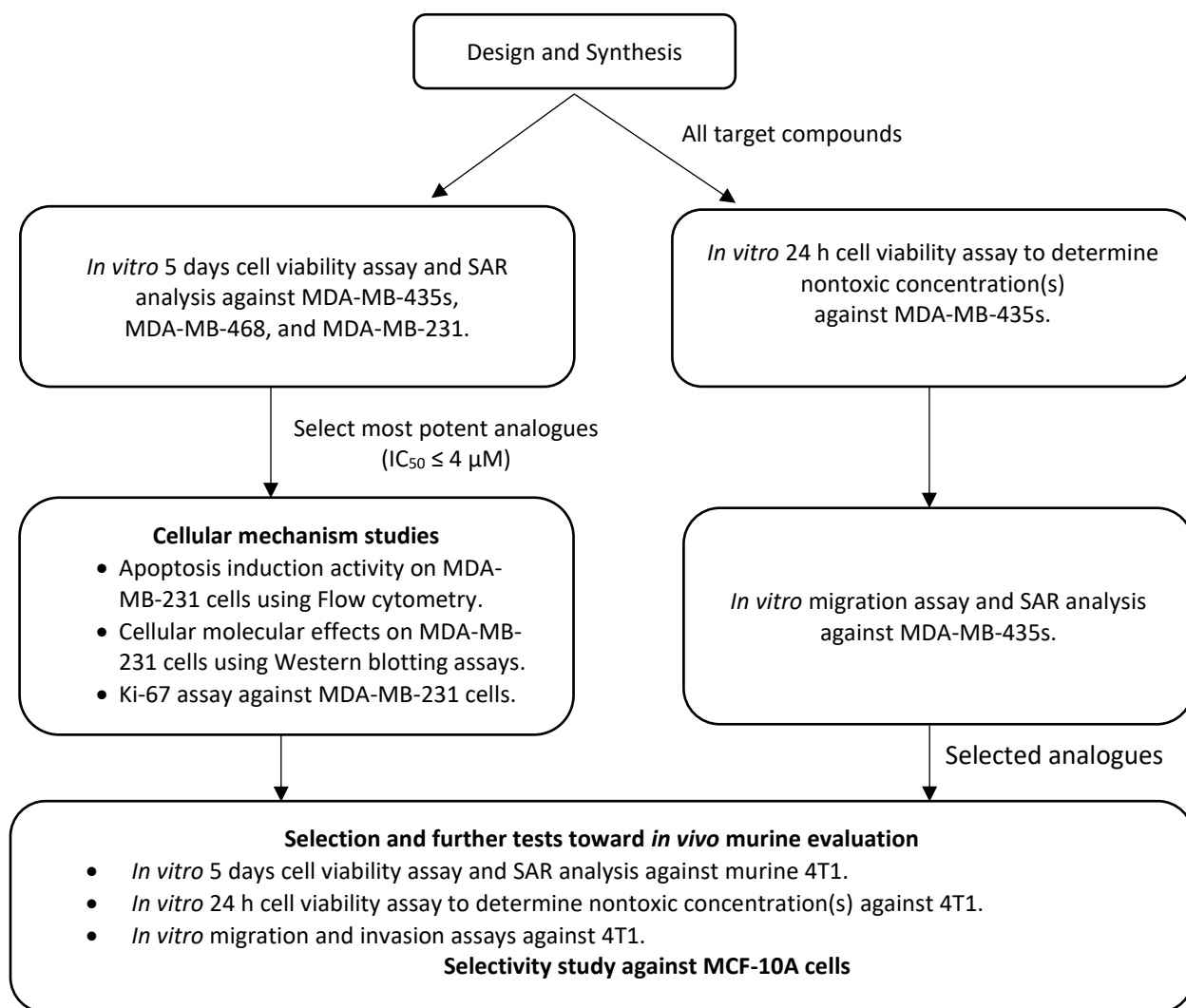


Figure 62: The screening cascade adopted in the biological evaluation of compounds

This chapter principally outlines the hit-to-lead optimization screens. It begins with a discussion on *in vitro* cancer growth inhibition activities as well as the cellular mechanistic studies which were carried out on selected potent compounds. Besides, it addresses the anti-migratory activities of the compounds. This chapter ends up with the selection and further testing toward *in vivo* murine evaluation and selectivity study against MCF-10A cells

II. *In Vitro* Cancer Growth Inhibition Activities

Once synthesized, the target analogues were examined for their *in vitro* growth inhibition of breast cancer cell lines, under replicating conditions. I conducted these assays under the supervision of Lucie Brisson and Sébastien Roger, at UMR INSERM 1069 N2C, Faculty of Medicine, Tours, France.

Three triple-negative human breast cancer (TNBC) cell lines were employed: the MDA-MB-435s-luc, MDA-MB-468-luc, and MDA-MB-231-luc. These cell lines are a representative array of cancerogenic and invasive properties (**Table 15**).²²⁷ MDA-MB-231-luc, MDA-MB-468-luc, and MDA-MB-435s-luc cell lines do not express nuclear progesterone, nuclear estrogen receptors of the ER type, and the HER2 (Human Epidermal Growth Factor Receptor-2) protein, therefore they are used as triple-negative cancer (TNBC) cell model.

Table 15: Characteristics of the human breast cancer cell lines used in the study

Cell line	Histopathological Diagnosis	ER Status	Cancer Stage	Metastasis
MDA-MB-231	IDC	-	IV	+
MDA-MB-435s	IDC	-	IV	+
MDA-MB-468	AC	-	IV	+2

Abbreviations: AC, adenocarcinoma; ER, estrogen receptors; IDC, infiltrating ductal carcinoma.

Test compounds were dissolved in DMSO at a stock solution of 100mM, diluted to 100 μ M in a culture medium, sterilized by passing through a 0.22 μ m pore size filter, then further

diluted to other four different concentrations (0.01, 0.1, 1, and 10 μM) in culture medium before use. The final concentration of DMSO in the culture medium was 0.1% or lower, a concentration without effect on cell replication.

Cell viability is assessed by the MTT (2-(4,5-dimethyl-2-thiazolyl bromide)-3,5-diphenyl-2*H*-tetrazolium). This colorimetric test is based on the reduction of yellow tetrazolium salts to insoluble violet formazan crystals. The reduction of MTT is carried out by oxidoreductases and dehydrogenases predominantly in mitochondria of the metabolically active cells, which makes it possible to assess the number of living cells (**Figure 63**). This relationship can be used to quantify the cytotoxic effects of a test compound; high MTT reduction correlates to high cell viability or low cell toxicity. The lowest concentration of the test compound that inhibited the growth of 50% of cancer cell line population [Inhibitory Concentration (IC_{50})] values were determined using a dose-response curve analysis of the relative fluorescence [emission wavelength at 570 nm] measured on a spectrophotometer.

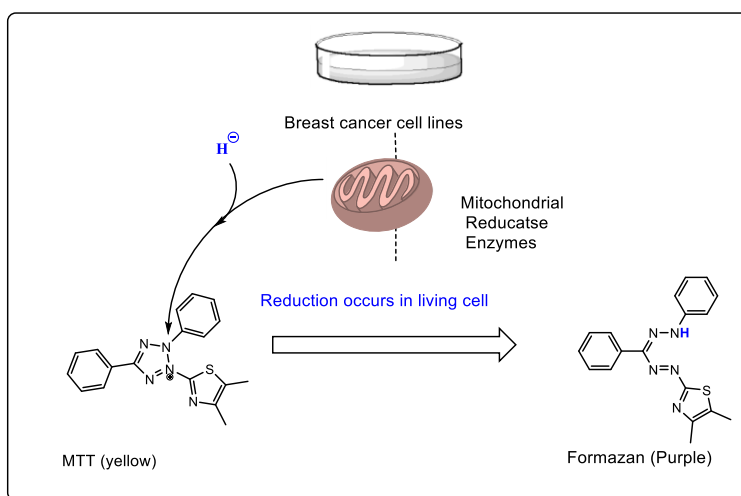
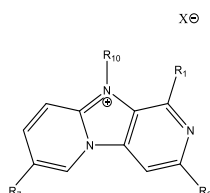


Figure 63: MTT cell viability assay

Taking into account the prevailing SAR of β -carboline, as well as the hits **POD108** and **POD118** from the preliminary screening of imidazo[1,2-*a*:4,5-*c'*]dipyridines, this thesis describes our efforts to introduce modifications at four positions of imidazo[1,2-*a*:4,5-*c'*]dipyridine core to further improve the structural diversity and the growth inhibition activity.

The *in vitro* growth inhibition activities (IC₅₀ values) are depicted in **Table 16** after 24h and 5-days of treatments with the analogues.

Table 16: *In vitro* growth inhibition activities of imidazo[1,2-*a*:4,5-*c'*]dipyridines



	R ₁	R ₃	R ₇	R ₁₀	X	5 days-cell viability (IC ₅₀ μM ± SEM)			MDA-MB-435s-luc 24h-cell viability (IC ₅₀ ± SEM)
						MDA-MB-468-luc	MDA-MB-435s-luc	MDA-MB-231	
POD118*	Me	c-Pr	H	Bn	Br	30.7±11.5	43.9±14.1	NT	>100
POD108*	Me	<i>t</i> -Bu	H	Bn	Br	18.4±6.1	16.4±3.1	NT	74.4±28.0
8	Et	c-Pr	H	Et	I	>100	28.3±4.8	>100	>100
9	Et	c-Pr	Br	Bn	Br	47.1±4.7	62.2±25.8	55.8±12.1	>100
10	Ph	c-Pr	H	Et	I	NT	47.6±20.4	NT	>100
11	Ph	c-Pr	H	Bn	Br	31.1±16.1	13.1±6.5	32.1±4.5	48.6±2.3
12	OMe	c-Pr	H	Et	I	37.7±5.4	6.3±3.0	24.8±3.7	>100
13	OMe	c-Pr	H	Bn	Br	3.6±1.2	1.3±0.1	3.1±0.4	16.3±3.3
14	Me	<i>t</i> -Bu	Br	Bn	Br	11.0±9.2	10.7±0.5	36.0±1.1	59.6±14.8
15	Me	<i>t</i> -Bu	H	Et	I	>100	90.5±0.5	>100	>100
16	Et	<i>t</i> -Bu	H	Bn	Br	8.7±1.7	4.8±0.3	10.7±2.6	35.4±14.6
17	OH	<i>t</i> -Bu	H	Bn	Br	NT	33.4±1.2	NT	>100
18	OMe	<i>t</i> -Bu	H	Bn	Br	0.4±0.4	1.1±0.1	1.7±0.3	11.9±1.7
19	Ph	<i>t</i> -Bu	H	Bn	Br	13.3±2.3	6.4±1.0	11.9±2.3	21.3±8.6
20	Ph	<i>t</i> -Bu	Br	Bn	Br	NT	5.2±0.4	27.6±4.9	29.14±1.7
21	Ph	<i>t</i> -Bu	Me	Bn	Br	NT	NT	>100	>100
22	Ph	<i>t</i> -Bu	Thien-2-yl	Bn	Br	NT	NT	62.9±0.4	30.8±6.5
23	Ph	<i>t</i> -Bu	1-benzyl pyridinium- 4-yl	H	-	NT	NT	>100	>100
24	Ph	<i>t</i> -Bu	Ph	Bn	Br	NT	NT	17.3±5.7	37.2±5.0
26	OMe	<i>t</i> -Bu	1-benzyl pyridinium- 4-yl	Bn	Br	NT	NT	14.3±0.2	NT
27	Me	Ph	H	Bn	Br	1.2±0.9	22.4±1.5	2.8±0.2	>100
28	OMe	Ph	H	Bn	Br	4.7±0.2	5.0±3.5	3.0±0.4	16.9±2.4

*hit compounds, NT = Not tested

As shown in **Table 16**, a general trend of relatively higher IC_{50} in 24h-cytotoxicity test compared to the 5 days antiproliferative activity in MDA-MB-435s-luc, was observed which account for low acute toxicity.

First, we investigated the effect of increasing the steric hindrance of the group at position 1. The influence of position 1 on the anti-proliferative activity will be detailed depending on the substitution at position 3. In the 3-cyclopropyl series, 1-phenyl-bearing compound **11** displayed good activity (IC_{50} = 13.1 μ M) against MDA-MB-435s compared to 1-methyl analogue **POD118** (IC_{50} = 43.9 μ M), while both compounds presented similar activities against MDA-MB-468 (31.1 μ M and 30.7 μ M respectively). In the 3-*tertio*-butyl series, the 1-ethyl- (**16**) and 1-phenyl- (**19**) bearing compounds, exhibited better activities compared to 1-methyl analogue **POD108** against MDA-MB-435s and MDA-MB-468. Moreover, **16** and **19** displayed good activity against MDA-MB-231 cells with IC_{50} values of 10.7 and 11.9 μ M, respectively.

To explore the effect of a methoxy group at C-1, the 1-methoxy analogues **13** (R_3 = *c*-Propyl) and **18** (R_3 = *t*-Butyl) of the corresponding 1-methyl **POD118** and **POD108** were synthesized and exhibited markedly enhanced growth inhibition activity in MDA-MB-435s and MDA-MB-468 cells (IC_{50} = 0.4–3.6 μ M). A similar trend was observed in the 3-phenyl series, comparing the 1-methyl **27** (IC_{50} = 22.4 μ M) and its 1-methoxy analogue **28** (IC_{50} = 5.0 μ M) against MDA-MB-435s. However, both **27** and **28** exhibited slightly similar activities against MDA-MB-468 and MDA-MB-231, and their IC_{50} values ranged from 1.2 to 4.7 μ M. Interestingly, analogues **13**, **18** and **28** (R_1 = OMe, R_7 = H, R_{10} = Bn) displayed remarkable growth inhibition activity regardless of R_3 moiety against the three TNBC cells examined with IC_{50} below 5 μ M.

As the 1-hydroxy compound **17** (analogue of **18**) appeared to be poorly active with a 33-fold drop of the activity (IC_{50} = 33.4 μ M), we concluded therefore at this stage that a methoxy group is the optimal R_1 moiety for growth inhibition activity. Moreover, we tried different synthetic approaches to install 1-ethoxy and 1-isopropoxy moieties to investigate their activity, without success (see chapter 3).

7-Bromo analogue **14** (R_1 = Me, R_3 = *t*-Butyl) exhibited better activities compared to 7-hydrogenated analogue **POD108** against MDA-MB-435s and MDA-MB-468 cells. Moreover, 7-

bromo **20** ($R_1 = \text{Ph}$, $R_3 = t\text{-Butyl}$, analogue of **19**) slightly improved activity against MDA-MB-435s but decreased activity against MDA-MB-231 cells. Besides, all the other substitutions (methyl or heteroaryl groups) were deleterious for the activity on MDA-MB-231. Only, compound **24** ($R_1 = \text{Ph}$, $R_7 = \text{Ph}$, $R_{10} = \text{Bn}$) and compound **26** ($R_1 = \text{OMe}$, $R_7 = 1\text{-benzylpyridinium-4-yl}$, $R_{10} = \text{Bn}$) displayed low activity against MDA-MB-231 (IC_{50} around 15 μM).

Next, we wished to investigate the steric effect at position 10 of **POD108**. The benzyl group of **POD108** was replaced by a smaller ethyl substituent leading to **15** ($R_3 = t\text{-Butyl}$). The growth inhibition activity of **15** was severely affected by this modification with an $\text{IC}_{50} > 90.5 \mu\text{M}$ in all cell lines tested. Also, replacement of 10-benzyl group of **11** ($\text{IC}_{50} = 13.1 \mu\text{M}$) by ethyl group resulted in **10** ($R_3 = c\text{-Propyl}$) with reduced activity ($\text{IC}_{50} = 47.6 \mu\text{M}$) against MDA-MB-435s. Further, the 10-ethyl compound **12** ($R_1 = \text{OMe}$, $R_3 = c\text{-Propyl}$) exhibited 5, 8 and 12-fold lower activity against MDA-MB-435s, MDA-MB-231 and MDA-MB-468, respectively, compared to its 10-benzyl analogue **13**. Moreover, 10-ethyl analogue **8** ($R_1 = \text{Ethyl}$, $R_3 = c\text{-Propyl}$) was poorly active against MDA-MB-435s and totally inactive against both MDA-MB 468 and MDA-MB 231. This clearly demonstrated the superiority of the benzyl group over the ethyl group at the 10 position for the growth inhibition activity.

Based on the previous findings, methoxy substituent at C-1 and 10-benzyl group enhance the activity.

Because of these promising results, the synthesis of selected analogues (**13**, **18**, and **27-28**) were scaled up and subjected to further cellular mechanistic studies.

III. Studies of the Imidazo[1,2-*a*:4,5-*c'*]dipyridines Cellular Mechanism

After determining the *in vitro* growth inhibition activities of imidazo[1,2-*a*:4,5-*c'*]dipyridines, potent analogues were selected and subjected to other biological screens, chiefly aimed at rapidly assessing the mechanism(s) of action for their growth inhibition activity. Although these biological tests do not furnish definitive mechanism(s) of action, they provide a first insight into the cellular processes involved in the showed activity.

A representative batch of imidazo[1,2-*a*:4,5-*c'*]dipyridines analogues **13**, **18**, and **27-28** (**Figure 64**) which demonstrated potent growth inhibition activity [$IC_{50} < 4 \mu M$] against the MDA-MB-231 were selected for further exploration of their mechanism of action. These biological tests include the flow cytometry assay, Western blot and Ki-67 assay described in the following sub-sections.

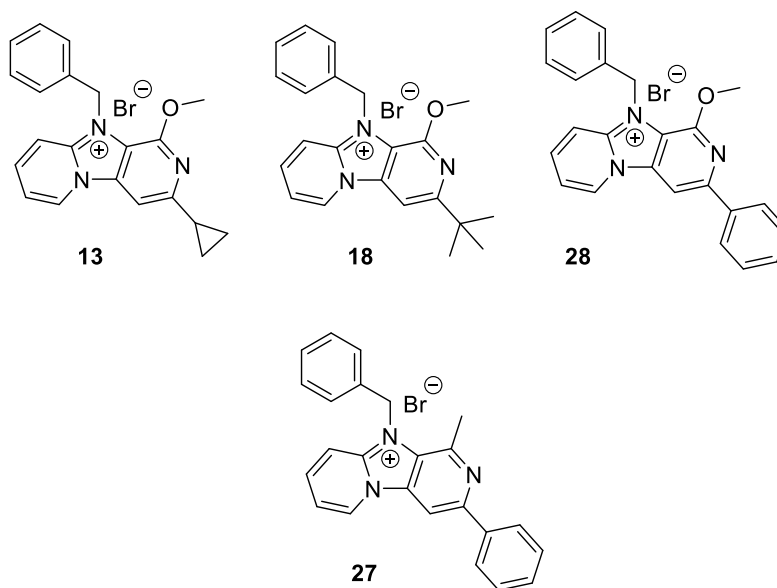


Figure 64: Selective analogues **13**, **18**, and **27-28** with potent growth inhibition activity

III-1. Apoptosis Induction Activity of Imidazo[1,2-*a*:4,5-*c'*]dipyridines

Imidazo[1,2-*a*:4,5-*c'*]dipyridines may induce cancer apoptosis. To further test this hypothesis, the effect of imidazo[1,2-*a*:4,5-*c'*]dipyridines on apoptosis induction were analyzed by using a double staining flow cytometric assay using Annexin-V fluorescein isothiocyanate (FITC) and Propidium Iodide (PI) in MDA-MB-231 cells. Annexin V competes for the phosphatidylserine binding site, which is normally found in the inner leaflet of the cell membrane and is externalized in the early stages of apoptosis while P.I. has the ability to DNA intercalation and is released after the damage of the cell nucleus in the late stage of apoptosis (**Figure 65**).

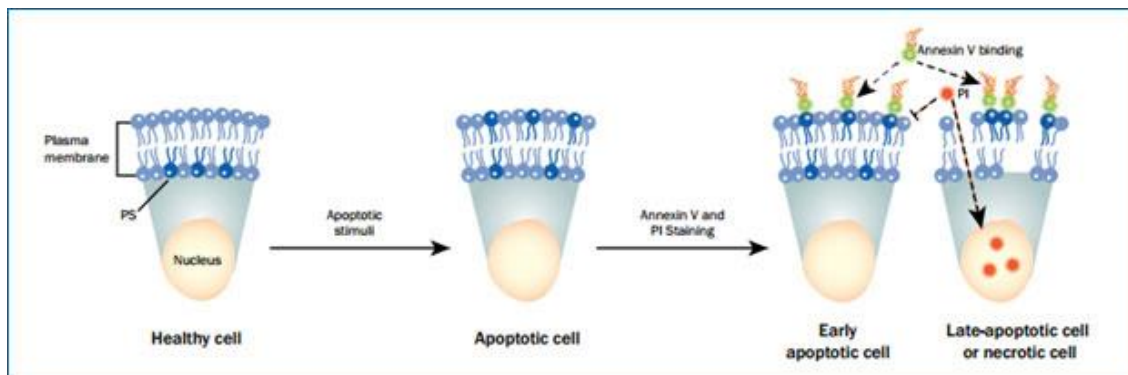


Figure 65: Principles of the FITC Annexin V Apoptosis Assay (Source: novusbio.com/research-topics/apoptosis/phosphatidylserine-externalization)

Data are analyzed as follows: Annexin V-negative/PI-negative population was used as a measure for live cells, Annexin V-positive/PI-negative cells as early apoptotic, and Annexin V-positive/PI-positive cells as late apoptotic and Annexin V-negative/PI-positive cells as necrotic population.

This double staining flow cytometric assay was carried out in MDA-MB-231 cells to evaluate the potential of compounds **13**, **18**, and **27-28** to induce apoptosis in cancer cells. The MDA-MB-231 cells were treated with two different concentrations (3 and 30 μM corresponding to about $1 \times \text{IC}_{50}$ and $10 \times \text{IC}_{50}$) of compounds **13**, **18**, and **27-28** for 48h to detect early apoptotic events (**Figure 66**). DMSO was used in the control condition. Compared to the control group with a total apoptosis rate of 4.87%, almost no effect was observed at 3 μM with apoptosis of 7.4, 6.7, 6.6, and 9.5% for compounds **13**, **18**, and **27-28**, respectively. Nevertheless, at 30 μM the total apoptosis rate strongly increased for compounds **13**, **18**, and **27-28** to 39.2, 37.1, 21.2, and 39.6%, respectively. Necrotic cell population also dramatically increased with 30 μM of 1-methoxy compounds **13**, **18**, and **28** to 26.7%, 24.2%, 43.1%, respectively compared to control (1.02%). Taken together, these compounds induced apoptosis and cell death in MDA-MB-231 cells.

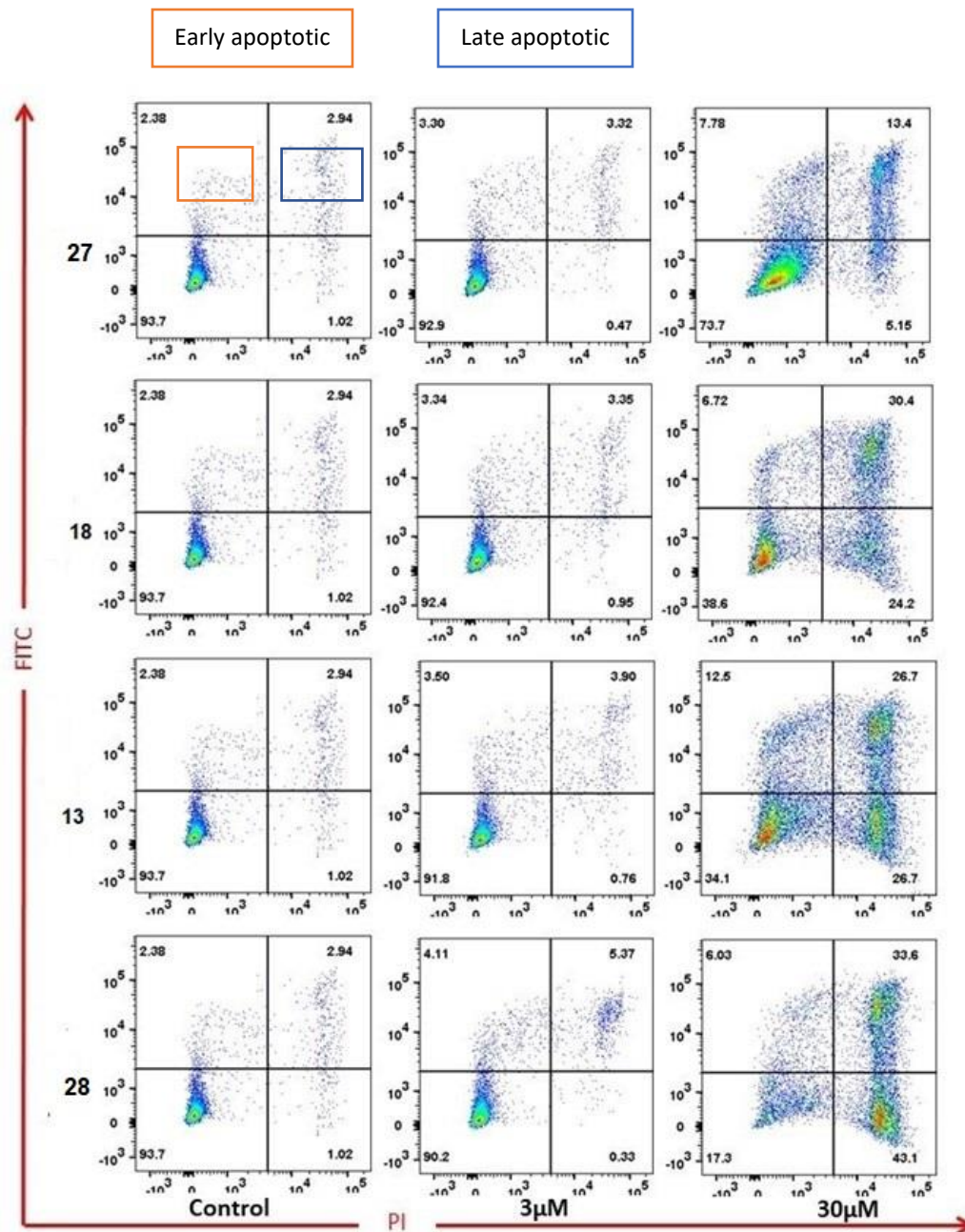


Figure 66: Annexin V and P.I. double staining flow cytometry of MDA-MB-231 cells treated with **13**, **18**, and **27-28** at 3 and 30 μ M for 48 hours. (Representative of n=3 independent experiments)

III-2. Cellular Molecular Effects of Imidazo[1,2-*a*:4,5-*c'*]dipyridines

To further explore the cellular molecular effects induced by our imidazo[1,2-*a*:4,5-*c'*]dipyridines, we examined the expression in MDA-MB-231 cells, of the pro-apoptotic proteins Bax and Bak, the anti-apoptotic Bcl-2 and Bcl-XL, and the cleavage state of PARP in response to compounds **13**, **18**, and **27-28** treatment at 30 μ M. MDA-MB-231 cells were treated with or without the tested compounds for 48h and then lysed and analyzed by Western blot. β -Actin expression was used as an internal control (**Figure 67**). It was revealed that the relative levels of pro-apoptotic Bax expression were increased in the presence of **27** (R_1 = Me), while **13**, **18**, and **28** (R_1 = OMe) reduced the levels of anti-apoptotic Bcl-2 expression. Furthermore, the four tested compounds resulted in more significant cleavage of PARP than the control group. Taken together, these results confirm that **13**, **18**, and **27-28** induced apoptosis in MDA-MB-231 cells. Nevertheless, a different signaling pathway seems to be impacted by 1-methyl compound **27** compared to 1-methoxy analogues **13**, **18**, and **28**.

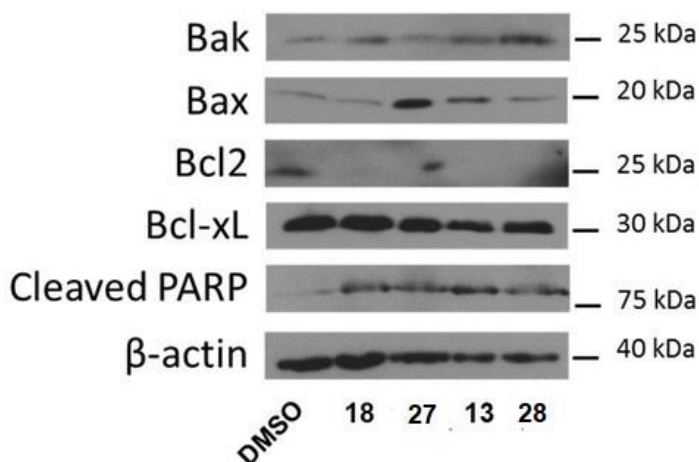


Figure 67: Western blot analysis of markers associated with apoptosis in MDA-MB-231 cells treated with compounds **13**, **18**, and **27-28** at 30 μ M for 48h. Markers include pro-apoptotic proteins Bax and Bak, the anti-apoptotic Bcl-2 and Bcl-XL, and the cleavage state of PARP. (Representative of n=3 independent experiments)

III-3. Ki-67 Staining Assay

In addition to the induction of apoptosis by compounds **13**, **18**, and **27-28**, the reduction of cell number could be attributed to reduced cell proliferation. Cell proliferation was evaluated using Ki-67 staining in MDA-MB-231 cells treated with 3 and 30 μ M of compounds **13**, **18**, and **27-28** during 48h. The Ki-67 protein is a nuclear antigen involved in cell proliferation and can be used as a marker for determining the cell proliferation as it is expressed throughout the active cell cycle (G_1 , S, G_2 , and M phases) except for the resting phase (G_0). Ki-67 ratio values were obtained by randomly enumerating Ki-67 positive cells through a microscope and expressed as percentages of positive cells. In which, Ki-67 positive cells stained by the green colour of GFP and total cancer cells nuclei stained by the blue colour of DAPI were counted. The ki-67 ratio (number of KI-67 positive cells/number of total cancer cells) is presented by the mean of the three independent experiments using five random microscopic fields counted for each concentration of a test compound \pm SEM. A decrease in nuclear Ki-67 staining indicates a blockage in the cell cycle and a decrease in cell proliferation.

Compared to the control, almost no effect was observed at 3 μ M for all compounds. However, at 30 μ M the Ki-67 ratio strongly decreased for compounds **13** (R_3 = c-Pr) and **18** (R_3 = *t*-Bu) to 36 and 28%, respectively, compared to **27** and **28** with 3-phenyl moieties as shown in **Table 17**. The images in **Figure 68** depict the Ki-67 staining of test compounds. Altogether, **13**, **18**, **27-28** lead to cancer cell growth inhibition with slightly different mechanisms. Compounds **13**, **18** and **28** strongly induced apoptosis and **13** and **18** also reduced cell proliferation.

Table 17: Cell proliferation activity of **13**, **18**, and **27-28** using Ki-67 assay

Compounds	Ki-67 ratio \pm SEM	
	3 μ M	30 μ M
13	1.12 \pm 0.14	0.36 \pm 0.21
18	1.05 \pm 0.09	0.28 \pm 0.12
27	1.09 \pm 0.13	0.86 \pm 0.09
28	1.15 \pm 0.08	0.68 \pm 0.04

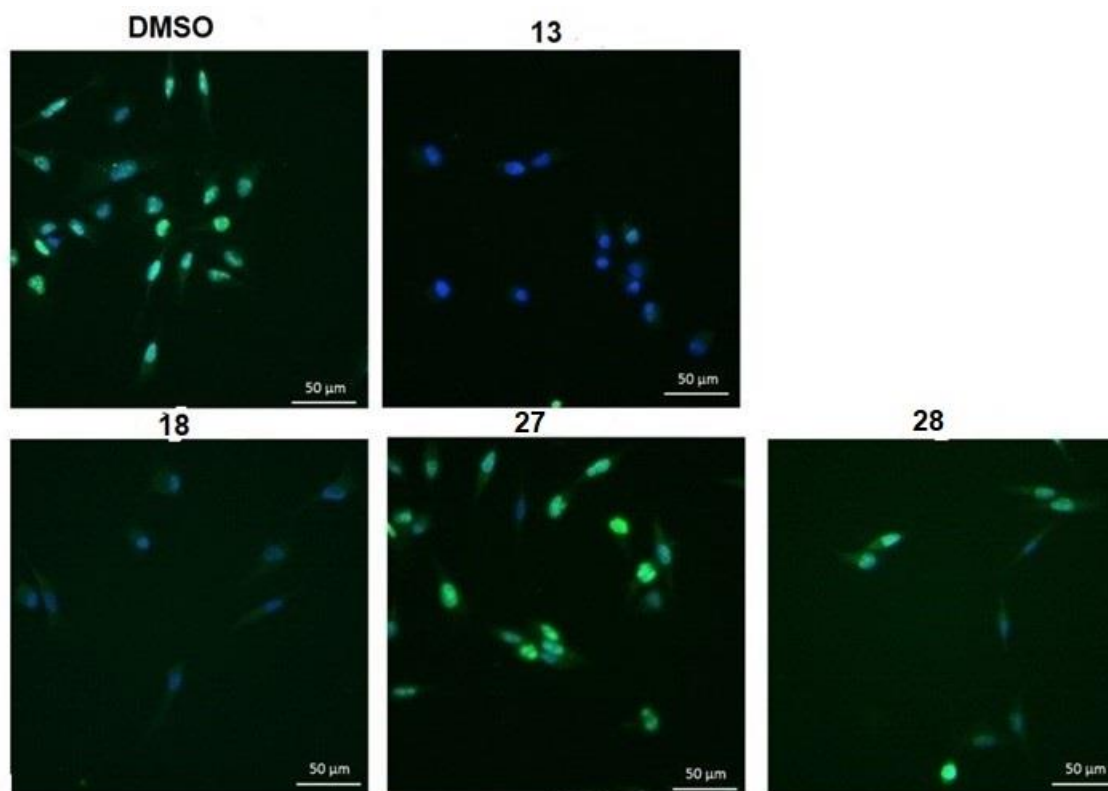


Figure 68: Ki-67 staining by the green colour of GFP for detection of cell proliferation of MDA-MB-231 cells treated with compounds **13**, **18**, and **27-28** at 30 μ M for 48h. Total nuclei are stained with the blue colour of Dapi.
(Representative of n=3 independent experiments)

IV. Anti-Migratory Activities

Cancer cells are capable of degrading their extracellular environment and migrate through the tissue to pass into the circulation and invade host tissues. It is possible to model these phenomena *in vitro* by assessing the migration and invasiveness of cells. The term migration has been defined as the ability of cells to migrate and close the defined 500 μ m cell-free gap created by culture inserts (**Figure 69**). Migration studies were performed using the 2 well culture inserts which were transferred into 24-well culture plate to form a well-defined gap without scratching the cell monolayer. Then, cells are treated with nontoxic concentrations of

compounds, monitored and photographed every 15 minutes for 24 hours for wound closure. The open area was analyzed with scratch software.

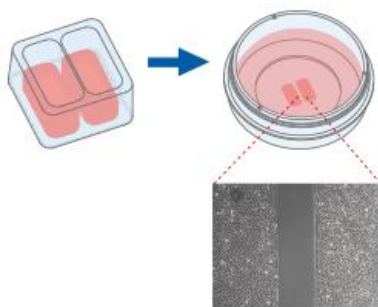
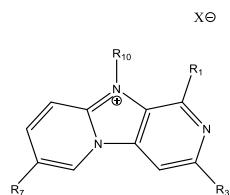


Figure 69: Inserts used in cell migration assay.

The highly metastatic human breast cancer cell line MDA-MB-435s was utilized to evaluate anti-migratory activity of the imidazo[1,2-*a*:4,5-*c'*]dipyridines using time-lapse microscopy of *in vitro* wound healing. Then, the open area was calculated with T-scratch software. The open areas were converted into distance migration and normalized to the control condition. First, I determined the 24h-cytotoxicity of our compounds to determine their nontoxic concentration(s) on MDA-MB-435s-luc cells as shown in **Table 18**. Also, **Table 18** provides the anti-migratory results at nontoxic concentrations, i.e. 0,1 μM and/or 1 μM depending on the compound. Of which, 1 μM was used to describe the anti-migratory SAR.

Table 18: Wound closure values for imidazo[1,2-*a*:4,5-*c'*]dipyridines

	R ₁	R ₃	R ₇	R ₁₀	X	Wound closure values \pm SEM in MDA-MB-435s-luc (24h) (concentrations)		Cytotox. (IC ₅₀ , μ M) MDA-MB-435s-luc
						0.1 μ M	1 μ M	
POD118	Me	c-Pr	H	Bn	Br	NT	0.76 \pm 0.14	>100
POD108	Me	<i>t</i> -Bu	H	Bn	Br	0.79 \pm 0.10	0.53 \pm 0.07	74.4 \pm 28.0
8	Et	c-Pr	H	Et	I	NT	0.79 \pm 0.16	>100
9	Et	c-Pr	Br	Bn	Br	0.92 \pm 0.00	0.58 \pm 0.05	>100
10	Ph	c-Pr	H	Et	I	0.73 \pm 0.19	1.05 \pm 0.27	>100
11	Ph	c-Pr	H	Bn	Br	0.94 \pm 0.11	0.75 \pm 0.21	48.6 \pm 2.3
12	OMe	c-Pr	H	Et	I	NT	0.82 \pm 0.11	>100
13	OMe	c-Pr	H	Bn	Br	0.70 \pm 0.11	0.86 \pm 0.14	16.3 \pm 3.3
14	Me	<i>t</i> -Bu	Br	Bn	Br	0.56 \pm 0.11	0.51 \pm 0.12	59.6 \pm 14.8
15	Me	<i>t</i> -Bu	H	Et	I	0.85 \pm 0.00	0.78 \pm 0.07	>100
16	Et	<i>t</i> -Bu	H	Bn	Br	0.77 \pm 0.05	0.80 \pm 0.06	35.4 \pm 14.6
17	OH	<i>t</i> -Bu	H	Bn	Br	0.73 \pm 0.06	0.57 \pm 0.07	>100
18	OMe	<i>t</i> -Bu	H	Bn	Br	0.77 \pm 0.10	0.59 \pm 0.01	11.9 \pm 1.7
19	Ph	<i>t</i> -Bu	H	Bn	Br	0.56 \pm 0.12	0.50 \pm 0.08	21.3 \pm 8.6
20	Ph	<i>t</i> -Bu	Br	Bn	Br	0.48 \pm 0.03	0.38 \pm 0.05	29.14 \pm 1.7
21	Ph	<i>t</i> -Bu	Me	Bn	Br	0.62 \pm 0.17	0.87 \pm 0.06	>100
22	Ph	<i>t</i> -Bu	Thien-2-yl	Bn	Br	0.61 \pm 0.04	0.63 \pm 0.03	30.8 \pm 6.5
23	Ph	<i>t</i> -Bu	1-benzyl pyridinium-4-yl	H	-	0.50 \pm 0.05	0.38 \pm 0.04	>100
24	Ph	<i>t</i> -Bu	Ph	Bn	Br	0.67 \pm 0.31	0.47 \pm 0.23	37.2 \pm 5.0
27	Me	Ph	H	Bn	Br	0.85 \pm 0.12	0.70 \pm 0.09	>100
28	OMe	Ph	H	Bn	Br	0.52 \pm 0.06	0.43 \pm 0.07	16.9 \pm 2.4

NT= Not tested

In this assay, six compounds inhibited the MDA-MB-435 cells migration by 41 to 50% (compounds **POD108**, **9**, **14**, **17-19**) while four inhibited the migration by 53 to 62% (**20**, **23**, **24**, **28**) at 1 μ M. From these ten compounds, eight present a *tertio*-butyl group in position 3 and a structural diversity in position 1, which seems to be less decisive for the anti-migrative activity.

Three closely related compounds **20**, **23** and **24**, deeply inhibited MDA-MB-435 cells migration by 62, 62 and 53% respectively at 1 μ M. Their structures present a phenyl group in position 1 and a *tertio*-butyl group in position 3. Diversity occurs in position 7 with either a bromine atom for compound **20**, a benzylpyridinium for **23** and a phenyl group for **24**. As the 10-benzyl part is absent in compound **23**, this substituent did not appear to be essential for the antimigration activity. Also, we can conclude that bromo, pyridin-4-yl-, and phenyl- moieties at C-7 may enhance the anti-migratory activity at 1 μ M. Interestingly, compound **28** presented dual antiproliferative and anti-migration activity with an average IC_{50} of 3.2 μ M for the inhibition of the MDA-MB-231, MDA-MB-468 and MDA-MB-435 cells proliferation, and 43% inhibition in the MDA-MB-435 migration assay at 1 μ M.

The images in **Figure 70** depict the wound healing closure of compound **28**.

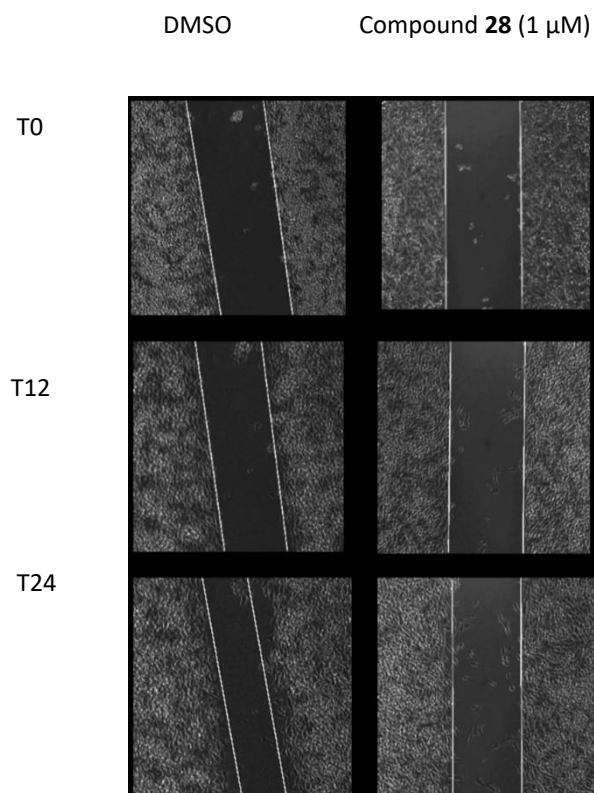


Figure 70: Wound healing activity of **28** (1 μ M) and DMSO (0.1%) against MDA-MB-435s-luc cells at selected periods

V. Selection and Further Tests Toward *In Vivo* Murine Evaluation

The *in vivo* evaluation of our best compounds will be performed at the Centre for Small Animal Imaging (CIPA-TAAM, UPS 44 CNRS at Orleans, France) in a syngeneic model of murine breast cancer cells (4T1) in immunocompetent mice Balb/c.

In mammary cancer models, murine 4T1 models are helpful tools for studying the anticancer and anti-metastatic effects of tested compounds as they are easily transplantable into the mammary gland. Thus the primary tumor growth is in the anatomically correct site, and metastasis develops spontaneously from the primary tumor.²²⁸ Moreover, 4T1-luc cells are

derived from murine BALB/c strain so they can grow in balbc immunocompetent mice compared to human cells who need immunodepressed mice.²²⁹

Thus to explore the *in vivo* biological activities of imidazo[1,2-*a*:4,5-*c'*]dipyridines **13**, **18**, **20** and **28** (Figure 71) in this syngeneic mouse model, we needed to determine their cell growth, migration and invasion inhibition activities against murine 4T1-luc cell line. Compounds **13** and **18** were selected due to their potent growth inhibition activities, compound **20** for its potent migration inhibition activity and compound **28** for both properties.

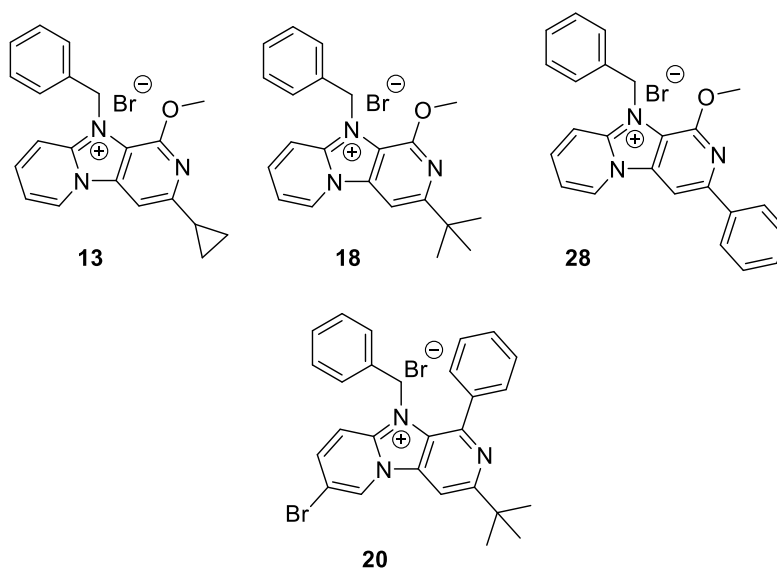
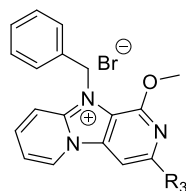


Figure 71: Analogues **13**, **18**, **20** and **28** which will be used for the *in vivo* biological activities

V-1. *In Vitro* Growth Inhibition Activity against Murine 4T1-luc Cells

As described previously in Section II, 1-methoxy analogues **13**, **18**, and **28** displayed potent growth inhibition activities against MDA-MB-435s-luc, MDA-MB-468-luc and MDA-MB-231 cancer cells ($IC_{50} \leq 5 \mu M$). Thus, compounds **13**, **18**, and **28** were further tested on 4T1-luc cells (Table 19). All three analogues retained their potent growth inhibition activities with IC_{50} values of 3.1, 1.7, 6 μM , respectively. This support the hypothesis that these analogues possess potent anticancer effect against TNBC cells.

Table 19: *In vitro* growth inhibition activities of selected imidazo[1,2-*a*:4,5-*c'*]dipyridines



Compound	R ₃	4T1-luc cells
		5 days-cell viability (IC ₅₀ μM ± SEM)
13	c-Pr	1.5±0.4
18	<i>t</i> -Bu	0.5±0.3
28	Ph	6.0±1.3

V-2. *In Vitro* Migration and Invasion Inhibition Activities against Murine 4T1-luc Cells

Thereafter, compound **20** which exhibited potent anti-migratory activities against MDA-MB-435s-luc cells (38%) at 1 μM was screened for its cell migration and invasion inhibition activities against 4T1-luc cell lines.

As described previously, cancer cells can degrade their extracellular environment and migrate through the tissue to pass into the circulation and invade host tissues. Cellular invasiveness measures the ability of cells to actively passing through an 8 μm pore size polyethylene terephthalate (PET) membrane that has been treated with Matrigel matrix, mimicking thus the extracellular matrix using Corning BioCoat Matrigel invasion chamber. Under these conditions, the cells must degrade the Matrigel matrix before migrating through the pores of the filter. The difference in FBS between the upper and lower compartments permits the establishment of a chemoattractant gradient (hormones and growth factor) (**Figure 72**).

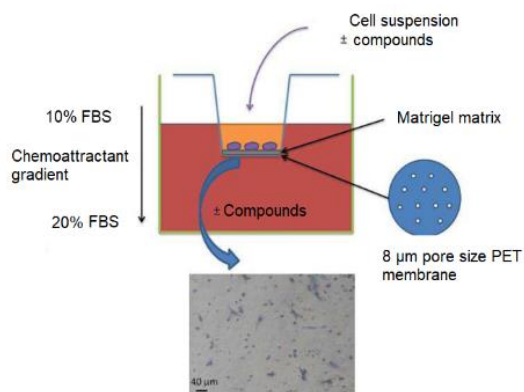
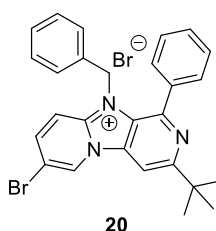


Figure 72: Matrigel invasion chamber used in cell invasiveness assays

First, I performed 24h-cytotoxicity tests for **20** at 1 μM and I found it was not toxic to the cells at this concentration (% of cell viability was 88.54% compared to 100% of DMSO). Thus, it was subsequently evaluated for its *in vitro* migration and invasion inhibition activities.

In the migration assay, compound **20** displayed lower activity than those obtained using MDA-MB-435s cells with value of 0.69 (**Table 20**). In the invasion assay, it exhibited potent cell invasion inhibition activity with value of 0.39. As shown in **Figure 73**, compound **20** greatly inhibited cell invasion compared to control (DMSO) through the matrix and thus lowered the number of invaded cells.

Table 20: 15h migration and invasion assay on 4T1-luc cells after treatment with **20** at 1 μM



4T1-luc \pm SEM (15h) (1 μM)	
Wound closure	Invasion
0.69 \pm 0.06	0.39 \pm 0.11

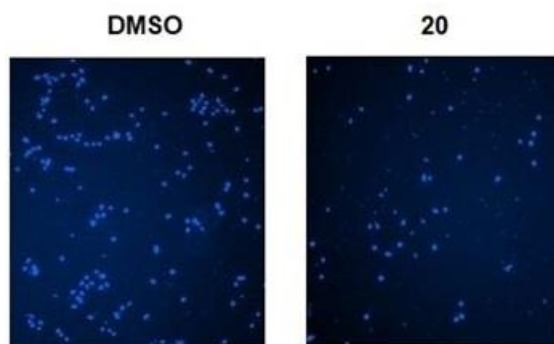


Figure 73: Invasion inhibitory activity of compound **20** against 4T1-luc cells. Cells treated with the compound at 1 μ M for 15h. Total nuclei are stained with Dapi. (Representative of n=3 independent experiments)

VI. Selectivity Study against MCF-10A Cells

Finally, in an effort to determine the selectivity of imidazo[1,2-*a*:4,5-*c'*]dipyridines for breast cancer cell lines, and in essence provide the predictive evidence of their safety profile, *in vitro* cytotoxicity studies were performed against human breast epithelial MCF-10A cell line which were conducted using MTT assay, which facilitates the measurement of cell proliferation and chemosensitivity. The non-cancerous epithelial cell line MCF-10A is derived from a mammaplasty and was immortalized by long-term culture in serum-free medium containing a low concentration of calcium.²³⁰ Cytotoxicity data for the representative imidazo[1,2-*a*:4,5-*c'*]dipyridines analogues **13**, **18**, and **28** are listed in **Table 21**. Compound **20** was not active as antiproliferative thus was not tested for selectivity study against MCF-10A cells

Table 21: *In vitro* 5 d cytotoxicity assay results for selected imidazo[1,2-*a*:4,5-*c'*]dipyridines

compound	5 days-cell viability (IC ₅₀ μ M \pm SEM)				
	MDA-MB-468	MDA-MB-435s	MDA-MB-231	4T1	MCF-10A
13	3.59 \pm 1.20	1.28 \pm 0.10	3.07 \pm 0.45	1.48 \pm 0.44	2.27 \pm 0.68
18	0.43 \pm 0.39	1.15 \pm 0.09	1.72 \pm 0.28	0.49 \pm 0.31	1.64 \pm 0.47
28	4.71 \pm 0.23	5.01 \pm 3.52	3.02 \pm 0.36	6.02 \pm 1.34	0.60 \pm 0.22

Compound **18** exhibited slightly lower cytotoxicity against non-cancer MCF-10A cells compared to MDA-MB-435s, MDA-MB-468 and 4T1 cancer cells, in contrast to compound **28** which exhibited higher cytotoxicity against non-cancer MCF-10A cells compared to cancer cells. Moreover, compound **13** displayed slightly lower cytotoxicity against noncancer MCF-10A cells compared to MDA-MB-435s and 4T1 but higher cytotoxicity compared to MDA-MB-468 and MDA-MB-231.

VII. Conclusion

This chapter described the various hit-to-lead biological investigations performed on the final target analogues. Initial SARs of imidazo[1,2-*a*:4,5-*c'*]dipyridines (**Figure 74**) indicated that: 1) Methoxy group enhances the growth inhibition activity; 2) Bromo, pyridin-4-yl-, and phenyl-moieties at position 7 enhance anti-migratory activity; 3) Benzyl substituent enhances cancer cell growth inhibition activity.

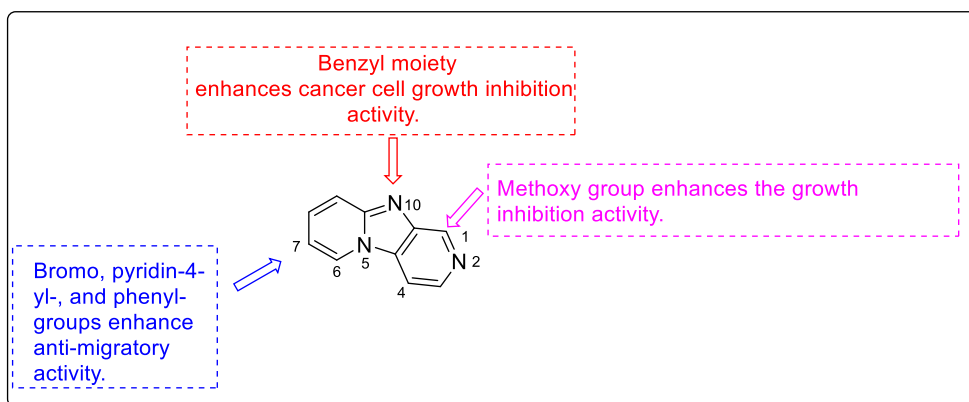


Figure 74: SAR analysis of imidazo[1,2-*a*:4,5-*c'*]dipyridines

The major findings of biological evaluation studies are summarized as follow (**Figure 75**):

- Analogues **13**, **18**, and **28** ($R_1 = \text{OMe}$, $R_{10} = \text{Bn}$) showed the most potent growth inhibition activity [that is, $\text{IC}_{50} \leq 6 \mu\text{M}$] against all four TNBC MDA-MB-231, MDA-MB-468, MDA-MB-435s and 4T1 cell lines tested.
- Analogues **POD108**, **14**, **19-20**, **23-24** and **28** exhibited potent anti-migratory activities against MDA-MB-435s at $1 \mu\text{M}$ with values range of 0.38-0.53.
- Analogue **20** displayed potent anti-invasion activities against 4T1 cell invasion at $1 \mu\text{M}$ with value of 0.39.
- Analogue **28** presented dual antiproliferative and anti-migration activity with an average IC_{50} of $3.2 \mu\text{M}$ for the inhibition of the MDA-MB-231, MDA-MB-468 and

- MDA-MB-435s cells proliferation, and 57% inhibition in the MDA-MB-435s cells migration assay at 1 μ M.
- Compounds **13**, **18** and **28** (R_1 = OMe, R_{10} = Bn) strongly induced apoptosis through decreasing the levels of anti-apoptotic Bcl-2 expression and increasing cleavage of PARP while compound **27** (R_1 = Me, R_{10} = Bn) increased levels of pro-apoptotic Bax expression and cleavage of PARP.
 - Compounds **13** and **18** also reduced cell proliferation through decrease of Ki-67.
 - Compound **18** exhibited slightly low cytotoxicity against the MCF-10A cell line compared to the three TNBC cells tested.

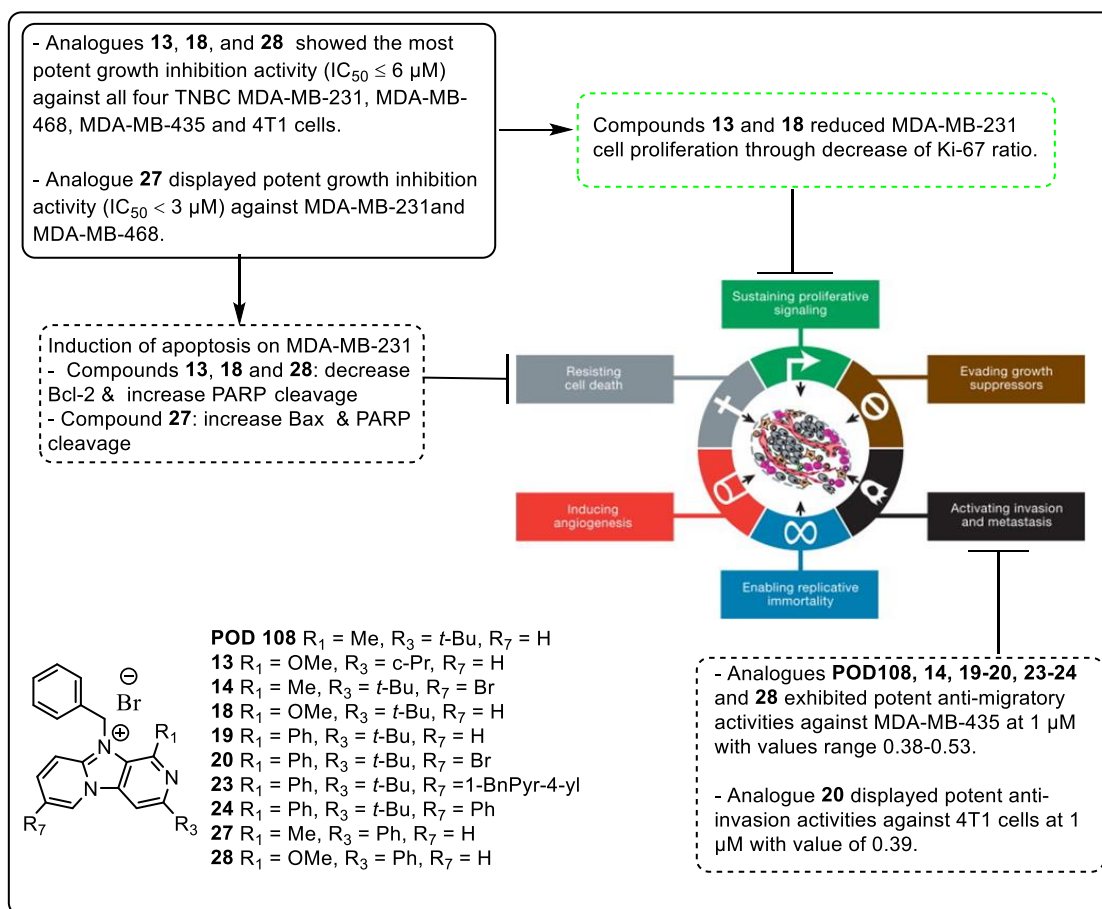


Figure 75: Effects of imidazo[1,2-*a*:4,5-*c'*]dipyridines on human breast cancer

Since the many imidazo[1,2-*a*:4,5-*c'*]dipyridine analogues showed excellent antiproliferative, anti-migratory, and anti-invasion activities, they might be useful as leads for further optimization.

All target compounds, regarding their growth inhibition activity against MDA-MB-435s-luc cell line, were subjected to *in silico* 3D-QSAR analysis to unravel and verify structure-activity relationships (SAR). These studies are discussed in the next chapter (Chapter 5).

Chapter 5:

***3D*-QSAR Study of Imidazo[1,2-*a*:4,5-*b'*]dipyridines**

I. Introduction

Chapter 5 shows a discussion of the three dimensional-quantitative structure-activity relationship (*3D*-QSAR) study on final target compounds. This *3D*-QSAR study aimed at unraveling and verify the main functional groups and positions responsible for the observed growth inhibition activity against MDA-MB-435s-luc cells showed in chapter 4.

The workflow that was followed towards achieving the above-mentioned objective of this chapter is depicted in **Figure 76**.

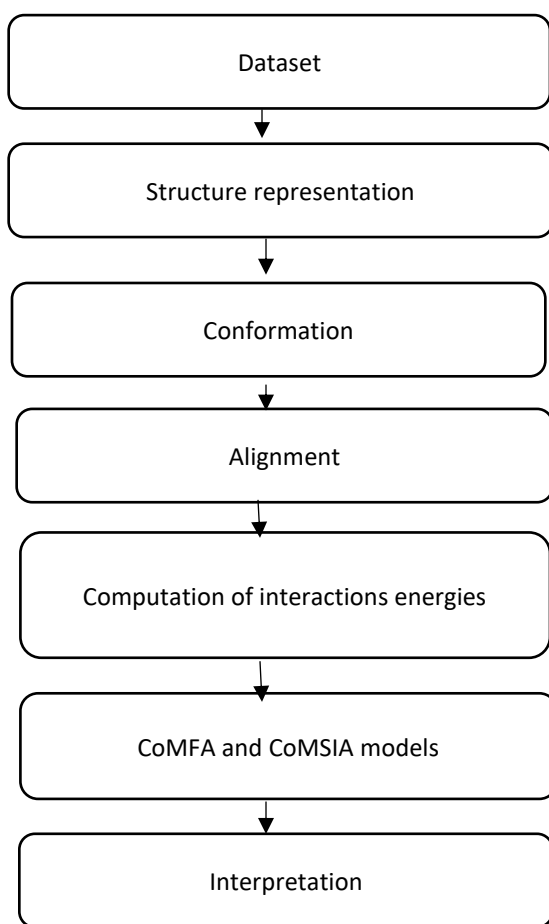


Figure 76: The workflow adapted in the *3D*-QSAR study

II. 3D-QSAR Study

The 3D-QSAR study is highlighted with respect to the data set; structure optimization and alignment; CoMFA and CoMISA studies as well as partial least squares (PLS) analysis.

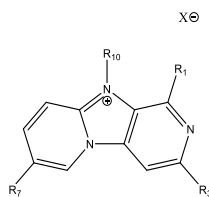
II-1. Data Set

To investigate the SARs of imidazo[1,2-*a*:4,5-*b'*]dipyridines, the growth inhibition data of the MDA-MB-435s-luc cell line was used to build the 3D-QSAR models. The compounds were divided into 13 and 4, the training and the test data sets respectively, and used for 3D-QSAR model generation and evaluation. The experimental IC₅₀ values of these compounds were converted to pIC₅₀ (-log IC₅₀) and shown in **Table 22**.

II-2. Structure Optimization and Alignment

All the 3D structures were constructed using Sybyl 2.1.1 sketcher (TRIPOS Associates Inc.). The geometries of the 3D structures were optimized using the tripos MMFF94 with the Powell method. The maximum iterations for the minimization were set to 10×10^3 and terminated when the energy gradient convergence criterion of 0.05 Kcal/mole was reached to obtain stable conformations. The electrostatic charges were assigned using the Gasteiger-Hucker method which was subsequently used for 3D-QSAR studies.²³¹

Molecular alignment is a crucial step in the 3D-QSAR study because the quality and the predictive ability of the model are directly dependent on this alignment. All of the compounds were aligned using the database alignment method. As no information about the nature of ligand-receptor complexes are provided, compound **18** which was one of the most active compounds against MDA-MB-435s-luc breast cancer cell lines was used as a template to align the other compounds from the dataset to it on the common three-ring substructure shown in **Figure 77**.²³²

Table 22: In vitro growth inhibition activities of analogues against MDA-MB-435s-luc

	R₁	R₃	R₇	R₁₀	X	MDA-MB-435s-luc 5 days-cell viability (IC₅₀, μM)	pIC₅₀
POD118	Me	<i>c</i> -Pr	H	Bn	Br	43.9+14.1	4.36
POD108	Me	<i>t</i> -Bu	H	Bn	Br	16.4+3.1	4.79
8	Et	<i>c</i> -Pr	H	Et	I	28.3+4.8	4.55
9	Et	<i>c</i> -Pr	Br	Bn	Br	62.2+25.8	4.21
10	Ph	<i>c</i> -Pr	H	Et	I	47.6+20.4	4.32
11	Ph	<i>c</i> -Pr	H	Bn	Br	13.1+6.5	4.88
12	OMe	<i>c</i> -Pr	H	Et	I	6.3+3.0	5.20
13	OMe	<i>c</i> -Pr	H	Bn	Br	1.3+0.1	5.89
14	Me	<i>t</i> -Bu	Br	Bn	Br	10.7+0.5	4.97
15	Me	<i>t</i> -Bu	H	Et	I	90.5+0.5	4.04
16	Et	<i>t</i> -Bu	H	Bn	Br	4.8+0.3	5.32
17	OH	<i>t</i> -Bu	H	Bn	Br	33.4+1.2	4.48
18	OMe	<i>t</i> -Bu	H	Bn	Br	1.1+0.1	5.94
19	Ph	<i>t</i> -Bu	H	Bn	Br	6.4+1.0	5.19
20	Ph	<i>t</i> -Bu	Br	Bn	Br	5.2+0.4	5.29
27	Me	Ph	H	Bn	Br	22.4+1.5	4.65
28	OMe	Ph	H	Bn	Br	5.0+3.5	5.30

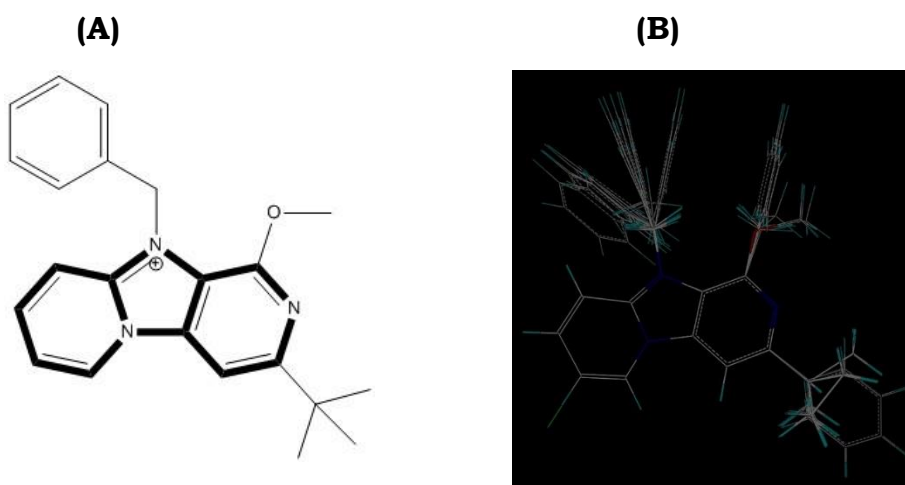


Figure 77: Database alignment method. (A) Structure of the template **18**, common core is in bold, (B) Alignment and superimposition of 17 compounds

II-3. CoMFA and CoMISA Studies

All the aligned compounds were placed in a lattice box with a grid spacing of 2Å, which was generated automatically by the software. CoMFA is based on the principle that changes in biological activity are correlated to changes in the steric and electrostatic components of compounds. CoMFA fields were generated using a sp^3 hybridized carbon atom as the steric probe (van der Waals radius of 1.53 Å) and the electrostatic probe (single positive charge) at each grid point. The cutoff was set to 30 kcal/mol. CoMSIA similarity indices descriptors, which include steric, electrostatic, hydrophobic, hydrogen acceptor and hydrogen donor, were calculated using the same lattice box used in CoMFA calculations. The attenuation factor (R) was set to the default value of 0.3.²³³

II-4. Partial Least Squares (PLS) Analysis

Partial Least Squares (PLS) method was used to linearly correlate the CoMFA and CoMSIA descriptors as independent variables to the pIC_{50} values as dependent variables.

The optimal number of components was determined using the Leave-One-Out (LOO) procedure using SAMPLS method. The final model (non-cross-validated analysis) was developed to produce the no validated correlation coefficient R^2 using the optimal number of components derived from the model with the highest cross-validated (q^2).²³⁴

II-5. Results

The experimental and predicted pIC_{50} values of the training set for the CoMFA and CoMSIA models were shown in **Table 23** and the plot of experimental pIC_{50} versus predicted pIC_{50} of the training set for the CoMFA and CoMSIA model was illustrated in **Figure 78**.

Table 23: The experimental pIC_{50} and predicted pIC_{50} of the training and test set molecules

Compound	Experimental pIC_{50}	CoMFA		CoMSIA	
		Predicted	Residual	Predicted	Residual
POD118^a	4.36	4.9983	0.6383	4.9743	0.6143
POD108	4.79	4.8668	0.0768	4.8602	0.0702
8	4.55	4.3363	-0.2137	4.3295	-0.2205
9^a	4.21	5.2932	1.0832	5.2258	1.0158
10	4.32	4.4268	0.1068	4.4449	0.1249
11	4.88	5.0767	0.1967	5.0897	0.2097
12^a	5.20	4.5554	-0.6446	4.7804	-0.4196
13	5.89	5.9623	0.0723	5.9409	0.0509
14	4.97	5.0217	0.0517	5.0012	0.0312
15	4.04	4.1355	0.0955	4.1668	0.1268
16	5.32	5.2468	-0.0732	5.1965	-0.1235
17^a	4.48	5.4233	0.9433	5.4646	0.9846
18	5.94	5.7904	-0.1496	5.8369	-0.1031
19	5.19	5.0946	-0.0954	5.0952	-0.0948
20	5.29	5.1681	-0.1219	5.1513	-0.1387
27	4.65	4.5703	-0.0797	4.5605	-0.0895
28	5.30	5.4338	0.1338	5.4565	0.1565

^a Test set molecule.

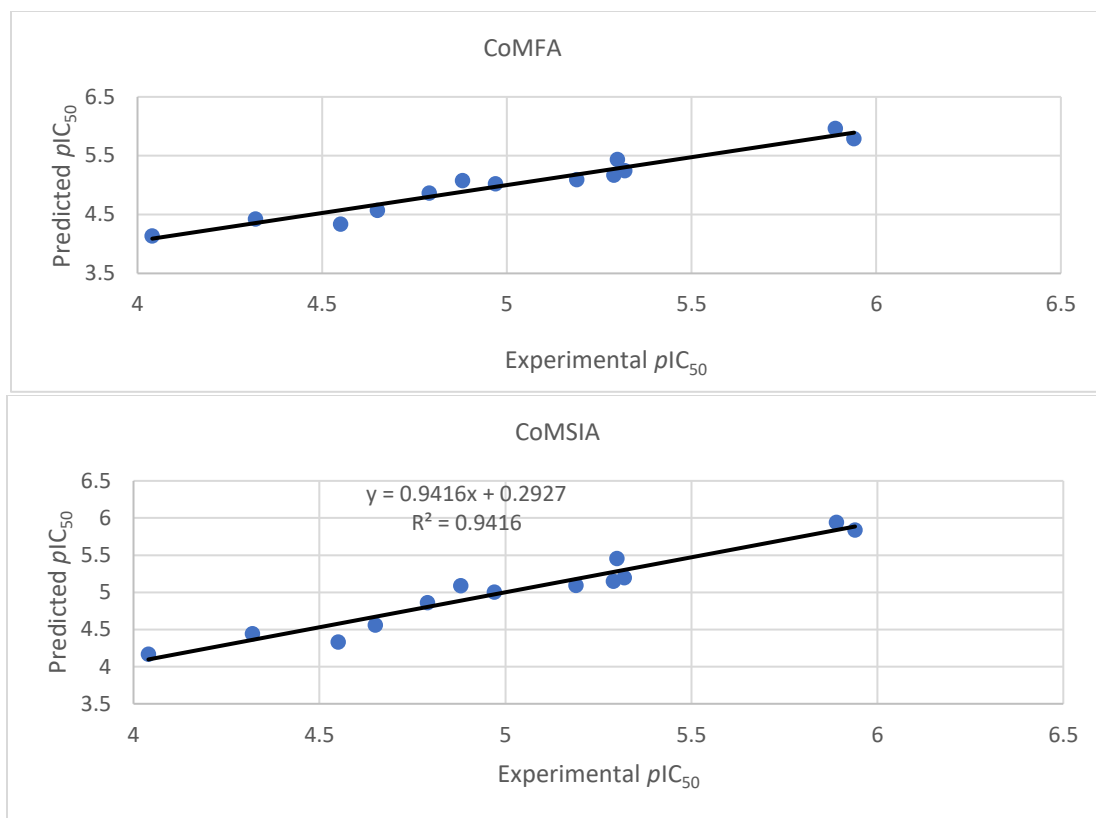


Figure 78: Predicted pIC_{50} vs. experimental pIC_{50} values for the 13 training set molecules obtained by PLS analysis using CoMFA and CoMSIA models

The partial least squares (PLS) results of CoMFA and CoMSIA models are listed in **Table 24**. The cross-validation correlation coefficient (q^2) and the Non-cross-validation correlation coefficient (r^2) are considered as two key parameters to evaluate the qualities of PLS analysis to indicate the predictive capacity and the self-consistency, respectively. Golbraikh and Tropsha reported that models are considered acceptable if they satisfy all of the following conditions: $q^2 > 0.5$ and $r^2 > 0.6$. PLS Statistics of both CoMFA and CoMSIA models indicated that CoMFA model was slightly better than CoMSIA model.²³⁵

The CoMFA and CoMSIA models gave a good cross-validated correlation coefficient q^2 of 0.681 and 0.677 respectively, with a number of components of 3, which were reasonable considering the number of compounds used to generate the models, suggesting that it has a good predictive capability. A high non-cross-validated correlation coefficient (r^2) of 0.948 for CoMFA

and 0.942 for CoMSIA with a low standard error estimate (SEE) of 0.147 and 0.156 for CoMFA and CoMSIA, respectively, were obtained.

Table 24: PLS Statistical results of CoMFA and CoMSIA Models

Model Name	q ^{2a}	r ^{2b}	Standard Error	Number of Components
CoMFA	0.681	0.948	0.147	3
CoMSIA	0.677	0.942	0.156	3

^a Cross-validation correlation coefficient.

^b Non-cross-validation correlation coefficient.

To verify the validity of the 3D-QSAR models, as well as their predictive utility, a test set made up of 4 compounds were employed as external testing data. The predictive pIC_{50} values of the test set were obtained by using the predict property function of the QSAR module in SYBYL X 2.1.1. The predictive results were summarized in **Table 25**.

Table 25: CoMFA and CoMSIA predictive pIC_{50} values of the test set

Compound	Experimental pIC_{50}	Predictive pIC_{50}	
		CoMFA	CoMSIA
POD118	4.36	4.9983	4.9743
9	4.21	5.2932	5.2258
12	5.20	4.5554	4.7804
17	4.48	5.4233	5.4646

3D-QSAR contour maps of both CoMFA and CoMSIA models were depicted in **Figure 79** using compound **18** as a reference structure. The steric field is represented by green and yellow contour maps in which green contours represent regions where the sterically bulky group would be favorable, while the yellow contours represent sterically less favorable. The electrostatic field is represented in red and blue, which demonstrates the regions where electron-rich groups and electron-deficient regions groups would be favorable, respectively.

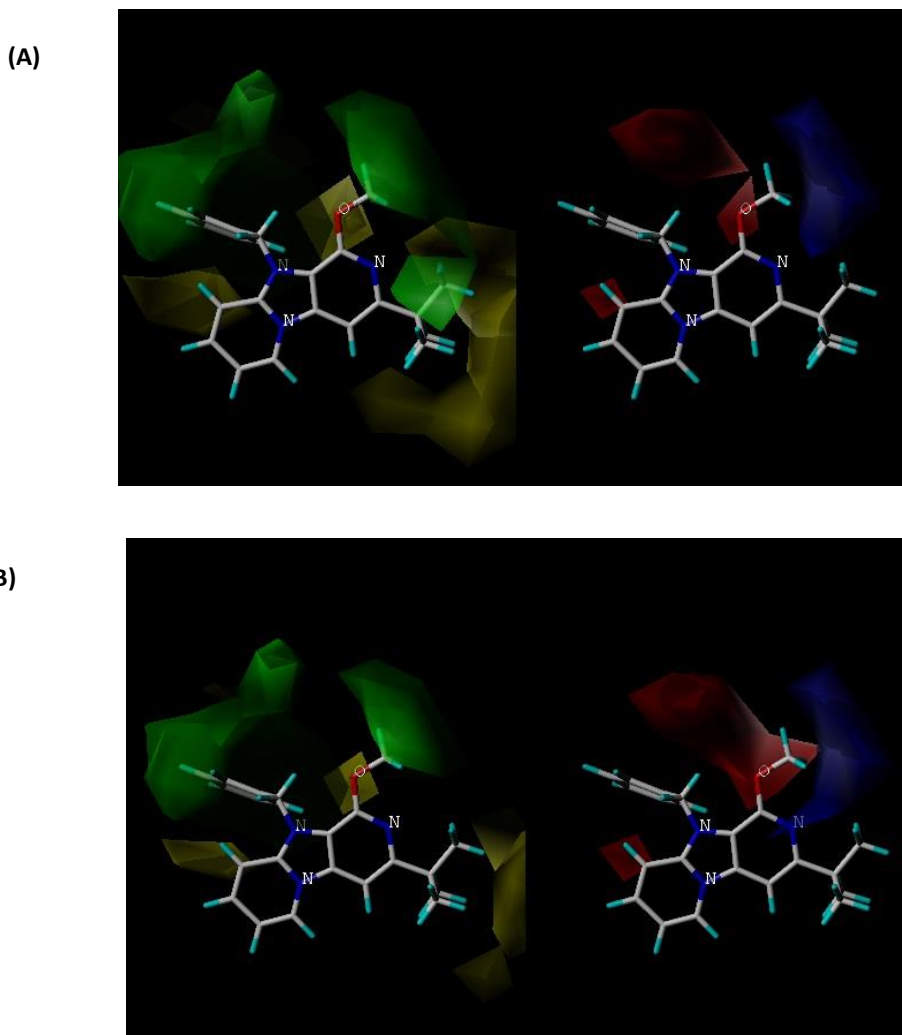


Figure 79: Contour maps of (A) CoMFA and (B) CoMSIA in combination with compound **18**. Green and yellow contours represent sterically bulky groups that increase activity and sterically bulky groups that decrease activity, respectively, while red and blue contours represent regions where electron-withdrawing groups increase activity and electron-donating groups increase activity, respectively.

Steric bulky green contour near **R₁** shows the existence of a bulky group may improve the growth inhibitory activity, which agrees well with the experimental results. For instance: compound **18** (OMe) > **17** (OH), compound **16** (ethyl) > **POD118** (methyl), compound **11** (phenyl) > **POD108** (methyl), and compound **20** (phenyl) > **14** (methyl). Besides, there is a green contour near the **R₁₀** region: compound **POD118** (benzyl) > **15** (ethyl) and compound **13** (benzyl) > **12** (ethyl).

Electrostatic blue and red contour maps are observed near **R₁** position and indicate that substituents presenting electronegative atoms in the middle and electropositive positive groups at the end are more favorable at this position. This can be seen by a great increase in activity of compounds **12**, **13**, and **28** including the most active compound **18** which contains both electronegative and electropositive substitution at this position. Besides, blue contour maps around the three electropositive nitrogen atoms in the skeleton indicate that they are essential for the activity.

In summary, analysis of compound **18**, which exhibits the greatest potency of all the compounds tested against MDA-MB-435s-luc cell lines, showed that it has a large electropositive group (methyl) at the end of the electronegative group (oxygen atom) at the C-1 and a large group (benzyl) at N-10 which is consistent with steric and electrostatic contour maps. In contrast, compound **15**, without an electronegative group but with a small group (methyl) at the C-1 and small group at N-10 (ethyl), did not match the model and have a weak activity.

III. Conclusion

Based on the CoMFA and CoMSIA models, we can conclude that the introduction of an electronegative atom in the middle and a large electropositive group at the extremity at the C-1 and a large group at the N-10 would improve the activity as shown in **Figure 80**. This SAR analysis is consistent with that obtained in chapter 4.

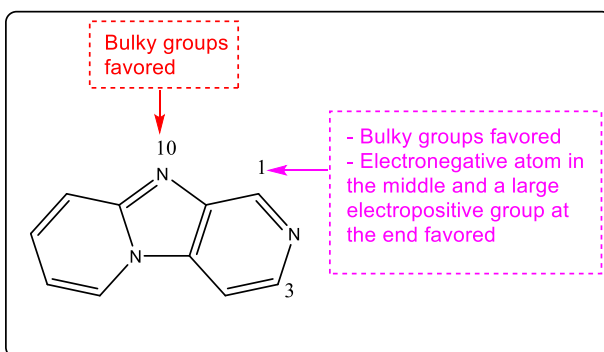


Figure 80: SAR summarized based on the 3D-QSAR analysis

Conclusion and Perspectives

I. Conclusions

This work is part of a collaborating program between University of Tours, France and University of Gezira, Sudan.

This thesis project is at the interface of chemistry and biology in field of cancerology and the aims were to design, synthesize and evaluate novel imidazo[1,2-*a*:4,5-*c'*]dipyridine analogues as anticancer agents. Inspired by the structure of the common core of β -carboline alkaloids and previous works from our laboratory, I elaborated new synthetic compounds as potential anticancer agents.

In chapter 1 and 2, a comprehensive literature review on breast cancer and *Peganum harmala* L. and β -carbolines was carried out. I took in consideration the literature's observation for identifying targeting approaches in breast cancer and designing new potential compounds inspired by anticancer SAR of β -carbolines.

In chapter 3, many new imidazo[1,2-*a*:4,5-*c'*]dipyridines were designed by applying rational medicinal chemistry principles, and thereafter successfully synthesized in accordance with synthetic procedures developed as well as methodologies adapted from literature.

In chapter 4, the synthesized compounds were evaluated for their *in vitro* growth inhibition, anti-migratory and anti-invasion activities, cellular mechanisms, and cytotoxicity studies. In particular, some imidazo[1,2-*a*:4,5-*c'*]dipyridine analogues showed potent *in vitro* growth inhibition activity against four TNBC cell lines, namely, MDA-MB-435s, MDA-MB-231, MDA-MB-468 and 4T1, and potent anti-migratory activities against 4T1 cells. In addition, one compound displayed good anti-invasion activity against murine 4T1-luc cells. Further studies, including the use of different *in vitro* assays, revealed that the potent growth inhibition activity of some imidazo[1,2-*a*:4,5-*c'*]dipyridines against MDA-MB-231 breast cancer cells is due to decrease proliferation and induction of apoptosis through expression increase of pro-apoptotic marker Bax, decrease expression of antiapoptotic marker Bcl-2, and increase cleavage of PARP. Nevertheless, selected potent compounds exhibited slightly lower cytotoxicity against the MCF-10A cell line.

In chapter 5, three dimensional-quantitative structure-activity relationships (3D-QSAR) study was carried on final target compounds with their growth inhibition activity against MDA-MB-435s-luc cells in which analogues were subjected to CoMFA and CoMSIA studies. The descriptors values obtained were then correlated with the experimentally determined growth inhibition activity values, to establish the SAR. In effect, correlations were deduced, and steric and electrostatic descriptors were found to be the most correlated factors with growth inhibition activities against MDA-MB-435s-luc cells.

In conclusion, a novel series of imidazo[1,2-*a*:4,5-*c'*]dipyridine were successfully developed. 1-Methoxy-based analogues with improved growth inhibition, anti-migratory and anti-invasion activities, are promising leads for further development.

II. Perspectives

During this thesis, it was difficult to install many moieties at C-1 (e.g. secondary amines), thus another synthetic approach can be used by preparing the tricyclic imidazo[1,2-*a*:4,5-*c'*]dipyridine core with chlorine leaving group at C-1 that permit introducing many moieties as secondary amine groups. Also, different tricyclics were produced in low yields as well as many were failed to be produced, thus we propose to introduce pyridine at C-7 to obtain the salt at this position as this synthetic approach was fast and produce the desired salts in high yields. This synthetic approach also permits the introduction of various salts with phenyl moieties at C-1 and C-3.

We didn't explore position 4, thus diverse moieties can be introduced in this position to investigate its anticancer effect.

Experimental Part

I. Introduction

This part describes the chemical and biological methods utilized in this thesis study and was divided into two sections, chemistry and biology. The chemistry section describes the synthetic protocols involved in Chapter 3 especially those that are not outlined in the main text. Moreover, this section provides the characterization information with respect to all the synthesized analogues. Additionally, the biology section addresses cellular and molecular investigations that utilized to investigate the anti-cancer activity of imidazo[1,2-*a*:4,5-*c'*]dipyridine compounds.

II. Chemistry

This section describes reagents and solvents, physical and spectroscopic characterization, chromatography, as well as synthesis and characterization of target compounds.

II-1. Reagents and Solvents

All commercially available chemicals and reagents were purchased from Sigma-Aldrich (France) and were used without prior purification.

II-2. Physical and Spectroscopic Characterization

Melting points were determined using on a capillary apparatus (Stuart, Staffordshire, United Kingdom), and are reported as uncorrected values. NMR spectra were recorded at 300 MHz (¹H) and 75 MHz (¹³C) on a Bruker-Avance 300 MHz spectrometer. Samples for NMR spectroscopy were dissolved in deuterated solvents such as dimethylsulfoxide (DMSO-*d*₆), chloroform (CDCl₃), or methanol (Methanol-*d*₄). Chemical shifts (δ) are reported in parts per

million (ppm) and rounded off to two decimals for ^1H and one for ^{13}C while coupling constants (J) are reported in Hertz (Hz) and rounded off to one decimal place. Abbreviations used to describe ^1H -NMR signal multiplicities are d (doublet), dd (doublet of doublets), ddd (doublet of doublet of doublets), dt (doublet of triplets), m (multiplet), q (quartet), s (singlet), t (triplet), and td (triplet of doublets). Assignment of carbons noted C* may be interchanged. Mass spectra were determined on a Hewlett Packard 5988A spectrometer or a Shimadzu QP 2010 spectrometer by a direct inlet at 70 eV.

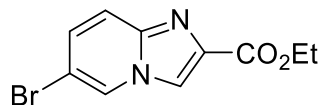
II-3. Chromatography

Reactions were monitored by analytical thin-layer chromatography (TLC) using Merk® silica gel 60F254 plates, which were visualized under UV light at a wavelength of 254 or 366 nm. Column chromatography was performed using Merck Geduran® Si 60 (40–63 μm) silica.

II-4. Synthesis and Characterization

Protocols reported in the literature were adapted in the synthesis of the target imidazo[1,2-a:4,5-c']dipyridine compounds. Compounds **1a-4a**, **5b-d**, **6a-b**, **6d**, and **6f-h** were prepared according to literature.^{8,9}

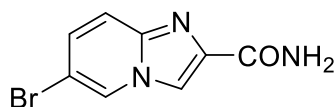
Synthesis of intermediate ethyl 6-bromoimidazo[1,2-a]pyridine-2-carboxylate **1b**



To a solution of 2-amino-5-bromopyridine (8.5 g, 49 mmol, 1 eq) in DME (300 mL) was added dropwise ethyl bromopyruvate (11 mL, 73.7 mmol, 1.5 eq). After stirring for 5h, the solid was filtered and washed with DME. The solid was then transferred in a second flask and heated in refluxing ethanol (500 mL) overnight. The ethanol was evaporated to dryness and the resulting solid was partitioned between water and dichloromethane (CH₂Cl₂) (300 mL/300 mL). The aqueous phase was alkalized with a saturated solution of sodium carbonate (Na₂CO₃) and extracted with twice 300 mL of CH₂Cl₂. The combined organic phases were dried over magnesium sulfate (MgSO₄) and evaporated to yield 11.5 g (42.7 mmol, 87%) of crude product, as a beige solid. **1b** was used directly for the next step without further purification.

m.p.: 122–126°C. ¹H NMR (300MHz, CDCl₃) δ: 8.31 (d, ⁴J = 1.0Hz, 1H, H-6), 8.14 (s, 1H, H-3), 7.61 (d, ³J = 9.6Hz, 1H, H-9), 7.32 (dd, ³J = 9.6Hz, ⁴J = 1.7Hz, 1H, H-8), 4.46 (q, ³J = 7.1Hz, 2H, OCH₂CH₃), 1.44 (t, ³J = 7.1Hz, 3H, OCH₂CH₃). ¹³C NMR (75MHz, CDCl₃) δ: 162.8 (CO), 143.7 (C-9a), 137.5 (C-2), 130.2 (C-8), 126.3 (C-6), 119.8 (C-3), 116.9 (C-9), 109.1 (C-7), 61.6 (OCH₂CH₃), 14.5 (OCH₂CH₃). HRMS (ESI): *m/z* calc. for C₁₀H₉⁷⁹BrN₂O₂ [M+I]⁺: 268.99202, found: 268.99118; *m/z* calc. for C₁₀H₉⁸¹BrN₂O₂ [M+I]⁺: 270.98997, found: 270.98902.

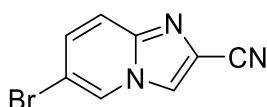
Synthesis of intermediate 6-bromoimidazo[1,2-a]pyridine-2-carboxamide **2b**



1b (11.5 g, 42.7 mmol) was stirred at room temperature overnight in a mixture of 65 mL of THF and 350 mL of an aqueous solution of ammonia (30%). Solvents were then evaporated to dryness. The obtained solid was washed with water and CH₂Cl₂ to afford 9.35 g of a beige solid (38.9 mmol, 91%). **2b** was used directly for the next step without further purification.

m.p.: 253–257°C. ^1H NMR (300MHz, DMSO- d_6) δ : 8.94 (d, 4J = 1.0Hz, 1H, H-6), 8.29 (s, 1H, H-3), 7.76 (bs, 1H, NH), 7.58 (d, 3J = 9.6Hz, 1H, H-9), 7.46-7.42 (m, 2H, H-8 & NH). ^{13}C NMR (75MHz, DMSO- d_6) δ : 163.8 (CO), 142.3 (C-9a*), 140.5 (C-2*), 129.1 (C-8), 127.7 (C-6), 118.4 (C-3), 115.1 (C-9), 106.8 (C-7). HRMS (ESI): m/z calc. for $\text{C}_8\text{H}_6^{79}\text{BrN}_3\text{O}$ $[\text{M}+\text{I}]^+$: 239.97670, found: 239.97592; m/z calc. for $\text{C}_8\text{H}_6^{81}\text{BrN}_3\text{O}$ $[\text{M}+\text{I}]^+$: 241.97465, found: 241.97374.

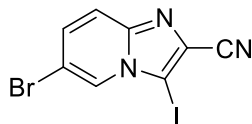
Synthesis of intermediate 6-bromoimidazo[1,2-a]pyridine-2-carbonitrile 3b



2b (8.47 g, 35 mmol) was charged in a 250 mL round bottom flask, followed by phosphoryl chloride (POCl_3) (66 mL, 705 mmol, 20 eq). The reaction mixture was heated at reflux for 4h. POCl_3 was then directly evaporated from the flask, using a vacuum pump equipped with an ice-cooled trap. The resulting solid was then suspended in a mixture of water and CH_2Cl_2 (200 mL/200 mL), followed by alkalization with an aqueous saturated solution of Na_2CO_3 . The aqueous phase was then extracted with CH_2Cl_2 (3 \times 200 mL). The combined organic phases were dried over MgSO_4 and evaporated to yield 6.5 g (29 mmol, 83%) of crude product, as a brown solid. **3b** was used directly for the next step without further purification.

m.p.: 223–227°C. ^1H NMR (300MHz, DMSO- d_6) δ : 8.97 (dd, 4J = 1.8Hz, 5J = 0.9Hz, 1H, H-6), 8.69 (s, 1H, H-3), 7.66 (d, 3J = 9.7Hz, 1H, H-9), 7.57 (dd, 3J = 9.7Hz, 4J = 1.9Hz, 1H, H-8). ^{13}C NMR (75MHz, DMSO- d_6) δ : 143.3 (C-9a), 130.9 (C-8), 127.7 (C-6), 121.5 (C-3), 118.4 (C-9), 116.5 (C-2), 115.0 (CN), 108.3 (C-7). HRMS (ESI): m/z calc. for $\text{C}_8\text{H}_4^{79}\text{BrN}_3$ $[\text{M}+\text{I}]^+$: 221.96614, found: 221.96547; m/z calc. for $\text{C}_8\text{H}_4^{81}\text{BrN}_3$ $[\text{M}+\text{I}]^+$: 223.96409, found: 223.96336.

Synthesis of intermediate 6-bromo-3-iodoimidazo[1,2-a]pyridine-2-carbonitrile **4b**



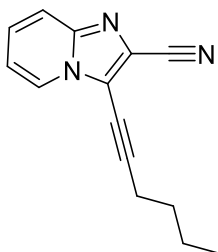
To a solution of **3b** (8.4 g, 37.8 mmol) in acetonitrile (CH₃CN) (170 mL) was added *N*-iodosuccinimide (NIS) (11.1 g, 49.2 mmol, 1.3 eq) in one portion. The reaction mixture was heated at reflux overnight. The CH₃CN was then evaporated to dryness and the solid was washed several times with water, petroleum ether (PE) and diethyl ether (Et₂O). The crude mixture was purified by flash chromatography on alumina using CH₂Cl₂ to afford 10.5 g (30 mmol, 80%) of **4b** as a white solid.

m.p.: 275–279°C. ¹H NMR (300MHz, DMSO-d₆) δ: 8.56 (dd, ⁴J = 1.7Hz, ⁵J = 1.0Hz, 1H, H-6), 7.67 (dd, ³J = 9.6Hz, ⁵J = 0.9Hz, 1H, H-9), 7.61 (dd, ³J = 9.6Hz, ⁴J = 1.7Hz, 1H, H-8). ¹³C NMR (75MHz, DMSO-d₆) δ: 145.8 (C-8a), 131.6 (C-8), 127.8 (C-6), 124.0 (C-2), 118.9 (C-9), 115.0 (CN), 110.0 (C-7), 78.3 (C-3). HRMS (ESI): *m/z* calc. for C₈H₃⁷⁹BrIN₃ [M+I]⁺: 347.86278, found: 347.86179; *m/z* calc. for C₈H₃⁸¹BrIN₃ [M+I]⁺: 349.86073, found: 349.85975.

General procedure for the Sonogashira coupling reaction (compounds **5a**, **5e-h**)

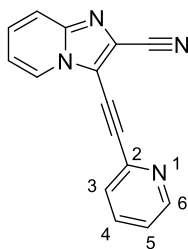
Carbonitriles **4a-b** (e.g., 5 mmol), Pd₂(dba)₃ (228 mg, 0.25 mmol, 5 mol%) and copper iodide (CuI) (95 mg, 0.5 mmol, 10mol%) were introduced in a sealed tube. Vacuum/refilling with argon cycles were repeated thrice and dioxane (5.5 mL), TEA (5.5 mL), and finally alkynes (1.2 eq) were added. The reaction mixture was stirred for 3h at room temperature. The reaction mixture was then filtered on celite® with CH₂Cl₂. The organic phase was washed with a saturated solution of NH₄Cl, dried over MgSO₄, and evaporated. The crude mixture was purified by flash chromatography with silica or alumina with appropriate eluent.

3-(hex-1-yn-1-yl)imidazo[1,2-a]pyridine-2-carbonitrile 5a



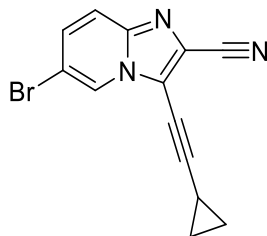
Silica, PE/Et₂O 80/20 → 50/50, white solid, 93 mg. Yield: 21%. ¹H NMR (300MHz, CDCl₃) δ 8.23 (dt, ³J = 6.9, ⁴J = ⁵J = 1.2 Hz, 1H, H-5), 7.66 (dt, ³J = 9.3, ⁴J = ⁵J = 1.2 Hz, 1H, H-8), 7.39 (ddd, ³J = 9.2, 6.8, ⁴J = 1.3 Hz, 1H, H-7), 7.05 (td, ³J = 6.8, ⁴J = 1.1 Hz, 1H, H-6), 2.64 (t, ³J = 7.0 Hz, 2H, CH₂), 1.79–1.63 (m, 2H, CH₂), 1.62–1.50 (m, 2H, CH₂), 1.01 (t, ³J = 7.3 Hz, 3H, CH₃). ¹³C NMR (75 MHz, CDCl₃) δ 144.3 (C-8a), 127.5 (C-7), 125.0 (C-5), 118.4 (C-8), 114.4 (C-6), 114.0 (C-2), 105.7 (C≡C-*n*-Bu), 64.8 (C≡C-*n*-Bu), 30.0 (CH₂), 21.8 (CH₂), 19.4 (CH₂), 13.3 (CH₃). *Two carbons are missing.*

3-(pyridin-2-ylethynyl)imidazo[1,2-a]pyridine-2-carbonitrile 5e



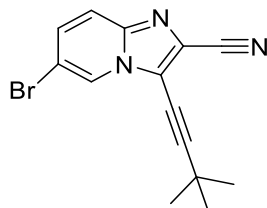
Begie solid, m.p.: 178°C, 303 mg. Yield: 27%. ¹H NMR (300MHz, CDCl₃) δ 8.69 (dt, ³J = 4.8 Hz, ⁴J = 1.4 Hz, 1H, pyr-6), 8.47 (dt, ³J = 6.9 Hz, ⁴J = 1.3 Hz, 1H, H-5), 7.84–7.67 (m, 3H, pyr-3,4 and H-8), 7.47 (ddd, ³J = 9.2, 6.8 Hz, ⁴J = 1.3 Hz, 1H, H-7), 7.36 (ddd, ³J = 7.6, 4.9 Hz, ⁴J = 1.3 Hz, 1H, pyr-5), 7.11 (td, ³J = 6.9 Hz, ⁴J = 1.2 Hz, 1H, H-6). ¹³C NMR (75 MHz, CDCl₃) δ 150.4 (pyr-6), 145.5 (C-8 a), 141.8 (pyr-2), 136.5 (pyr-4), 128.7 (C-7), 127.8 (pyr-3), 125.9 (C-5), 124.0 (pyr-5), 118.8 (C-8), 115.3 (C-6), 113.8 (CN), 102.5 (C≡C-pyr), 72.8 (C≡C-pyr). *Two carbons are missing.*

6-Bromo-3-(cyclopropylethynyl)imidazo[1,2-a]pyridine-2-carbonitrile 5f



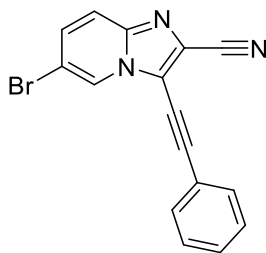
Alumina, CH₂Cl₂, yellow solid, m.p.: 161–165°C, 1.05 g. Yield: 74%. ¹H NMR (300MHz, CDCl₃) δ: 8.33 (dd, ⁴J = 1.8Hz, ⁵J = 0.9Hz, 1H, H-6), 7.52 (dd, ³J = 9.6Hz, ⁵J = 0.9Hz, 1H, H-9), 7.41 (dd, ³J = 9.6Hz, ⁴J = 1.8Hz, 1H, H-8), 1.72-1.58 (m, 1H, CH c-Pr), 1.13-0.95 (m, 4H 2 CH₂ c-Pr). ¹³C NMR (75MHz, CDCl₃) δ: 143.0 (C-9a), 131.6 (C-8), 125.5 (C-6), 121.3 (C-2), 119.3 (C-9), 113.9 (C-3), 110.14 (CN*), 110.06 (C-7*), 59.6 (–C≡C-c-Pr), 9.9 (CH₂ c-Pr), 0.7 (CH c-Pr). *One carbon is missing.* HRMS (ESI): *m/z* calc. for C₁₃H₈⁷⁹BrN₃ [M+I]⁺: 285.99744, found: 285.99663; *m/z* calc. for C₁₃H₈⁸¹BrN₃ [M+I]⁺: 287.99539, found: 287.99444.

6-bromo-3-(3,3-dimethylbut-1-yn-1-yl)imidazo[1,2-a]pyridine-2-carbonitrile 5g



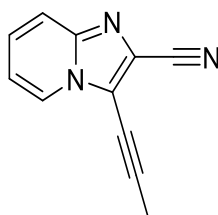
Silica, PE/Et₂O 80/20 → 50/50, yellow solid, m.p.: 137–141°C, 3.26 g. Yield: 94%. ¹H NMR (300MHz, CDCl₃) δ: 8.26 (dd, ⁴J = 1.8Hz, ⁵J = 0.9Hz, 1H, H-6), 7.53 (dd, ³J = 9.6Hz, ⁵J = 0.8Hz, 1H, H-9), 7.42 (dd, ³J = 9.6Hz, ⁴J = 1.8Hz, 1H, H-8), 1.42 (s, 9H, *t*-Bu). ¹³C NMR (75MHz, CDCl₃) δ: 143.1 (C-9a), 131.6 (C-8), 125.4 (C-6), 121.1 (C-2), 119.3 (C-9), 114.7 (C-3*), 113.9 (C-7*), 110.1 (CN), 63.5 (–C≡C-*t*-Bu), 30.7 (CH₃ *t*-Bu), 29.0 (Cq *t*-Bu). *One carbon is missing.* HRMS (ESI): *m/z* calc. for C₁₄H₁₂⁷⁹BrN₃ [M+I]⁺: 302.02874, found: 302.02784; *m/z* calc. for C₁₄H₁₂⁸¹BrN₃ [M+I]⁺: 304.02669, found: 304.02566.

6-bromo-3-(phenylethynyl)imidazo[1,2-a]pyridine-2-carbonitrile 5h



Beige solid, m.p.: 221.8°C, 327 mg. Yield: 50%. ¹H NMR (300MHz, CDCl₃) δ 8.44 (dd, ⁴J = 1.8 Hz, ⁵J = 0.8Hz, 1H, H-5), 7.68–7.63 (m, 2H, Ph-2,6), 7.59 (dd, ³J = 9.6Hz, ⁵J = 0.9 Hz, 1H, H-8), 7.52–7.42 (m, 4H, Ph-3,4,5 and H-7). ¹³C NMR (75 MHz, CDCl₃) δ 143.4 (C-8a), 131.9 (C-7 & Ph-2,6), 130.1 (Ph-4), 128.7 (Ph-3,5), 125.5 (C-5), 121.6 (C-2), 120.7 (Ph-1), 119.4 (C-8), 115.8 (C-6), 113.6 (CN), 110.4 (C-3), 104.3 (-C≡C-Ph), 72.5 (-C≡C-Ph).

Synthesis of 3-(prop-1-yn-1-yl)imidazo[1,2-a]pyridine-2-carbonitrile 5i



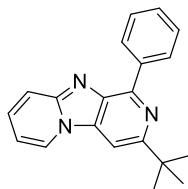
A sealed tube was loaded with 3-iodoimidazo [1,2-a] pyridine-2-carbonitrile **4a** (520 mg, 22 mmol), 2-butanoic acid (336 mg, 4 mmol, 2 eq), in DMF (6 ml), CuI (91.2 mg, 0.1 mmole, 0.05 eq) was added, palladium acetate (Pd(OAc)₂) (44.9 mg, 0.2 mmol, 0.1 eq), PdCl₂(PPh₃)₂ (140 mg, 0.2 mmole, 0.1 eq) and TEA (4 ml, 2 eq). The tube was filled with argon and sealed. The mixture was heated at 50°C for 2 hours by microwave. After that, the mixture was diluted with water (40 ml) and extracted with CH₂Cl₂. The organic layer was washed with brine, dried with MgSO₄, filtered, and concentrated under reduced pressure. The crude mixture was purified by column chromatography with PE and Et₂O (50:50).

Begie solid, m.p.: 172°C, 200 mg. Yield: 55%. ^1H NMR (300 MHz, CDCl_3) δ 8.22 (d, 3J = 6.7Hz, 1H, H-5), 7.62 (d, 3J = 9.1Hz, 1H, H-8), 7.36 (t, 3J = 9.0Hz, 1H, H-7), 7.01 (m, 1H, H-6), 2.27 (s, 3H, CH_3). ^{13}C NMR δ 144.7 (C-8a), 128.0 (C-6), 125.4 (C-5), 120.6 (C-3*), 118.7 (C-8), 116.5 (C-2*), 114.8 (C-7), 114.3 (CN), 101.6 ($-\text{C}\equiv\text{C}-\text{Me}$), 64.5 ($-\text{C}\equiv\text{C}-\text{Me}$), 5.2 (CH_3).

The general method for cyclization with Grignard reagent (compounds 6c, 6e, 6i-o)

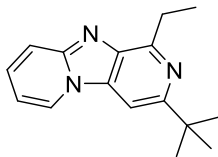
To a solution of 3-alkynylimidazo [1,2-*a*] pyridine-2-carbonitriles (e.g. 1 mmol) in cyclopentyl methyl ether (CPME) (10 mL) were added dropwise Grignard reagent (2 eq) at room temperature. After completion of the reaction (followed by TLC, *ca.* 15 min-5h), 10 mL of NH_4Cl aqueous saturated solution was added. After 30 minutes of hydrolysis, the phases are separated, and the aqueous phase was extracted with 15 mL of ethyl acetate (EtOAc). The crude mixture was purified by flash chromatography on silica gel with appropriate eluent.

3-(tert-Butyl)-1-phenylimidazo[1,2-*a*:4,5-*c'*]dipyridine 6c



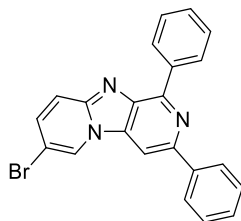
PE/ Et_2O : 50/50, yellow solid, m.p.: 128–132°C, 105 mg. Yield: 77%. ^1H NMR (300MHz, CDCl_3) δ : 8.93-8.91 (m, 2H, Ph-2,6), 8.42 (d, 3J = 6.9Hz, 1H, H-6), 7.76 (d, 3J = 9.4Hz, 1H, H-9), 7.72 (s, 1H, H-4), 7.60-7.55 (m, 2H, Ph-3,5), 7.47-7.39 (m, 2H, Ph-4 & H-8), 6.83 (td, 3J = 6.8Hz, 4J = 0.7Hz, 1H, H-7), 1.56 (s, 9H, *t*-Bu). ^{13}C NMR (75MHz, CDCl_3) δ : 159.8 (C-3), 148.7 (C-9a), 147.7 (C-1), 138.8 (Ph-1), 137.0 (C-10a*), 135.2 (C-4a*), 130.2 (C-8), 129.5 (Ph-2,6), 128.9 (Ph-4), 128.5 (Ph-3,5), 125.5 (C-6), 119.1 (C-9), 111.0 (C-7), 98.8 (C-4), 38.0 (Cq *t*-Bu), 30.9 (CH_3 *t*-Bu). HRMS (ESI): *m/z* calc. for $\text{C}_{20}\text{H}_{19}\text{N}_3$ [$\text{M}+\text{I}$] $^+$: 302.16517, found: 302.16415.

3-(tert-Butyl)-1-ethylimidazo[1,2-a:4,5-c']dipyridine 6e



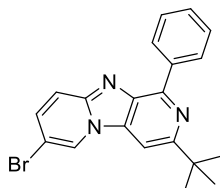
PE/Et₂O: 50/50, yellow solid, m.p.: 121–125°C, 45 mg. Yield: 40%. ¹H NMR (300MHz, CDCl₃) δ: 8.41 (d, ³J = 6.9Hz, 1H, H-6), 7.73 (d, ³J = 9.4Hz, 1H, H-9), 7.60 (s, 1H, H-4), 7.42 (ddd, ³J = 9.3Hz, 6.6Hz, ⁴J = 1.1Hz, 1H, H-8), 6.84 (td, ³J = 6.7Hz, ⁴J = 0.9Hz, 1H, H-7), 3.39 (q, ³J = 7.5Hz, 2H, CH₂CH₃), 1.51-1.46 (m, 12H, *t*-Bu & CH₂CH₃). ¹³C NMR (75MHz, CDCl₃) δ: 160.0 (C-3), 155.7 (C-1), 148.2 (C-9a), 137.1 (C-10a), 133.4 (C-4a), 129.9 (C-8), 125.6 (C-6), 119.0 (C-9), 110.9 (C-7), 97.6 (C-4), 37.8 (Cq *t*-Bu), 30.8 (CH₃, *t*-Bu), 27.2 (CH₂CH₃), 13.0 (CH₂CH₃). HRMS (ESI): *m/z* calc. for C₁₆H₁₉N₃ [M+I]⁺: 254.16517, found: 254.16426.

7-bromo-1,3-diphenylimidazo[1,2-a:4,5-c']dipyridine 6i



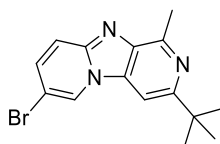
CH₂Cl₂, yellow solid, m.p.: 255–259°C, 210 mg. Yield: 85%. ¹H NMR (300 MHz, CDCl₃) δ 8.88 (d, ³J = 7.3Hz, 2H, 1-Ph-2,6), 8.61 (s, 1H, H-6), 8.23 (d, ³J = 7.3Hz, 2H, 3-Ph-2,6), 8.07 (s, 1H, H-4), 7.70 (d, ³J = 9.7Hz, 1H, H-9), 7.62–7.40 (m, 7H, 1-Ph-3,4,5, 3-Ph-3,4,5 & H-8). ¹³C NMR (75 MHz, CDCl₃) δ 149.4 (C-1), 148.5 (C-3), 147.1 (C-9a), 139.6 (1-Ph-1), 137.89 (C-4a*), 137.85 (3-Ph-1), 135.2 (C-10a*), 134.2 (C-8), 129.6 (1-Ph-2,6), 129.4 (1-Ph-4*), 128.8 (1-Ph-3,5*), 128.52 (3-Ph-4*), 128.48 (3-Ph-3,5*), 127.0 (3-Ph-2,6), 125.7 (C-6), 119.8 (C-9), 105.9 (C-7), 100.1 (C-4).

7-bromo-3-(tert-butyl)-1-phenylimidazo [1,2-a:4,5-c']dipyridine 6j



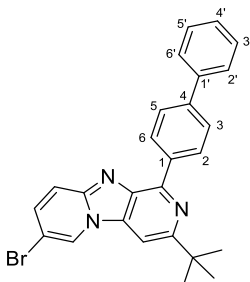
PE/Et₂O: 10/90, yellow solid, m.p.: 216–220°C, 230 mg. Yield: 91%. ¹H NMR (300MHz, CDCl₃) δ: 8.85-8.83 (m, 2H, Ph-2,6), 8.63 (s, 1H, H-6), 7.76 (d, ³J = 9.7Hz, 1H, H-9), 7.60-7.43 (m, 4H, H-8 & Ph-3,4,5), 1.55 (s, 9H, *t*-Bu). ¹³C NMR (75MHz, CDCl₃) δ: 160.7 (C-3), 148.3 (C-1), 146.8 (C-9a), 138.5 (Ph-1), 136.9 (C-4a*), 134.9 (C-10a*), 133.7 (C-8), 129.6 (Ph-2,6), 129.2 (Ph-4), 128.5 (Ph-3,5), 125.7 (C-6), 119.9 (C-9), 105.4 (C-7), 98.7 (C-4), 38.1 (Cq *t*-Bu), 30.8 (CH₃ *t*-Bu). HRMS (ESI): *m/z* calc. for C₂₀H₁₈⁷⁹BrN₃ [M+I]⁺: 380.07569, found: 380.07470; *m/z* calc. for C₂₀H₁₈⁸¹BrN₃ [M+I]⁺: 382.07364, found: 382.07253.

7-bromo-3-(tert-butyl)-1-methylimidazo[1,2-a:4,5-c']dipyridine 6k



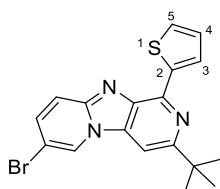
PE/Et₂O: 10/90, yellow solid, m.p.: 226–230°C, 90 mg. Yield: 42%. ¹H NMR (300MHz, CDCl₃) δ: 8.54 (s, 1H, H-6), 7.62 (d, ³J = 9.8Hz, 1H, H-9), 7.57 (s, 1H, H-4), 7.44 (d, ³J = 9.8Hz, 1H, H-8), 2.97 (s, 3H, CH₃), 1.46 (s, 9H, *t*-Bu). ¹³C NMR (75MHz, CDCl₃) δ: 160.8 (C-3), 151.8 (C-1), 146.4 (C-9a), 137.9 (C-10a), 133.3 (C-8), 132.9 (C-4a), 125.8 (C-6), 119.7 (C-9), 105.3 (C-7), 97.8 (C-4), 37.7 (Cq *t*-Bu), 30.7 (CH₃ *t*-Bu), 20.7 (Me). HRMS (ESI): *m/z* calc. for C₁₅H₁₆⁷⁹BrN₃ [M+I]⁺: 318.06004, found: 318.05912; *m/z* calc. for C₁₅H₁₆⁸¹BrN₃ [M+I]⁺: 320.05799, found: 320.05698.

1-([1,1'-biphenyl]-4-yl)-7-bromo-3-(tert-butyl)imidazo[1,2-a:4,5-c']dipyridine 6l



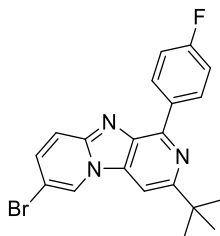
PE/Et₂O: 90/10, yellow solid, m.p.: 230–234°C, 120 mg. Yield: 40%. ¹H NMR (300 MHz, CDCl₃) δ 8.96 (m, 2H, biPh-2,6), 8.64 (s, 1H, H-6), 7.83 (m, 2H, biPh-2',6'), 7.79–7.64 (m, 4H, biPh-3,5*, H-4 and H-9), 7.58–7.45 (m, 3H, biPh-3',5'* and H-8), 7.41 (m, 1H, biPh-4'), 1.58 (s, 9H, *t*-Bu). ¹³C NMR (75 MHz, CDCl₃) δ 160.7 (C-3), 147.9 (C-1), 146.7 (C-9a), 141.7 (biPh-1), 141.1 (biPh-1'), 137.4 (C-4a*), 136.9 (biPh-4'*), 134.8 (C-10a*), 133.6 (C-8), 129.8 (biPh-2,6), 128.8 (biPh-3,5*), 127.4 (biPh-4'), 127.19 (biPh-2',6'*), 127.17 (biPh-3',5'*), 125.6 (C-6), 119.8 (C-9), 105.3 (C-7), 98.6 (C-4), 38.0 (Cq *t*-Bu), 30.7 (CH₃ *t*-Bu).

7-bromo-3-(tert-butyl)-1-(thiophen-2-yl)imidazo[1,2-a:4,5-c']dipyridine 6m



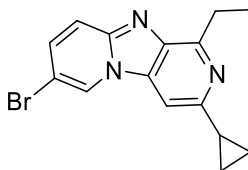
PE/Et₂O: 80/20, yellow solid, m.p.: 192–196°C, 160 mg. Yield: 63%. ¹H NMR (300 MHz, CDCl₃) δ 8.71 (d, ³*J* = 3.6 Hz, 1H, thienyl-3), 8.57 (s, 1H, H-6), 7.69 (d, ³*J* = 9.8 Hz, 1H, H-9), 7.61 (s, 1H, H-4), 7.54–7.44 (m, 2H, thienyl-5 and H-8), 7.25 (dd, ³*J* = 5.0, 3.7 Hz, 1H, thienyl-4), 1.53 (s, 9H, 3CH₃). ¹³C NMR (75 MHz, CDCl₃) δ 160.6 (C-3), 146.9 (C-9 a), 144.0 (C-1*), 143.8 (thienyl-2*), 135.1 (C-4 a), 134.4 (C-10 a), 133.5 (C-8), 129.4 (thienyl-3), 128.3 (thienyl-4*), 128.2 (thienyl-5*), 125.5 (C-6), 119.8 (C-9), 105.4 (C-7), 98.1 (C-4), 37.8 (Cq *t*-Bu), 30.6 (CH₃ *t*-Bu).

7-bromo-3-(tert-butyl)-1-(4-fluorophenyl)imidazo[1,2-a:4,5-c']dipyridine 6n



PE/Et₂O: 90/10, yellow solid, m.p.: > 260°C, 90 mg. Yield: 34%. ¹H NMR (300 MHz, CDCl₃) δ 9.00 – 8.88 (m, 2H, F-Ph-2,6), 8.62 (s, 1H, H-6), 7.75–7.65 (m, 2H, H-4 and H-9), 7.52 (dd, ³J = 9.8Hz, ⁴J = 1.9Hz, 1H, H-8), 7.33–7.19 (m, 2H, F-Ph-3,5), 1.56 (s, 9H, t-Bu). ¹³C NMR (75 MHz, CDCl₃) δ 163.7 (d, ¹J_{C-F} = 246.7Hz, F-Ph-4), 160.7 (C-3), 147.2 (C-9 a*), 146.9 (C-1*), 136.8 (C-4 a*), 135.0 (C-10 a*), 134.7 (d, ⁴J_{C-F} = 3.0Hz, F-Ph-1), 133.8 (C-8), 131.4 (d, ³J_{C-F} = 8.2Hz, F-Ph-2,6), 125.7 (C-6), 119.9 (C-9), 115.4 (d, ²J_{C-F} = 21.0Hz, F-Ph-3,5), 105.5 (C-7), 98.7 (C-4), 38.1 (Cq t-Bu), 30.8 (CH₃ t-Bu).

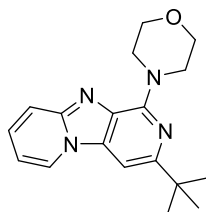
7-Bromo-3-cyclopropyl-1-ethylimidazo[1,2-a:4,5-c']dipyridine 6o



CH₂Cl₂/EtOAc: 70/30 → 60/40, tan solid, m.p.: 121–125°C, 164 mg. Yield: 74%. ¹H NMR (300MHz, CDCl₃) δ: 8.46 (dd, ⁴J = 1.5Hz, ⁵J = 0.6Hz, 1H, H-6), 7.60 (dd, ³J = 9.6Hz, ⁵J = 0.6Hz, 1H, H-9), 7.43 (dd, ³J = 9.6Hz, ⁴J = 1.8Hz, 1H, H-8), 7.36 (s, 1H, H-4), 3.30 (q, ³J = 7.5Hz, 2H, CH₂CH₃), 2.25-2.16 (m, 1H, CH c-Pr), 1.43 (t, ³J = 7.5Hz, 3H, CH₂CH₃), 1.11-0.99 (m, 4H, 2 CH₂ c-Pr). ¹³C NMR (75MHz, CDCl₃) δ: 157.2 (C-1), 153.9 (C-3), 146.1 (C-9a), 137.6 (C-10a), 133.3 (C-8), 125.7 (C-6), 119.8 (C-9), 105.2 (C-7), 99.2 (C-4), 27.4 (CH₂CH₃), 17.9 (CH c-Pr), 13.1 (CH₂CH₃), 9.8 (CH₂ c-Pr). One carbon is missing. HRMS (ESI): *m/z* calc. for C₁₅H₁₄⁷⁹BrN₃ [M+I]⁺: 316.04439, found: 316.04351; *m/z* calc. for C₁₅H₁₄⁸¹BrN₃ [M+I]⁺: 318.04234, found: 318.04135.

Synthesis of 4-(3-(tert-butyl)imidazo[1,2-a:4,5-c']dipyridin-1-yl)morpholine 6p

A mixture of 3-(3,3-Dimethylbut-1-yn-1-yl)imidazo[1,2-*a*]pyridine-2-carbonitrile **5c** (444 mg, 2 mmol), Pd(OAc)₂ (5 mol %, 0.1 mmol, 22.4 mg), PPh₃ (10 mol %, 0.2 mmol, 52.4 mg), morpholine (2 eq, 4 mmol, 348 μ L), and K₂CO₃ (2 eq, 4 mmol, 553 mg) in acetonitrile (16 ml) was stirred under argon at 80°C. Then, the mixture was washed with water, the organic layer was extracted with ethyl acetate, dried with MgSO₄, and concentrated under vacuum. The residue was purified by chromatography on silica gel with CH₂Cl₂/EtOAc (80/20) as eluent.

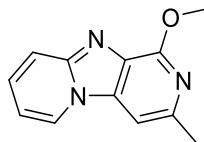


White solid, m.p.: 138–142°C, 50 mg. Yield: 8%. ¹H NMR (300 MHz, CDCl₃) δ 8.31 (d, ³*J* = 6.9 Hz, 1H, H-6), 7.63 (d, ³*J* = 9.3 Hz, 1H, H-9), 7.33 (ddd, ³*J* = 9.3, 6.6, ⁴*J* = 1.3 Hz, 1H, H-8), 7.13 (s, 1H, H-4), 6.84 (td, ³*J* = 6.8 Hz, ⁴*J* = 0.9 Hz, 1H, H-7), 4.26 (m, 4H, 2 CH₂N), 3.93 (m, 4H, 2 CH₂O), 1.41 (s, 9H, 3CH₃). ¹³C NMR (75 MHz, CDCl₃) δ 159.1 (C-3), 150.5 (C-1), 145.7 (C-9a), 135.0 (C-4a), 128.4 (C-8), 124.9 (C-6), 118.6 (C-9), 110.8 (C-7), 91.1 (C-4), 67.3 (2 CH₂O), 47.0 (2 CH₂N), 37.6 (Cq *t*-Bu), 30.4 (CH₃ *t*-Bu). One carbon is missing.

The general method for cyclization with sodium methoxide 6q-v

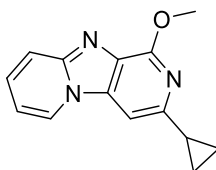
3-Alkynylimidazo[1,2-*a*]pyridine-2-carbonitriles (*e.g.* 1 mmol) were added in one portion to a 0.4M solution of MeONa in MeOH (12 mL). The reaction mixture was refluxed overnight. Methanol was then evaporated and crude solid was partitioned between 25 mL of water and 25 mL of CH₂Cl₂. The aqueous phase was extracted several times with 20 mL of CH₂Cl₂. The combined organic phases were dried over MgSO₄, filtered, and evaporated to dryness. The crude mixture was purified by flash chromatography on silica gel with appropriate eluent.

1-methoxy-3-methylimidazo[1,2-a:4,5-c']dipyridine 6q



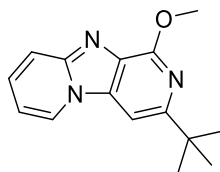
PE/Et₂O: 20/80 → 0/100, solid, m.p.: 130–134°C, 50 mg. Yield: 21%. ¹H NMR (300 MHz, CDCl₃) δ 8.27 (dt, ³J = 7.0 Hz, ⁴J = ⁵J = 1.3 Hz, 1H, H-6), 7.70 (dt, ³J = 9.3 Hz, ⁴J = ⁵J = 1.2 Hz, 1H, H-9), 7.38 (ddd, ³J = 9.4, 6.6 Hz, ⁴J = 1.3 Hz, 1H, H-8), 7.21 (s, 1H, H-4), 6.85 (td, ³J = 6.8 Hz, ⁴J = 1.2 Hz, 1H, H-7), 4.19 (s, 3H, OCH₃), 2.63 (s, 3H, CH₃). ¹³C NMR (75 MHz, CDCl₃) δ 155.7 (C-1), 147.5 (C-9a*), 146.7 (C-3*), 135.0 (C-10a), 129.0 (C-8), 127.9 (C-4a), 125.1 (C-6), 119.2 (C-9), 111.2 (C-7), 98.4 (C-4), 53.6 (OCH₃), 24.5 (CH₃).

3-cyclopropyl-1-methoxyimidazo[1,2-a:4,5-c']dipyridine 6r



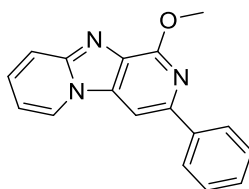
PE/Et₂O: 10/90, yellow solid, m.p.: 188–192°C, 88 mg. Yield: 57%. ¹H NMR (300 MHz, CDCl₃) δ: 8.26 (dt, ³J = 6.9 Hz, ⁴J = 1.0 Hz, 1H, H-6), 7.69 (d, ³J = 9.3 Hz, 1H, H-9), 7.36 (ddd, ³J = 9.3 Hz, 6.6 Hz, ⁴J = 1.2 Hz, 1H, H-8), 7.23 (s, 1H, H-4), 6.83 (td, ³J = 6.8 Hz, ⁴J = 1.0 Hz, 1H, H-7), 4.11 (s, 3H, OCH₃), 2.12–2.04 (m, 1H, CH c-Pr), 1.14–1.09 (m, 2H, 2 CH_aH_b c-Pr), 0.97–0.91 (m, 2H, 2 CH_aH_b c-Pr). ¹³C NMR (75 MHz, CDCl₃) δ: 155.9 (C-1), 151.5 (C-3), 147.3 (C-9a), 135.0 (C-10a*), 129.2 (C-8), 127.5 (C-4a*), 125.3 (C-6), 119.1 (C-9), 111.4 (C-7), 96.6 (C-4), 53.4 (OCH₃), 17.5 (CH c-Pr), 9.3 (CH₂ c-Pr). HRMS (ESI): *m/z* calc. for C₁₄H₁₃N₃O [M+]⁺: 240.11314, found: 240.11230.

3-(tert-Butyl)-1-methoxyimidazo[1,2-a:4,5-c']dipyridine 6s



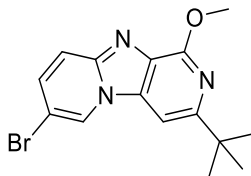
PE/Et₂O: 10/90, beige solid, m.p.: 80–84°C, 45 mg. Yield: 39%. ¹H NMR (300MHz, CDCl₃) δ : 8.40 (d, ³J = 6.5Hz, 1H, H-6), 7.81 (d, ³J = 9.2Hz, 1H, H-9), 7.44 (dd, ³J = 8.8Hz, ⁴J = 6.8Hz, 1H, H-8), 7.34 (s, 1H, H-4), 6.92 (t, ³J = 6.4Hz, 1H, H-7), 4.19 (s, 3H, OCH₃), 1.43 (s, 9H, t-Bu). ¹³C NMR (75MHz, CDCl₃) δ : 159.2 (C-3), 154.7 (C-1), 147.2 (C-9a), 134.8 (C-4a*), 129.9 (C-8), 126.3 (C-10a*), 125.4 (C-6), 118.8 (C-9), 111.9 (C-7), 94.4 (C-4), 53.6 (OCH₃), 37.8 (Cq t-Bu), 30.4 (CH₃ t-Bu). HRMS (ESI): *m/z* calc. for C₁₅H₁₇N₃O [M+I]⁺: 256.14444, found: 256.14351.

1-methoxy-3-phenylimidazo[1,2-a:4,5-c']dipyridine 6t



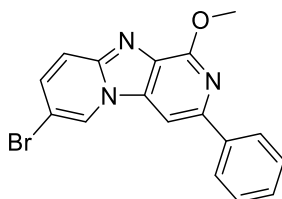
PE/EtOAc: 50/50 → 30/70, beige solid, m.p.: 248–252°C, 100 mg. Yield: 44%. ¹H NMR (300MHz, CDCl₃) δ : 8.37 (d, ³J = 6.9Hz, 1H, H-6), 8.15–8.12 (m, 2H, Ph-2,6), 7.80 (s, 1H, H-4), 7.72 (d, ³J = 9.4Hz, 1H, H-9), 7.50–7.35 (m, 4H, H-8 & Ph-3,4,5), 6.89 (t, ³J = 6.8Hz, 1H, H-7), 4.30 (s, 3H, OCH₃). ¹³C NMR (75MHz, CDCl₃) δ : 155.9 (C-1), 148.3 (C-9a), 146.0 (C-3), 139.6 (Ph-1), 135.4 (C-4a), 129.6 (C-8*), 129.4 (C-10a), 128.8 (Ph-3,5), 128.3 (Ph-4*), 126.7 (Ph-2,6), 125.4 (C-6), 119.3 (C-9), 111.7 (C-7), 96.3 (C-4), 53.8 (OCH₃). HRMS (ESI): *m/z* calc. for C₁₇H₁₃N₃O [M+I]⁺: 276.11314, found: 276.11235.

7-bromo-3-(tert-butyl)-1-methoxyimidazo[1,2-a:4,5-c']dipyridine 6u



CH₂Cl₂, beige solid, m.p.: 207–211°C, 143 mg. Yield: 43%. ¹H NMR (300MHz, CDCl₃) δ: 8.51 (d, ⁴J = 1.5Hz, 1H, H-6), 7.66 (d, ³J = 9.7Hz, 1H, H-9), 7.44 (dd, ³J = 9.7Hz, ⁴J = 1.8Hz, 1H, H-8), 7.30 (s, 1H, H-4), 4.19 (s, 3H, OCH₃), 1.43 (s, 9H, *t*-Bu). ¹³C NMR (75MHz, CDCl₃) δ: 159.7 (C-3), 155.1 (C-1), 145.7 (C-9a), 134.7 (C-10a), 132.7 (C-8), 127.6 (C-4a), 125.5 (C-6), 119.8 (C-9), 105.9 (C-7), 94.2 (C-4), 53.6 (OCH₃), 37.8 (Cq *t*-Bu), 30.4 (CH₃ *t*-Bu). HRMS (ESI): *m/z* calc. for C₁₅H₁₆⁷⁹BrN₃O [M+I]⁺: 334.05495, found: 334.05389; *m/z* calc. for C₁₅H₁₆⁸¹BrN₃O [M+I]⁺: 336.05290, found: 336.05169.

7-bromo-1-methoxy-3-phenylimidazo[1,2-a:4,5-c']dipyridine 6v

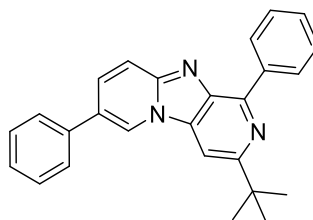


CH₂Cl₂, brown solid, m.p.: 240–244°C, 220 mg. Yield: 47%. ¹H NMR (300 MHz, CDCl₃) δ 8.56 (s, 1H, H-6), 8.15 (m, 2H, Ph-2,6), 7.81 (s, 1H, H-4), 7.67 (d, ³J = 9.8Hz, 1H, H-9), 7.57–7.44 (m, 3H, Ph-3,5 and H-8), 7.42 (m, 1H, Ph-4), 4.32 (s, 3H, OCH₃). ¹³C NMR (75 MHz, CDCl₃) δ 155.8 (C-1), 146.8 (C-3*), 146.2 (C-9a*), 139.2 (Ph-1), 134.9 (C-4a*), 133.1 (C-8), 129.0 (C-10a*), 128.7 (Ph-3,5), 128.5 (Ph-4), 126.7 (Ph-2,6), 125.5 (C-6), 119.8 (C-9), 106.3 (C-7), 95.9 (C-4), 53.8 (OCH₃).

The general method for Suzuki-Miyaura cross-coupling (compounds 7a-e)

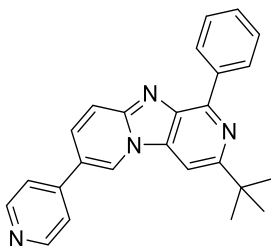
7- Bromo-imidazo[1,2-a:4,5-c']dipyridine **6u** and **6j** (e.g. 100 mg), PdCl₂(PPh₃)₂ (10 mol%), Na₂CO₃ (2 eq) and boronic acid (1.1 eq) were introduced in a microwave reaction vial. DME (1 mL) and water (500 µL) were then added. The mixture was heated using a microwave oven until completion (ca. 1–3 h). The crude mixture was partitioned between 20 mL of water and 20 mL of CH₂Cl₂. The aqueous phase was then extracted with twice 20 mL of CH₂Cl₂. The combined organic phases were dried over MgSO₄, filtered, and evaporated to dryness. The crude mixture was purified by flash chromatography on silica gel with appropriate eluent.

3-(tert-butyl)-1,7-diphenylimidazo[1,2-a:4,5-c']dipyridine 7a



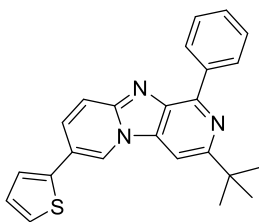
CH₂Cl₂, orange solid, m.p.: 267–271°C, 92 mg. Yield: 93%. ¹H NMR (300MHz, CDCl₃) δ: 8.93-8.89 (m, 2H, 1-Ph-2,6), 8.60 (m, 1H, H-6), 7.86 (dd, ³J = 9.6Hz, ⁵J = 0.8Hz, 1H, H-9), 7.78 (s, 1H, H-4), 7.75 (dd, ³J = 9.6Hz, ⁴J = 1.8Hz, 1H, H-8), 7.68-7.67 (m, 2H, 7-Ph-2,6), 7.60-7.41 (m, 6H, 1-Ph-3,4,5 & 7-Ph-3,4,5), 1.56 (s, 9H, t-Bu). ¹³C NMR (75MHz, CDCl₃) δ: 160.1 (C-3), 148.1 (C-1*), 148.0 (C-9a*), 138.8 (1-Ph-1), 137.4 (7-Ph-1), 136.9 (C-10a), 135.6 (C-4a), 131.3 (C-8), 129.6 (1-Ph-2,6), 129.4 (1-Ph-3,5*), 129.0 (1-Ph-4*), 128.5 (7-Ph-3,5*), 128.3 (7-Ph-4*), 127.0 (7-Ph-2,6), 125.6 (C-7), 122.5 (C-6), 119.1 (C-9), 98.9 (C-4), 38.1 (Cq t-Bu), 30.1 (CH₃ t-Bu). HRMS (ESI): m/z calc. for C₂₆H₂₃N₃ [M+]⁺: 378.19647, found: 378.19548.

3-(tert-butyl)-1-phenyl-7-(pyridin-4-yl)imidazo[1,2-a:4,5-c']dipyridine 7b



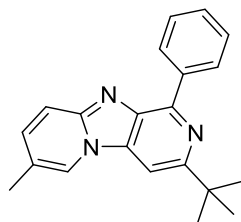
CH₂Cl₂ → CH₂Cl₂/MeOH 99/1, pale yellow solid, m.p.: 254–258°C, 72 mg. Yield: 73%. ¹H NMR (300MHz, CDCl₃) δ: 8.89-8.86 (m, 2H, Ph-2,6), 8.72 (bs, 2H, pyr-2,6), 8.67 (s, 1H, H-6), 7.82 (d, ³J = 9.6Hz, 1H, H-9), 7.77 (s, 1H, H-4), 7.67 (dd, 3J = 9.6Hz, ⁴J = 1.5Hz, 1H, H-8), 7.56-7.51 (m, 4H, Ph-3,5 & pyr-3,5), 7.45-7.40 (m, 1H, Ph-4), 1.56 (s, 9H, t-Bu). ¹³C NMR (75MHz, CDCl₃) δ: 160.5 (C-3), 150.7 (pyr-2,6), 148.1 (C-1*), 147.9 (C-9a*), 144.1 (pyr-4), 138.5 (Ph-1), 137.3 (C-4a), 135.5 (C-10a), 129.55 (C-8), 129.50 (Ph-2,6), 129.1 (Ph-4), 128.4 (Ph-3,5), 123.5 (C-6), 122.5 (C-7), 121.2 (pyr-3,5), 119.5 (C-9), 98.9 (C-4), 38.1 (Cq t-Bu), 30.8 (CH₃ t-Bu). HRMS (ESI): *m/z* calc. for C₂₅H₂₂N₄ [M+I]⁺: 379.19172, found: 379.19058.

3-(tert-butyl)-1-phenyl-7-(thiophen-2-yl)imidazo[1,2-a:4,5-c']dipyridine 7c



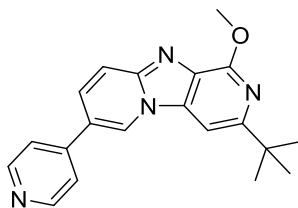
CH₂Cl₂, pale yellow solid, m.p.: 229–233°C, 90 mg. Yield: 89%. ¹H NMR (300MHz, CDCl₃) δ: 8.91-8.88 (m, 2H, Ph-2,6), 8.60 (s, 1H, H-6), 7.80 (dd, ³J = 9.6Hz, ⁵J = 0.8Hz, 1H, H-9), 7.75 (s, 1H, H-4), 7.71 (dd, ³J = 9.6Hz, ⁴J = 1.8Hz, 1H, H-8), 7.60-7.55 (m, 2H, Ph-3,5), 7.47-7.42 (m, 1H, Ph-4), 7.37-7.35 (m, 2H, thienyl-3,5), 7.15 (dd, ³J = 4.9Hz, 3.8Hz, 1H, thienyl-4), 1.57 (s, 9H, t-Bu). ¹³C NMR (75MHz, CDCl₃) δ: 160.3 (C-3), 148.0 (C-1), 147.8 (C-9a), 139.4 (thienyl-2), 138.7 (Ph-1), 137.3 (C-4a), 135.5 (C-10a), 130.4 (C-8), 129.5 (Ph-2,6), 129.0 (Ph-4), 128.5 (Ph-3,5 & thienyl-4), 125.6 (thienyl-5*), 124.4 (thienyl-3*), 121.1 (C-6), 119.6 (C-7), 119.1 (C-9), 98.9 (C-4), 38.1 (Cq t-Bu), 30.9 (CH₃ t-Bu). HRMS (ESI): *m/z* calc. for C₂₄H₂₁N₃S [M+I]⁺: 384.15289, found: 384.15177.

3-(tert-butyl)-7-methyl-1-phenylimidazo[1,2-a:4,5-c']dipyridine 7d



CH₂Cl₂, pale yellow solid, m.p.: 190–194°C, 74 mg. Yield: 89%. ¹H NMR (300MHz, CDCl₃) δ : 8.91-8.88 (m, 2H, Ph-2,6), 8.23 (s, 1H, H-6), 7.71-7.68 (m, 2H, H-4 & H-9), 7.59-7.54 (m, 2H, Ph-3,5), 7.46-7.40 (m, 1H, Ph-4), 7.31 (dd, ³J = 9.5Hz, ⁴J = 1.7Hz, 1H, H-8), 2.41 (s, 3H, Me), 1.55 (s, 9H, t-Bu). ¹³C NMR (75MHz, CDCl₃) δ : 159.6 (C-3), 148.1 (C-9a), 147.7 (C-1), 138.9 (Ph-1), 137.2 (C-10a*), 135.1 (C-4a*), 133.7 (C-8), 129.5 (Ph-2,6), 128.9 (Ph-4), 128.5 (Ph-3,5), 122.8 (C-6), 120.7 (C-7), 118.5 (C-9), 98.8 (C-4), 38.0 (Cq t-Bu), 30.9 (CH₃ t-Bu), 18.3 (Me). HRMS (ESI): *m/z* calc. for C₂₁H₂₁N₃ [M+]⁺: 316.18082, found: 316.17996.

3-(tert-butyl)-1-methoxy-7-(pyridin-4-yl)imidazo[1,2-a:4,5-c']dipyridine 7e

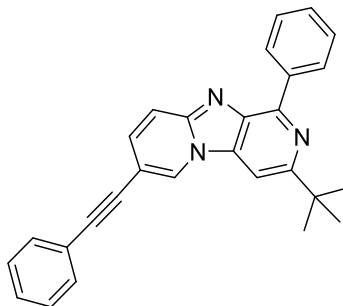


CH₂Cl₂/MeOH 99/1 → CH₂Cl₂/MeOH 96/4, brown solid, m.p.: 190–194°C, 106 mg. Yield: 99%. ¹H NMR (300MHz, CDCl₃) δ : 8.75-8.73 (m, 2H, pyr-2,6), 8.62 (dd, ⁴J = 1.5Hz, ⁵J = 0.9Hz, 1H, H-6), 7.81 (dd, ³J = 9.6Hz, ⁵J = 0.7Hz, 1H, H-9), 7.65 (dd, ³J = 9.6Hz, ⁴J = 1.7Hz, 1H, H-8), 7.59-7.56 (m, 2H, pyr-3,5), 7.39 (s, 1H, H-4), 4.19 (s, 3H, OCH₃), 1.45 (s, 9H, t-Bu). ¹³C NMR (75MHz, CDCl₃) δ : 159.4 (C-3), 155.2 (C-1), 150.7 (pyr-2,6), 147.0 (C-9a), 144.5 (pyr-4), 135.4 (C-4a*), 128.4 (C-10a*), 128.3 (C-8), 123.4 (C-6), 122.8 (C-7), 121.3 (pyr-3,5), 119.7 (C-9), 94.3 (C-4), 53.5 (OCH₃), 37.9 (Cq t-Bu), 30.5 (CH₃ t-Bu). HRMS (ESI): *m/z* calc. for C₂₀H₂₀N₄O [M+]⁺: 333.17099, found: 333.06997.

General procedure for the Sonogashira coupling reaction for the synthesis of compounds 7f-g

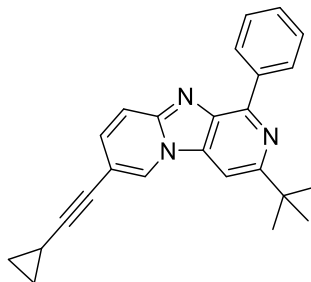
To a screw-capped test tube were added 100 mg of **6j** (0.263 mmol), copper iodide (10 mol%), $\text{PdCl}_2(\text{PPh}_3)_2$ (10 mol%). The tube was evacuated and backfilled with nitrogen. Triethylamine (0.25 mL), DMF (0.25 mL) and alkyne (2 mmol) were added successively by syringe at heated at 80 °C overnight. The suspension was then diluted with a saturated aqueous ammonium chloride solution and extracted with CH_2Cl_2 . The organic phase was dried over MgSO_4 . After concentration to dryness, the residue is purified on silica gel.

3-(tert-butyl)-1-phenyl-7-(phenylethynyl)imidazo[1,2-a:4,5-c']dipyridine 7f



CH_2Cl_2 , clear brown solid, m.p.: 94–98°C, 105 mg. Yield: 69%. ^1H NMR (300 MHz, CDCl_3) δ 8.87 (m, 2H, 1-Ph-2,6), 8.70 (s, 1H, H-6), 7.79 (d, $3J = 9.5\text{Hz}$, 1H, H-9), 7.75 (s, 1H, H-4), 7.60–7.37 (m, 9H, 1-Ph-3,4,5, $-\text{C}\equiv\text{C}-\text{Ph}$, and H-8), 1.55 (s, 9H, 3CH_3 t-Bu). ^{13}C NMR (75 MHz, CDCl_3) δ 160.7 (C-3), 148.1 (C-1*), 147.3 (C-9a*), 138.6 (1-Ph-1), 137.2 (C-10a*), 135.2 (C-4a*), 133.0 (C-8), 131.7 ($-\text{C}\equiv\text{C}-\text{Ph}$ -1), 129.6 (1-Ph-2,6), 129.1 (1-Ph-4*), 129.0 ($-\text{C}\equiv\text{C}-\text{Ph}$ -4*), 128.7 (1-Ph-3,5*), 128.5 ($-\text{C}\equiv\text{C}-\text{Ph}$ -3,5*), 128.3 (C-6), 122.6 ($-\text{C}\equiv\text{C}-\text{Ph}$ -1), 118.8 (C-9), 108.1 (C-7), 98.9 (C-4), 91.6 ($-\text{C}\equiv\text{C}-\text{Ph}$), 85.1 ($-\text{C}\equiv\text{C}-\text{Ph}$), 38.1 (Cq t-Bu), 30.9 (CH_3 t-Bu).

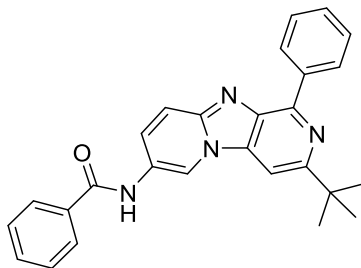
3-(tert-butyl)-7-(cyclopropylethynyl)-1-phenylimidazo[1,2-a:4,5-c']dipyridine 7g



PE/EtOAc: 95/5, yellow solid, m.p.: 167–171°C, 96 mg. Yield: 19%. ¹H NMR (300 MHz, CDCl₃) δ 8.86 (m, 2H, Ph-2,6), 8.51 (s, 1H, H6), 7.71–7.63 (m, 2H, H-4 and H-9), 7.55 (m, 2H, Ph-3,5), 7.49–7.43 (m, 1H, Ph-4), 7.40 (dd, ³J = 9.6 Hz, ⁴J = 1.7 Hz, 1H, H-8), 1.55–1.51 (m, 10H, 3CH₃ *t*-Bu and CH *c*-Pr), 0.89 (m, 4H, 2CH₂ *c*-Pr). ¹³C NMR (75 MHz, CDCl₃) δ 160.3 (C-3), 147.8 (C-1), 147.1 (C-9a), 138.5 (Ph-1), 137.0 (C-4a), 135.0 (C-10a), 133.4 (C-8), 129.4 (Ph-2,6), 128.9 (Ph-4), 128.3 (Ph-3,5), 127.9 (C-6), 118.4 (C-9), 108.5 (C-7), 98.7 (C-4), 95.8 (C≡C-*c*-Pr), 71.4 (C≡C-*c*-Pr), 37.9 (Cq *t*-Bu), 30.7 (3CH₃ *t*-Bu), 8.7 (2CH₂ *c*-Pr), 0.13 (CH *c*-Pr).

Synthesis of N-(3-(tert-butyl)-1-phenylimidazo[1,2-a:4,5-c']dipyridin-7-yl)benzamide 7h

In a microwave tube, to a solution of **6j** (100 mg, 0.263 mmol, 1 eq) in 0.3 mL of toluene, CuI (5 mg, 0.026 mmol, 0.1 eq), 1,2-trans-cyclohexane diamine (4 μl, 4 mg, 0.026 mmol, 0.1 eq), benzamide (38 mg, 0.316 mmole, 1.2 eq) and K₃PO₄ (112 mg, 0.526 mmol, 2eq) were added. The mixture was heated using microwave irradiation at 100 °C for 30 minutes. Then, heated at 130 °C for 30 minutes. After cooling, the reaction mixture was concentrated under reduced pressure. The residue was purified by silica gel chromatography (eluent: PE/EtOAc, 70:30 to 50:50).

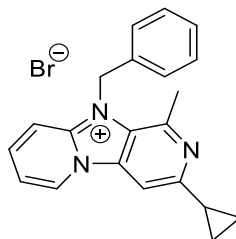


Yellow solid, m.p.: 260–264°C, 111 mg. Yield: 72%. ^1H NMR (300 MHz, CD_3OD) δ 9.76 (s, 1H, H-6), 8.42–8.40 (m, 2H, 1-Ph-2,6), 8.21 (s, 1H, H-4), 8.03–8.00 (m, 2H, CPh-2,6), 7.94 (dd, $^3J = 9.8\text{Hz}$, $^4J = 1.7\text{Hz}$, 1H, H-8), 7.81 (d, $^3J = 9.8\text{Hz}$, 1H, H-9), 7.66–7.50 (m, 6H, 1-Ph-3,4,5 and CPh-3,4,5), 1.54 (s, 9H, 3CH₃ *t*-Bu). ^{13}C NMR (75 MHz, CD_3OD) δ 168.9, 148.3, 135.2, 133.4, 132.0, 130.9, 130.6, 129.8, 129.6, 128.8, 128.4, 119.1, 117.6, 116.2, 110.0, 102.3, 101.0, 38.8, 30.9. Two carbons are missing.

The general method for salt formation (POD118, POD108, POD147 and 8-29)

To the appropriate solutions of imidazo[1,2-*a*:4,5-*c'*]dipyridines (e.g., 0.5 mmol) in CH_3CN (5 mL) was added 8 eq of benzyl bromide or ethyl iodide (1.5 eq for 1-methoxy analogues). The tube was sealed and the reaction heated to 80 °C for ca. 1-5 d (24h for 1-methoxy analogues). After cooling in an ice bath, the solid was filtered and washed with EtOAc.

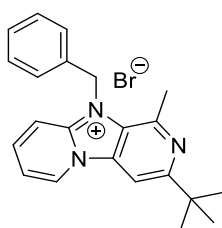
10-benzyl-3-cyclopropyl-1-methylimidazo[1,2-*a*:4,5-*c'*]dipyridin-10-ium bromide (POD118)



Brown solid, m.p.: 158–162°C, 7 mg. Yield: 39%. ^1H NMR (300MHz, CD_3OD) δ : 9.54 (d, $^3J = 6.8\text{Hz}$, 1H, H-6), 8.49–8.43 (m, 2H, H-8 & H-4), 8.31 (d, $^3J = 9.3\text{Hz}$, 1H, H-9), 7.81 (td, $^3J = 7.0\text{Hz}$, $^4J = 0.8\text{Hz}$, 1H, H-7), 7.44–7.36 (m, 3H, Ph-3,4,5), 7.25–7.22 (m, 2H, Ph-2,6), 6.17 (s, 2H, CH_2Ph), 2.90

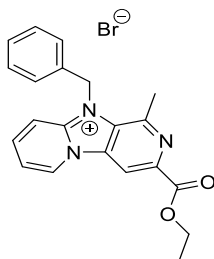
(s, 3H, CH_3), 2.47-2.39 (m, 1H, CH c-Pr), 1.26-1.20 (m, 4H, 2 CH_2 c-Pr). ^{13}C NMR (75MHz, CD_3OD) δ : 158.6 (C-3), 146.9 (C-1*), 146.0 (C-9a*), 143.7 (C-8), 137.2 (Ph-1), 135.7 (C-4a), 131.5 (C-6), 130.6 (Ph-3,5), 129.7 (Ph-4), 127.9 (C-10a), 126.8 (Ph-2,6), 119.2 (C-7), 112.5 (C-9), 105.1 (C-4), 50.3 (CH_2Ph), 20.6 (Me), 16.8 (CH c-Pr), 11.6 (CH_2 c-Pr). HRMS (ESI): m/z calc. for $\text{C}_{21}\text{H}_{20}\text{N}_3$ $[\text{M}]^+$: 314.16517, found: 314.16443.

10-benzyl-3-(tert-butyl)-1-methylimidazo[1,2-a:4,5-c']dipyridin-10-ium bromide (POD108)



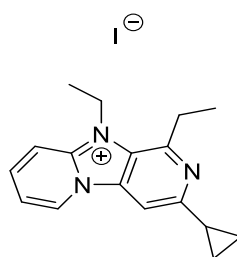
Beige solid, m.p.: 138–142°C, 156 mg. Yield: 69%. ^1H NMR (300MHz, DMSO-d_6) δ : 9.84 (d, $^3J = 6.6\text{Hz}$, 1H, H-6), 8.70 (s, 1H, H-4), 8.50-8.42 (m, 2H, H-8 & H-9), 7.82 (ddd, $^3J = 6.9\text{Hz}$, 6.0Hz, $^4J = 2.4\text{Hz}$, 1H, H-7), 7.40-7.36 (m, 3H, Ph-3,4,5), 7.25-7.23 (m, 2H, Ph-2,6), 6.18 (s, 2H, CH_2Ph), 2.76 (s, 3H, CH_3), 1.43 (s, 9H, *t*-Bu). ^{13}C NMR (75MHz, DMSO-d_6) δ : 163.3 (C-3), 144.0 (C-1*), 143.6 (C-9a*), 141.0 (C-8), 135.7 (Ph-1), 133.9 (C-4a), 130.3 (C-6), 129.1 (Ph-3,5), 128.0 (Ph-4), 125.7 (Ph-2,6), 125.5 (C-10a), 117.0 (C-7), 111.2 (C-9), 102.0 (C-4), 48.2 (CH_2Ph), 37.7 (Cq *t*-Bu), 30.2 (CH_3 *t*-Bu), 22.4 (Me). HRMS (ESI): m/z calc. for $\text{C}_{22}\text{H}_{24}\text{N}_3$ $[\text{M}]^+$: 330.19647, found: 330.19572.

10-benzyl-3-(ethoxycarbonyl)-1-methylimidazo[1,2-a:4,5-c']dipyridin-10-ium bromide (POD147)



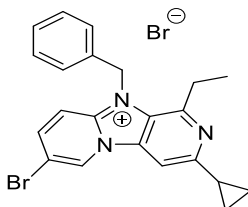
Beige solid, m.p.: 256–260°C, 5 mg. Yield: 15%. ^1H NMR (300MHz, CD_3OD) δ : 9.73 (d, $^3J = 6.9\text{Hz}$, 1H, H-6), 9.28 (s, 1H, H-4), 8.52 (ddd, $^3J = 9.3\text{Hz}$, 7.2Hz , $^4J = 0.9\text{Hz}$, 1H, H-8), 8.37 (d, $^3J = 9.3\text{Hz}$, 1H, H-9), 7.87 (t, $^3J = 6.9\text{Hz}$, 1H, H-7), 7.44-7.37 (m, 3H, Ph-3,4,5), 7.26-7.23 (m, 2H, Ph-2,6), 6.24 (s, 2H, CH_2Ph), 4.55 (q, $^3J = 7.1\text{Hz}$, 2H, OCH_2CH_3), 2.99 (s, 3H, CH_3), 1.49 (t, $^3J = 7.1\text{Hz}$, 3H, OCH_2CH_3). ^{13}C NMR (75MHz, CD_3OD) δ : 165.3 (C-3), 147.8 (C-1), 146.6 (C-9a), 143.53 (C-4a), 143.47 (C-8), 135.9 (C-10a), 135.2 (Ph-1), 131.7 (C-6), 130.6 (Ph-3,5), 129.7 (Ph-4), 126.7 (Ph-2,6), 119.4 (C-7), 112.6 (C-9), 110.4 (C-4), 63.5 (OCH_2CH_3), 50.3 (CH_2Ph), 22.4 (Me), 14.6 (OCH_2CH_3). CO is missing. HRMS (ESI): m/z calc. for $\text{C}_{21}\text{H}_{20}\text{N}_3\text{O}_2$ $[\text{M}]^+$: 346.15500, found: 346.15400.

3-cyclopropyl-1,10-diethylimidazo[1,2-a:4,5-c']dipyridin-10-ium iodide (8)



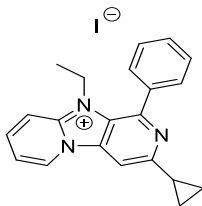
Pale yellow solid, m.p.: 256–260°C, 30 mg. Yield: 15%. ^1H NMR (300MHz, DMSO-d_6) δ : 9.52 (d, $^3J = 6.9\text{Hz}$, 1H, H-6), 8.47-8.38 (m, 3H, H-4, H-8 & H-9), 7.75 (td, $^3J = 6.6\text{Hz}$, $^4J = 1.5\text{Hz}$, 1H, H-7), 4.83 (q, $^3J = 7.1\text{Hz}$, 2H, CH_2CH_3), 3.32 (q, $^3J = 7.5\text{Hz}$, 2H, CH_2CH_3), 2.35-2.27 (m, 1H, CH c-Pr), 1.47 (t, $^3J = 7.1\text{Hz}$, 3H, CH_2CH_3), 1.38 (t, $^3J = 7.3\text{Hz}$, 3H, CH_2CH_3), 1.13-1.02 (m, 4H, 2 CH_2 c-Pr). ^{13}C NMR (75MHz, DMSO-d_6) δ : 156.2 (C-3), 148.7 (C-1), 142.7 (C-9a), 140.2 (C-8), 133.5 (C-4a), 129.6 (C-6), 124.5 (C-10a), 116.7 (C-7), 111.4 (C-9), 102.7 (C-4), 41.1 (CH_2CH_3), 27.1 (CH_2CH_3), 17.2 (CH c-Pr), 15.0 (CH_2CH_3), 12.2 (CH_2CH_3), 10.2 (CH_2 c-Pr). HRMS (ESI): m/z calc. for $\text{C}_{17}\text{H}_{20}\text{N}_3$ $[\text{M}]^+$: 266.16517, found: 266.16450.

10-benzyl-7-bromo-3-cyclopropyl-1-ethylimidazo[1,2-a:4,5-c']dipyridin-10-ium bromide (9)



Pale yellow solid, m.p.: 232–236°C, 31 mg. Yield: 20%. ^1H NMR (300MHz, DMSO- d_6) δ : 10.09 (s, 1H, H-6), 8.65 (dd, $^3J = 9.7\text{Hz}$, $^4J = 1.2\text{Hz}$, 1H, H-8), 8.51-8.47 (m, 2H, H-4 & H-9), 7.36-7.34 (m, 3H, Ph-3,4,5), 7.22-7.19 (m, 2H, Ph-2,6), 6.16 (s, 2H, CH_2Ph), 3.01 (q, $^3J = 7.3\text{Hz}$, 2H, CH_2CH_3), 2.34-2.24 (m, 1H, CH c-Pr), 1.11-1.02 (m, 7H, 2CH_2 c-Pr & CH_2CH_3). ^{13}C NMR (75MHz, DMSO- d_6) δ : 157.1 (C-3), 149.0 (C-1), 143.3 (C-8), 142.8 (C-9a), 135.2 (Ph-1), 133.7 (C-4a), 130.3 (C-6), 129.0 (Ph-3,5), 128.1 (Ph-4), 125.7 (Ph-2,6), 124.7 (C-10a), 112.5 (C-9), 110.6 (C-7), 102.8 (C-4), 48.7 (CH_2Ph), 26.8 (CH_2CH_3), 17.3 (CH c-Pr), 12.1 (CH_2CH_3), 10.4 (2 CH_2 c-Pr). HRMS (ESI): m/z calc. for $\text{C}_{22}\text{H}_{21}^{79}\text{BrN}_3$ $[\text{M}]^+$: 406.09134, found: 406.09033; m/z calc. for $\text{C}_{22}\text{H}_{21}^{81}\text{BrN}_3$ $[\text{M}]^+$: 408.08929, found: 408.08815.

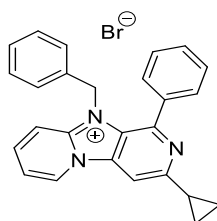
3-cyclopropyl-10-ethyl-1-phenylimidazo[1,2-a:4,5-c']dipyridin-10-ium iodide (10)



Pale yellow solid, m.p.: 237–241°C, 103 mg. Yield: 44%. ^1H NMR (300MHz, DMSO- d_6) δ : 9.62 (d, $^3J = 6.9\text{Hz}$, 1H, H-6), 8.63 (s, 1H, H-4), 8.48-8.43 (m, 2H, H-8 & H-9), 7.81 (td, $^3J = 6.6\text{Hz}$, $^4J = 1.5\text{Hz}$, 1H, H-7), 7.68-7.60 (m, 5H, Ph), 4.29 (q, $^3J = 7.1\text{Hz}$, 2H, CH_2CH_3), 2.45-2.35 (m, 1H, CH c-Pr), 1.16-1.02 (m, 4H, 2CH_2 c-Pr), 0.95 (t, $^3J = 7.1\text{Hz}$, 3H, CH_2CH_3). ^{13}C NMR (75MHz, DMSO- d_6) δ : 156.8 (C-3), 145.9 (C-1), 143.4 (C-9a), 140.8 (C-8), 136.9 (Ph-1), 134.4 (C-4a), 129.8 (C-6*), 129.7 (Ph-4*), 129.1 (Ph-2,6*), 128.5 (Ph-3,5*), 124.4 (C-10a), 117.0 (C-7), 111.7 (C-9), 103.9 (C-4), 40.7

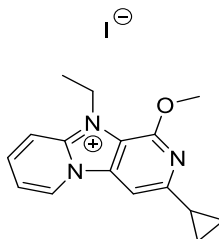
(CH₂CH₃), 17.3 (CH c-Pr), 13.5 (CH₂CH₃), 10.5 (CH₂ c-Pr). HRMS (ESI): *m/z* calc. for C₂₁H₂₀N₃ [M]⁺: 314.16517, found: 314.16421.

10-benzyl-3-cyclopropyl-1-phenylimidazo[1,2-a:4,5-c']dipyridin-10-ium bromide (11)



Beige solid, m.p.: 252–256°C, 133 mg. Yield: 55%. ¹H NMR (300MHz, CD₃OD) δ: 9.57 (d, ³*J* = 6.8Hz, 1H, H-6), 8.46 (s, 1H, H-4), 8.41 (ddd, ³*J* = 9.1Hz, 7.1Hz, ⁴*J* = 1.1Hz, 1H, H-8), 8.18 (d, ³*J* = 9.3Hz, 1H, H-9), 7.79 (td, ³*J* = 7.0Hz, ⁴*J* = 0.9Hz, 1H, H-7), 7.56-7.49 (m, 1H, Ph-4), 7.44-7.40 (m, 4H, Ph-2,3,5,6), 7.25-7.14 (m, 3H, Bn-3,4,5), 6.69-6.67 (m, 2H, Bn-2,6), 5.60 (s, 2H, CH₂Ph), 2.48-2.39 (m, 1H, CH c-Pr), 1.16-1.14 (m, 4H, CH₂ c-Pr). ¹³C NMR (75MHz, CD₃OD) δ: 160.1 (C-3), 148.4 (C-1), 145.9 (C-9a), 142.5 (C-8), 138.0 (1-Ph-1), 136.2 (C-4a), 135.0 (CH₂Ph-1), 131.2 (C-6), 130.9 (1-Ph-4), 130.4 (1-Ph-3,5*), 130.0 (1-Ph-2,6*), 129.5 (CH₂Ph-3,5*), 129.2 (CH₂Ph-4), 126.8 (CH₂Ph-2,6), 126.2 (C-10a), 118.6 (C-7), 112.7 (C-9), 104.7 (C-4), 50.2 (CH₂Ph), 18.3 (CH c-Pr), 11.3 (CH₂ c-Pr). HRMS (ESI): *m/z* calc. for C₂₆H₂₂N₃ [M]⁺: 376.18082, found: 376.18001.

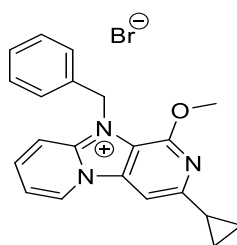
3-cyclopropyl-10-ethyl-1-methoxyimidazo[1,2-a:4,5-c']dipyridin-10-ium iodide (12)



Yellow solid, m.p.: >260 °C, 69 mg. Yield: 47%. ¹H NMR (300MHz, DMSO-d₆) δ: 9.46 (d, ³*J* = 6.8Hz, 1H, H-6), 8.45 (d, ³*J* = 9.3Hz, 1H, H-9), 8.36 (ddd, ³*J* = 9.0Hz, 6.9Hz, ⁴*J* = 1.2Hz, 1H, H-8), 8.17 (s, 1H, H-4), 7.73 (td, ³*J* = 6.8Hz, ⁴*J* = 1.0Hz, 1H, H-7), 4.77 (q, ³*J* = 7.1Hz, 2H, CH₂CH₃), 4.13 (s,

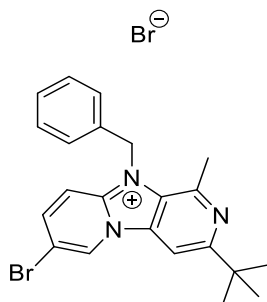
3H, OCH₃), 2.28-2.20 (m, 1H, CH c-Pr), 1.45 (t, ³J = 7.1Hz, 3H, , CH₂CH₃), 1.08-1.06 (m, 4H, 2 CH₂ c-Pr). ¹³C NMR (75MHz, DMSO-d₆) δ: 155.1 (C-3), 150.8 (C-1), 142.0 (C-9a), 139.2 (C-8), 134.8 (C-4a), 129.4 (C-6), 116.7 (C-7), 114.9 (C-10a), 111.6 (C-9), 99.0 (C-4), 54.2 (OCH₃), 41.5 (CH₂CH₃), 17.1 (CH c-Pr), 15.1 (CH₂CH₃), 9.9 (CH₂ c-Pr). HRMS (ESI): *m/z* calc. for C₁₆H₁₈N₃O [M]⁺: 268.14444, found: 268.14368.

10-benzyl-3-cyclopropyl-1-methoxyimidazo[1,2-a:4,5-c']dipyridin-10-ium bromide (13)



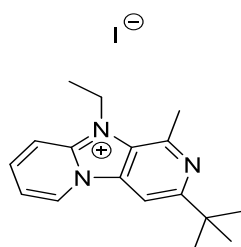
Off-white solid, m.p.: 218–222°C, 88 mg. Yield: 43%. ¹H NMR (300MHz, CDCl₃) δ: 10.08 (d, ³J = 6.8Hz, 1H, H-6), 8.53 (s, 1H, H-4), 8.35 (d, ³J = 9.3Hz, 1H, H-9), 8.14 (t, ³J = 7.2Hz, 1H, H-8), 7.54 (t, ³J = 6.9Hz, H-7), 7.37-7.29 (m, 5H, Ph), 6.21 (s, 2H, CH₂Ph), 4.14 (s, 3H, OCH₃), 2.34-2.26 (m, 1H, CH c-Pr), 1.17-1.01 (m, 4H, 2 CH₂ c-Pr). ¹³C NMR (75MHz, CDCl₃) δ: 158.1 (C-3), 151.0 (C-1), 141.9 (C-9a), 139.5 (C-8), 134.6 (C-4a*), 134.2 (Ph-1*), 131.2 (C-6), 129.5 (Ph-3,5), 129.1 (Ph-4), 127.5 (Ph-2,6), 117.7 (C-7), 115.0 (C-10a), 112.5 (C-9), 100.3 (C-4), 54.4 (OCH₃), 50.5 (CH₂Ph), 17.8 (CH c-Pr), 10.8 (CH₂ c-Pr). HRMS (ESI): *m/z* calc. for C₂₁H₂₀N₃O [M]⁺: 330.16009, found: 330.15921.

10-benzyl-7-bromo-3-(tert-butyl)-1-methylimidazo[1,2-a:4,5-c']dipyridin-10-ium bromide (14)



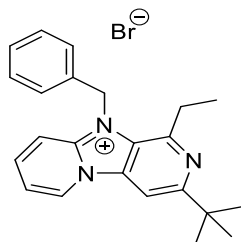
Pale yellow solid, m.p.: 220–224°C, 145 mg. Yield: 99%. ^1H NMR (300MHz, DMSO- d_6) δ : 10.23 (d, $^4J = 1.2\text{Hz}$, 1H, H-6), 8.70 (s, 1H, H-4), 8.66 (dd, $^3J = 9.7\text{Hz}$, $^4J = 1.7\text{Hz}$, 1H, H-8), 8.49 (d, $^3J = 9.8\text{Hz}$, 1H, H-9), 7.41-7.31 (m, 3H, Ph-3,4,5), 7.24-7.21 (m, 2H, Ph-2,6), 6.19 (s, 2H, CH_2Ph), 2.74 (s, 3H, Me), 1.45 (s, 9H, *t*-Bu). ^{13}C NMR (75MHz, DMSO- d_6) δ : 163.6 (C-3), 143.9 (C-1), 143.3 (C-9a), 142.9 (C-8), 135.6 (C-4a), 133.6 (Ph-1), 130.6 (C-6), 129.1 (Ph-3,5), 128.1 (Ph-4), 125.7 (Ph-2,6), 125.5 (C-10a), 112.5 (C-9), 110.7 (C-7), 102.2 (C-4), 48.4 (CH_2Ph), 37.7 (Cq *t*-Bu), 30.1 (CH_3 *t*-Bu), 22.4 (Me). HRMS (ESI): m/z calc. for $\text{C}_{22}\text{H}_{23}^{79}\text{BrN}_3$ $[\text{M}]^+$: 408.10699, found: 408.10601; m/z calc. for $\text{C}_{22}\text{H}_{23}^{81}\text{BrN}_3$ $[\text{M}]^+$: 410.10494, found: 410.10392.

3-(*tert*-Butyl)-10-ethyl-1-methylimidazo[1,2-*a*:4,5-*c'*]dipyridin-10-ium iodide (15)



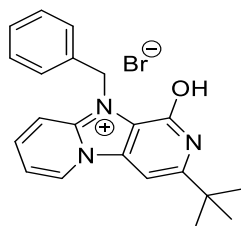
Brown solid, m.p.: 244–248°C, 52 mg. Yield: 63%. ^1H NMR (300MHz, DMSO- d_6) δ : 9.72 (d, $^3J = 6.9\text{Hz}$, 1H, H-6), 8.61 (s, 1H, H-4), 8.50-8.40 (m, 2H, H-9 & H-8), 7.76 (td, $^3J = 6.7\text{Hz}$, $^4J = 1.2\text{Hz}$, 1H, H-7), 4.88 (q, $^3J = 7.1\text{Hz}$, 2H, CH_2CH_3), 3.08 (s, 3H, Me), 1.49 (t, $^3J = 7.2\text{Hz}$, 3H, CH_2CH_3), 1.44 (s, 9H, *t*-Bu). ^{13}C NMR (75MHz, DMSO- d_6) δ : 162.9 (C-3), 143.6 (C-1*), 142.8 (C-9a*), 140.3 (C-8), 133.4 (C-4a), 129.9 (C-6), 125.2 (C-10a), 116.6 (C-7), 111.4 (C-9), 101.8 (C-4), 40.8 (CH_2CH_3), 37.6 (Cq *t*-Bu), 30.2 (CH_3 *t*-Bu), 22.7 (Me), 15.2 (CH_2CH_3). HRMS (ESI): m/z calc. for $\text{C}_{17}\text{H}_{22}\text{N}_3$ $[\text{M}]^+$: 268.18082, found: 268.17990.

10-benzyl-3-(tert-butyl)-1-ethylimidazo[1,2-a:4,5-c']dipyridin-10-ium bromide (16)



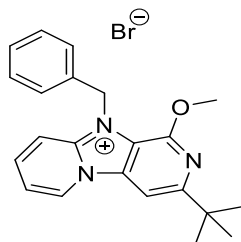
Beige solid, m.p.: 158–162°C, 30 mg. Yield: 40%. ^1H NMR (300MHz, CD_3OD) δ : 9.68 (d, $^3J = 6.8\text{Hz}$, 1H, H-6), 8.52 (s, 1H, H-4), 8.42 (ddd, $^3J = 9.3\text{Hz}$, 6.9Hz, $^4J = 0.9\text{Hz}$, 1H, H-8), 8.29 (d, $^3J = 9.3\text{Hz}$, 1H, H-9), 7.78 (t, $^3J = 6.9\text{Hz}$, 1H, H-7), 7.43-7.21 (m, 5H, Ph), 6.18 (s, 2H, CH_2Ph), 3.23 (q, $^3J = 7.4\text{Hz}$, 2H, CH_2CH_3), 1.52 (s, 9H, *t*-Bu), 1.30 (t, $^3J = 7.4\text{Hz}$, 3H, CH_2CH_3). ^{13}C NMR (75MHz, CD_3OD) δ : 165.8 (C-3), 150.1 (C-1), 145.5 (C-9a), 142.2 (C-8), 136.0 (Ph-1*), 135.4 (C-4a*), 131.1 (C-6), 130.5 (Ph-3,5), 129.5 (Ph-4), 126.7 (Ph-2,6), 126.5 (C-10a), 118.5 (C-7), 112.3 (C-9), 102.5 (C-4), 50.4 (CH_2Ph), 39.2 (Cq *t*-Bu), 30.7 (CH_3 *t*-Bu), 28.7 (CH_2CH_3), 12.6 (CH_2CH_3). HRMS (ESI): m/z calc. for $\text{C}_{23}\text{H}_{26}\text{N}_3$ $[\text{M}]^+$: 344.21212, found: 344.21126.

1-benzyl-3-(tert-butyl)-1-hydroxyimidazo[1,2-a:4,5-c']dipyridin-10-ium bromide (17)



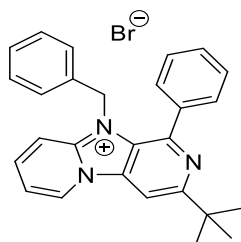
Yellow solid, m.p.: >260 °C, 31 mg. Yield: 80%. ^1H NMR (300MHz, CD_3OD) δ : 9.31 (dt, $^3J = 6.9\text{Hz}$, $^4J = ^5J = 0.9\text{Hz}$, 1H, H-6), 8.24-8.22 (m, 2H, H-8 & H-9), 7.69 (m, 1H, H-7), 7.51-7.48 (m, 2H, Ph-2,6), 7.36-7.33 (m, 4H, Ph-3,4,5 & H-4), 6.20 (s, 2H, CH_2Ph), 1.48 (s, 9H, *t*-Bu). ^{13}C NMR (75MHz, CD_3OD) δ : 156.9 (C-3*), 156.8 (C-1*), 143.4 (C-9a), 139.3 (C-8), 136.1 (Ph-1), 134.9 (C-4a), 130.4 (C-6), 130.2 (Ph-3,5), 129.8 (Ph-4), 128.8 (Ph-2,6), 120.2 (C-10a), 118.9 (C-7), 112.7 (C-9), 89.6 (C-4), 49.8 (CH_2Ph), 36.8 (Cq *t*-Bu), 29.3 (CH_3 *t*-Bu). HRMS (ESI): m/z calc. for $\text{C}_{21}\text{H}_{22}\text{N}_3\text{O}$ $[\text{M}]^+$: 332.17574, found: 332.17473.

10-benzyl-3-(tert-butyl)-1-methoxyimidazo[1,2-a:4,5-c']dipyridin-10-ium bromide (18)



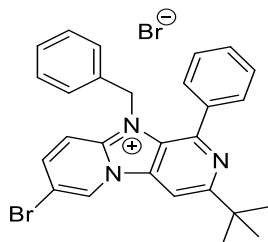
White solid, m.p.: 188–192°C, 38 mg. Yield: 50%. ^1H NMR (300MHz, DMSO- d_6) δ : 9.71 (d, $^3J = 6.6\text{Hz}$, 1H, H-6), 8.49–8.38 (m, 2H, H-8 & H-9), 8.34 (s, 1H, H-4), 7.79 (t, $^3J = 6.6\text{Hz}$, 1H, H-7), 7.43–7.33 (m, 5H, Ph), 6.03 (s, 2H, CH_2Ph), 4.11 (s, 3H, OCH₃), 1.43 (s, 9H, *t*-Bu). ^{13}C NMR (75MHz, DMSO- d_6) δ : 161.9 (C-3); 149.8 (C-1), 142.8 (C-9a), 140.0 (C-8), 135.3 (C-4a*), 135.1 (Ph-1*), 130.1 (C-6), 128.8 (Ph-3,5), 128.2 (Ph-4), 127.2 (Ph-2,6), 117.0 (C-7), 115.2 (C-10a), 111.5 (C-9), 98.0 (C-4), 54.0 (OCH₃), 48.9 (CH_2Ph), 37.8 (Cq *t*-Bu), 29.9 (CH₃ *t*-Bu). HRMS (ESI): m/z calc. for C₂₂H₂₄N₃O [M]⁺: 346.19139, found: 346.19042.

10-benzyl-3-(tert-butyl)-1-phenylimidazo[1,2-a:4,5-c']dipyridin-10-ium bromide (19)



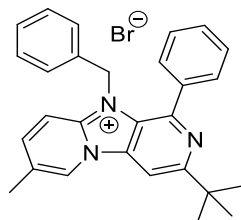
Yellow solid, m.p.: 208–212°C, 54 mg. Yield: 34%. ^1H NMR (300MHz, DMSO- d_6) δ : 9.94 (d, $^3J = 6.6\text{Hz}$, 1H, H-6), 8.92 (s, 1H, H-4), 8.49 (t, $^3J = 8.7\text{Hz}$, 1H, H-8), 8.42 (d, $^3J = 9.0\text{Hz}$, 1H, H-9), 7.88 (t, $^3J = 6.6\text{Hz}$, 1H, H-7), 7.52–7.41 (m, 5H, 1-Ph), 7.20–7.13 (m, 3H, CH₂Ph-3,4,5), 6.56 (d, $^3J = 7.2\text{Hz}$, 2H, CH₂Ph-2,6), 5.64 (s, 2H, CH_2Ph), 1.46 (s, 9H, *t*-Bu). ^{13}C NMR (75MHz, DMSO- d_6) δ : 163.3 (C-3), 145.2 (C-1), 144.3 (C-9a), 141.5 (C-8), 136.8 (1-Ph-1), 134.9 (C-4a), 134.0 (CH₂Ph-1), 130.6 (C-6), 129.4 (1-Ph-4), 129.2 (1-Ph-2,6), 128.5 (1-Ph-3,5*), 128.3 (CH₂Ph-3,5*), 127.8 (CH₂Ph-4), 125.8 (CH₂Ph-2,6), 124.5 (C-10a), 117.3 (C-7), 111.5 (C-9), 103.3 (C-4), 48.5 (CH_2Ph), 37.9 (Cq *t*-Bu), 30.2 (CH₃ *t*-Bu). HRMS (ESI): m/z calc. for C₂₇H₂₆N₃ [M]⁺: 392.21212, found: 392.21099.

10-benzyl-7-bromo-3-(tert-butyl)-1-phenylimidazo[1,2-a:4,5-c']dipyridin-10-ium bromide (20)



Yellow solid, m.p.: 156–160°C, 112 mg. Yield: 33%. ^1H NMR (300MHz, CDCl_3) δ : 10.67 (d, $^4J = 0.9\text{Hz}$, 1H, H-6), 9.05 (s, 1H, H-4), 8.50 (d, $^3J = 9.7\text{Hz}$, 1H, H-9), 8.15 (dd, $^3J = 9.6\text{Hz}$, $^4J = 1.1\text{Hz}$, 1H, H-8), 7.57–7.41 (m, 5H, 1-Ph), 7.18–7.10 (m, 3H, CH_2Ph -3,4,5), 6.75–6.72 (m, 2H, CH_2Ph -2,6), 5.92 (s, 2H, CH_2Ph), 1.48 (s, 9H, *t*-Bu). ^{13}C NMR (75MHz, CDCl_3) δ : 166.3 (C-3), 146.3 (C-1), 143.2 (C-8), 142.5 (C-9a), 136.7 (1-Ph-1), 133.9 (CH_2Ph -1*), 133.4 (C-4a*), 130.7 (C-6), 130.1 (1-Ph-4), 129.7 (1-Ph-2,6), 129.2 (1-Ph-3,5*), 128.8 (CH_2Ph -3,5*), 128.7 (CH_2Ph -4), 126.4 (CH_2Ph -2,6), 124.7 (C10a), 114.6 (C-9), 112.1 (C-7), 104.1 (C-4), 50.4 (CH_2Ph), 38.8 (Cq *t*-Bu), 30.7 (CH_3 *t*-Bu). HRMS (ESI): m/z calc. for $\text{C}_{27}\text{H}_{25}^{79}\text{BrN}_3$ $[\text{M}]^+$: 470.12264, found: 470.12126; m/z calc. for $\text{C}_{27}\text{H}_{25}^{81}\text{BrN}_3$ $[\text{M}]^+$: 472.12059, found: 472.11915.

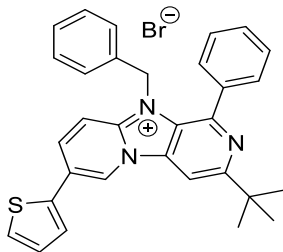
10-benzyl-3-(tert-butyl)-7-methyl-1-phenylimidazo [1,2-a:4,5-c']dipyridin-10-ium bromide (21)



White solid, m.p.: 237–241°C, 57 mg. Yield: 53%. ^1H NMR (300MHz, CD_3OD) δ : 9.56 (s, 1H, H-6), 8.62 (s, 1H, H-4), 8.30 (dd, $^3J = 9.4\text{Hz}$, $^4J = 1.5\text{Hz}$, 1H, H-8), 8.10 (d, $^3J = 9.4\text{Hz}$, 1H, H-9), 7.57–7.40 (m, 5H, 1-Ph), 7.25–7.13 (m, 3H, CH_2Ph -3,4,5), 6.69–6.66 (m, 2H, CH_2Ph -2,6), 5.61 (s, 2H, CH_2Ph), 2.65 (s, 3H, Me), 1.53 (s, 9H, *t*-Bu). ^{13}C NMR (75MHz, CD_3OD) δ : 166.1 (C-3), 147.6 (C-1), 144.9 (C-8), 144.8 (C-9a), 138.5 (1-Ph-1), 135.9 (C-4a), 135.1 (CH_2Ph -1), 130.8 (1-Ph-4), 130.6 (1-Ph-2,6), 130.0 (1-Ph-3,5*), 129.8 (C-7), 129.5 (CH_2Ph -3,5*), 129.2 (CH_2Ph -4), 129.0 (C-6), 126.9

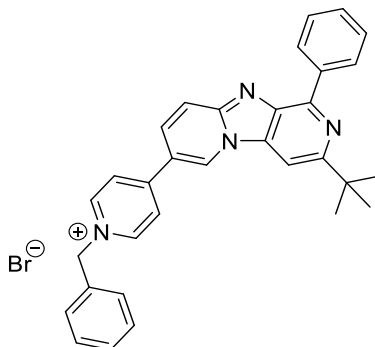
(CH₂Ph-2,6), 126.2 (C-10a), 111.9 (C-9), 103.5 (C-4), 50.1 (CH₂Ph), 39.2 (Cq *t*-Bu), 30.7 (CH₃ *t*-Bu), 17.9 (Me). HRMS (ESI): *m/z* calc. for C₂₈H₂₈N₃ [M]⁺: 406.22777, found: 406.22663.

**10-benzyl-3-(tert-butyl)-1-phenyl-7-(thiophen-2-yl)imidazo[1,2-a:4,5-c']dipyridin-10-ium
bromide (22)**



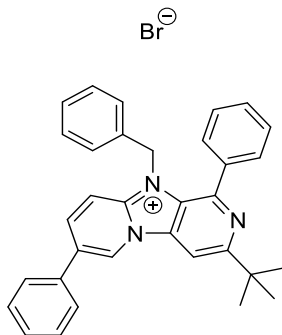
Off-white solid, m.p.: 251–255°C, 119 mg. Yield: 90%. ¹H NMR (300MHz, CD₃OD) δ: 10.0 (q, ⁴*J* = 1.8Hz, ⁵*J* = 0.9Hz, 1H, H-6), 8.87 (s, 1H, H-4), 8.70 (dd, ³*J* = 9.6Hz, ⁴*J* = 1.8Hz, 1H, H-8), 8.23 (dd, ³*J* = 9.6Hz, ⁵*J* = 0.7Hz, 1H, H-9), 7.85 (dd, ³*J* = 3.7Hz, ⁴*J* = 1.1Hz, 1H, thienyl-3), 7.71 (dd, ³*J* = 5.1Hz, ⁴*J* = 1.1Hz, 1H, thienyl-5), 7.59-7.41 (m, 5H, 1-Ph), 7.29 (dd, ³*J* = 5.1Hz, 3.7Hz, 1H, thienyl-4), 7.24-7.15 (m, 3H, CH₂Ph-3,4,5), 6.72-6.70 (m, 2H, CH₂Ph-2,6), 5.65 (s, 2H, CH₂Ph), 1.55 (s, 9H, *t*-Bu). ¹³C NMR (75MHz, CD₃OD) δ: 166.4 (C-3), 147.7 (C-1), 144.8 (C-9a), 140.9 (C-8), 138.4 (1-Ph-1), 137.6 (thienyl-2), 136.4 (C-4a), 135.0 (CH₂Ph-1), 130.8 (1-Ph-4), 130.6 (1-Ph-2,6), 130.03 (1-Ph-3,5*), 130.00 (thienyl-4), 129.6 (CH₂Ph-3,5*), 129.34 (CH₂Ph-4*), 129.32 (thienyl-5*), 128.2 (thienyl-3), 127.4 (C-7), 126.9 (CH₂Ph-2,6), 126.4 (C-6), 126.3 (C-10a), 112.9 (C-9), 104.0 (C-4), 50.3 (CH₂Ph), 39.3 (Cq *t*-Bu), 30.7 (CH₃ *t*-Bu). HRMS (ESI): *m/z* calc. for C₃₁H₂₈N₃S [M]⁺: 474.20039, found: 474.19820.

1-benzyl-4-(3-(tert-butyl)-1-phenylimidazo[1,2-a:4,5-c']dipyridin-7-yl)pyridin-1-ium bromide (23)



Orange solid, m.p.: 324–328°C, 103 mg. Yield: 97%. ^1H NMR (300MHz, DMSO- d_6) δ : 10.09 (s, 1H, H-6), 9.34 (d, $^3J = 7.0\text{Hz}$, 2H, pyr-2,6), 8.92–8.84 (m, 2H, 1-Ph-2,6), 8.69 (d, $^3J = 7.0\text{Hz}$, 2H, pyr-3,5), 8.53 (s, 1H, H-4), 8.21 (dd, $^3J = 9.9\text{Hz}$, $^4J = 1.8\text{Hz}$, 1H, H-8), 7.94 (d, $^3J = 9.7\text{Hz}$, 1H, H-9), 7.64–7.61 (m, 2H, CH₂Ph-2,6), 7.56–7.40 (m, 6H, 1-Ph-3,4,5 & CH₂Ph-3,4,5), 5.88 (s, 2H, CH₂Ph), 1.54 (s, 9H, *t*-Bu). ^{13}C NMR (75MHz, DMSO- d_6) δ : 159.7 (C-3), 151.8 (pyr-4), 147.6 (C-9a), 145.7 (C-1), 144.6 (pyr-2,6), 137.8 (1-Ph-1), 136.7 (C-4a), 136.2 (C-10a), 134.6 (CH₂Ph-1), 130.2 (C-6), 129.4 (C-8), 129.3 (1-Ph-4*), 129.2 (1-Ph-3,5*), 129.1 (CH₂Ph-4*), 128.8 (1-Ph-2,6), 128.6 (CH₂Ph-2,6), 128.3 (CH₂Ph-3,5*), 124.1 (pyr-3,5), 118.2 (C-7), 117.7 (C-9), 101.7 (C-4), 62.4 (CH₂Ph), 37.7 (Cq *t*-Bu), 30.6 (CH₃ *t*-Bu). HRMS (ESI): m/z calc. for C₃₂H₂₉N₄ [M]⁺: 469.23867, found: 469.23716.

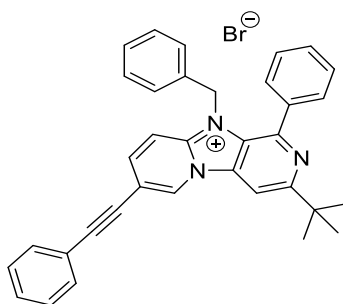
10-benzyl-3-(tert-butyl)-1,7-diphenylimidazo[1,2-a:4,5-c']dipyridin-10-ium bromide (24)



White solid, m.p.: 244–248°C, 103 mg. Yield: 97%. ^1H NMR (300MHz, CD₃OD) δ : 9.99 (s, 1H, H-6), 8.86 (s, 1H, H-4), 8.74 (dd, $^3J = 9.6\text{Hz}$, $^4J = 1.7\text{Hz}$, 1H, H-8), 8.27 (d, $^3J = 9.6\text{Hz}$, 1H, H-9),

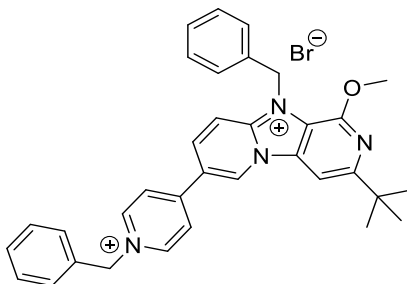
7.97-7.94 (m, 2H, 7-Ph-2,6), 7.72-7.39 (m, 8H, 7-Ph-3,4,5 & 1-Ph), 7.30-7.12 (m, 3H, CH₂Ph-3,4,5), 6.74-6.72 (m, 2H, CH₂Ph-2,6), 5.67 (s, 2H, CH₂Ph), 1.54 (s, 9H, *t*-Bu). ¹³C NMR (75MHz, CD₃OD) δ: 166.4 (C-3), 147.7 (C-1), 145.1 (C-9a), 142.1 (C-8), 138.4 (1-Ph-1), 136.5 (C-4a), 135.5 (7-Ph-1), 135.1 (CH₂Ph-1), 133.1 (C-7), 130.8 (7-Ph-4), 130.7 (1-Ph-3,4,5), 130.6 (7-Ph-3,5), 130.0 (CH₂Ph-3,5*), 129.6 (1-Ph-3,5*), 129.3 (CH₂Ph-4), 128.6 (7-Ph-2,6), 128.3 (C-6), 126.9 (CH₂Ph-2,6), 126.4 (C-10a), 112.6 (C-9), 104.0 (C-4), 50.3 (CH₂Ph), 39.3 (Cq *t*-Bu), 30.7 (CH₃ *t*-Bu). HRMS (ESI): *m/z* calc. for C₃₃H₃₀N₃ [M]⁺: 468.24342, found: 468.21191.

**10-benzyl-3-(tert-butyl)-1-phenyl-7-(phenylethynyl)imidazo[1,2-a:4,5-c']dipyridin-10-ium
bromide (25)**



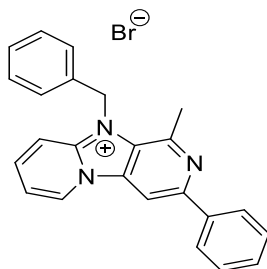
Beige solid, m.p.: 229–233°C, 94 mg. Yield: 56%. ¹H NMR (300 MHz, CD₃OD) δ 10.04 (s, 1H, H-6), 8.73 (s, 1H, H-4), 8.50 (dd, ³*J* = 9.5 Hz, ⁴*J* = 1.6 Hz, 1H, H-8), 8.25 (dd, ³*J* = 9.5, ⁵*J* = 0.9 Hz, 1H, H-9), 7.74 – 7.63 (m, 2H, 1-Ph-2,6), 7.68 – 7.39 (m, 8H, 1-Ph-3,4,5 and -C≡C-Ph), 7.32–7.14 (m, 3H, Bn-3,4,5), 6.78–6.68 (m, 2H, Bn-2,6), 4.90 (s, 2H, CH₂Ph), 1.55 (s, 9H, *t*-Bu). ¹³C NMR (75 MHz, CD₃OD) δ 165.3 (C-3), 146.5 (C-1), 143.4 (C-9a), 142.7 (C-8), 136.9 (1-Ph-1), 134.7 (C-4a), 133.4 (Bn-1), 132.1 (C-6), 131.5 (-C≡C-Ph-2,6), 129.50 (1-Ph-4*), 129.46 (-C≡C-Ph-4*), 129.1 (1-Ph-2,6*), 128.6 (1-Ph-3,5*), 128.5 (-C≡C-Ph-3,5*), 128.2 (Bn-3,5*), 127.9 (Bn-4*), 125.5 (Bn-2,6), 124.8 (C-10a), 121.4 (-C≡C-Ph-1), 114.5 (C-7), 111.4 (C-9), 102.3 (C-4), 94.0 (-C≡C-Ph), 82.0 (-C≡C-Ph), 49.1 (CH₂Ph), 37.9 (Cq *t*-Bu), 29.3 (CH₃ *t*-Bu).

10-benzyl-7-(1-benzylpyridin-1-ium bromide-4-yl)-3-(tert-butyl)-1-methoxyimidazo[1,2-a:4,5-c']dipyridin-10-ium bromide (26)



Red solid, m.p.: 208–212°C, 65 mg. Yield: 32%. ^1H NMR (300MHz, CD_3OD) δ : 10.38 (s, 1H, H-6), 9.28 (d, $^3J = 6.7\text{Hz}$, 2H, pyr-2,6), 8.89 (dd, $^3J = 9.7\text{Hz}$, $^4J = 1.5\text{Hz}$, 1H, H-8), 8.79 (d, $^3J = 6.7\text{Hz}$, 2H, pyr-3,5), 8.52 (d, $^3J = 9.7\text{Hz}$, 1H, H-9), 8.45 (s, 1H, H-4), 7.67–7.29 (m, 10H, Ph), 6.16 (s, 2H, 10- CH_2Ph), 5.95 (s, 2H, pyr- CH_2Ph), 4.24 (s, 3H, OCH_3), 1.52 (s, 9H, *t*-Bu). ^{13}C NMR (75MHz, CD_3OD) δ : 165.8 (C-3), 152.3 (C-1*), 152.0 (pyr-4*), 146.5 (pyr-2,6), 144.4 (C-9a), 139.2 (C-8), 137.1 (C-4a), 135.9 (10- CH_2Ph -1), 134.6 (pyr- CH_2Ph -1), 132.3 (C-6), 131.1 (10- CH_2Ph -4*), 130.8 (10- CH_2Ph -3,5*), 130.32 (pyr- CH_2Ph -3,5*), 130.26 (10- CH_2Ph -2,6*), 129.8 (pyr- CH_2Ph -4*), 128.4 (pyr- CH_2Ph -2,6*), 127.4 (pyr-3,5), 125.9 (C-7), 117.3 (C-10a), 113.5 (C-9), 99.2 (C-4), 65.4 (pyr- CH_2Ph), 54.9 (OCH_3), 51.3 (10- CH_2Ph), 39.4 (Cq *t*-Bu), 30.6 (CH_3 *t*-Bu). HRMS (ESI): m/z calc. for $\text{C}_{34}\text{H}_{34}\text{N}_4\text{O} [\text{M}]^{2+}$: 257.13608, found: 257.13525.

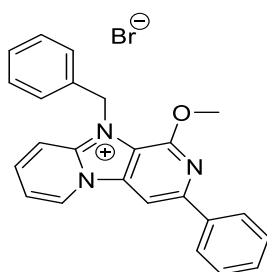
10-benzyl-1-methyl-3-phenylimidazo [1,2-a:4,5-c'] dipyridin-10-ium bromide (27)



Brown solid, m.p.: 238–242°C, 35 mg. Yield: 30%. ^1H NMR (300MHz, $\text{DMSO}-d_6$) δ : 9.85 (d, $^3J = 6.9\text{Hz}$, 1H, H-6), 9.37 (s, 1H, H-4), 8.54–8.47 (m, 2H, H-8 & H-9), 8.26 (d, $^3J = 7.2\text{Hz}$, 2H, Ph-2,6), 7.91 (td, $^3J = 6.9\text{Hz}$, $^4J = 0.9\text{Hz}$, 1H, H-7), 7.61–7.47 (m, 3H, Ph-3,4,5), 7.42–7.26 (m, 5H, CH_2Ph),

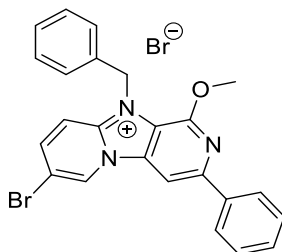
6.23 (s, 2H, $\underline{\text{CH}_2\text{Ph}}$); 2.84 (s, 3H, CH_3). ^{13}C NMR (75MHz, DMSO-d_6) δ : 150.4 (C-3), 144.8 (C-1), 144.2 (C-9a), 141.5 (C-8), 137.5 (3-Ph-1), 135.7 ($\text{CH}_2\text{Ph-1}^*$), 134.7 (C-4a*), 130.4 (C-6), 129.5 (3-Ph-4), 129.1 ($\text{CH}_2\text{Ph-3,5}^*$), 129.0 (3-Ph-3,5*), 128.1 ($\text{CH}_2\text{Ph-4}$), 126.75 (C-10a), 126.68 (3-Ph-2,6), 125.7 ($\text{CH}_2\text{Ph-2,6}$), 117.4 (C-7), 111.4 (C-9), 103.2 (C-4), 48.3 ($\underline{\text{CH}_2\text{Ph}}$), 22.4 (Me). HRMS (ESI): m/z calc. for $\text{C}_{24}\text{H}_{20}\text{N}_3$ $[\text{M}]^+$: 350.16517, found: 350.16432.

10-benzyl-1-methoxy-3-phenylimidazo[1,2-a:4,5-c']dipyridin-10-ium bromide (28)



Off-white solid, m.p.: 190–194°C, 48 mg. Yield: 49%. ^1H NMR (300MHz, DMSO-d_6) δ : 9.71 (d, $^3J = 6.6\text{Hz}$, 1H, H-6), 9.06 (s, 1H, H-4), 8.53-8.42 (m, 2H, H-8 & H-9), 8.26 (d, $^3J = 7.5\text{Hz}$, 2H, 3-Ph-2,6), 7.86 (t, $^3J = 6.6\text{Hz}$, 1H, H-7), 7.60-7.31 (m, 8H, 3-Ph-3,4,5 & CH_2Ph), 6.08 (s, 2H, $\underline{\text{CH}_2\text{Ph}}$), 4.23 (s, 3H, OCH_3). ^{13}C NMR (75MHz, DMSO-d_6) δ : 150.6 (C-1), 148.6 (C-3), 143.0 (C-9a), 140.4 (C-8), 137.1 (C-4a), 135.7 (3-Ph-1), 135.2 ($\text{CH}_2\text{Ph-1}$), 130.2 (C-6), 129.6 (3-Ph-4), 129.0 (3-Ph-3,5*), 128.8 ($\text{CH}_2\text{Ph-3,5}^*$), 128.2 ($\text{CH}_2\text{Ph-4}$), 127.2 ($\text{CH}_2\text{Ph-2,6}$), 126.5 (3-Ph-2,6), 117.4 (C-7), 116.4 (C-10a), 111.7 (C-9), 99.2 (C-4), 54.4 (OCH_3), 49.0 ($\underline{\text{CH}_2\text{Ph}}$). HRMS (ESI): m/z calc. for $\text{C}_{24}\text{H}_{20}\text{N}_3\text{O}$ $[\text{M}]^+$: 366.16009, found: 366.15899.

10-benzyl-7-bromo-1-methoxy-3-phenylimidazo[1,2-a:4,5-c']dipyridin-10-ium bromide (29)



White solid, m.p.: 231.8°C, 135 mg. Yield: 85%. ^1H NMR (300 MHz, DMSO- d_6) δ 10.11 (s, 1H, H-6), 9.03 (s, 1H, H-4), 8.65 (dd, $^3J = 9.7\text{Hz}$, $^4J = 1.8\text{Hz}$, 1H, H-8), 8.53 (dd, $^3J = 9.7\text{Hz}$, $^5J = 0.8\text{Hz}$, 1H, H-9), 8.28–8.18 (m, 2H, 3-Ph-2,6), 7.66–7.56 (m, 2H, 3-Ph-3,5), 7.56–7.46 (m, 1H, 3-Ph-4), 7.45–7.27 (m, 5H, CH_2Ph), 6.09 (s, 2H, CH_2Ph), 4.23 (s, 3H, OMe). ^{13}C NMR (75 MHz, DMSO- d_6) δ 151.2 (C-1), 149.5 (C-3), 143.1 (C-8), 142.5 (C-9a), 137.5 (C-4a), 135.8 (3-Ph-1*), 135.5 (Bn-1*), 130.9 (C-6), 130.2 (3-Ph-4), 129.6 (3-Ph-3,5), 129.3 (Bn-2,6*), 128.7 (Bn-4), 127.6 (Bn-3,5*), 127.0 (3-Ph-2,6), 116.9 (C-10a), 113.3 (C-9), 111.5 (C-7), 99.6 (C-4), 55.0 (OCH₃), 49.8 (CH_2Ph).

III. Biology

This section describes cell culture techniques, the evaluation of the effects of test compounds on cancer cell viability (apoptosis using flow cytometry, apoptosis analysis using the western blotting and proliferation using Ki-67), migration and invasion, and statistics.

III-1. Cell Culture Techniques

Here I discuss cell lines, test compounds, and cell culture protocol used in this thesis study.

III-1. 1. Cell lines

The cells used in this study are all breast cell lines from the American Type Culture Collection (ATCC, USA). The non-cancerous epithelial cell line MCF-10A is derived from a mammaplasty and was immortalized by long-term culture in serum-free medium containing a low concentration of calcium.²³⁰ The human triple-negative breast cancer (TNBC) cells MDA-MB-231, MDA-MB-435s, and MDA-MB-468 are derived from metastases present in pleural effusions in patients with metastatic mammary adenocarcinomas.⁴⁹ Stable murine TNBC 4T1-luc and MDA-MB-468-luc cell lines were obtained by transduction with lentiviral vectors containing the luciferase gene and the blasticidin resistance gene for selection (GIGA Viral Vectors, Belgium). MDA-MB-435s-luc was obtained as described previously.²³⁶ **Table 15** in chapter 4 displayed the characteristics of the MDA-MBA family of cell lines which were used in the thesis study.

MDA-MB-231, MDA-MB-468-luc, MDA-MB-435s-Luc and 4T1-Luc cell lines do not express nuclear progesterone, nuclear estrogen receptors of the ER type, and oncogene encoding the HER2 (Human Epidermal Growth Factor Receptor-2) protein, therefore they are used as triple-negative cancer (TNBC) cell model. 4T1-luc cells possess many characteristics that make them suitable for the experimental animal model for breast cancer. Among these characteristics, they are easily transplantable into the mammary gland so the primary tumor growth is in the anatomically correct site, and metastasis develops spontaneously from the primary tumor.²²⁸

Moreover, 4T1-luc cells derived from murine BALB/c strain so they can grow in balbc immunocompetent mice compared to human cells who need immunodepressed mice.²²⁹

MCF-10A was cultured in DMEM/Ham's F-12, 1:1 mix containing 5% fetal bovine serum (FBS) (Invitrogen, France), 10 µg/ml insulin, 20 ng/ml epidermal growth factor, 0.5 µg/ml hydrocortisone and 100 ng/ml cholera toxin. MDA-MB-231, MDA-MB-468-luc, and MDA-MB-435s-Luc breast cancer cells are cultured in DMEM (Lonza, USA) supplemented with 5% FBS. 4T1-luc cells were cultivated in RPMI 1640 medium (Lonza, USA) supplemented with 10% FBS.

All breast cancer cells were placed in an incubator with a controlled atmosphere and humidity, at 37 °C and containing 5% carbon dioxide to maintain the pH using the bicarbonate buffer system.

III-1. 2. Test compounds

Test compounds were dissolved in DMSO at a stock solution of 100 mM, diluted to 100 µM in a culture medium, sterilized by passing through a 0.22 µm pore size filter, then further diluted to other four concentrations (0.01, 0.1, 1, and 10 µM) in culture medium before use. The final concentration of DMSO in the culture medium was 0.1% or lower, a concentration without effect on cell replication.

III-1. 3. Cell culture protocol

The cells were first washed twice with calcium- and magnesium-free Dulbecco's Phosphate Buffered Saline (DPBS) to eliminate proteins in the serum that could inhibit the action of trypsin. DPBS also removes calcium from the medium to facilitate the dissociation of cells. Trypsin-EDTA solution was added to the cell culture flask and incubated for 2–5 minutes for cell detachment. Trypsin activity was stopped by adding media containing fetal bovine serum (FBS) after ensuring the complete detachment of cells. The determination of the cell number was carried out using Malassez hemocytometers.

III-2. Evaluation of the Effects of Test Compounds on Cancer Cell Viability

In this section, I describe various *in vitro* assays that were conducted to examine the anticancer activity of test compounds including a study of cell viability using MTT assay, apoptosis using flow cytometry, apoptosis analysis using the western blotting and proliferation using Ki-67 assay.

III-2. 1. Study of cell viability using MTT assay

Cell viability is assessed by the MTT (2-(4,5-dimethyl-2-thiazolyl bromide)-3,5-diphenyl-2H-tetrazolium). This colorimetric test is based on the reduction of yellow tetrazolium salts to insoluble violet formazan crystals as shown in **Figure 63** in chapter 4. The reduction of MTT is carried out by oxidoreductases and dehydrogenases (NADH-dependent) predominantly in mitochondria of the metabolically active cells, which makes it possible to assess the number of living cells. The measure by absorbance spectrophotometry at 570 nm is directly proportional to the number of viable cells.

Human cancer cells divide through a sequence of steps that are collectively called the cell cycle which lasts 24h or less. Thus, we treated the cancer cells with our compounds for 5 days to investigate their effect on cancer growth. Besides, we explored the cytotoxic activity of these compounds by evaluating cell survival after 24h treatment to exclude any compound with an acute toxic effect that could induce high toxicity *in vivo*.

Breast cancer cells were seeded in 24-well plates at a final volume of 0.5 ml and allowed to adhere overnight. Then, cells were treated with five concentrations (0.01, 0.1, 1, 10, and 100 μ M) of compounds and the control (0.1% DMSO) for 24h and 5 days to measure cytotoxicity and proliferation, respectively.

For MDA-MB family and MCF-10A cells, densities of 30×10^3 and 5×10^3 cells per well were used in 24h and 5 days cell viability assays, respectively. Because of the rapid growth of 4T1-luc, densities of 15×10^3 and 2×10^3 cells per well were used in 24h and 5 days cell viability assays, respectively.

Then, MDA-MB-231 cells are incubated for 1 hour while MDA-MB-435s-luc, MDA-MB-468-luc and 4T1-luc are incubated for 30 minutes with 400 μ L of prepared 0.5 mg/mL MTT solution in the growing medium. The formazan crystals formed are dissolved in 400 μ L of DMSO. Following 5 minutes of gentle shaking, the absorbance was measured using a microplate spectrophotometer (Epoch, BioTek Instruments Inc, USA) at 570 nm. The obtained data were normalized to the DMSO treated cells and IC₅₀ which is the concentration of the test compound giving 50% inhibition of growth were calculated by using nonlinear regression with variable slope using GraphPad Prism™ v.5 (GraphPad Software, Incorporation, California, USA). Data are presented by the mean of the two or three independent experiments performed in four replicate wells for each concentration of a test compound \pm SEM.

III-2. 2. Study of cell apoptosis using flow cytometry

FITC Annexin V is a quantitative assay used to determine the percentage of cells within a population that are actively undergoing apoptosis. It depends on the property of cells to lose membrane asymmetry in the early phases of apoptosis. In apoptotic cells, the membrane phospholipid phosphatidylserine (PS) is translocated from the inner leaflet to the outer leaflet of the plasma membrane, therefore, exposing PS to the external environment. Annexin V is a member of the annexin family of intracellular proteins that has a high binding affinity for PS and is useful for identifying apoptotic cells with exposed PS. Propidium Iodide (PI) is a standard flow cytometry viability probe and is used to differentiate between viable and nonviable cells. Viable cells with intact membranes exclude PI, whereas the membranes of dead and damaged cells are permeable to PI as displayed in **Figure 65** in chapter 4.

Apoptosis cells were quantified by FITC Annexin V Apoptosis Detection Kit (Ref: 556547, BD Biosciences, France) following the manufacturer's instructions.

MDA-MB-231 cells were seeded at a density of 150×10^3 cells/well in 6-well plates at a final volume of 2 ml overnight to settle down, then treated with two concentrations (3 and 30 μ M corresponding to about 1xIC₅₀ and 10xIC₅₀) of compounds **13**, **18**, and **27–28** and the control (0.1% DMSO) for 48h to detect any earlier phenomenon that preceded cell death.

MDA-MB-231 cells were washed with PBS and were separated into single cells after Accutase dissociation (0.5 ml) (Innovative cell technologies). Both floating and adherent cells were collected and pelleted by centrifugation at 480x g for 5 minutes. The supernatant was removed, and 400 µL of 1X binding buffer was used to resuspend the pellet. The mixtures were incubated with 5 µL propidium iodide (PI) and 5 µL FITC-Annexin V and kept in the dark for 15 min at RT (25 °C). Then, the samples were maintained with 400 µL of 1X binding buffer, and stained cells were analyzed by using a FACSCanto flow cytometer (BD Biosciences). The analysis was performed using BD FACS Diva software (BD Biosciences).

Data are analyzed as follows: Annexin V-negative/PI-negative population was used as a measure for live cells, Annexin V-positive/PI-negative cells as early apoptotic, and Annexin V-positive/PI-positive cells as late apoptotic and Annexin V-negative/PI-positive cells as necrotic population.

III-2. 3. Analysis of apoptosis using western blotting

Western blot is a widely used method for the electrophoretic separation of proteins of a sample according to their molecular weight and their identification by immunostaining. This method is based on the migration capacity of negatively charged proteins by sodium dodecyl sulphate (SDS) in an acrylamide gel under an electric field. The proteins are then transferred from the acrylamide gel to a membrane allowing the binding of an antibody specific for the protein of interest. The identification of proteins is done by the binding of antibodies then by detection of the antigen-antibody complex.

MDA-MB-231 cells were seeded at a density of 200×10^3 cells/well in 6-well plates at a final volume of 2 ml overnight and then treated with two concentrations (3 µM and 30 µM) of compounds **13**, **18**, and **27–28** and the control (0.1% DMSO) for 48 h.

The total protein was extracted from the MDA-MB-231 cells via protein lysis buffer (0.1% SDS, 1% NP-40, 50 µM Tris, 150 µM NaCl, and 1% SDOC) supplemented with protease inhibitors and quantified using the Pierce® BCA kit Protein Assay Kit according to manufacturer recommendations (Pierce, Thermo Fischer Scientific, France).

After being boiled with Sample Loading Buffer (10% glycerol, 5% β -mercaptoethanol, 2.3% SDS, 0.125 M Tris pH 6.8 and bromophenol blue dye) at 95 °C for 3 minutes, 20 μ g protein samples were subjected to electrophoresis in 12% sodium dodecyl sulphate-polyacrylamide gel electrophoresis (SDS-PAGE) gels. Precision Plus Protein Dual Color Standards (Bio-Rad Laboratories) were used as a molecular mass standard to monitor the electrophoresis and to estimate the size of protein of interest. The electrophoresis was carried out at a constant voltage of 90 mV during the concentration of the samples and then at 130 mV for about 1h30 during the separation of the proteins, in Tris-glycine-SDS buffer (25 mM Tris, 190 mM glycine, 0.1% SDS, pH 8.3). Proteins that have migrated according to their molecular weight are then transferred to a polyvinylidene fluoride (PVDF) membrane (immobilon-P Membrane, Millipore, France). The transfer was carried out in a liquid medium in a Tris-glycine ethanol buffer (25 mM Tris, 190 mM glycine, 10% ethanol, pH 8.3) for 90 minutes at constant 300 mA for proteins detected with the cocktail primary antibodies and 45 minutes at 75 mV for other proteins.

The membrane spaces not occupied by proteins are saturated for 1 to 2 hours at room temperature under agitation in a solution of TTBS (Tween Tris-Buffered-Saline) containing 5% nonfat dry milk. Then, the membrane is incubated overnight with the primary antibody specific for the protein studied at 4°C with agitation (**Table 26**). The membranes are washed 5 times for 5 minutes with TTBS to remove excess primary antibody and then incubated with a secondary antibody specifically directed against the species of the primary antibody (**Table 27**) for 45 minutes at room temperature with agitation. Finally, the membranes are washed again 5 times for 5 minutes with TTBS. The dilution of primary and secondary antibodies is carried out in the TTBS solution containing 5% nonfat dry milk.

The secondary antibodies are coupled to horseradish peroxidase, which allows the revelation of the protein of interest (HorseRadish, HRP) except in the case of the anti- β -actin antibody which is directly coupled to the HRP. Horseradish peroxidase, coupled with the secondary antibody, enables oxidation of luminol in the presence of hydrogen peroxide present in the kit reagents (Thermo Fischer Scientific, France). The membrane is exposed to the kit reagents for approximately one minute and then is placed between two plastic films. Conventional autoradiographic development enables signal detection on photographic film

(Kodak® BioMax™ light film, Sigma, France) after processing and fixation with Kodak® processing chemical reagents for autoradiography films (Sigma, France). The film is then dried, scanned, and analyzed. The images were analyzed using ImageJ.

Table 26: List of primary antibodies used in western blotting

Primary antibody	Reference	Supplier	Dilution	Species reactivity	Molecular weight
Cocktail (pro/p17 caspase 3, cleaved PARP1, muscle actin)	ab136812	Abcam	1:250	Human	
Bak (D4E4)	12105	Cell signaling	1:1000	Human, mouse, rabbit	25 kDa
Bax (D55G8)	4223	Cell signaling	1:1000	Human	26 kDa
Bcl-xl (54h6)	2764	Cell signaling	1:1000	Human, mouse, rabbit	30 kDa
Bcl-2 (D55G8)	4223	Cell signaling	1:1000	Human	26 kDa
IgG1 monoclonal anti-β-actin HRP	(C4) sc-47778	Tebu-Bio France	1:5000	Mouse	43 kDa

Table 27: List of secondary antibodies used in western blotting

Secondary antibody	Reference	Supplier	Dilution	Species
Antirabbit IgG-HRP	sc-2004	Santa-Cruz, Tebu-Bio France	1:10,000	Goat
100X HRP conjugated secondary antibodies cocktail	sc-2005	Abcam	1:100	Goat

III-2. 4. Study of cell proliferation using Ki-67 assay

The Ki-67 protein is a nuclear antigen involved in cell proliferation and can be used as a marker for determining the cell proliferation because it is expressed throughout the active cell cycle (G1, S, G2, and M phases) except for the resting phase (G0).

A density of 20×10^3 MDA-MB-231 cells was seeded in each well of 8-well Lab-Tek™ slides in a final volume of 200 µL overnight. After adhesion, cells were treated with 3 and 30 µM of compounds **13**, **18**, and **27–28** and the control (0.1% DMSO) for 48h.

MDA-MB-231 cells were rinsed two times with PBS, fixed with 4% paraformaldehyde (PFA) at room temperature for 10 minutes and washed three times with PBS. For intracellular proteins, it is vital to permeabilize the cells, thus, PBS containing 0.3% Triton (PBST) solution was used for 5 minutes at room temperature. Cells were blocked with PBS containing 5% BSA for 1 hour at room temperature to block unspecific binding of the antibodies. Cells were labeled with Ki-67 Monoclonal Antibody in 1% BSA (1:1000 dilution, BD Bioscience) for 1 hour at room temperature. Cells were washed three times with PBS and then labeled with Goat anti-Mouse IgG (H+L) Secondary Antibody, Alexa Fluor® 488 conjugate in 1% BSA (1:1000 dilution) for 1 hour at room temperature. Cells were washed three times with PBS and mounted with Vectashield Vibrance (Eurobio, France) containing Dapi to stain cell nuclei. Slides were imaged and analyzed with a fluorescent microscope equipped with NIS Elements software. Ki-67 ratio was obtained by randomly enumerating Ki-67 positive cells through a microscope and expressed as percentages of positive cells. In which, Ki-67 positive cells stained by the green colour of GFP and total cancer cell nuclei stained by the blue colour of DAPI were counted. The ki-67 ratio is presented by the mean of the three independent experiments using five random microscopic fields counted for each concentration of a test compound \pm SEM.

III-3. Study of *In Vitro* Cell Migration and Invasiveness

Cancer cells are capable of degrading their extracellular environment and migrate through the tissue to pass into the circulation and invade host tissues. It is possible to model these phenomena *in vitro* by assessing the migration and invasiveness of cells. We have defined the term migration as the ability of cells to migrate and close the 500 μ m cell-free gap created by culture inserts (Ref: 80206, Ibidi, Regensburg, Germany). Cell invasiveness measures the ability of cells to actively pass through an 8 μ m pore size poly(ethylene terephthalate (PET) membrane that has been covered with Matrigel matrix, mimicking thus the extracellular matrix using Corning BioCoat Matrigel invasion chamber (Ref: 354480, Corning, USA). Under these conditions, the cells must degrade the Matrigel matrix before migrating through the pores of the filter as displayed in **Figure 69** and **71** in chapter 4.

Migration and invasiveness tests are a simple and accurate way to evaluate the behavior of cancer cells *in vitro*. However, it is necessary to ensure that the substance to be tested has no toxic effect on the cells, thus, a cytotoxicity test was carried to determine the nontoxic concentrations which are subsequently used for migration and invasion studies.

Migration studies were performed using the 2 well culture inserts which were transferred into 24-well culture plate to form a well-defined gap without scratching the cell monolayer. MDA-MB-435s-luc and MDA-MB-231 Cells were cultivated in 70 μ L of growth medium in a density of 40×10^3 cells per chamber of the culture insert and incubated overnight. Due to their rapid growth, 4T1-luc cells were cultivated at a density of 20×10^3 cells per chamber of the culture insert.

The inserts were removed carefully using sterile forceps, and different nontoxic concentrations of each test compound in 500 μ L culture medium and the control (0.1% DMSO) were added to each well plate. Then, cells were monitored and photographed every 15 minutes for 24 hours for MDA-MB-435s-luc and MDA-MB-231 cells and 15 hours for 4T1-luc cells for wound closure using Nikon Eclipse (Nikon Corp., Tokyo, Japan) equipped with NIS Elements software. The open area was calculated with Tscratch software (CSElab, Zurich, Switzerland). The open areas were converted into distance migration and normalized to the control condition. Analyses was performed using GraphPad Prism™ to calculate the percentage of inhibition of migration and SEM values. Experiments were run at least three times for each condition.

Invasion assays (Corning® BioCoat™ Matrigel Invasion chamber) were performed according to the manufacturer's instructions. 800 μ L of 20% FBS RPMI medium containing test compounds or DMSO was added to the lower chambers. 40×10^3 4T1-luc cells in 200 μ L of 10% FBS RPMI medium with the same compounds at final concentration of 1 μ M or 0.1% DMSO (as control) were added to the upper chambers. The difference in FBS between the upper and lower compartments permits the establishment of a chemoattractant gradient (hormones and growth factor). Cells were incubated in the chambers for 15 h at 37°C and 5% CO₂. At the end of the experiment, inserts were washed with DPBS, cells were fixed for 10 minutes in ice-cold methanol and washed with water. Cell nuclei were stained with DAPI for 2 minutes. The upper side of insets was scrapped to remove the non-invading cells, washed two times with water, and imaged with

a fluorescent microscope equipped with NIS Elements software. Duplicate inserts were used for each experiment, and five random microscopic fields were counted per insert. Data are represented as total cell invading in 5 fields per insert and normalized to the control condition.

III-4. Statistics

The results are represented as an average plus or minus the standard error of the mean (SEM). The statistical analysis is carried out using GraphPad Prism v5 (GraphPad Software, USA).

Bibliography

1. Li C, Wang Y, Wang C, Yi X, Li M, He X. Anticancer activities of harmine by inducing a pro-death autophagy and apoptosis in human gastric cancer cells. *Phytomedicine*. 2017;28:10-18.
2. Nafisi S, Bonsaii M, Maali P, Khalilzadeh MA, Manouchehri F. β -Carboline alkaloids bind DNA. *J Photochem Photobiol B Biol*. 2010;100(2):84-91.
3. Cao R, Peng W, Wang Z, Xu A. β -Carboline alkaloids: biochemical and pharmacological functions. *Curr Med Chem*. 2007;14(4):479-500.
4. Zaker F, Oody A, Arjmand A. A study on the antitumoral and differentiation effects of *Peganum harmala* derivatives in combination with atra on leukaemic cells. *Arch Pharm Res*. 2007;30(7):844-849.
5. Hamsa TP, Kuttan G. Harmine activates intrinsic and extrinsic pathways of apoptosis in B16F-10 melanoma. *Chin Med*. 2011;6(1):11.
6. Hamsa TP, Kuttan G. Harmine inhibits tumour specific neo-vessel formation by regulating VEGF, MMP, TIMP and pro-inflammatory mediators both *in vivo* and *in vitro*. *Eur J Pharmacol*. 2010;649(1-3):64-73.
7. Ishida J, Wang HK, Bastow KF, Hu CQ, Lee KH. Antitumor agents 201. Cytotoxicity of harmine and β -carboline analogs. *Bioorganic Med Chem Lett*. 1999;9(23):3319-3324.
8. Enguehard-Gueiffier C, Delaye P-O, Pénichon M, Denevault-Sabourin C, Allouchi H, Gueiffier A. Domino 6-endo-dig Cyclization/Halogenation Reactions: Three-Component Synthesis of 1,3-Disubstituted 4-Haloimidazo[1,2-*a*:4,5-*c'*]dipyridines. *Synthesis (Stuttg)*. 2015;47(24):3983-3989.
9. Oudot R, Costes P, Allouchi H, et al. Grignard reagent-promoted 6-endo-dig cyclization: Instantaneous synthesis of original dipyrido[1,2-*a*:3',4'-*d'*]imidazole. *Tetrahedron*. 2011;67(49):9576-9581.
10. Torre LA, Bray F, Siegel RL, Ferlay J, Lortet-Tieulent J, Jemal A. Global cancer statistics, 2012. *CA Cancer J Clin*. 2015;65(2):87-108.
11. WHO. Breast cancer. Accessed January 31, 2020.
<https://www.who.int/cancer/prevention/diagnosis-screening/breast-cancer/en/>
12. Hanahan D, Weinberg RA. Hallmarks of cancer: The next generation. *Cell*. 2011;144:646-674.

13. Bhatt AN, Mathur R, Farooque A, Verma A, Dwarakanath BS. Cancer biomarkers - current perspectives. *Indian J Med Res.* 2010;132:129-149.
14. Masuda H, Zhang D, Bartholomeusz C, Doihara H, Hortobagyi GN, Ueno NT. Role of epidermal growth factor receptor in breast cancer. *Breast Cancer Res Treat.* 2012;136(2):331-345.
15. Cheang MCU, Chia SK, Voduc D, et al. Ki67 Index, HER2 Status, and Prognosis of Patients With Luminal B Breast Cancer. *JNCI J Natl Cancer Inst.* 2009;101(10):736-750.
16. Velez AA, Howard M. Tumor-suppressor genes, cell cycle regulatory checkpoints, and the skin. *N Am J Med Sci.* 2015;7(5):176.
17. Bryan TM, Englezou A, Dalla-Pozza L, Dunham MA, Reddel RR. Evidence for an alternative mechanism for maintaining telomere length in human tumors and tumor-derived cell lines. *Nat Med.* 1997;3(11):1271-1274.
18. Bryan TM, Englezou A, Gupta J, Bacchetti S, Reddel RR. Telomere elongation in immortal human cells without detectable telomerase activity. *EMBO J.* 1995;14(17):4240-4248.
19. Stewart SA, Weinberg RA. Telomeres: Cancer to Human Aging. *Annu Rev Cell Dev Biol.* 2006;22(1):531-557.
20. Hanahan D, Folkman J. Patterns and emerging mechanisms of the angiogenic switch during tumorigenesis. *Cell.* 1996;86(3):353-364.
21. Toomey DP, Murphy JF, Conlon KC. COX-2, vegf and tumour angiogenesis. *Surgeon.* 2009;7(3):174-180.
22. Mittal V. Epithelial Mesenchymal Transition in Tumor Metastasis. *Annu Rev Pathol Mech Dis.* 2018;13(1):395-412.
23. Cominetti MR, Altei WF, Selistre-De-araujo HS. Metastasis inhibition in breast cancer by targeting cancer cell extravasation. *Breast Cancer Targets Ther.* 2019;11:165-178.
24. Revenco T, Nicodème A, Pastushenko I, et al. Context Dependency of Epithelial-to-Mesenchymal Transition for Metastasis. *Cell Rep.* 2019;29(6):1458-1468.e3.
25. Talmadge JE, Fidler IJ. AACR Centennial Series: The Biology of Cancer Metastasis: Historical Perspective. *Cancer Res.* 2010;70(14):5649-5669.
26. Polyak K, Weinberg RA. Transitions between epithelial and mesenchymal states:

- acquisition of malignant and stem cell traits. *Nat Rev Cancer*. 2009;9(4):265-273.
27. Rankin EB, Nam JM, Giaccia AJ. Hypoxia: Signaling the Metastatic Cascade. *Trends in Cancer*. 2016;2(6):295-304.
 28. Jain RK. Normalizing tumor vasculature with anti-angiogenic therapy: A new paradigm for combination therapy. *Nat Med*. 2001;7(9):987-989.
 29. Brown JM, Attardi LD. The role of apoptosis in cancer development and treatment response. *Nat Rev Cancer*. 2005;5(3):231-237.
 30. Walensky LD. BCL-2 in the crosshairs: tipping the balance of life and death. *Cell Death Differ*. 2006;13(8):1339-1350.
 31. Sankari SL, Babu NA, Rajesh E, Kasthuri M. Apoptosis in immune-mediated diseases. *J Pharm Bioallied Sci*. 2015;7(Suppl 1):S200-2.
 32. Bajwa N, Liao C, Nikolovska-Coleska Z. Inhibitors of the anti-apoptotic Bcl-2 proteins: a patent review. *Expert Opin Ther Pat*. 2012;22(1):37-55.
 33. Souers AJ, Levenson JD, Boghaert ER, et al. ABT-199, a potent and selective BCL-2 inhibitor, achieves antitumor activity while sparing platelets. *Nat Med*. 2013;19(2):202-208.
 34. Lessene G, Czabotar PE, Sleebs BE, et al. Structure-guided design of a selective BCL-X(L) inhibitor. *Nat Chem Biol*. 2013;9(6):390-397.
 35. Zhou H, Aguilar A, Chen J, et al. Structure-based design of potent Bcl-2/Bcl-xL inhibitors with strong *in vivo* antitumor activity. *J Med Chem*. 2012;55(13):6149-6161.
 36. Morganti S, Tarantino P, Ferraro E, et al. Complexity of genome sequencing and reporting: Next generation sequencing (NGS) technologies and implementation of precision medicine in real life. *Crit Rev Oncol Hematol*. 2019;133:171-182.
 37. Provenzano E, Chin S-F. Molecular Classification of Breast Cancer. *PET Clin*. 2018;13(3):325-338.
 38. Ades F, Zardavas D, Bozovic-Spasojevic I, et al. Luminal B breast cancer: molecular characterization, clinical management, and future perspectives. *J Clin Oncol*. 2014;32(25):2794-2803.
 39. Hynes NE, MacDonald G. ErbB receptors and signaling pathways in cancer. *Curr Opin Cell*

- Biol.* 2009;21(2):177-184.
40. Lyu H, Han A, Polsdofer E, Liu S, Liu B. Understanding the biology of HER3 receptor as a therapeutic target in human cancer. *Acta Pharm Sin B.* 2018;8(4):503-510.
 41. Dieci MV, Miglietta F, Griguolo G, Guarneri V. Biomarkers for HER2-positive metastatic breast cancer: Beyond hormone receptors. *Cancer Treat Rev.* 2020;88:102064.
 42. Citri A, Yarden Y. EGF–ERBB signalling: towards the systems level. *Nat Rev Mol Cell Biol.* 2006;7(7):505-516.
 43. Slamon DJ, Godolphin W, Jones LA, et al. Studies of the HER-2/neu proto-oncogene in human breast and ovarian cancer. *Science.* 1989;244(4905):707-712.
 44. Rimawi MF. Metastatic human epidermal growth factor receptor 2-positive breast cancer: Management, challenges, and future directions. *Curr Probl Cancer.* 2016;40(2-4):117-129.
 45. Lee A, Djamgoz MBA. Triple negative breast cancer: Emerging therapeutic modalities and novel combination therapies. *Cancer Treat Rev.* 2018;62:110-122.
 46. Chang-Qing Y, Jie L, Shi-Qi Z, et al. Recent treatment progress of triple negative breast cancer. *Prog Biophys Mol Biol.* 2020;151:40-53.
 47. Dent R, Trudeau M, Pritchard KI, et al. Triple-negative breast cancer: Clinical features and patterns of recurrence. *Clin Cancer Res.* 2007;13(15):4429-4434.
 48. Lehmann BD, Bauer JA, Chen X, et al. Identification of human triple-negative breast cancer subtypes and preclinical models for selection of targeted therapies. *J Clin Invest.* 2011;121(7):2750-2767.
 49. Chavez KJ, Garimella S V., Lipkowitz S. Triple negative breast cancer cell lines: One tool in the search for better treatment of triple negative breast cancer. *Breast Dis.* 2010;32(1-2):35-48.
 50. da Silva JL, Cardoso Nunes NC, Izetti P, de Mesquita GG, de Melo AC. Triple negative breast cancer: A thorough review of biomarkers. *Crit Rev Oncol Hematol.* 2020;145:102855.
 51. Greenwalt I, Zaza N, Das S, Li BD. Precision Medicine and Targeted Therapies in Breast Cancer. *Surg Oncol Clin N Am.* 2020;29(1):51-62.

52. Tsimberidou AM, Kurzrock R, Anderson KC. *Targeted Therapy in Translational Cancer Research*. 1st ed. Wiley-Blackwell; 2015.
53. Jeselsohn R, Yelensky R, Buchwalter G, et al. Emergence of constitutively active estrogen receptor- α mutations in pretreated advanced estrogen receptor-positive breast cancer. *Clin Cancer Res*. 2014;20(7):1757-1767.
54. Schiavon G, Smith IE. Status of adjuvant endocrine therapy for breast cancer. *Breast Cancer Res*. 2014;16(2):206.
55. Basu A. Molecular Targets of Breast Cancer: AKTing in Concert. *Breast Cancer Basic Clin Res*. 2008;2:11-16.
56. Huerta-Reyes M, Maya-Núñez G, Pérez-Solis MA, et al. Treatment of Breast Cancer With Gonadotropin-Releasing Hormone Analogs. *Front Oncol*. 2019;9:943.
57. Slamon D, Clark G, Wong S, Levin W, Ullrich A, McGuire W. Human breast cancer: correlation of relapse and survival with amplification of the HER-2/neu oncogene. *Science (80-)*. 1987;235(4785):177-182.
58. Khodadust F, Ahmadpour S, Aligholikhamsheh N, Abedi SM, HosseiniMehr SJ. An improved 99mTc-HYNIC-(Ser)3-LTVSPWY peptide with EDDA/tricine as co-ligands for targeting and imaging of HER2 overexpression tumor. *Eur J Med Chem*. 2018;144:767-773.
59. Slamon DJ, Leyland-Jones B, Shak S, et al. Use of chemotherapy plus a monoclonal antibody against her2 for metastatic breast cancer that overexpresses HER2. *N Engl J Med*. 2001;344(11):783-792.
60. Romond EH, Perez EA, Bryant J, et al. Trastuzumab plus adjuvant chemotherapy for operable HER2-positive breast cancer. *N Engl J Med*. 2005;353(16):1673-1684.
61. Pegram MD. Treating the HER2 pathway in early and advanced breast cancer. *Hematol Oncol Clin North Am*. 2013;27(4):751-765.
62. Baselga J, Cortés J, Kim S-B, et al. Pertuzumab plus Trastuzumab plus Docetaxel for Metastatic Breast Cancer. *N Engl J Med*. 2012;366(2):109-119.
63. Rugo HS, Keck S. Reversing hormone resistance: Have we found the golden key? *J Clin Oncol*. 2012;30(22):2707-2709.
64. Hua H, Kong Q, Zhang H, Wang J, Luo T, Jiang Y. Targeting mTOR for cancer therapy. *J*

- Hematol Oncol.* 2019;12(1):71.
65. Dickson MA. Molecular pathways: CDK4 inhibitors for cancer therapy. *Clin Cancer Res.* 2014;20(13):3379-3383.
 66. Robson M, Offit K. Management of an inherited predisposition to breast cancer. *N Engl J Med.* 2007;357(2):154-162.
 67. Ohmoto A, Yachida S. Current status of poly(ADP-ribose) polymerase inhibitors and future directions. *Onco Targets Ther.* 2017;10:5195-5208.
 68. Boussios S, Abson C, Moschetta M, et al. Poly (ADP-Ribose) Polymerase Inhibitors: Talazoparib in Ovarian Cancer and Beyond. *Drugs R D.* 2020;20(2):55-73.
 69. Lamchouri F, Settaf A, Cherrah Y, et al. *In vitro* cell-toxicity of *Peganum harmala* alkaloids on cancerous cell-lines. *Fitoterapia.* 2000;71(1):50-54.
 70. Moloudizargari M, Mikaili P, Aghajanshakeri S, Asghari M, Shayegh J. Pharmacological and Therapeutic effects of *Peganum harmala* and its main alkaloids. *Pharmacogn Rev.* 2013;7(14):199-212.
 71. Niroumand MC, Farzaei MH, Amin G. Medicinal properties of *Peganum harmala* L. in traditional Iranian medicine and modern phytotherapy: A review. *J Tradit Chinese Med.* 2015;35(1):104-109.
 72. Moazeni M, Saadaty Ardakani ZS, Saharkhiz MJ, et al. *In vitro* ovicidal activity of *Peganum harmala* seeds extract on the eggs of *Fasciola hepatica*. *J Parasit Dis.* 2017;41(2):467-472.
 73. Yousefi R, Ghaffarifar F, Asl AD. The Effect of *Alkanna tinctoria* and *Peganum harmala* Extracts on *Leishmania major* (MRHO/IR/75/ER) *in vitro*. *Iran J Parasitol.* 2009;4(1):40-47.
 74. Airaksinen MM, Kari I. β -carboline, psychoactive compounds in the mammalian body. Part I: Occurrence, origin and metabolism. *Med Biol.* 1981;59(1):21-34.
 75. Zhao T, He Y, Wang J, Ding K, Wang C, Wang Z. Inhibition of Human Cytochrome P450 Enzymes 3A4 and 2D6 by β -Carboline Alkaloids, Harmine Derivatives. *Phyther Res.* 2011;25(11):1671-1677.
 76. Bournine L, Bensalem S, Fatmi S, et al. Evaluation of the cytotoxic and cytostatic activities of alkaloid extracts from different parts of *Peganum harmala* L. (Zygophyllaceae). *Eur J Integr Med.* 2017;9:91-96.

77. Astulla A, Zaima K, Matsuno Y, et al. Alkaloids from the seeds of *Peganum harmala* showing antiplasmodial and vasorelaxant activities. *J Nat Med*. 2008;62(4):470-472.
78. Arshad N, Neubauer C, Hasnain S, Hess M. *Peganum harmala* Can Minimize Escherichia coli Infection in Poultry, but Long-Term Feeding May Induce Side Effects. *Poult Sci*. 2008;87(2):240-249.
79. Pulpati H, Biradar. High-performance thin-layer chromatography densitometric method for the quantification of harmine, harmaline, vasicine, and vasicinone in *Peganum harmala*. *J AOAC Int*. 2008;91(5):1179-1185.
80. Herraiz T, González D, Ancín-Azpilicueta C, Arán VJ, Guillén H. β -Carboline alkaloids in *Peganum harmala* and inhibition of human monoamine oxidase (MAO). *Food Chem Toxicol*. 2010;48(3):839-845.
81. Frison G, Favretto D, Zancanaro F, Fazzin G, Ferrara SD. A case of β -carboline alkaloid intoxication following ingestion of *Peganum harmala* seed extract. *Forensic Sci Int*. 2008;179(2-3):37-43.
82. Allen JRF, Holmstedt BR. The simple β -carboline alkaloids. *Phytochemistry*. 1980;19(8):1573-1582.
83. Callaway JC. Various alkaloid profiles in decoctions of *Banisteriopsis caapi*. *J Psychoactive Drugs*. 2005;37(2):151-155.
84. Valin N, Haybron D, Groves L, Mower HF. The nitrosation of alcohol-induced metabolites produces mutagenic substances. *Mutat Res Toxicol*. 1985;158(3):159-168.
85. FARREL G and WMM. Adrenoglomerulotropin. *Arch Biochem*. 1961;94:543-544.
86. Laine A, Lood C, Koskinen A. Pharmacological Importance of Optically Active Tetrahydro- β -carbolines and Synthetic Approaches to Create the C1 Stereocenter. *Molecules*. 2014;19(2):1544-1567.
87. Ding S, Shi Z, Jiao N. Pd(II)-catalyzed synthesis of carbolines by iminoannulation of internal alkynes via direct C-H bond cleavage using dioxygen as oxidant. *Org Lett*. 2010;12(7):1540-1543.
88. Shi Z, Cui Y, Jiao N. Synthesis of β - and γ -Carbolinones via Pd-Catalyzed Direct Dehydrogenative Annulation (DDA) of Indole-carboxamides with Alkynes Using Air as the

- Oxidant. *Org Lett.* 2010;12(13):2908-2911.
89. Verniest G, England D, De Kimpe N, Padwa A. Synthesis of substituted β -carbolines via gold(III)-catalyzed cycloisomerization of N-propargylamides. *Tetrahedron.* 2010;66(7):1496-1502.
 90. Nissen F, Richard V, Alayrac C, Witulski B. Synthesis of β - And γ -carbolines via ruthenium and rhodium catalysed [2+2+2] cycloadditions of yne-ynamides with methylcyanoformate. *Chem Commun.* 2011;47(23):6656-6658.
 91. Dhara S, Singha R, Ahmed A, et al. Synthesis of α , β and γ -carbolines via Pd-mediated C sp²-H/N-H activation. *RSC Adv.* 2014;4(85):45163-45167.
 92. Winkler JD, Axten JM. The first total syntheses of ircinol A, ircinal A, and manzamines A and D. *J Am Chem Soc.* 1998;120(25):6425-6426.
 93. Samoylenko V, Khan SI, Jacoba MR, et al. Bioactive (+)-manzamine A and (+)-8-hydroxymanzamine A tertiary bases and salts from *Acanthostrongylophora ingens* and their preparations. *Nat Prod Commun.* 2009;4(2):185-192.
 94. Boursereau Y, Coldham I. Synthesis and biological studies of 1-amino β -carbolines. *Bioorg Med Chem Lett.* 2004;14(23):5841-5844.
 95. Thompson MJ, Louth JC, Little SM, et al. Synthesis and Evaluation of 1-Amino-6-halo- β -carbolines as Antimalarial and Antiprion Agents. *ChemMedChem.* 2012;7(4):578-586.
 96. Chauhan SS, Gupta L, Mittal M, Vishwakarma P, Gupta S, Chauhan PMS. Synthesis and biological evaluation of indolyl glyoxylamides as a new class of antileishmanial agents. *Bioorg Med Chem Lett.* 2010;20(21):6191-6194.
 97. Baréa P, Barbosa VA, Bidóia DL, et al. Synthesis, antileishmanial activity and mechanism of action studies of novel β -carboline-1,3,5-triazine hybrids. *Eur J Med Chem.* 2018;150:579-590.
 98. Peng J, Kudrimoti S, Prasanna S, et al. Structure–Activity Relationship and Mechanism of Action Studies of Manzamine Analogues for the Control of Neuroinflammation and Cerebral Infections. *J Med Chem.* 2010;53(1):61-76.
 99. Venkataramana Reddy PO, Hridhay M, Nikhil K, et al. Synthesis and investigations into the anticancer and antibacterial activity studies of β -carboline chalcones and their

- bromide salts. *Bioorg Med Chem Lett*. 2018;28(8):1278-1282.
100. Xu Z, Chang FR, Wang HK, et al. Anti-HIV agents 45(1) and antitumor agents 205.(2) two new sesquiterpenes, leitneridanins A and B, and the cytotoxic and anti-HIV principles from *Leitneria floridana*. *J Nat Prod*. 2000;63(12):1712-1715.
 101. Ishida J, Wang HK, Oyama M, Cosentino ML, Hu CQ, Lee KH. Anti-AIDS agents. 46.1 Anti-HIV activity of harman, an anti-HIV principle from *Symplocos setchuensis*, and its derivatives. *J Nat Prod*. 2001;64(7):958-960.
 102. Brahmbhatt KG, Ahmed N, Sabde S, Mitra D, Singh IP, Bhutani KK. Synthesis and evaluation of β -carboline derivatives as inhibitors of human immunodeficiency virus. *Bioorg Med Chem Lett*. 2010;20(15):4416-4419.
 103. Ashok P, Lu C-L, Chander S, Zheng Y-T, Murugesan S. Design, Synthesis, and Biological Evaluation of 1-(thiophen-2-yl)-9 *H* -pyrido[3,4- *b*]indole Derivatives as Anti-HIV-1 Agents. *Chem Biol Drug Des*. 2015;85(6):722-728.
 104. Ashok P, Chander S, Balzarini J, Pannecouque C, Murugesan S. Design, synthesis of new β -carboline derivatives and their selective anti-HIV-2 activity. *Bioorg Med Chem Lett*. 2015;25(6):1232-1235.
 105. Ahmed NS, Ali AH, El-Nashar SM, et al. Exploring the PDE5 H-pocket by ensemble docking and structure-based design and synthesis of novel β -carboline derivatives. *Eur J Med Chem*. 2012;57:329-343.
 106. El-Gamil DS, Ahmed NS, Gary BD, et al. Design of Novel β -Carboline Derivatives with Pendant 5-Bromothieryl and Their Evaluation as Phosphodiesterase-5 Inhibitors. *Arch Pharm (Weinheim)*. 2013;346(1):23-33.
 107. Evans AK, Lowry CA. Pharmacology of the β -carboline FG-7,142, a partial inverse agonist at the benzodiazepine allosteric site of the GABA A receptor: neurochemical, neurophysiological, and behavioral effects. *CNS Drug Rev*. 2007;13(4):475-501.
 108. Bracher F, Hildebrand D, Häberlein H. 1-substituted β -carboline-3-carboxylates with high affinities to the benzodiazepine recognition site. *Nat Prod Res*. 2004;18(5):391-396.
 109. Ma C, Cao R, Shi B, et al. Synthesis and cytotoxic evaluation of 1-carboxamide and 1-amino side chain substituted β -carbolines. *Eur J Med Chem*. 2010;45(11):5513-5519.

110. Liew LPP, Fleming JM, Longeon A, et al. Synthesis of 1-indolyl substituted β -carboline natural products and discovery of antimalarial and cytotoxic activities. *Tetrahedron*. 2014;70(33):4910-4920.
111. Xiao S, Lin W, Wang C, Yang M. Synthesis and biological evaluation of DNA targeting flexible side-chain substituted β -carboline derivatives. *Bioorg Med Chem Lett*. 2001;11(4):437-441.
112. Formagio ASN, Tonin LTD, Foglio MA, et al. Synthesis and antitumoral activity of novel 3-(2-substituted-1,3,4-oxadiazol-5-yl) and 3-(5-substituted-1,2,4-triazol-3-yl) β -carboline derivatives. *Bioorg Med Chem*. 2008;16(22):9660-9667.
113. Savariz FC, Foglio MA, Goes Ruiz ALT, et al. Synthesis and antitumor activity of novel 1-substituted phenyl 3-(2-oxo-1,3,4-oxadiazol-5-yl) β -carbolines and their Mannich bases. *Bioorg Med Chem*. 2014;22(24):6867-6875.
114. Kamal A, Srinivasulu V, Nayak VL, et al. Design and Synthesis of C3-Pyrazole/Chalcone-Linked β -Carboline Hybrids: Antitopoisomerase I, DNA-Interactive, and Apoptosis-Inducing Anticancer Agents. *ChemMedChem*. 2014;9(9):2084-2098.
115. Barbosa VA, Formagio ASN, Savariz FC, et al. Synthesis and antitumor activity of β -carboline 3-(substituted-carbohydrazide) derivatives. *Bioorg Med Chem*. 2011;19(21):6400-6408.
116. Yang C-R, Peng B, Cao S-L, et al. Synthesis, cytotoxic evaluation and target identification of thieno[2,3- d]pyrimidine derivatives with a dithiocarbamate side chain at C2 position. *Eur J Med Chem*. 2018;154:324-340.
117. Guo X, Fu Y, Wang Z, et al. Di-2-pyridylhydrazone Dithiocarbamate Butyric Acid Ester Exerted Its Proliferative Inhibition against Gastric Cell via ROS-Mediated Apoptosis and Autophagy. *Oxid Med Cell Longev*. 2018;2018:1-11.
118. Kamal A, Sathish M, Nayak VL, et al. Design and synthesis of dithiocarbamate linked β -carboline derivatives: DNA topoisomerase II inhibition with DNA binding and apoptosis inducing ability. *Bioorg Med Chem*. 2015;23(17):5511-5526.
119. Cao R, Fan W, Guo L, et al. Synthesis and structure–activity relationships of harmine derivatives as potential antitumor agents. *Eur J Med Chem*. 2013;60:135-143.

120. Chen Z, Cao R, Shi B, et al. Synthesis of novel β -carbolines with efficient DNA-binding capacity and potent cytotoxicity. *Bioorg Med Chem Lett*. 2010;20(13):3876-3879.
121. Chen Z, Cao R, Yu L, et al. Synthesis, cytotoxic activities and DNA binding properties of β -carboline derivatives. *Eur J Med Chem*. 2010;45(11):4740-4745.
122. Cao R, Yi W, Wu Q, et al. Synthesis and cytotoxic activities of 1-benzylidine substituted β -carboline derivatives. *Bioorg Med Chem Lett*. 2008;18(24):6558-6561.
123. Ma C, Cao R, Shi B, et al. Synthesis and cytotoxic evaluation of N2-benzylated quaternary β -carboline amino acid ester conjugates. *Eur J Med Chem*. 2010;45(4):1515-1523.
124. Zhang G, Cao R, Guo L, et al. Synthesis and structure--activity relationships of N2-alkylated quaternary β -carbolines as novel antitumor agents. *Eur J Med Chem*. 2013;65:21-31.
125. Bérubé G. An overview of molecular hybrids in drug discovery. *Expert Opin Drug Discov*. 2016;11(3):281-305.
126. Ferland CL, Schrader LA. Regulation of histone acetylation in the hippocampus of chronically stressed rats: a potential role of sirtuins. *Neuroscience*. 2011;174:104-114.
127. Celano M, Mio C, Sponziello M, et al. Targeting post-translational histone modifications for the treatment of non-medullary thyroid cancer. *Mol Cell Endocrinol*. 2018;469:38-47.
128. Gryder BE, Sodji QH, Oyeler AK. Targeted cancer therapy: giving histone deacetylase inhibitors all they need to succeed. *Future Med Chem*. 2012;4(4):505-524.
129. Papavassiliou KA, Papavassiliou AG. Histone deacetylases inhibitors: conjugation to other anti-tumour pharmacophores provides novel tools for cancer treatment. *Expert Opin Investig Drugs*. 2014;23(3):291-294.
130. Amin SA, Adhikari N, Jha T. Structure-activity relationships of HDAC8 inhibitors: Non-hydroxamates as anticancer agents. *Pharmacol Res*. 2018;131:128-142.
131. Ropero S, Esteller M. The role of histone deacetylases (HDACs) in human cancer. *Mol Oncol*. 2007;1(1):19-25.
132. Lai C-J, Bao R, Tao X, et al. CUDC-101, a multitargeted inhibitor of histone deacetylase, epidermal growth factor receptor, and human epidermal growth factor receptor 2, exerts potent anticancer activity. *Cancer Res*. 2010;70(9):3647-3656.

133. Zhou Y, Pan D-S, Shan S, et al. Non-toxic dose chidamide synergistically enhances platinum-induced DNA damage responses and apoptosis in Non-Small-Cell lung cancer cells. *Biomed Pharmacother.* 2014;68(4):483-491.
134. Zhao X, Tan Q, Zhang Z, Zhao Y. 1,3,5-Triazine inhibitors of histone deacetylases: synthesis and biological activity. *Med Chem Res.* 2014;23(12):5188-5196.
135. Grayson DR, Kundakovic M, Sharma RP. Is there a future for histone deacetylase inhibitors in the pharmacotherapy of psychiatric disorders? *Mol Pharmacol.* 2010;77(2):126-135.
136. Grant S, Easley C, Kirkpatrick P. Vorinostat. *Nat Rev Drug Discov.* 2007;6(1):21-22.
137. Thompson CA. Belinostat approved for use in treating rare lymphoma. *Am J Health Syst Pharm.* 2014;71(16):1328.
138. Garnock-Jones KP. Panobinostat: First Global Approval. *Drugs.* 2015;75(6):695-704.
139. Ling Y, Xu C, Luo L, et al. Novel β -Carboline/Hydroxamic Acid Hybrids Targeting Both Histone Deacetylase and DNA Display High Anticancer Activity via Regulation of the p53 Signaling Pathway. *J Med Chem.* 2015;58(23):9214-9227.
140. Ling Y, Feng J, Luo L, et al. Design and Synthesis of C3-Substituted β -Carboline-Based Histone Deacetylase Inhibitors with Potent Antitumor Activities. *ChemMedChem.* 2017;12(9):646-651.
141. Ling Y, Guo J, Yang Q, et al. Development of novel β -carboline-based hydroxamate derivatives as HDAC inhibitors with antiproliferative and antimetastatic activities in human cancer cells. *Eur J Med Chem.* 2018;144:398-409.
142. Karimi-Sales E, Mohaddes G, Alipour MR. Chalcones as putative hepatoprotective agents: Preclinical evidence and molecular mechanisms. *Pharmacol Res.* 2018;129:177-187.
143. Singh P, Anand A, Kumar V. Recent developments in biological activities of chalcones: A mini review. *Eur J Med Chem.* 2014;85:758-777.
144. Mirossay L, Varinská L, Mojžiš J. Antiangiogenic Effect of Flavonoids and Chalcones: An Update. *Int J Mol Sci.* 2017;19(1):27.
145. Shankaraiah N, Siraj KP, Nekkanti S, et al. DNA-binding affinity and anticancer activity of β -carboline–chalcone conjugates as potential DNA intercalators: Molecular modelling

- and synthesis. *Bioorg Chem*. 2015;59:130-139.
146. Lai M-Y, Huang J-A, Liang Z-H, Jiang H-X, Tang G-D. Mechanisms underlying aspirin-mediated growth inhibition and apoptosis induction of cyclooxygenase-2 negative colon cancer cell line SW480. *World J Gastroenterol*. 2008;14(26):4227-4233.
 147. Cuzick J, Otto F, Baron JA, et al. Aspirin and non-steroidal anti-inflammatory drugs for cancer prevention: an international consensus statement. *Lancet Oncol*. 2009;10(5):501-507.
 148. Langley RE, Burdett S, Tierney JF, Cafferty F, Parmar MKB, Venning G. Aspirin and cancer: has aspirin been overlooked as an adjuvant therapy? *Br J Cancer*. 2011;105(8):1107-1113.
 149. Hao W, Shen Y, Feng M, et al. Aspirin acts in esophageal cancer: a brief review. *J Thorac Dis*. 2018;10(4):2490-2497.
 150. Hua H, Zhang H, Kong Q, Wang J, Jiang Y. Complex roles of the old drug aspirin in cancer chemoprevention and therapy. *Med Res Rev*. 2019;39(1):114-145.
 151. Zhao M, Wang Y, Du C, Liu Y, Zhang N, Luo F. Aspirin and metformin exhibit antitumor activity in murine breast cancer. *Oncol Rep*. 2018;39(3):1414-1422.
 152. Verdoodt F, Kjaer SK, Dehlendorff C, Friis S. Aspirin use and ovarian cancer mortality in a Danish nationwide cohort study. *Br J Cancer*. 2018;118(4):611-615.
 153. Algra AM, Rothwell PM. Effects of regular aspirin on long-term cancer incidence and metastasis: a systematic comparison of evidence from observational studies versus randomised trials. *Lancet Oncol*. 2012;13(5):518-527.
 154. Bosetti C, Rosato V, Gallus S, Cuzick J, La Vecchia C. Aspirin and cancer risk: a quantitative review to 2011. *Ann Oncol*. 2012;23(6):1403-1415.
 155. Gray RT, Coleman HG, Hughes C, Murray LJ, Cardwell CR. Low-dose aspirin use and survival in colorectal cancer: results from a population-based cohort study. *BMC Cancer*. 2018;18(1):228.
 156. Patrignani P, Patrono C. Aspirin and Cancer. *J Am Coll Cardiol*. 2016;68(9):967-976.
 157. Rothwell PM, Wilson M, Elwin C-E, et al. Long-term effect of aspirin on colorectal cancer incidence and mortality: 20-year follow-up of five randomised trials. *Lancet*.

- 2010;376(9754):1741-1750.
158. Rothwell PM, Fowkes FGR, Belch JF, Ogawa H, Warlow CP, Meade TW. Effect of daily aspirin on long-term risk of death due to cancer: analysis of individual patient data from randomised trials. *Lancet*. 2011;377(9759):31-41.
 159. Alfonso L, Ai G, Spitale RC, Bhat GJ. Molecular targets of aspirin and cancer prevention. *Br J Cancer*. 2014;111(1):61-67.
 160. García-Heredia JM, Hervás M, De la Rosa MA, Navarro JA. Acetylsalicylic acid induces programmed cell death in Arabidopsis cell cultures. *Planta*. 2008;228(1):89-97.
 161. Yu H-G, Huang J-A, Yang Y-N, et al. The effects of acetylsalicylic acid on proliferation, apoptosis, and invasion of cyclooxygenase-2 negative colon cancer cells. *Eur J Clin Invest*. 2002;32(11):838-846.
 162. Wang Z-Q, Chang R-A, Huang H-Y, et al. Synthesis and biological evaluation of novel farnesylthiosalicylic acid/salicylic acid hybrids as potential anti-tumor agents. *Chinese Chem Lett*. 2014;25(12):1545-1549.
 163. Zhu Y, Fu J, Shurlknight KL, et al. Novel Resveratrol-Based Aspirin Prodrugs: Synthesis, Metabolism, and Anticancer Activity. *J Med Chem*. 2015;58(16):6494-6506.
 164. Xu Q-B, Chen X-F, Feng J, et al. Design, synthesis and biological evaluation of hybrids of β -carboline and salicylic acid as potential anticancer and apoptosis inducing agents. *Sci Rep*. 2016;6(1):36238.
 165. Misra S, Ghatak S, Patil N, et al. Novel dual cyclooxygenase and lipoxygenase inhibitors targeting hyaluronan-CD44v6 pathway and inducing cytotoxicity in colon cancer cells. *Bioorg Med Chem*. 2013;21(9):2551-2559.
 166. Barbosa VA, Baréa P, Mazia RS, et al. Synthesis and evaluation of novel hybrids β -carboline-4-thiazolidinones as potential antitumor and antiviral agents. *Eur J Med Chem*. 2016;124:1093-1104.
 167. Liu T, Sun C, Xing X, et al. Synthesis and evaluation of 2-[2-(phenylthiomethyl)-1H-benzo[d]imidazol-1-yl]acetohydrazide derivatives as antitumor agents. *Bioorg Med Chem Lett*. 2012;22(9):3122-3125.
 168. Li F-Y, Wang X, Duan W-G, Lin G-S. Synthesis and *In Vitro* Anticancer Activity of Novel

- Dehydroabiatic Acid-Based Acylhydrazones. *Molecules*. 2017;22(7):1087.
169. Zheng Y, Ren J, Wu Y, Meng X, Zhao Y, Wu C. Proteolytic Unlocking of Ultrastable Twin-Acylhydrazone Linkers for Lysosomal Acid-Triggered Release of Anticancer Drugs. *Bioconjug Chem*. 2017;28(10):2620-2626.
170. Cardoso LNF, Nogueira TCM, Rodrigues FAR, et al. N-acylhydrazones containing thiophene nucleus: a new anticancer class. *Med Chem Res*. 2017;26(8):1605-1608.
171. Sun K, Peng J-D, Suo F-Z, et al. Discovery of tranlylcypromine analogs with an acylhydrazone substituent as LSD1 inactivators: Design, synthesis and their biological evaluation. *Bioorg Med Chem Lett*. 2017;27(22):5036-5039.
172. Masunari A, Tavares LC. A new class of nifuroxazide analogues: Synthesis of 5-nitrothiophene derivatives with antimicrobial activity against multidrug-resistant *Staphylococcus aureus*. *Bioorg Med Chem*. 2007;15(12):4229-4236.
173. Zhang M, Xian D-M, Li H-H, Zhang J-C, You Z-L. Synthesis and Structures of Halo-Substituted Aroylhydrazones with Antimicrobial Activity. *Aust J Chem*. 2012;65(4):343-350.
174. Li Y, Yan W, Yang J, et al. Discovery of novel β -carboline/acylhydrazone hybrids as potent antitumor agents and overcome drug resistance. *Eur J Med Chem*. 2018;152:516-526.
175. Zhou J, Qu Z, Yan S, et al. Differential roles of STAT3 in the initiation and growth of lung cancer. *Oncogene*. 2015;34(29):3804-3814.
176. Kaur, R., Kapoor, K., Kaur H. Plants as a source of anticancer agents. *J Nat Prod Plant Resour*. 2014;1(1):119-124.
177. Kamal A, Tamboli JR, Nayak VL, Adil SF, Vishnuvardhan MVPS, Ramakrishna S. Synthesis of a terphenyl substituted 4-aza-2,3-didehydropodophyllotoxin analogues as inhibitors of tubulin polymerization and apoptosis inducers. *Bioorg Med Chem*. 2014;22(9):2714-2723.
178. QI Y, LIAO F, ZHAO C, LIN Y, ZUO M. Cytotoxicity, apoptosis induction, and mitotic arrest by a novel podophyllotoxin glucoside, 4DPG, in tumor cells¹. *Acta Pharmacol Sin*. 2005;26(8):1000-1008.
179. Kamal A, Ashwini Kumar B, Suresh P, Juvekar A, Zingde S. Synthesis of 4 β -carbamoyl

- epipodophyllotoxins as potential antitumour agents. *Bioorg Med Chem*. 2011;19(9):2975-2979.
180. Zhang X, Rakesh KP, Shantharam CS, et al. Podophyllotoxin derivatives as an excellent anticancer aspirant for future chemotherapy: A key current imminent needs. *Bioorg Med Chem*. 2018;26(2):340-355.
 181. Xu H, Lv M, Tian X. A Review on Hemisynthesis, Biosynthesis, Biological Activities, Mode of Action, and Structure-Activity Relationship of Podophyllotoxins: 2003- 2007. *Curr Med Chem*. 2009;16(3):327-349.
 182. Sathish M, Kavitha B, Nayak VL, et al. Synthesis of podophyllotoxin linked β -carboline congeners as potential anticancer agents and DNA topoisomerase II inhibitors. *Eur J Med Chem*. 2018;144:557-571.
 183. deStevens G, Lukaszewski H, Sklar M, Halamandaris A, Blatter HM. Investigations in Heterocycles. XI. Tetracyclic and Pentacyclic Indolo[2,3-a]quinolizines. *J Org Chem*. 1962;27(7):2457-2462.
 184. SUNG Y, KOIKE K, NIKAIDO T, OHMOTO T, SANKAWA U. Inhibitors of cyclic AMP phosphodiesterase in *Picrasma quassioides* Bennet, and inhibitory activities of related β -carboline alkaloids. *Chem Pharm Bull (Tokyo)*. 1984;32(5):1872-1877.
 185. Shi B, Cao R, Fan W, et al. Design, synthesis and *in vivo* antitumor activities of novel bivalent β -carbolines. *Eur J Med Chem*. 2013;60:10-22.
 186. Guo L, Chen W, Cao R, et al. Synthesis and structure-activity relationships of asymmetric dimeric β -carboline derivatives as potential antitumor agents. *Eur J Med Chem*. 2018;147:253-265.
 187. Daoud A, Song J, Xiao F, Shang J. B-9-3, a novel β -carboline derivative exhibits anti-cancer activity via induction of apoptosis and inhibition of cell migration *in vitro*. *Eur J Pharmacol*. 2014;724:219-230.
 188. Chatwichien J, Basu S, Budina-Kolomets A, Murphy ME, Winkler JD. PUMA-dependent apoptosis in NSCLC cancer cells by a dimeric β -carboline. *Bioorg Med Chem Lett*. 2016;26(20):4884-4887.
 189. Alderden RA, Hall MD, Hambley TW. The Discovery and Development of Cisplatin. *J Chem*

- Educ.* 2006;83(5):728.
190. Zhang CX, Lippard SJ. New metal complexes as potential therapeutics. *Curr Opin Chem Biol.* 2003;7(4):481-489.
 191. Liu H-K, Berners-Price SJ, Wang F, et al. Diversity in Guanine-Selective DNA Binding Modes for an Organometallic Ruthenium Arene Complex. *Angew Chemie Int Ed.* 2006;45(48):8153-8156.
 192. Li L, Cao W, Zheng W, Fan C, Chen T. Ruthenium complexes containing 2,6-bis(benzimidazolyl)pyridine derivatives induce cancer cell apoptosis by triggering DNA damage-mediated p53 phosphorylation. *Dalt Trans.* 2012;41(41):12766.
 193. Tan C, Wu S, Lai S, et al. Synthesis, structures, cellular uptake and apoptosis-inducing properties of highly cytotoxic ruthenium-Norharman complexes. *Dalt Trans.* 2011;40(34):8611.
 194. Bruijninx PC, Sadler PJ. New trends for metal complexes with anticancer activity. *Curr Opin Chem Biol.* 2008;12(2):197-206.
 195. Liu H-K, Sadler PJ. Metal Complexes as DNA Intercalators. *Acc Chem Res.* 2011;44(5):349-359.
 196. Liu H-K, Parkinson JA, Bella J, Wang F, Sadler PJ. Penetrative DNA intercalation and G-base selectivity of an organometallic tetrahydroanthracene RuII anticancer complex. *Chem Sci.* 2010;1(2):258.
 197. Chen X, Gao F, Zhou Z-X, Yang W-Y, Guo L-T, Ji L-N. Effect of ancillary ligands on the topoisomerases II and transcription inhibition activity of polypyridyl ruthenium(II) complexes. *J Inorg Biochem.* 2010;104(5):576-582.
 198. Castonguay A, Doucet C, Juhas M, Maysinger D. New Ruthenium(II)–Letrozole Complexes as Anticancer Therapeutics. *J Med Chem.* 2012;55(20):8799-8806.
 199. Corral E, Hotze ACG, den Dulk H, et al. Ruthenium polypyridyl complexes and their modes of interaction with DNA: Is there a correlation between these interactions and the antitumor activity of the compounds? *JBIC J Biol Inorg Chem.* 2009;14(3):439-448.
 200. Morais TS, Santos F, Côrte-Real L, et al. Biological activity and cellular uptake of [Ru(η^5 -C₅H₅)(PPh₃)(Me₂bpy)][CF₃SO₃] complex. *J Inorg Biochem.* 2013;122:8-17.

201. Tan C, Lai S, Wu S, et al. Nuclear Permeable Ruthenium (II) β -Carboline Complexes Induce Autophagy To Antagonize Mitochondrial-Mediated Apoptosis. *J Med Chem.* 2010;53:7613-7624.
202. Chen Y, Qin M, Wu J, et al. Synthesis , characterization , and anticancer activity of ruthenium (II) - β -carboline complex. *Eur J Med Chem.* 2013;70:120-129.
203. Chen Y, Qin M, Wang L, Chao H, Ji L, Xu A. A ruthenium (II) β -carboline complex induced p53-mediated apoptosis in cancer cells. *Biochimie.* 2013;95(11):2050-2059.
204. Chen J, Peng F, Zhang Y, et al. Synthesis, characterization, cellular uptake and apoptosis-inducing properties of two highly cytotoxic cyclometalated ruthenium(II) β carboline complexes. *Eur J Med Chem.* 2017;140:104-117.
205. Jin Q, Lu Y, Jin J, et al. Synthesis , characterization , DNA binding ability and cytotoxicity of the novel platinum (II), copper (II), cobalt (II) and nickel (II) complexes with 3- (1 H - benzo [d] imidazol-2-yl) - β -carboline. *Inorg Chim Acta.* 2014;421:91-99.
206. Yang J-M, Zhu Y-H, Chen S, et al. A β -carboline derivative-based nickel(ii) complex as a potential antitumor agent: synthesis, characterization, and cytotoxicity. *Medchemcomm.* 2018;9(1):100-107.
207. Ding Y, He J, Huang J, et al. Harmine induces anticancer activity in breast cancer cells via targeting TAZ. *Int J Oncol.* 2019;54(6):1995-2004.
208. Geng X, Ren Y, Wang F, et al. Harmines inhibit cancer cell growth through coordinated activation of apoptosis and inhibition of autophagy. *Biochem Biophys Res Commun.* 2018;498(1):99-104.
209. Marx S, Bodart L, Tumanov N, Wouters J. Design and Synthesis of a New Soluble Natural β -Carboline Derivative for Preclinical Study by Intravenous Injection. *Int J Mol Sci.* 2019;20(6):1491.
210. Meinguet C, Masereel B, Wouters J. Preparation and characterization of a new harmine-based antiproliferative compound in complex with cyclodextrin: Increasing solubility while maintaining biological activity. *Eur J Pharm Sci.* 2015;77:135-140.
211. Sniady A. N-iodosuccinimide (NIS). *Synlett.* 2006;(6):960-961.
212. Wang D, Gao S. Sonogashira coupling in natural product synthesis. *Org Chem Front.*

- 2014;1(5):556-566.
213. Bakherad M, Jajarmi S. Pd/C-catalyzed, copper-free Sonogashira coupling: One-pot synthesis of 1-aryl-4-(2-phenylethynyl)[1,2,4]triazolo[4,3-a]quinoxalines in water. *Monatshefte fur Chemie*. 2013;144(6):885-890.
 214. Maaliki C, Chevalier Y, Thiery E, Thibonnet J. Palladium and copper catalyzed Sonogashira decarboxylative coupling of aryl iodides and alkynyl carboxylic acids. *Tetrahedron Lett*. 2016;57(30):3358-3362.
 215. Matulenko MA, Paight ES, Frey RR, et al. 4-Amino-5-aryl-6-arylethynylpyrimidines: Structure-activity relationships of non-nucleoside adenosine kinase inhibitors. *Bioorganic Med Chem*. 2007;15(4):1586-1605.
 216. Kassoum N, Lohitha R, Joseph C, Anders P. Heteroaryl alkyne derivatives and uses thereof. Published online 2015:109-110.
 217. Kumar R, Asthana M, Singh RM. Pd-Catalyzed One-Pot Stepwise Synthesis of Benzo[b][1,6]naphthyridines from 2-Chloroquinoline-3-carbonitriles Using Sulfur and Amines As Nucleophiles. *J Org Chem*. 2017;82(21):11531-11542.
 218. Ding MW, Sun Y, Liu XP, Liu ZJ. A direct synthesis of 2-alkoxy-4H-imidazol-4-ones. *Heterocycl Commun*. 2003;9(2):135-138.
 219. Li J, Chen L, Chin E, Lui AS, Zecic H. Platinum(II)-catalyzed intramolecular cyclization of alkynylbenzonitriles: Synthesis of 1-alkoxyisoquinolines and isoquinolones. *Tetrahedron Lett*. 2010;51(49):6422-6425.
 220. Miyaura N, Yamada K, Suzuki A. A new stereospecific cross-coupling by the palladium-catalyzed reaction of 1-alkenylboranes with 1-alkenyl or 1-alkynyl halides. *Tetrahedron Lett*. 1979;20(36):3437-3440.
 221. Andappan MMS, Nilsson P, Larhed M. Arylboronic acids as versatile coupling partners in fast microwave promoted oxidative Heck chemistry. *Mol Divers*. 2003;7(2-4):97-106.
 222. Braga AAC, Morgon NH, Ujaque G, Maseras F. Computational characterization of the role of the base in the Suzuki-Miyaura cross-coupling reaction. *J Am Chem Soc*. 2005;127(25):9298-9307.
 223. Braga AAC, Ujaque G, Maseras F. A DFT study of the full catalytic cycle of the Suzuki-

- Miyaura cross-coupling on a model system. *Organometallics*. 2006;25(15):3647-3658.
224. Enguehard-Gueiffier C, Thery I, Gueiffier A, Buchwald SL. A general and efficient method for the copper-catalyzed cross-coupling of amides and thiophenols with 6-halogenoimidazo[1,2-*a*]pyridines. *Tetrahedron*. 2006;62(25):6042-6049.
225. Thomas A, Sujatha A, Anilkumar G. Goldberg Reaction: Development, Mechanistic Insights and Applications. *Mini Rev Org Chem*. 2014;12(1):3-23.
226. Sato S, Inokuma T, Otsubo N, Burton DR, Barbas CF. Chemically Programmed Antibodies As HIV-1 Attachment Inhibitors. *ACS Med Chem Lett*. 2013;4(5):460-465.
227. Sutherland RL, Watts CKW, Lee CSL, Musgrove EA. Breast Cancer. In: J.R.W. M, B. P, eds. *Human Cell Culture*. 1st ed. Springer, Dordrecht; 1999:79-106.
228. Pulaski BA, Ostrand-Rosenberg S. Mouse 4T1 Breast Tumor Model. *Curr Protoc Immunol*. 2000;39(1):20.2.1-20.2.16.
229. Zhang Y, Zhang GL, Sun X, et al. Establishment of a murine breast tumor model by subcutaneous or orthotopic implantation. *Oncol Lett*. 2018;15(5):6233-6240.
230. Soule HD, Maloney TM, Wolman SR, et al. Isolation and Characterization of a Spontaneously Immortalized Human Breast Epithelial Cell Line, MCF-10. *Cancer Res*. 1990;50(18):6075-6086.
231. Mohan Krishna K, Inturi B, Pujar G V., Purohit MN, Vijaykumar GS. Design, synthesis and 3D-QSAR studies of new diphenylamine containing 1,2,4-triazoles as potential antitubercular agents. *Eur J Med Chem*. 2014;84:516-529.
232. Zhu W, Liu Y, Zhai X, et al. Design, synthesis and 3D-QSAR analysis of novel 2-hydrazinyl-4- morpholinothieno[3,2-*d*]pyrimidine derivatives as potential antitumor agents. *Eur J Med Chem*. 2012;57:162-175.
233. Zhao B, Zhao C, Hu X, et al. Design, synthesis and 3D-QSAR analysis of novel thiopyranopyrimidine derivatives as potential antitumor agents inhibiting A549 and Hela cancer cells. *Eur J Med Chem*. 2020;185:111809.
234. Meinguet C, Bruyère C, Frédérick R, et al. 3D-QSAR, design, synthesis and characterization of trisubstituted harmine derivatives with *in vitro* antiproliferative properties. *Eur J Med Chem*. 2015;94:45-55.

235. Golbraikh A, Tropsha A. Beware of q²! In: *Journal of Molecular Graphics and Modelling*. Vol 20. Elsevier; 2002:269-276.
236. Chantôme A, Potier-Cartereau M, Clarysse L, et al. Pivotal role of the lipid raft SK3-orai1 complex in human cancer cell migration and bone metastases. *Cancer Res*. 2013;73(15):4852-4861.

Résumé

Dans le cadre de cette thèse, un travail approfondi a été réalisé pour développer de nouveaux agents anticancéreux de structure imidazo[1,2-*a*:4,5-*c'*]dipyridine. Un aperçu des β -carboline décrites dans la littérature est donné dans le chapitre 2, ainsi qu'une analyse des relations structure-activité (SAR) anticancéreuse de ce squelette. Cette thèse décrit dans le chapitre 3 nos efforts pour introduire une variabilité structurale sur quatre positions du noyau imidazo[1,2-*a*:4,5-*c'*]dipyridine. Ensuite, les produits cibles ont été testés pour leur capacité à inhiber la prolifération, la migration et l'invasion des cellules TNBC (chapitre 4). Les composés anti-prolifératifs les plus puissants [$IC_{50} \leq 6 \mu M$] contre les quatre lignées cellulaires TNBC étudiées ont été testés quant à leur capacité d'induire l'apoptose. De plus, deux composés ont réduit l'expression nucléaire de KI67, démontrant une activité inhibitrice de la prolifération cellulaire. Enfin, de nombreux analogues ont présenté de puissantes activités anti-migratoires sur MDA-MB-435s à 1 μM . En outre, un composé a inhibé l'invasion des cellules murines 4T1 à 1 μM . Dans le chapitre 5, nous discutons de l'étude *in silico* des relations structure-activité quantitatives tridimensionnelles (3D-QSAR) de nos composés.

En résumé, de nouveaux inhibiteurs puissants de la prolifération, de la migration et de l'invasion des cellules du cancer du sein ont été mis au point au cours de cette recherche doctorale.

Mots-clés: Cancer du sein triple négatif (TNBC); imidazo[1,2-*a*:4,5-*c'*]dipyridine, activité antiproliférative; apoptose; activité anti-migrative; activité anti-invasion.

Summary

In this thesis, an extensive work was done to develop new anticancer agents based on the imidazo[1,2-*a*:4,5-*c'*]dipyridine scaffold. An overview of β -carboline described in the literature was given in Chapter 2, together with an analysis of the anticancer structure-activity relationships (SAR) of this skeleton. This thesis describes in Chapter 3 our efforts to introduce modifications at four positions of imidazo[1,2-*a*:4,5-*c'*]dipyridine core. Then, the target products were tested for their ability to inhibit the proliferation, migration, and invasion of TNBC cells (Chapter 4). The most potent anti-proliferative compounds [$IC_{50} \leq 6 \mu M$] against all four TNBC cell lines studied, were tested for their apoptotic induction capacity. Also, two compounds reduced nuclear Ki-67 staining indicating a decrease in cell proliferation. Many analogues exhibited potent anti-migratory activities against MDA-MB-435s at 1 μM . Besides, one compound inhibited murine 4T1 cell invasion at 1 μM . In chapter 5, we discuss the *in silico* three dimensional-quantitative structure-activity relationships (3D-QSAR) study of these compounds.

In summary, novel potent inhibitors of breast cancer cell proliferation, migration, and invasion were developed during this doctoral research, which may lead to novel anti-cancer agents.

Keywords: Triple-negative breast cancer (TNBC); imidazo[1,2-*a*:4,5-*c'*]dipyridine, antiproliferative activity; apoptosis; anti-migrative activity; anti-Invasion activity.